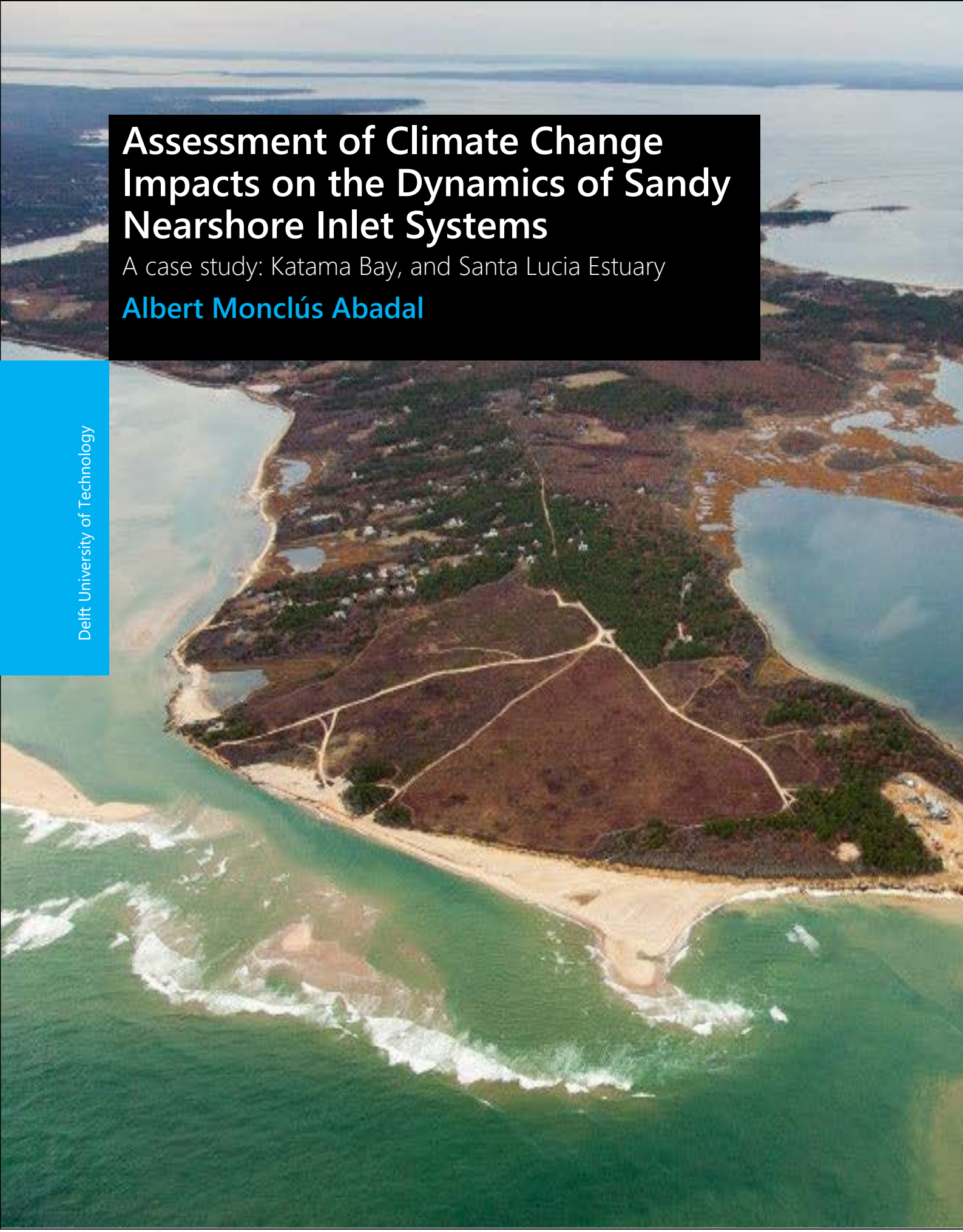

Assessment of Climate Change Impacts on the Dynamics of Sandy Nearshore Inlet Systems

A case study: Katama Bay, and Santa Lucia Estuary

Albert Monclús Abadal

Delft University of Technology

TU Delft Delft University of Technology

Challenge the future

Assessment of Climate Change Impacts on the Dynamics of Sandy Nearshore Inlet Systems

A Case Study: Katama Bay, and Santa Lucia Estuary

by

Albert Monclús Abadal

In partial fulfillment of the requirements for the degree of

ERASMUS +: ERASMUS MUNDUS MOBILITY PROGRAMME

Master of Science

Coastal & Marine Engineering and Management (CoMEM)

at the Delft University of Technology,

to be defended publicly on Wednesday, July 18, 2018, at 10:00 AM.

Thesis committee:

Prof. dr. Ir. S.G.J. Aarninkhof, TU Delft

Ir. J. Bosboom, TU Delft

Ir. dr J.A. Hopkins, TU Delft

Ir. S. G. Pearson, TU Delft

Ir. dr H. M. Schuttelaars, TU Delft

An electronic version of this thesis is available at

http://repository.tudelft.nl/

Correspondence with the author may be directed to:

monclus.albert@gmail.com

Keywords: Tidal inlet, climate change, copula analysis, hydrodynamics, morphodynamics, Delft3D, inlet migration, sediment pathways, Katama Bay, Santa Lucia Estuary.

Front Cover: Aerial view of Katama Bay inlet, Massachusetts (USA). It is appreciable the interaction between waves and currents. Strong currents flow from the inlet during ebb, inducing wave blocking and breaking. (Source: Bill Brine)

The Erasmus+: Erasmus Mundus MSc in Coastal and Marine Engineering and Management is an integrated programme including mobility organized by five European partner institutions, coordinated by Norwegian University of Science and Technology (NTNU).

The joint study programme of 120 ECTS credits (two years full-time) has been obtained at two or three of the five CoMEM partner institutions:

- Norges Teknisk- Naturvitenskapelige Universitet (NTNU) Trondheim, Norway
- Technische Universiteit (TU) Delft, The Netherlands
- Universitat Politècnica de Catalunya (UPC). BarcelonaTech. Barcelona, Spain
- University of Southampton, Southampton, Great Britain
- City University London, London, Great Britain

During the first three semesters of the programme, students study at two or three different universities depending on their track of study. In the fourth and final semester an MSc project and thesis has to be completed. The two-year CoMEM programme leads to a multiple set of officially recognized MSc diploma certificates. These will be issued by the universities that have been attended by the student. The transcripts issued with the MSc Diploma Certificate of each university include grades/marks and credits for each subject.

Information regarding the CoMEM programme can be obtained from the programme coordinator:

Øivind A. Arntsen, Dr.ing.
Associate Professor in Marine Civil Engineering
Department of Civil and Transport Engineering
NTNU Norway
Telephone: +4773594625 Cell: +4792650455 Fax: + 4773597021
Email: oivind.arntsen@ntnu.no

CoMEM URL: https://www.ntnu.edu/studies/mscomem

Disclaimer:

"The European Commission support for the production of this publication does not constitute an endorsement of the contents which reflects the views only of the authors, and the Commission cannot be held responsible for any use which may be made of the information contained therein."

CoMEM Thesis

This thesis was completed by:

Albert Monclús Abadal

Under supervision of:

Prof. dr. Ir. S.G.J. Aarninkhof, TU Delft

Ir. J. Bosboom, TU Delft

Ir. dr J.A. Hopkins, TU Delft

Ir. S. G. Pearson, TU Delft

Ir. dr H. M. Schuttelaars, TU Delft

As a requirement to attend the degree of

Erasmus+: Erasmus Mundus Master in Coastal and Marine Engineering and Management (CoMEM)

Taught at the following educational institutions:

Norges Teknisk- Naturvitenskapelige Universitet (NTNU)

Trondheim, Norway

Technische Universiteit (TU) Delft

Delft, The Netherlands

University of Southampton,

Southampton, Great Britain

At which the student has studied from August 2016 to July 2018.

ACKNOWLEDGEMENTS

This thesis is the culmination of the Master of Science in Coastal & Marine Engineering and Management (CoMEM) program imparted at Delft University of Technology (TU Delft), the Norwegian University of Science and Technology (NTNU), and the University of Southampton.

First and foremost, I would like to thank my committee for their contributions to this thesis. Julia, thanks for generously offering your time, support, and guidance throughout these past five months. You helped me to be critical and were always quick to respond with valuable feedback. Stuart, thank you for being my "second" daily supervisor. You have always been there to resolve any doubt and encourage me to improve my work. Thank you Stefan, Judith, and Henk, for proposing several ideas during the meetings that made this thesis more concise and thoughtful.

Outside TU Delft, I am grateful to Jordi Hoek for providing the initial models of Santa Lucia, and to the researchers of IH Cantabria, Paula Camus and Jorge Pérez, for offering me the projected changes in wave conditions. Without this information, this study would not have been possible.

Most of all, I would like to thank my parents for their unconditional support during all these years. *Mama, gràcies per emparar-me en els moments més difícils. Papa, gràcies pel teu suport diari durant aquesta llarga travessia. Sense vosaltres això no hauria estat possible. Mil gràcies.* And also, to my grandmas. You are always waiting with the biggest smiles.

Thanks to the CoMEM family. These last two years have been the best experience of my life, and without all of you, that would not be possible. Claude thanks for making every day an adventure. *Inés gracias por aguantar mis estupideces y sacarme siempre una sonrisa.* Michelle, thanks for your delightful craziness. Tom, Chris, David, and Charles, cheers for the beers, movies, and inappropriate conversations. Nader and Al, I will miss the Iranian hospitality. And thank you Tessa, Esther, John, Mao, Nan, Mohamed, Maria, and Mohammad for all the unforgettable moments. I hope our friendship will last a lifetime, regardless of where we are. And you all know that you have a home wherever I am.

Thanks to my friends in Barcelona and Sevilla for their unwavering support. *Hèctor, David, Albert, Roger, Raquel us veig aviat!. David B. gracias por motivarme a intentar esta aventura*.

And finally, I would like to acknowledge the support and funding sources of the EACEA/EU that provided the opportunity to study abroad for two years. And obviously, the effort and hosting of the organizers of this master. *Tussen Takk* Øivind Arntsen and Sonja Marie Ekrann.

Albert Monclus Abadal

Delft, July 2018

SUMMARY

Sandy barriers comprise 12% of coastlines around the world, and most of these barriers enclose tidal bays and lagoons. These systems accommodate human settlements vulnerable to climate change, which offer enough economic, social, and environmental utility to require further research on the impact of climate change and subsequent best management practices.

The present work aims to analyze how climate change impacts the hydrodynamics and morphodynamics of two barrier inlet systems: Katama Bay (United States of America), and the Santa Lucia Estuary (South Africa). The goal is to estimate future changes in forcing variables (e.g., sea level rise, wave climate, river discharge, tides), implement them in process-based models (coupled SWAN and Delft3D), and identify changes in the dynamics of both systems by comparing present and future state simulations.

This thesis develops a replicable and flexible methodology that can be used as a systematic tool to assess the impacts of climate change on the overall dynamics of tidal inlet systems. A novel approach (copula analysis) was used to derive the wave climate implemented in Delft3D, which was then qualitatively validated for both sites. Model results were used to compare changes to inlet stability, inlet geometry, and sediment pathways for present and future hydrodynamic conditions.

Results show that sea level rise is the primary contributor to the overall morphodynamics at both sites, whereas changes in wave direction strongly impact the rate of inlet migration. Other changes (e.g., significant wave height, wave period, and river discharge) play a secondary role in the dynamics of both systems. Comparisons with previous studies suggest that wave direction impacts each system differently. These impacts must be specifically addressed for each tidal inlet, as the results from one site should not be used to determine a general behavior for the assessment of CC impacts in tidal inlet systems.

CONTENTS

LIST OF FIGURES

LIST OF TABLES

LIST OF SYMBOLS

Symbol	Units	Description
A_b	m^2	Inlet cross section area
f'_c	-	Bedload friction owing to currents
h	m	Water depth
H_S	m	Significant wave height
$k_{s,grain}$	m	Bed roughness
M_{TOT}	m^3	Annual littoral drift
P	m^3	Tidal prism
Q_F	m^3	Future river discharge
Q_P	m^3	Present river discharge
Q_S	m^3	Littoral drift
r	-	Bruun stability criterion
T_M	s	Mean wave period
T_P	s	Peak wave period
$U_{\delta, back}$	m/s	Offshore peak orbital velocity
$U_{\delta, for}$	m/s	Onshore peak orbital velocity
V_d	m^3	Downdrift barrier migration rate
V_u	m^3	Updrift barrier migration rate
α	m^3	Barrier transport fraction
α_d	m^3	Barrier transport fraction from the flood-tidal delta
β	m^3	Bypassing transport fraction
β_d	m^3	Bypassing transport fraction from the barrier
δ	m^3	Flood-tidal delta transport fraction
δ_d	m^3	Flood-tidal delta transport fraction from the barrier
ΔH_S	m	Change in significant wave height
ΔT_P	s	Change in peak wave period
θ	degrees	Wave direction
θ^-	degrees	Anticlockwise changes in wave direction
θ^+	degrees	Clockwise changes in wave direction
θ_M	degrees	Mean wave direction
θ_P	degrees	Peak wave direction
ρ	-	Correlation factor
$\tau'_{b,cw,t}$	Pa	Grain-related bed shear stress

LIST OF ABBREVIATIONS

Abbreviation	Description
AR5	Fifth Assessment Report
ASMITA	Aggregated Scale Morphological Interaction between Tidal basin and Adjacent coast
BLT	Bedload Transport
BN	Bayesian Network
CC	Climate Change
CMIP5	Coupled Model Intercomparison Project Phase 5
DD	Dynamically Downscaling
DIVA	Dynamic Interactive Vulnerability Assessment
FS	Future State
GCM	Global Climate Model
GEV	Generalized Extreme Value
GIA	Glacial Isostatic Adjustment
IPCC	Intergovernmental Panel on Climate Change
JOWSAP	Joint North Sea Wave Project
KB	Katama Bay
LS	Land Subsidence
MA	Massachusetts
MAR	Mean Annual Runoff
MORFAC	Morphological acceleration factor
MSL	Mean Sea Level
MVCO	Martha's Vineyard Coastal Observatory
NE	North East
NOAA	National Oceanic and Atmospheric Administration
PS	Present State
RCM	Regional Climate Model
RCP	Representative Concentration Pathways
RMS	Root Mean Square
RMSE	Root Mean Square Error
RSLR	Relative Sea Level Rise
SD	Statistical Downscaling
SE	South East
SI	Scatter Index
SL	Santa Lucia

Abbreviation	Description
SLR	Sea Level Rise
SRES	Special Report on Emissions Scenarios
SSE	South South-East
SSW	South South-West
ST	Suspended Transport
SW	South West
TT	Total Transport
USA	United States of America
WWIII	WaveWatch III

CHAPTER 1. INTRODUCTION

CHAPTER SUMMARY

Climate change may alter the hydrodynamics along the global coast, thus impacting society, environment, and economy on a worldwide scale. Coastal systems such as tidal inlets are vulnerable to climate change effects, but to date, the focus has been on the consequences of sea level rise. The present study analyzes the influences of climate change on different and diverse sandy inlet systems examining effects of and on wave height, wave direction, tides, mean water levels and river flow. Furthermore, the potential effects on the nearshore hydrodynamics and morphodynamics are studied on the selected inlet systems using process-based models (Delft3D).

1.1. Motivation

This study is motivated by the unknown but probable consequences of climate change (hereafter CC) on sandy inlets and associated socio-economic damages. Projected CC-driven variations in wave conditions, mean sea level, tidal forcings, and river flow have the potential to affect the coastal zone (Ranasinghe 2016). Hence, understanding CC effects on coastal systems, such as tidal inlets, is crucial to predicting the potential consequences of CC on society and nature.

Climate Change: a global problem

Humans tend to settle in areas with readily accessible water, such as river edges or coastal zones (Figure 1.1). Settlements in coastal lowlands are especially vulnerable to CC-driven risks, owing to high-density population and rapid increase of inhabitants (McGranahan, Balk, and Anderson 2007). Nearly 13% of the world's urban areas (counting an estimated 634 million inhabitants) are in coastal lowland zones (Johnson et al. 2015).

Multiple systems around the world are vulnerable to CC. Indeed, sandy barriers comprise 12% of the coastal shoreline around the world, and most of these barriers enclose tidal bays and lagoons (Glaeser 1978). Tidal basins are a system with enough economic, social, and environmental utility to require further research on the impact of CC and following best management practices.

Diverse factors contribute to societal and economic vulnerability in tidal basins (e.g., areas with large flood-plain populations that are exposed to significant storm surge hazards; areas with tourist-based economies where major adverse effects on tourism are likely; highly sensitive coastal areas where the scope for inland migration is limited; areas where there are substantial barriers to adaptation (R.J. Nicholls et al. 2007)). Similarly, environmental vulnerability depends on different factors (e.g., vertical changes in wetland elevation, spatial landscape-scale feedbacks, wetland saltmarsh deterioration, human interference with ecosystem feedbacks (Kirwan and Megonigal 2013)).

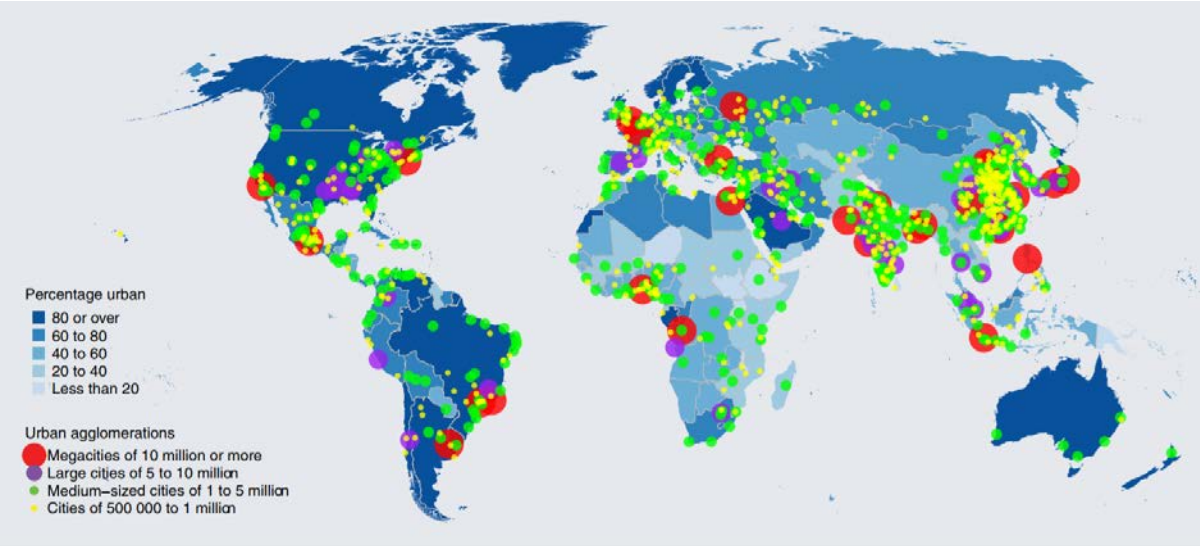

Figure 1.1. Percentage (in blue colors) and location (dots, legend on the left) of urban agglomerations with at least 500,000 inhabitants, 2014 (from Nations 2014)

Many examples of tidal basins where CC may have a significant impact exist around the world, such as Venice Lagoon, Wadden Sea or Galveston Bay. Indeed, the area around Venice lagoon exhibits large population density in low lying areas which increases flood risk vulnerability. Here, the relative sea level rise may increase flood events (considered when the level is 110 cm above the datum) from 4 times a year to 20-250 times a year. Thus, there is a need to advance ad hoc management and planning of the Venice defense. (Carbognin et al. 2010).

Similarly, around the United States Coast, it is possible to find multiple bays that are sensitive to CC (Figure 1.2). For instance, Galveston Bay is semi-enclosed with a barrier system that shelters it from waves (Rego and Li 2010), where flood risk is increasing due to the population growth in the area and the potential effects of sea level rise (SLR). Moreover, Warner and Tissot (2012) showed that by the year 2100 the increase of flooding frequency due to small but regular surges could have a more significant impact on the coast than SLR.

On the other side of the Atlantic Ocean, the Wadden Sea is a site with enough present-condition knowledge (Eysink 1993; Wang et al. 1995; Elias 2006; Elias et al. 2012; Wang et al. 2012; and many others) use to study potential changes owing to CC. Multiple effects of SLR have been studied at this site (Reed 1995; Flemming and Bartholomä 1997; Beukema 2002; and many others), showing that SLR may impact the coastline in more ways than merely flooding. For instance, loss of intertidal sand and muds in tidal flats over the Wadden Sea (Flemming and Bartholomä 1997) or the decline in saltmarsh population owing to SLR-driven changes on wetland elevation (Reed 1995).

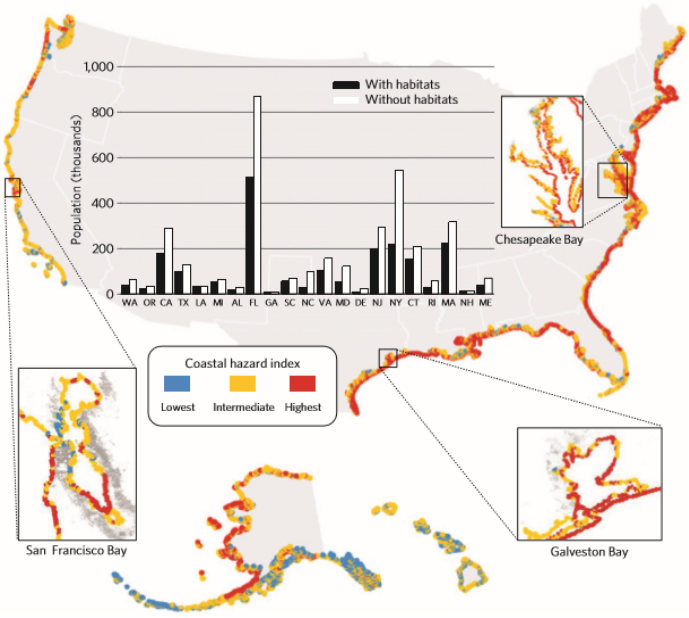

Figure 1.2. Exposure of the US coastline and coastal population to sea-level rise in 2100 and storms. Warmer colors indicate regions with more exposure to coastal hazards. The analysis is done using an A2 scenario. This scenario projects a very heterogeneous world, preserving the local identities and the self-reliance. Therefore, the economic development is primarily regional (which results in a significant population growth), and the technological development is slow (IPCC 2000). The bar graph shows the population living in areas most exposed to hazards (red 1km² coastal segments in the map). It is divided into protection provided by inhabitants (black bars) and increase in a population exposed to hazards were lost owing to CC or human impacts (white bars). Letters on the x-axis represent US state abbreviations. (from Arkema et al. 2013).

Climate Change is not only Sea Level Rise

However, SLR is a small part of the "climate change loading spectrum," which includes changes on wave height, wave period, wave direction, wind climate, storminess, storm surges, and rainfall among others. Recently, multiple models have hypothesized changes to other loadings than SLR (e.g., wave height (Young et al. 2011; Mori et al. 2013; Hemer et al. 2013; Camus et al. 2014; Perez et al. 2015; Camus et al. 2017), wave direction (Hemer et al. 2013; Perez et al. 2015), wave period (Hemer et al. 2013; Camus et al. 2014; Perez et al. 2015; Camus et al. 2017), rainfall (Hirabayashi et al. 2013), storminess (Bender et al. 2009; Shope et al. 2016), and wind (Young et al. 2011; Mori et al. 2013; Storlazzi et al. 2015; Sterl et al. 2015)). Some of the projected changes are large (e.g., Hemer et al. (2013) projected wave direction changes of 10º (Figure 1.3)) and its impacts may have considerable consequences on tidal inlets around the world.

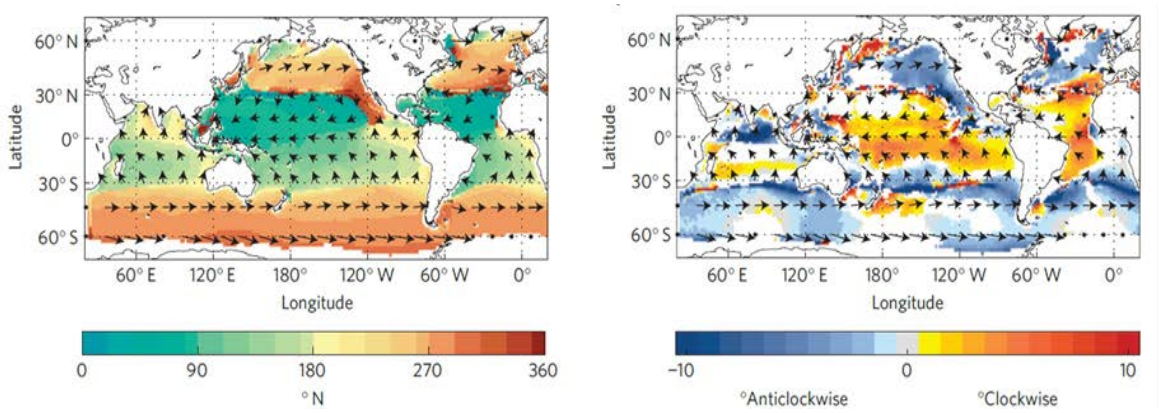

Figure 1.3. Averaged multi-model annual mean wave direction (ºN) for a historical time-slice (~1979-2009) (Left). Averaged multi-model changes in annual mean wave direction for the future time slice (2070-2100) relative to the present climate time-scale (1979-2009) (right). Black arrows show the predominant wave direction (from Hemer et al. 2013).

Opportunity to expand research further

The vulnerability of tidal inlets to CC has been established based on changes of SLR at different sites around the world (Van Goor et al. 2003; Lopes et al. 2011; Dissanayake et al. 2012; Ranasinghe et al. 2013; Valentim et al. 2013; and many others). However, recent studies show that other variables (changes in wave height, river flow or wave direction) could also contribute to changes in the hydrodynamics and morphodynamics on tidal inlets (Ranasinghe 2016; Duong et al. 2017; Duong et al. 2018). These systems exhibit irregular geometry and branch into multiple channels at the flood- and ebb- side creating complicated flow patterns (van de Kreeke 1992). The problem is complex, and 3D computational models are useful to understand the hydrodynamics and morphodynamics behind them.

Duong et al. (2017) and Duong et al. (2018) focus their research on understanding how CC-driven forcings would affect the stability of small tidal inlets by looking at the inlet migration distance, the inlet migration speed, and the Bruun stability criterion (ratio between tidal prism and littoral drift). Small tidal inlets are characterized by inlet channels less than 500 meters-wide connected to small (less than 50 km^2) and relatively shallow estuaries/lagoons (Duong et al. 2016). The study is divided into two approaches (a poor data approach (Duong et al. 2017) and a rich data approach (Duong et al. 2018)) using process-based computational models (Delft3D) at three tidal inlets in Sri Lanka (Negombo Lagoon,

Kalutara Lagoon, and Maha Oya River). Both approaches have shown that changes in wave conditions (significant wave height and wave direction) have the largest impact on a small inlet's stability. Figure 1.4 (from Duong et al. 2017) illustrates the Bruun criterion variation at Negombo Lagoon for all the simulations attained. C9 simulation (no SLR, increase in wave height, increase in wave direction, and a decrease of river flow) is the one that has the most significant impact on the inlet stability. Considering all the simulations, changes in wave conditions account for almost 70% of the CC-modified Bruun criterion.

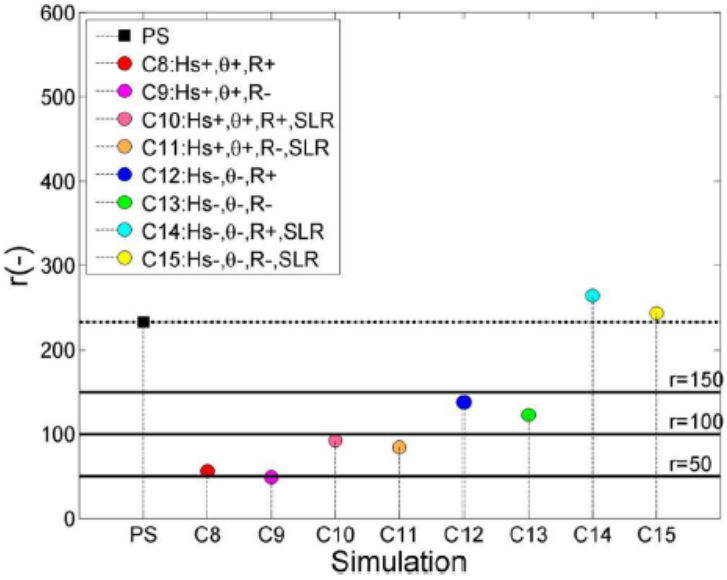

Figure 1.4. Bruun stability criterion (r) for CC-driven forcings at Negombo Lagoon. The r value for the PS (Present Simulation) is shown in the left side and compared with the other simulations that include variations in significant wave height (H_S), wave direction (θ) and river flow (R) (from Duong et al. 2017).

Main Motivation for the Research:

- Climate change effects on inlet systems may have severe impacts on society, economy, and environment.
- Models show that other variables (e.g., wave height, wave period, wave direction, rainfall) are likely to vary due to CC within the next century.
- There is an opportunity to explore the effects of CC-driven loadings in addition to SLR on inlet systems.

1.2. Research Objectives

Predicting CC effects is a complex and uncertain science even in well-studied environments like sandy coastlines due to multiple variables involved, such as hydrodynamics forcings, changing morphology characteristics, uncertainty in projected changes, and human adaption. Predicting CC effects on tidal inlets is complicated even further by more complex hydrodynamics and morphodynamics. The inclusion of forcing in addition to SLR increases the complexity. Thus, improved understanding of the response of such systems to CC is needed. To understand the potential consequences of such forcings on inlet systems, this thesis focuses on several research questions:

Main Question:

How does climate change (sea level rise, wave derived changes, rainfall derived changes, changes in tidal range) impact the hydrodynamics and morphodynamics of sandy nearshore inlet systems?

Sub-questions:

- To what degree does SLR affect sandy nearshore inlet systems?
- Other than SLR, which are the most critical CC processes that impact sandy nearshore inlet systems?
- Concretely, how do changes in wave direction affect sandy nearshore inlet systems?
- Are process-based numerical models suitable for this analysis?
- Can these tools be applied to develop a systematic analytical method to analyze the impact of CC on different sandy nearshore inlet systems?

In the process of answering these questions, we expect to further develop the existing body of CC assessment in inlet systems, presenting a suitable methodology applicable to similar sites. Therefore, an analysis of two sites (Katama Bay (USA) and Santa Lucia Estuary (South Africa)) is achieved through six primary objectives:

Main Objectives:

- To analyze and estimate the future changes in forcing variables, such as wave height, wave direction, river-flow discharges, and changes in tidal ranges and phases.
- To examine the potential effects of CC on the hydrodynamics of the selected inlet systems using process-based models (based on Delft3D).
- To study the potential effects of CC on the inlet migration morphodynamics of the selected systems using process-based models (Delft3D) with simplified geometry.
- To determine the relative importance of various CC impacts on changes of inlet stability, inlet geometry, and sediment pathways during the inlet migration on each site.
- To compare the results with similar existing studies, particularly the relative importance of each CC-driven forcing.
- To develop a replicable methodology to assess CC impacts on sandy nearshore inlet systems.

1.3. Relevance

This thesis is innovative in that it includes CC-driven forcings other than SLR in the study of the hydrodynamics and the morphodynamics of inlet systems. It builds on recent studies and methodologies (Ranasinghe 2016; Duong et al. 2016; Duong et al. 2017; Duong et al. 2018) to include such CC-driven forcings as wave direction, river discharge, tidal elevation, and SLR.

Duong et al. (2017) and Duong et al. (2018) are both focused on the analysis of the stability of small tidal inlets, while this research is focused also on changes in geometry (e.g., inlet width, depth, and length), changes on the main tidal features (e.g., ebb- and flood-tidal deltas) and analyzing the sediment pathways causing inlet migration (e.g., littoral sediment bypassing, sediment transport through the inlet, and import of sediment into the basin). The sediment pathways analysis provides a better framework to understand the morphodynamic behavior of each system and hence, helping to find management solutions for the future.

This thesis also isolates the effects of CC-driven wave direction changes on tidal inlet migration, an investigation that has yet to be undertaken in the literature. Systems with strong wave climate dependency (Katama Bay (USA) and Santa Lucia Estuary (South Africa)) are selected to examine the sensitivity of inlet migration to changes in wave direction. Figure 1.5 shows the location of both sites. Katama Bay is in a storm environment, primarily affected by hurricanes, whereas Santa Lucia is in a swell environment. These distinct wave climates allow an evaluation of the differences between CC-driven impacts in different wave environments.

Figure 1.5. Location of the analyzed sites (Katama Bay (USA), and the Santa Lucia Estuary (South Africa). Katama Bay satellite image from (Google Earth 2018a) and Santa Lucia Estuary image from (Google Earth 2018b).

1.4. Thesis Approach

The current thesis is divided into three parts (Figure 1.6):

Thesis stages:

- CC data analysis for the present and future states.
- Numerical modeling of the tidal inlet systems via coupled Delft3D and SWAN models for the present and future state simulations.
- Results analysis and comparisons with previous literature.

1. CC data analysis

The present state data is obtained from hindcast models (waves, tides) or site studies (river discharge). We derive projected conditions for 2100 using an intermediate climate scenario (Representative Concentration Pathways 4.5 (IPCC 2014b)). Projected wave climates are collected from statistical downscaling projections (Perez et al. 2015; Camus et al. 2017) or dynamic downscaling projections (Hemer et al. 2013). Here, we use statistical tools (copula distributions) to derive the wave boundary conditions along the outermost domains at both sites using WaveWatch III (WWIII) hindcast data. This procedure is used as a wave reduction method for both sites when a morphological acceleration factor (MORFAC) is applied in Delft3D.

2. Numerical modeling with Delft3D

Coupled wave (SWAN) and flow (Delft3D-FLOW) models are used to investigate the inlet system hydrodynamics and morphodynamics at both sites. Waves are simulated over several nested SWAN model domains, whereas water levels, currents, and sediment transport are modeled using Delft3D-FLOW on a single grid in Santa Lucia and two nested grids in Katama Bay. The same "snap-shot" methodology is applied at both sites (Figure 1.6). First, a present state (PS) simulation is run. Next, future state (FS) simulations are run by changing the forcings to introduce CC effects.

3. Result analysis and comparison

We analyze changes to inlet stability, inlet geometry, main tidal features, and sediment pathways for present and future hydrodynamic conditions. The results for both sites are compared for similarities and differences. The discussion is focused on the link between the result divergences and the particular conditions of each site. Similarly, results are qualitatively compared with other previous studies in other sites (Duong et al. 2017; Duong et al. 2018) to contextualize this analysis with the existing body of CC assessment in inlet systems.

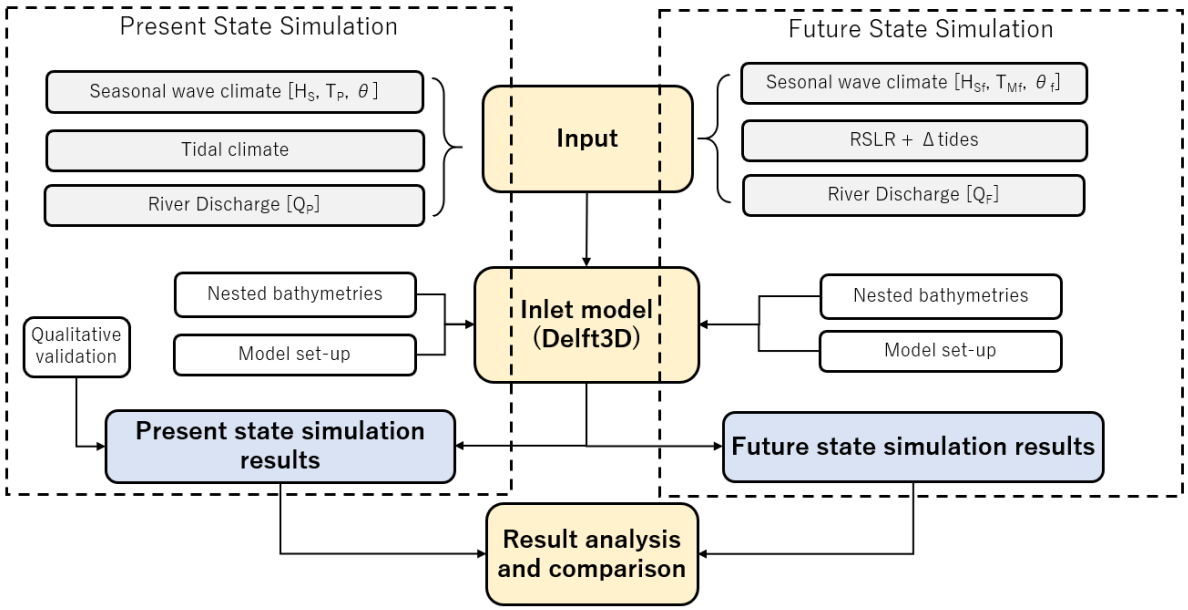

Figure 1.6. Methodology scheme used to analyze the potential CC impacts at both sites. Subscripts 'p' and 'f' refer to 'present' and 'future' situation.

1.5. Thesis Outline

This thesis is divided into seven chapters. Chapter 1 outlines the motivation, the objectives, the research approach, and the thesis relevance. The relevant background information is presented in Chapter 2, where both analyzed sites are described. Then, Chapter 3 describes the methodology followed in both sites, including the data analysis for hindcast and forecast climate, and the process-based model set-ups. Chapter 4 shows the results for Katama Bay, analyzing the present state simulation and comparing it with six future state simulations. Chapter 5 illustrates the result analysis done at Santa Lucia Estuary for both, present state, and future state simulations. The discussion of the results is carried out in Chapter 6, emphasizing the results comparison between both sites and with previous studies. Finally, Chapter 7 outlines the conclusions, recommendations, study limitations and proposed next steps.

CHAPTER 2. LITERATURE REVIEW

CHAPTER SUMMARY

This chapter describes the main aspects of the literature review that are necessary to construct the methodology presented in Chapter 3. First, a description of the analyzed sites (Katama Bay, and Santa Lucia Estuary) is achieved. Then, an analysis of the physics and the mechanisms behind inlet morphodynamics is attained. Finally, the potential CC drivers (sea level rise, variations in wave conditions, variations in tidal conditions, and variation in river discharge) are explained.

2.1. Site descriptions

2.1.1. Katama Bay

Katama Bay, Martha's Vineyard, MA (Figure 2.1) is a shallow bay connected to Vineyard Sound by the narrow, deep Edgartown Channel and episodically connected to the Atlantic Ocean via Katama Inlet. This is a migrating tidal inlet (Figure 2.1) which opens during large storms, migrates east, and within ten years closes upon reaching Chappaquiddick Island (Arpin 1970; Dunlop 2014). When the inlet exists, it turns the Bay into a channel owing to tides flowing between Vineyard Sound and the Atlantic Ocean. When the inlet is closed, the bay becomes stagnant, affecting the water quality in Edgartown Harbor and hence the shellfish farms (J. A. Hopkins 2017). Edgartown Channel is 2 to 10 meters deep, 2500 meters long and 350 meters wide channel (M. Orescanin, Raubenheimer, and Elgar 2014) connected to a basin with shallow flats (~1 meter deep) interrupted by stagnant channels shaped during previous openings.

Multiple openings of the inlet have been recorded during the past two centuries (1776, 1795, 1830, 1846, 1856, 1869, 1871, 1886, 1953, 1976, 1991, and 2007). Moreover, multiple attempts to open the barrier have been attempted (1919, 1921, 1932, 1937) to improve the water quality inside the bay (Dunlop 2014). The last breaching was during the Patriots' Day Storm (April 17, 2007). The combination of a great storm, with a narrow and low barrier, and an exceptionally high tide produced a breach at the Norton Point. The inlet migrated for eight years (2007-2015) (Figure 2.1) with an average velocity of 300-400 meters per year, and finally, it closed at the Wasque Point.

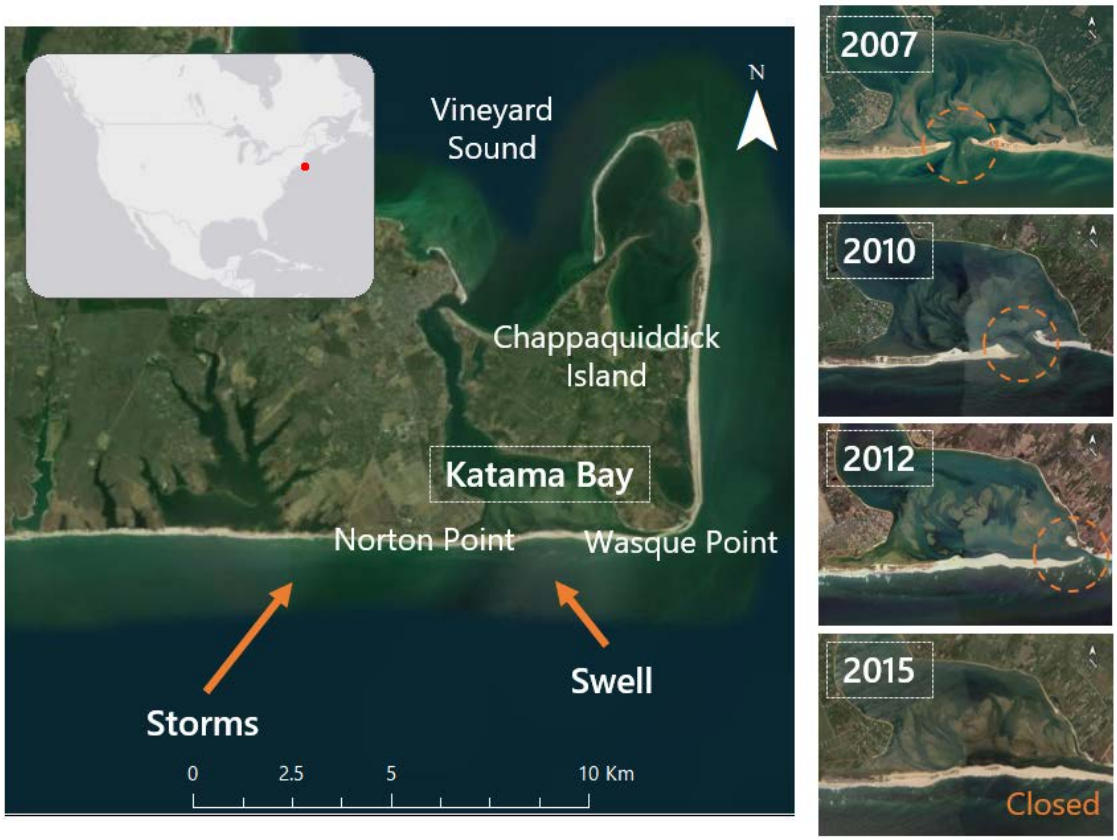

Figure 2.1. Katama Bay main features (left) and inlet migration (right). Orange dashed circles highlight the inlet position over time. Orange arrows show the predominant wave climates. Satellite images from (Google Earth 2018a).

Hydrodynamics

Tides around Martha's Vineyard are profoundly influenced by abrupt changes in bed level and jet formation between the islands (Martha's Vineyard, Nantucket Island, and Naushon Island). Tidal amplitudes (dominated by M2) are asymmetric, resulting in a residual tidal flow that circulates counterclockwise around Martha's Vineyard (Brandon 2006). This anticlockwise rotation leads to a difference in the phases and amplitudes between the south-east corner of the Chappaquiddick Island and Vineyard's Sound. Strong currents (up to 2 m/s) develop at the south-east edge of Chappaquiddick Island, creating a flow separation depending on the curvature of that corner (J. Hopkins, Elgar, and Raubenheimer 2017). When the inlet is open, the difference in tidal conditions among the south of Martha's Vineyard and the Vineyard's Sound induce strong currents (up to 2 m/s) through the inlet.

Katama Bay is located in a storm climate environment with swell presence (Figure 2.1). Storm waves are higher (up to 5-6 meters), with medium periods (around 6-7 seconds) and eastward directed (around 200 degrees North). Swell is characterized to be smaller (less than 4 meters), with higher periods (10-12 seconds), and westward directed (170 degrees North). Wave climate is variant throughout the year, the swell being more persistent during summer than during winter (Figure 2.2).

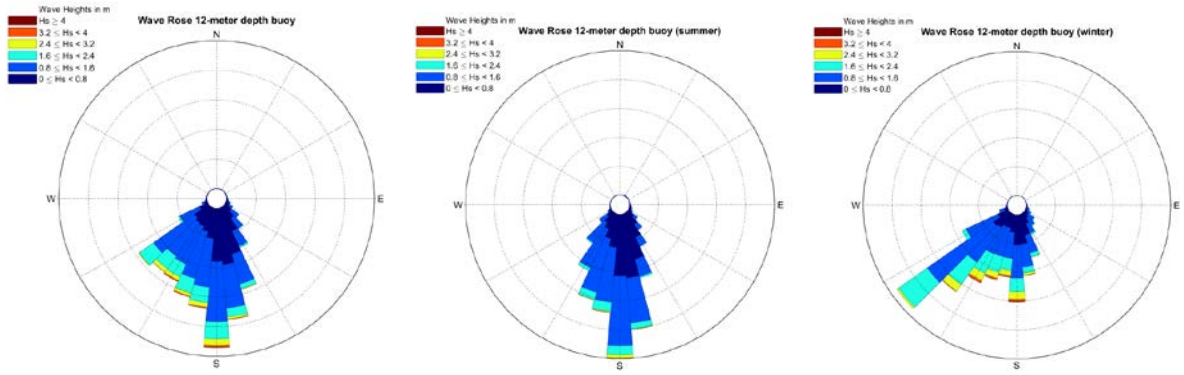

Figure 2.2. Wave rose for a full year (top), summer (July, August, September) (left), and winter (December, January, and February) (right). Data from 12-meter depth buoy MVCO (2006-2017 period).

Morphodynamics

The interaction between waves and currents governs the morphodynamics of the system and shapes the littoral and the nearshore bathymetry. Sediment transport is affected by wave-orbital velocities, breaking wave-driven currents, tidal currents, and inlet inflows (J. A. Hopkins 2017). The inlet presence interrupts the longshore sediment transport, by trapping material inside the basin and into the ebb tidal delta. The system is dynamic and changes hastily. Big shoals in front of the Wasque Point develop owing to strong tidal-driven currents. When the barrier is open, the inlet migrates rapidly (approximately 300 to 400 meters per year), inducing fast changes in the shallow bay by creating new channels and making stagnant the old ones. Strong currents along the inlet are the responsible of the formation of the ebb and flood deltas. The ebb delta migrates with the inlet pushed by waves when the inlet migrates.

During the last breach (2007-2015), the inlet migration was faster for the first couple of years, and the inlet was wider (up to 1 km in 2008). Longshore sediment transport built up the updrift barrier, making

the inlet migrate further, until interaction between currents and waves made the inlet shift (i.e. becomes narrower and larger). Then, the barrier elongated towards the Wasque point, making the beach wider and affecting the transport in that area (Figure 2.1). The orientation of the beach around the Wasque points affects the current separation, and hence affects the sediment transport. When the inlet is open, larger transport is expected around the Wasque Point area (J. Hopkins, Elgar, and Raubenheimer 2017).

2.1.2. Santa Lucia Estuary

Santa Lucia Estuary is the biggest estuary in South Africa (accounting for 60% of South Africa's estuarine area), and it is part of the largest estuarine system of Africa, the Isimangaliso Wetland Park. Furthermore, it is ranked the 5th estuary in South Africa based on conservation importance (i.e., estuaries are scored regarding their size, type, and biogeographical zone) (Turpie et al. 2002). Therefore, it is an essential habitat for birds and important nursery ground for marine fish and prawns along the east coast.

The estuary is connected at the north part of the Santa Lucia Lakes via the Narrows, which is a long (20 km), but very shallow (1 m deep) channel. The estuary is episodically connected on the north to the Indian Ocean by a temporary open inlet. Five main rivers (the Mfolozi, Mzinene, Hluhluwe, Nyalazi, and Mkhuze) provide fresh water and sediments to the whole Isimangalso Wetland. Contrary to the other main rivers, the Mfolozi River (the largest freshwater inflow) discharges directly to the St Lucia estuary.

This system has gone through several changes since 1952 when it was in its natural state. The natural state consisted to a combined mouth for both, the Mfolozi River, and the St Lucia Estuary. The river mouth was opened most of the time (Taylor 1993), being wider during wet periods and tending to close during dry seasons. Decades before (the 1920s), canals were constructed upstream of the Mfolozi River to prevent sugar cane farms to flood. This caused an increase of the velocities through the floodplain of the river, moving the fine sediments towards the estuary (Taylor 1993).

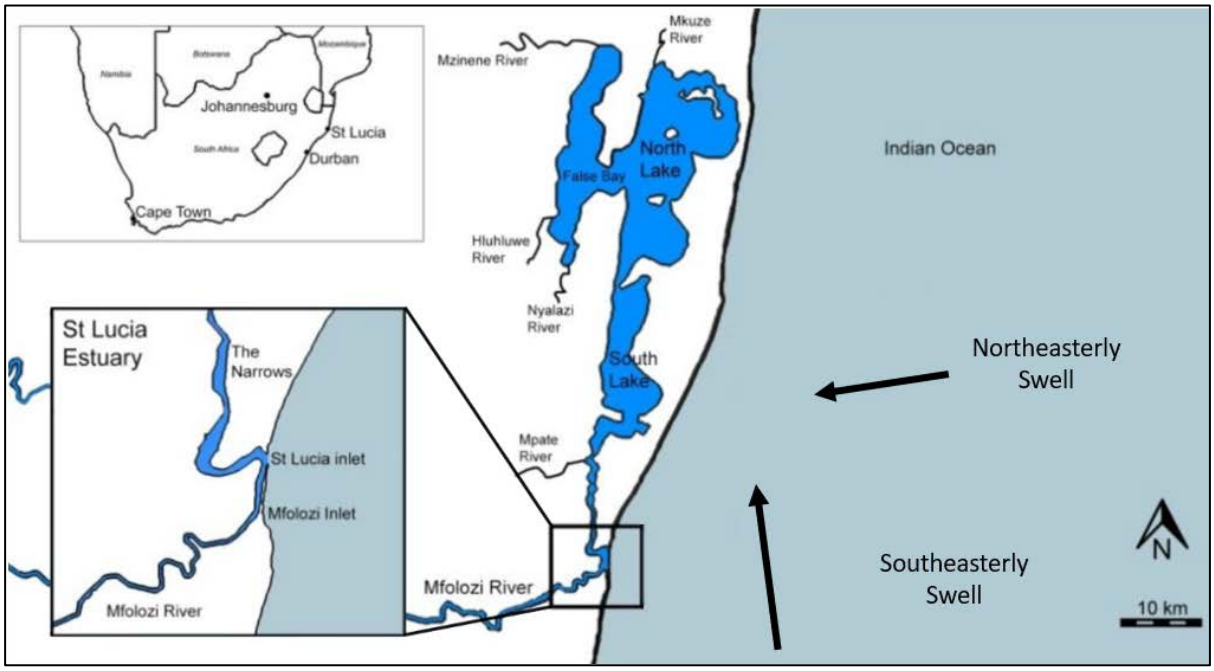

Santa Lucia Estuary main features. Black arrows show the predominant wave climates. Adjusted from (Hoek 2017).

The canal construction, combined with an extreme drought during the 1950s, produced a blockage of the entire mouth, closing the whole system to the Indic Ocean. Consequently, an artificial canal was constructed to discharge river water into the ocean preventing the sugar cane farmlands from flooding by the back-up of Mfolozi River (Kriel 1966). Afterward, the authorities opted to maintain two continuity open mouths (one for the Mfolozi River and a second one for the estuary) for 50 years.

During the drought from 2001 to 2012 the management policy changed (i.e., not to actively manipulate the mouths). The authorities were concerned about the adverse effects on the ecosystem owing to the extreme salinity. The previous management policy adopted during the late 60s drought was disastrous; shoreline vegetation was killed, and endemic species had difficulties to survive (Whitfield and Taylor 2009). By leaving the system to develop naturally, the salinity levels were less alarming. However, the drought was long, and the freshwater volume on the lakes decreased reaching 10% of the normal flooded area on July 2006. After (March 2007), cyclone Gamede breached the barrier, allowing sea water to penetrate to Santa Lucia system increasing the salinity levels significantly. The system was opened to the sea for 175 days (Whitfield and Taylor 2009).

As the drought continued, local authorities decided to create a backchannel connecting the Mfolozi River with the Santa Lucia Estuary. This construction was demonstrated to be effective, diverting Mfolozi winter low-flows (when freshwater contains fewer sediments) into the estuary. After this intervention, the Mfolozi River mouth closed, and salinity levels declined. However, the flow into the lakes was limited, and high salinity levels persisted. The last solution (2016-2017) aimed to bring more fresh water into St Lucia System. The primary idea was to recreate the natural system by dredging 1.2 million cubic meters of dredged spoil in two phases. An early-2016 small removal (100.000 m^3) and a large one (1.1 million m^3) during mid-2017.

The modeling done before the intervention did not contain the effects of waves, tides, currents, cross-shore sediment transport, longshore sediment transport, nor inlet morphodynamics. Hoek (2017) introduce these processes on a Delft3D model showing that the relinkage of the Mfolozi River reduces the closure times of the inlet drastically, but the spoil dredge does have a limited impact. Nevertheless, this study shows that the removal of the dredge spoil changed the behavior of the estuary. The tidal prism increased, making the estuary more flood dominated. The input of sediment from the ocean increased by a factor of 2.7 (from 92,000m^3 to 247,000 m^3).

Hoek (2017) showed that the relinkage (100,000 m^3 removal) of the system was closer to its equilibrium. Also, future management policies can drastically change. Therefore, the analysis of the system excluding the last spoil removal is achieved to study the hydrodynamics and morphodynamics.

Hydrodynamics

Tides in South Africa coast propagates as Kelvin waves from the west to east direction, with an amphidromic point situated in the Southern Ocean (Schumann 2013). At Santa Lucia Estuary, the average tidal range at spring and neap tides are 2.1 m and 0.5 m respectively (Perissinotto, Stretch, and Taylor

2013). Hindcast data from the last 19 years shows a mean tidal range of 1.33 meters (SANHO 2018). Tides produce an exchange of water from the estuary to the Indic Ocean when the inlet is opened. The volume of water that flows in (during flood) or out (during ebb) through the inlet throughout one tidal cycle is defined as the tidal prism. Lawrie and Stretch (2011) did field measurements of the tidal conditions at Santa Lucia Estuary during six months in 2007. The measurements show that the tidal prism fluctuated between ~400,000 m^3 and ~1,600,000 m^3 (Table 2.1), mainly owing to the tidal cycle (e.g., neap, spring, mean) and the mouth conditions.

Santa Lucia Estuary is in a high energetic wave climate. Waves that impact the system can be generated either by cold fronts, tropical cyclones, or cut-off lows (Corbella and Stretch 2012). Cut-off low-pressure systems have the largest impact on the morphodynamics along the beach owing to higher wave heights and wave periods. These are low pressure systems that develop south of South Africa when a preexisting cold trough extends equatorward, stemming from the main westerly trough and leaving a cyclonic closed vortex. Cut off lows are associated with extreme rainfall, and flash flooding, particularly over southern and eastern coastal regions of South Africa (Singleton and Reason 2007). Conversely, tropical cyclones generated in the Mozambique Channel cause north-easterly swells, whereas cold fronts produce smaller waves with southern direction.

A directional GPS buoy and a directional waverider buoy are available at Richards Bay (60 km south of Santa Lucia Estuary). Winter is the most wave energetic season (Figure 2.3) due to the presence of southeasterly waves from the cut off low-pressure systems. During summer the energy extends over a bigger range of directions owing to the existence of northeasterly and southeasterly waves. Therefore, waves are higher and longer during winter (H_S = 1.66 m, and T_P =12.5 s) than in summer (H_S=1.51 m and T_P = 10.2 s). For a full year, the mean significant wave height is 1.6 m, the mean peak period is 11 seconds, and the mean wave direction is 139ºN. Wave Watch III data is available 10 km offshore from Santa Lucia Estuary. Data from the model indicates that the continental shelf may alter Richard's Bay buoy data. Waves from WWIII show a larger wave angle spreading with two picks, one at 100 ºN and another at 190ºN.

Table 2.1. Tidal stages and tidal prisms at Santa Lucia Estuary. Data from (Lawrie and Stretch 2011) summarized by (Chrystal and Stretch 2014). [1]. The ebb volumes are large due to a strong river discharge.

Date	Tidal Stage	Peak flows (m^3/s)		Volume (m^3)		Net volume (m^3)
		Flood	Ebb	Flood	Ebb	
20/04/2007	Spring	131	68	1,600,000	1,333,668	266,332
25/05/2007	Neap	48.7	24.8	851,397	332,996	518,401
28/05/2007	Mid	57.8	24.4	822,890	445,099	377,881
31/05/2007	Spring	63.9	25.6	965,566	454,445	511,121
22/06/2007	Neap	49.7	30.9	495,003	594,964	-99,960
11/07/1972	Spring	187.0	115.0	2,067,179	1,829,419	237,760
12/07/1972	Mid	176.0	100.0	1,887,813	1,586,904	300,909
13/07/1972	Mid	150.0	91.0	1,338,517	1,495,033	-106,516
14/07/1972[1]	Mid	105.0	147.0	1,198,524	2,984,691	-1,786,167

Two major river discharges highly influence the system; the Mfolozi River (discharging to the south of the estuary), and the discharge from the Lakes throughout the Narrows to the north of the estuary. The Mfolozi discharge represents ~60% of the input of fresh water into the system, with a mean annual runoff (MAR) of 940 x10^6 m^3. Nevertheless, significant fluctuations occur during dry (15% of averaged MAR) and wet years (420% of averaged MAR) and within seasons (Bate, Whitfield, and Forbes 2011). During summer (November-March) the river has higher flow with higher content of sediment (2.49 kg/m^3), whereas, during winter (June – August), when the runoff is small, the sediment content decreases until 0.078kg/m^3. On the other hand, the annual river discharge into the Lakes (five rivers) is 362x10^6 m^3. However, the annual balance is altered by the evaporation (-420x10^6 m^3), the rainfall (243x10^6 m^3), and the ground flow (23x10^6 m^3) (Whitfield and Taylor 2009), leading to an averaged discharge of 208x10^6 m^3 into the Santa Lucia Estuary.

Four different states are distinguished in this system depending on the condition of the mouth (open or closed), and the discharges of the Lakes and the Mfolozi River. If the mouth is closed and the water levels on the Mfolozi River are higher than in the lakes, water flows from the river via the Narrows. When Mfolozi River and the lakes have similar water levels, water floods the adjacent land until the inlet breaches. If the mouth is open and the water levels are higher in the river than in the lakes, the river discharge is divided into two fractions; one into the sea and another into the lakes. Finally, if the mouth is open and the water levels in the lakes and Mfolozi River are similar, all the discharge goes to the Indian Ocean.

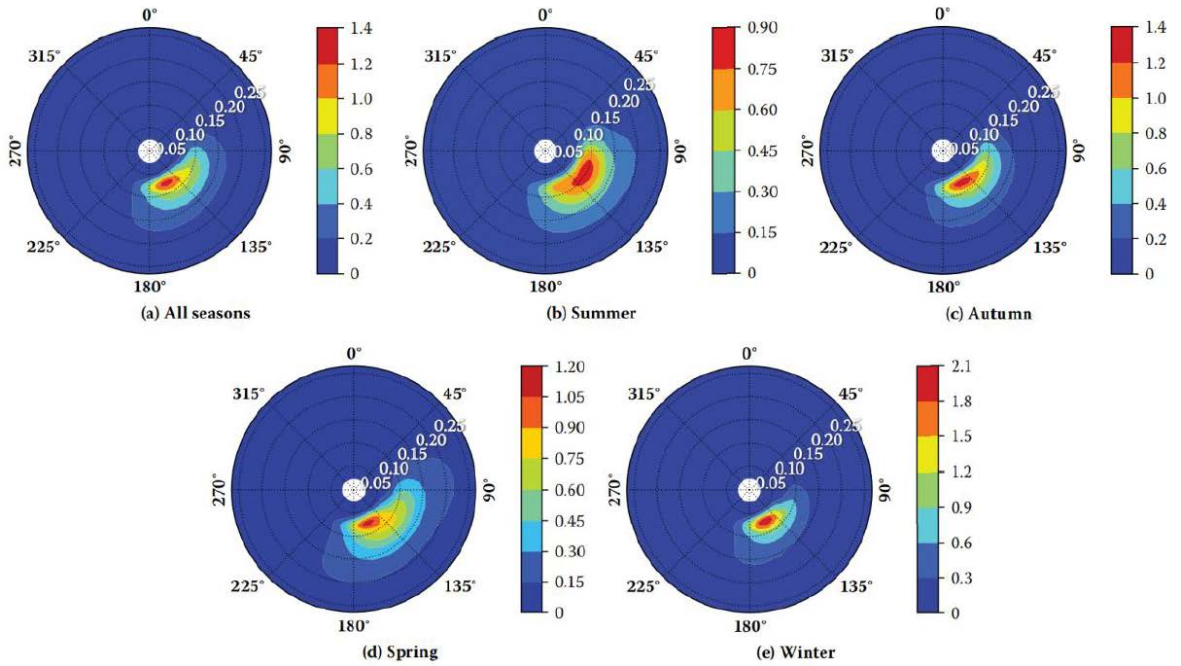

Figure 2.3. Richards Bay's averaged seasonal wave climate for (a) All seasons, (b) summer, (c) autumn, (d) spring and (e) winter, (from Corbella & Stretch 2014).

Morphodynamics

In a high energetic wave climate, it is expected to have a sizeable longshore transport. Waves are high (annually averaged H_S = 1.6 m) and with a high incidence angle (10-20 degrees). The sediment (sand

with a grain diameter of 0.1-0.3 mm (C. I. Wright and Mason 1990)) is carried through a beach with an average slope of 1/100. Longshore transport rates were calcualted in Richards Bay by Schoonees (2000). The measured sediment transport rates were obtained calibrating the Kamphuis (1991) formula using volumetric differences, hydrographic surveys, and wave recordings by means of a Waverider and a clinometer. Results show a mean longshore annual rate of 850,000 m^3 with a large variation of the transport over the years (from 21.2 $x10^5$ m^3 in 1983 to -4.2$x10^5$ m^3 in 1986).

Figure 2.4 shows the evolution of the Santa Lucia Estuary from 1990 until 2017. The Santa Lucia inlet is locationally stable and seasonally open owing to big storms (e.g., cyclone Gamede in 2007). Santa Lucia Inlet is maintained mainly due to tidal flow, and it closes owing to high longshore sediment transport rates. When two mouths were present (first row of images on Figure 2.4), the Mfolozi mouth migrated around 300 to 400 meters per year in a northern direction, discharging large quantities of sediment on the sea that were carried out in northern direction. Now, with the re-linkage of the Mfolozi River with the Santa Lucia Estuary (2016 and 2017 images on Figure 2.4), it is expected that one inlet (located in the North) opens more frequently owing to the river discharge.

Figure 2.4. Santa Lucia Estuary evolution from 1990 to 2017. Satellite images from (Google Earth 2018b).

2.2. Tidal Inlet Theory

2.2.1. Inlet classification

Tidal inlets are systems maintained by tidal flow that connect bays, lagoons, or estuaries to the open sea. These systems are mainly formed by two barrier islands, an ebb-tidal delta, a tidal flood delta, and tidal channels (see Appendix **¡Error! No se encuentra el origen de la referencia.** for a detailed explanation). Each of these features is shaped by tides, waves, and river discharges. Therefore, the ratio among these three describes the morphology of the inlets and basins.

The tidal environment can be classified depending on its tidal character (e.g., diurnal, semidiurnal, or mixed), or depending on its magnitude (micro-tidal regime, meso-tidal regime, or macro-tidal regime). Tidal regime depends primarily on the ocean tide propagation and their interaction with the continental

shelf (i.e., friction and resonance). Systems with macro-tidal regimes are characterized to have developed deltas, whereas systems with micro-tidal regimes are more vulnerable to the effects of waves.

Similarly, wave climates can be classified regarding their energy (low wave energy (H_S<0.6 m), medium wave energy (0.6 m<H_S<1.5 m), or high wave energy ((H_S>1.5 m)), or regarding their wave steepness (swell waves or storm waves).

M.O. Hayes (1979) and Richard A. Davis and Hayes (1984) distinguish five regimes combining the wave energy classification and the tidal range regimes (Figure 2.5). Katama Bay and Santa Lucia Estuary are wave-dominant sites. Therefore, it is expected that these systems are going to be influenced by waves (e.g., ebb tidal deltas would not be fully developed, and waves will penetrate the basin, affecting their features).

River discharge plays a vital role on shaping the coast. Systems with a high fluvial power (i.e., significant river discharge) resemble progressive coasts, whereas systems with insufficient river sediment supply are characterized to be transgressive coasts. The sufficiency or insufficiency of sediment supply is dictated by the balance between the hydrodynamic forcings (e.g. river power, tide power, and wave power). Galloway (1975) proposed a triangular classification for deltas regarding the relative influence of waves, tides, and sediment input. Figure 2.6 illustrates different examples of tidal, wave, river, and mixed dominated deltas. The amount of material accumulated in the delta depends on the forcing roles. For instance, deltas with high wave energy flux have a smooth shoreline with developed beaches and dunes, while deltas with big tides feature like estuaries (Boyd, Dalrymple, and Zaitlin 1992). Santa Lucia estuary is a mixed system, with a smooth shoreline but with enough tidal power to resemble an estuary.

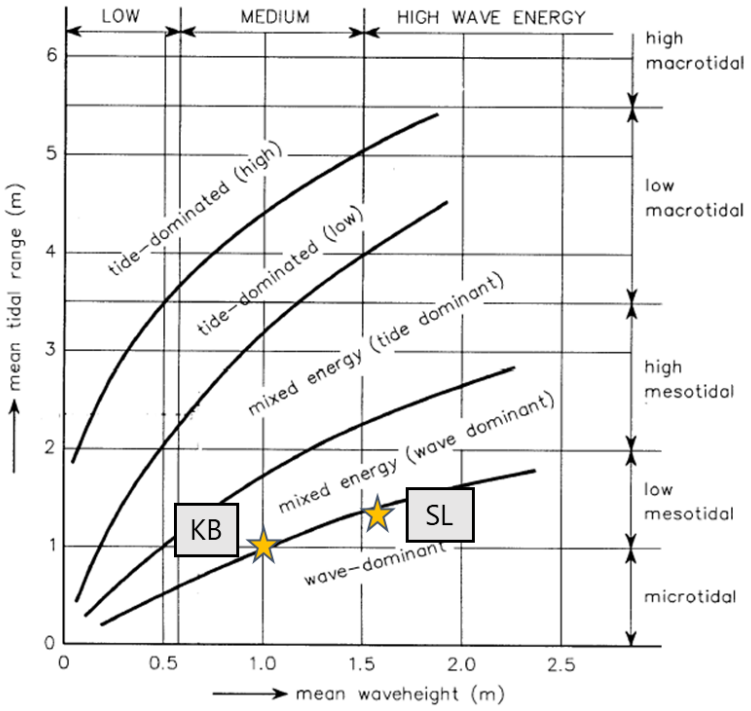

Figure 2.5. Hydrodynamical classification of tidal inlets regarding its tidal regime and its wave climate energy classification. The figure included the classification for Katama Bay (KB) and Santa Lucia Estuary (SL). Adjusted from (M.O. Hayes 1979).

Table 2.2. Inlet hydrodynamic conditions (tidal range, mean significant wave height, and river discharge).

	Mean Tidal Range [m]	Mean H_S [m]	Mean River Discharge [m^3/s]
Katama	1	1	-
St Lucía	1.2	1.6	30

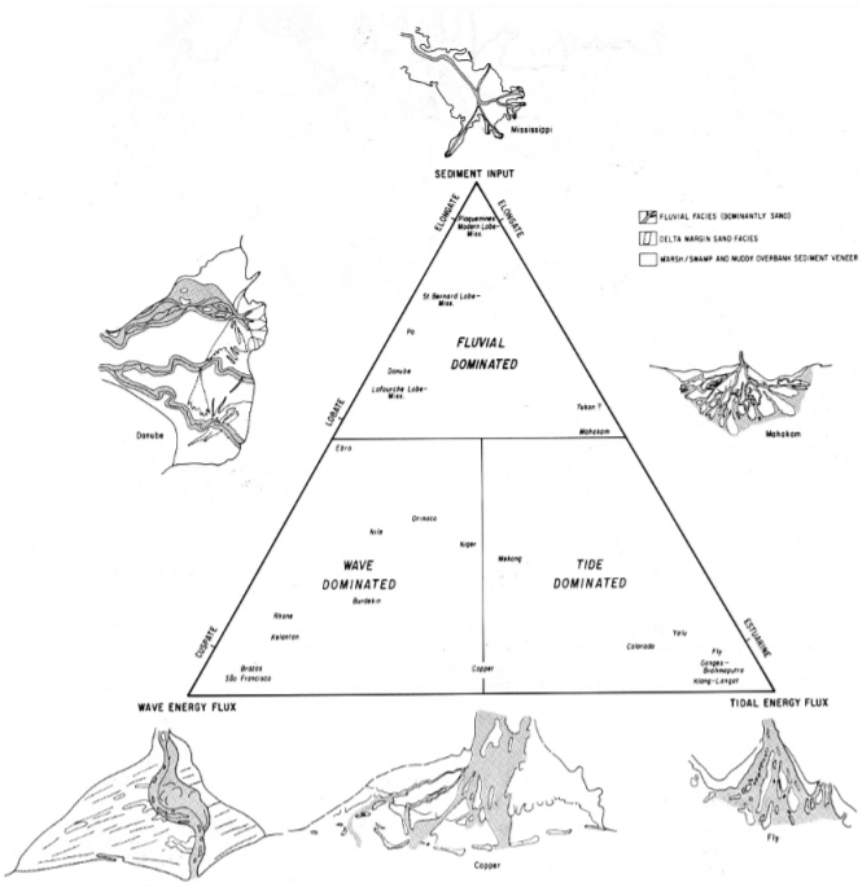

Figure 2.6. Delta classification diagram. The deltas are divided into fluvial- or river-dominated, wave-dominated, and tide-dominated types. From (Galloway 1975).

2.2.2. Inlet Stability

Inlet stability is governed by the flow through the inlet and the nearshore sediment transport around the inlet. Therefore, inlet stablity depends on the balance between tides, waves, and river discharge, that can potentially be affected by CC. An inlet can be either cross-sectionally stable or locationally. The first refers to inlets that preserve the same cross-section over time, whereas the second applies to inlets that remain in the same position over time. Duong et al. 2016 characterized small tidal inlets into three main categories on their morphodynamic behavior:

- Permanently open, locationally stable inlets (Type 1).
- Permanently open, alongshore migrating inlets (Type 2).
- Seasonally open, locationally stable inlets (Type 3).

Locationally stable inlets, can either be cross-sectionally stable (Type 1) or be cross-sectionally unstable (Type 3). The closure of the inlet may be owing to a strong longshore sediment transport (oblique wave-dominated environments) or due to onshore bar transport (on swash dominated coasts). Permanently

open, alongshore migrating inlets (Type 2) phenomenon is conceptually described in Figure 2.7 (R.A. Davis and FitzGerald 2009). Littoral drift induced by longshore currents leads to accumulation of sediments at the updrift side of the inlet. The flow velocities through the inlet increases owing to a reduction of the channel section. Then, tidal currents erode the downdrift side of the inlet, causing the migration of it (most of the time in the prevailing littoral drift direction). The migration rate depends on the longshore sediment transport, ebb tidal current velocity, river flow, and composition of the channel banks. At a particular moment, extreme river flow and severe storms may breach the updrift sand spit stopping the elongation of the channel. This new inlet will provide a more efficient tidal exchange, making the old channel close gradually.

The evolution of Santa Lucia Estuary from December 1984 until December 2016 is illustrated in Figure 2.4. Santa Lucia is seasonally open and remains in the same location (Type 3). Nevertheless, the mouth of the Mfolozi River migrates approximately 300 to 400 meters per year in northern direction (equally as the predominant littoral drift) and hence can be classified as Type 2. On the other hand, Katama Bay is a seasonally open inlet (decadal cycle), that migrates and changes in cross-shore dimensions (i.e., cross-sectionally unstable). While the inlet is open, it can be classified as Type 2, that stops migrating owing to be at the edge of the Martha's Vineyard island. The migration of Katama Inlet can be found in Figure 2.1.

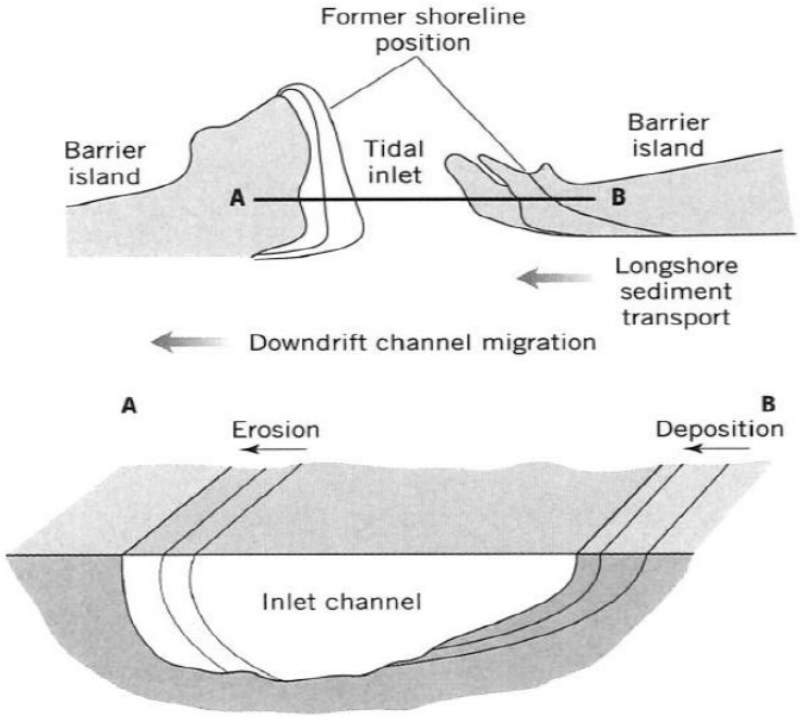

Figure 2.7. A conceptual model of inlet migration (from R.A. Davis and FitzGerald 2009).

Empirical relationships to assess inlet stability

The inlet condition governs the dynamics of the estuary/lagoon/bay connected to it. Therefore, inlet stability is a crucial indicator for investigating the potential impacts of CC. The processes involving stability are complicated, and a simplified results analysis can improve the understanding of it. Simple empirical relationships provide a practical framework for this analysis.

There are two extended used empirical methods to predict the cross-sectional stability, the Escoffier closure diagram (Escoffier 1940), and the relationship between the tidal prism and the inlet minimum cross-section (O'Brien and Dean 1972). The Escoffier diagram (Figure 2.8) shows the maximum flow velocity at the inlet against the cross-sectional area. According to this diagram, inlets that have a cross-sectional area larger than the critical flow area (point A in Figure 2.8) are stable. In this case, if the velocity is larger than the critical one, the inlet would be scouring (until reach point B), whereas if the velocity smaller than the critical one, shoals will appear. On the other hand, inlets that have a smaller area than the critical, will tend to close.

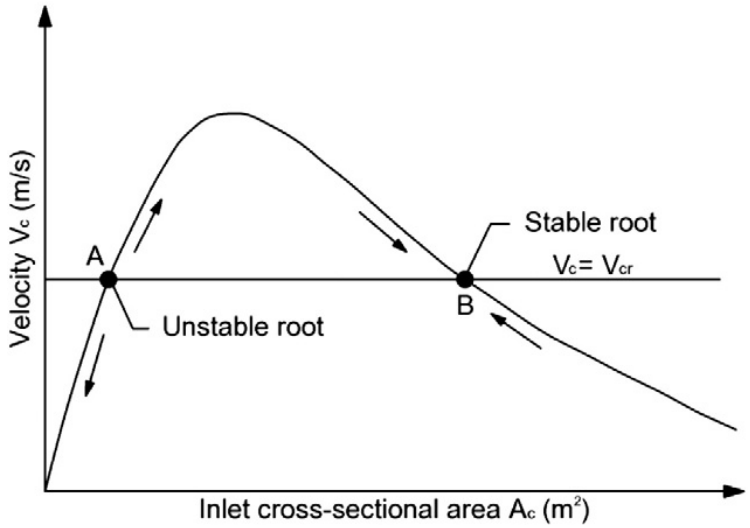

Figure 2.8. Escoffier closure diagram (after Escoffier 1940).

Moreover, Bruun et al. (1978) defined a parameter (Bruun Criterion) that involves both (locational and cross-sectional) stability (see Equation [1]). Then, Duong et al. 2016 related the Bruun criterion with the previous inlet classification (Table 2.3).

$$r = \frac{P}{M_{tot}} \qquad [1]$$

where:

M_{tot}	total annual littoral transport in the surrounds of the inlet (m^3/year).
P	Tidal prism (m^3/cycle).

Table 2.3. Classification scheme for small inlet Type and stability conditions (from Duong et al. 2016 and Duong et al. 2017).

Inlet Type	$r = \frac{P}{M_{tot}}$	Bruun Classification	Inlet condition
Type 1	> 150	Good	These inlets are typically tide-dominated and reasonably stable.
	100 - 150	Fair	A mix of bar-by-passing and flow-by-passing
	50 - 100	Fair to Poor	Inlet is mainly bar-by-passing and unstable
	20 - 50	Poor	Inlet becomes unstable with non-permanent overflow channels
Type 2	10 - 20	Unstable	Open and migrating
Type 2/3	5 - 10	Unstable	Migrating or intermittently closing
Type 3	0 - 5	Unstable	Intermittently closing

2.2.3. Mass Balance of a Migrating Inlet

To quantify inlet migration Nienhuis & Ashton (2016) proposed a mass balance framework of sediment fluxes. Two sources of material were suggested as a supply for the migrating inlet; the littoral sediment from the updrift surf zone, and the eroded barrier from the retreating downdrift barrier.

For an inlet with a cross section A_b (m^2) and a littoral drift (Q_S in Figure 2.9), three fractions can be considered around the tidal inlet:

(1) A bypassing fraction (β) that accounts for the littoral sediment that bypasses the tidal flood delta.
(2) A flood tidal delta fraction (δ) that describes the sediment that ends up in the flood tidal delta.
(3) A barrier fraction (α) of material deposited in the updrift of the inlet as part of the barrier.

Sediment eroded from the downdrift barrier can end up either to the updrift of the inlet as part of the barrier (β_d), to the flood tidal delta (δ_d), or continue downdrift as part of the littoral sediment transport (α_d) (Figure 2.9). Sediment eroded from the retreating downdrift barrier can be deposited either in the flood delta ($Q_S \cdot \delta_d$), as part of the updrift barrier ($Q_S \cdot \alpha_d$), or continue moving downdrift (Nienhuis and Ashton 2016).

This study considers that the ebb delta remains constant during the inlet migration. Therefore, the rate of updrift migration of the channel can be described as shown in Equation [2], whereas the rate of downdrift migration can be defined as shown in Equation [3].

$$V_u = \frac{Q_s \times (\alpha + \alpha_d)}{A_b} \quad [2]$$

$$V_d = \frac{Q_s \times (\alpha_d + \beta_d + \delta_d)}{A_b} \quad [3]$$

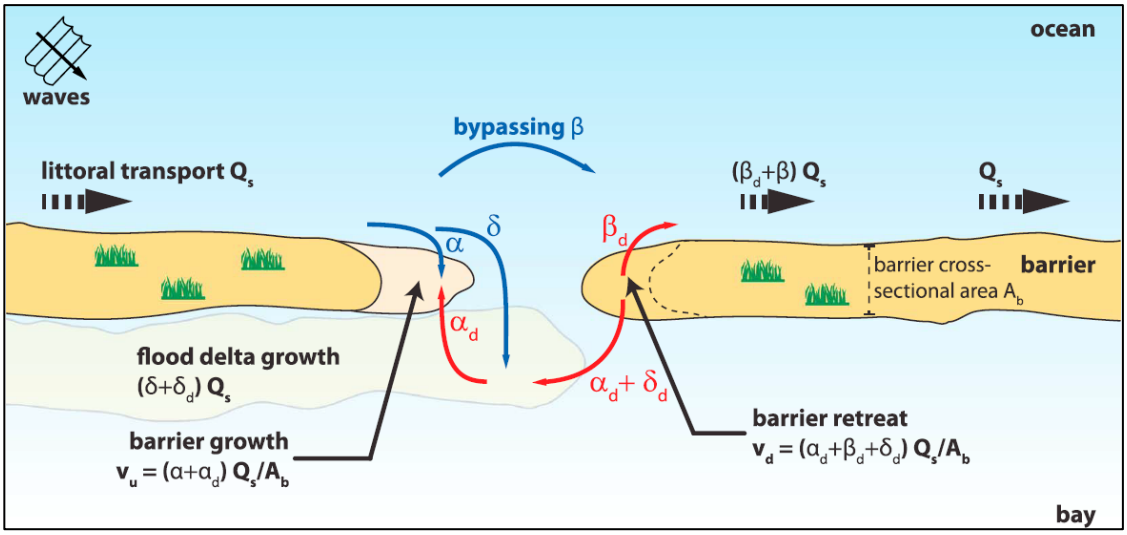

Figure 2.9. Mass balance framework of a migrating tidal inlet. All sediment fluxes (α, β, δ, α_d, β_d, and δ_d) are normalized by the littoral drift Q_S to quantify the changes in the distinct features (flood delta growth, up barrier growth and downdrift barrier retreat). Blue arrows represent circulation of sediment from outside the inlet system, whereas red arrows represent circulation of sediment within the inlet system. (from Nienhuis & Ashton 2016)

2.3. Potential CC drivers

2.3.1. Sea level rise and relative level rise

The Fifth Assessment Report (AR5) of Intergovernmental Panel on Climate Change (IPCC) projects that global mean sea level will rise with an accelerated trend during the 21st Century. This is owing to thermal expansion of seawater due to ocean warming, and water mass input from land ice melt and land water reservoirs (IPCC 2014b). The AR5 suggests four different Representative Concentration Pathways (RCP) scenarios (RCP2.6, RCP4.5, RCP6.0, and RCP8.5) which provide a quantitative description of CC pollutant concentrations in the atmosphere over time (van Vuuren et al. 2011). The projected global SLR for 2081-2100 (relative to 1986-2005) is from 0.17 to 0.38 meters in the mid-century and from 0.26 to 0.82 meters in the late century (Table 2.4).

In addition to global SLR (Figure 2.10), relative sea-level change for a specific site relies on regional contributions, such as meteo-oceanographic factors (e.g., ocean circulation, regionally distinct rates in changes of ocean density), changes in the regional gravity of the earth (i.e., the farther away the area is from the ice melting, the higher the SLR) and vertical land movement (e.g. subsidence due gas/water extraction) (Robert J. Nicholls et al. 2014). In the AR5 an ensemble projection of SLR is presented for mean regional sea level change (Figure 2.11) which includes meteo-oceanographic factors, glacial isostatic adjustment, and terrestrial water sources for the four scenarios (RCP2.6, RCP4.5, RCP6.0, and RCP8.5). Locally land subsidence should be added to regional sea level change to obtain the relative sea level rise for each site (Figure 2.12).

Table 2.4. Projected global mean sea level rise during the 21st Century, relative to the 1986-2005 period (IPCC 2014b). The likely ranges are calculated from projections as 5 to 95% model ranges.

Scenario	2046-2065		2081-2100	
	Mean	Likely range	Mean	Likely range
RCP2.6	0.24	0.17 to 0.32	0.40	0.26 to 0.55
RCP4.5	0.26	0.19 to 0.33	0.47	0.32 to 0.63
RCP6.0	0.25	0.18 to 0.32	0.48	0.33 to 0.63
RCP8.5	0.3	0.22 to 0.38	0.63	0.45 to 0.82

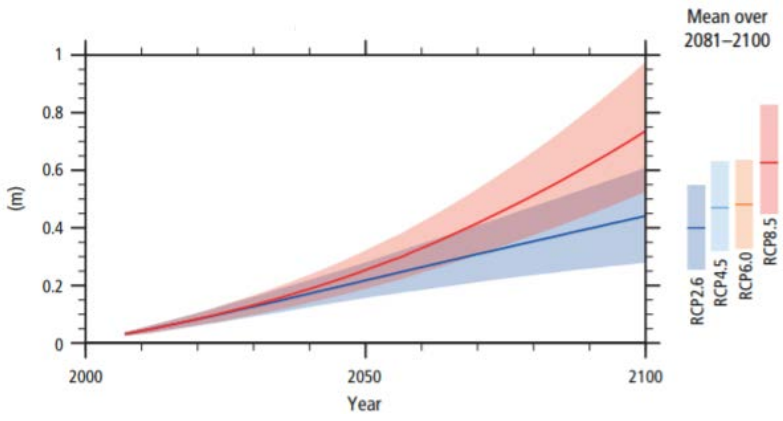

Figure 2.10. Global mean sea level rise, relative to 1986-2005. The shaded bands show the likely ranges for scenarios RCP2.6 (blue) and RCP8.5 (red). The colored vertical bars represent the mean and associated uncertainties for all the scenarios (from IPCC 2014b).

Table 2.5 summarizes the projected regional SLR at both sites for an RCP4.5 scenario showing the mean, the maximum and the minimum value based on a 95% confidence interval. Both sites present similar mean values (~0.5 meters), but there is more confidence in Santa Lucia than in Katama Bay. For the present analysis, an intermediate scenario is chosen owing to the uncertainty of the effects of CC on the different systems.

Table 2.5. Projected regional mean, maximum and minimum SLR for an RCP4.5 scenario.

	Regional SLR	Max RSLR (95% interval)	Min RSLR (95% interval)
Katama Bay	0.53	0.85	0.21
Santa Lucia Estuary	0.54	0.78	0.32

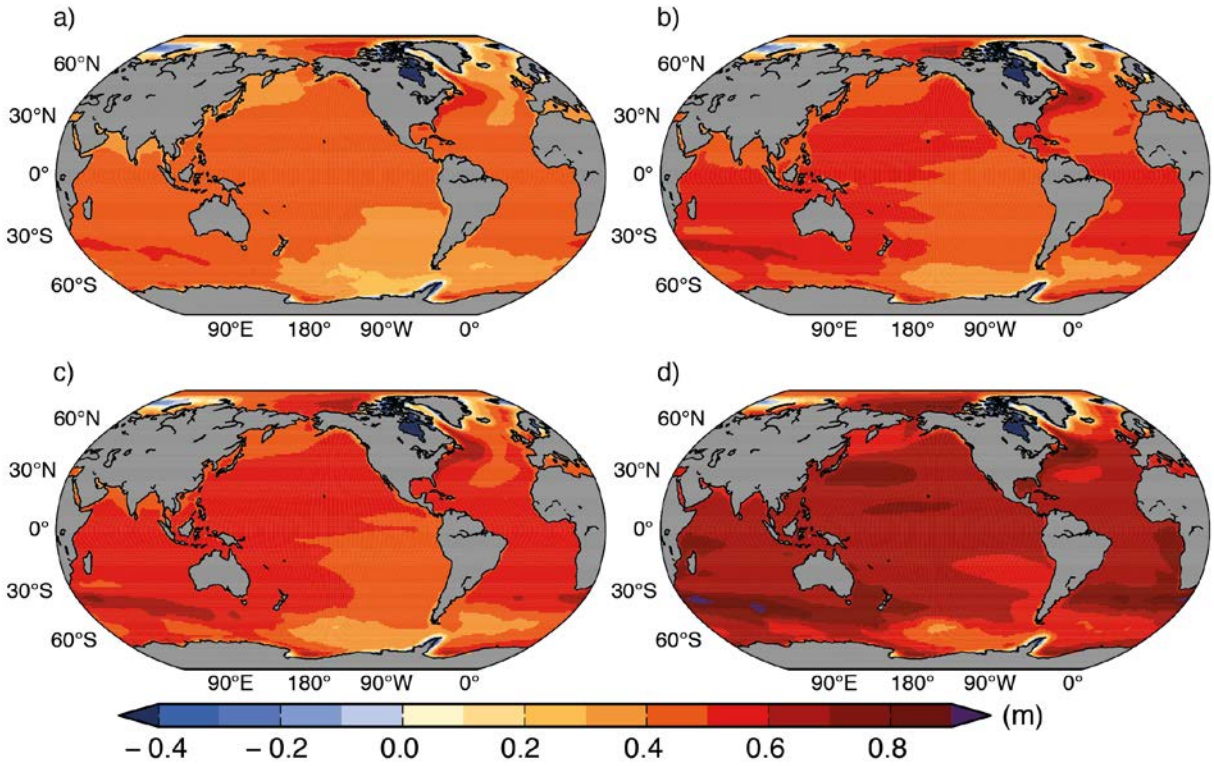

Figure 2.11. Ensemble mean regional relative sea level change (meters) evaluated from 21 Coupled Model Intercomparison Project Phase 5 (CMIP5) models for the RCP scenarios (a) 2.6, (b) 4.5, (c) 6.0 and (d) 8.5 between 1986–2005 and 2081–2100. Each map includes effects of atmospheric loading, plus land ice, glacial isostatic adjustment (GIA) and terrestrial water sources (Church et al. 2013).

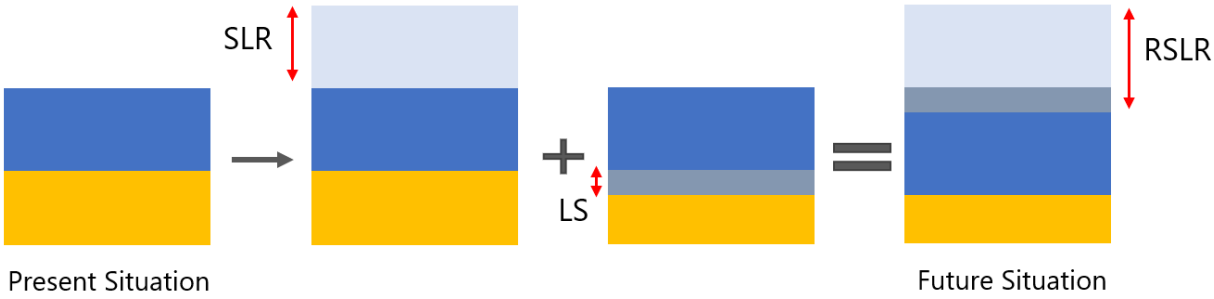

Figure 2.12. Schematic illustration of relative sea level rise example. SLR (sea level rise including regional contributions, LS (land subsidence), RSLR (relative sea level rise).

2.3.2. Tidal amplitudes and phases

Changes on tidal amplitudes and phases of tidal harmonics may alter the hydrodynamics and the morphodynamics of the inlet systems around the world. SLR in the open oceans (Müller, Arbic, and Mitrovica 2011), and changes in radiative forcing (Ray 2009) have been suggested as possible contributors.

Pickering et al. (2017) investigated the effect of future SLR on the tides globally using a global tidal model. They showed that changes in the semidiurnal constituents (M2 and S2) occur globally in most shelf seas, whereas changes in the diurnal constituents (K1 and O1) are confined to Asian shelves. Nevertheless, the regionality effects (e.g., bottom friction, resonance) have a substantial impact on the results (see Figure 2.13). Areas with large tidal amplification (e.g., the North Sea, the northern North-America Coast, the Yellow Sea) suggest the most prominent changes, being them fluctuating. Therefore, regional analysis (if available) become a preferred approach to predict the potential changes on tidal harmonics.

Müller et al. (2011) analyzed sea level data in the North Atlantic and found long-term trends in the amplitude and phase of individual tidal harmonics. The principal solar semidiurnal (S2) tide shows the largest amplitude trends (a decrease of 1.2% per decade). M2 shows an average increase of 0.3% per decade, and the diurnal components (K1 and O1) a decrease of 0.4% per decade and an increase of 0.3% per decade respectively.

Moreover, they studied these changes in some specific locations along the USA East Coast. One of the studied sites was Newport (USA), which is located 50 km West from Katama Bay. Here, the S2 amplitude is decreasing by 1.48% per decade, and its phase is changing 0.29ºN per decade anticlockwise directed. The M2 amplitude is decreasing by 0.22% per decade, and its phase is changing 0.15ºN per decade anticlockwise directed. Diurnal changes do not show a good correlation, therefore there not considered in the present analysis. Additionally, Müller et al. (2011) showed that the sum of all the amplitude trends (diurnal and semidiurnal) in Newport is between 5-10% of the mean sea level trend.

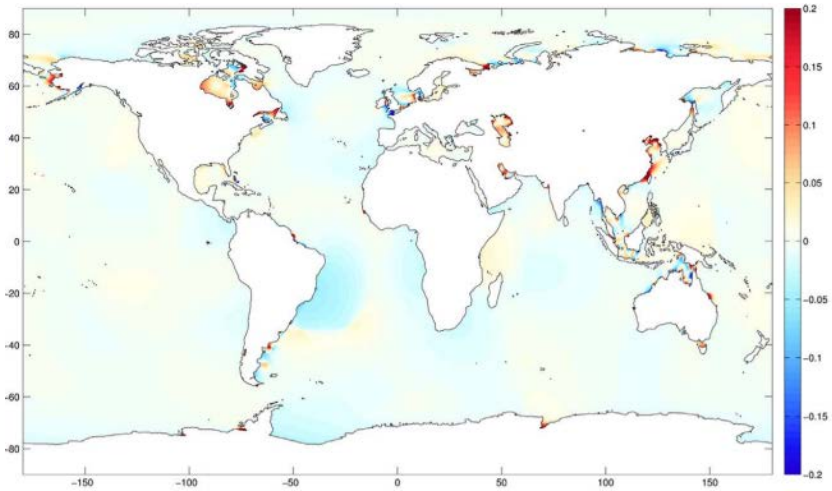

Figure 2.13. Change in amplitude (m) of M2 (left) with 2 m of uniform SLR assuming a fixed present-day coastline (from Pickering et al. 2017)

2.3.3. CC driven variations in wave conditions

CC is expected to affect the global mean and extreme wave conditions (Young et al. 2011; Mori et al. 2013; Hemer et al. 2013; Camus et al. 2014; Perez et al. 2015; Shope et al. 2016; Camus et al. 2017; and many others). A dynamical or statistical downscaling approach is often used to obtain wave climate changes due to CC. Dynamical downscaling (DD) approaches are better for reproducing the climate response to climate projected surface winds, but they need high computational time. Statistical downscaling (SD) approaches need lower computational time, and hence they can use many Global Climate Models (GCMs) providing a more robust multi-model projection ensemble (Camus et al. 2017).

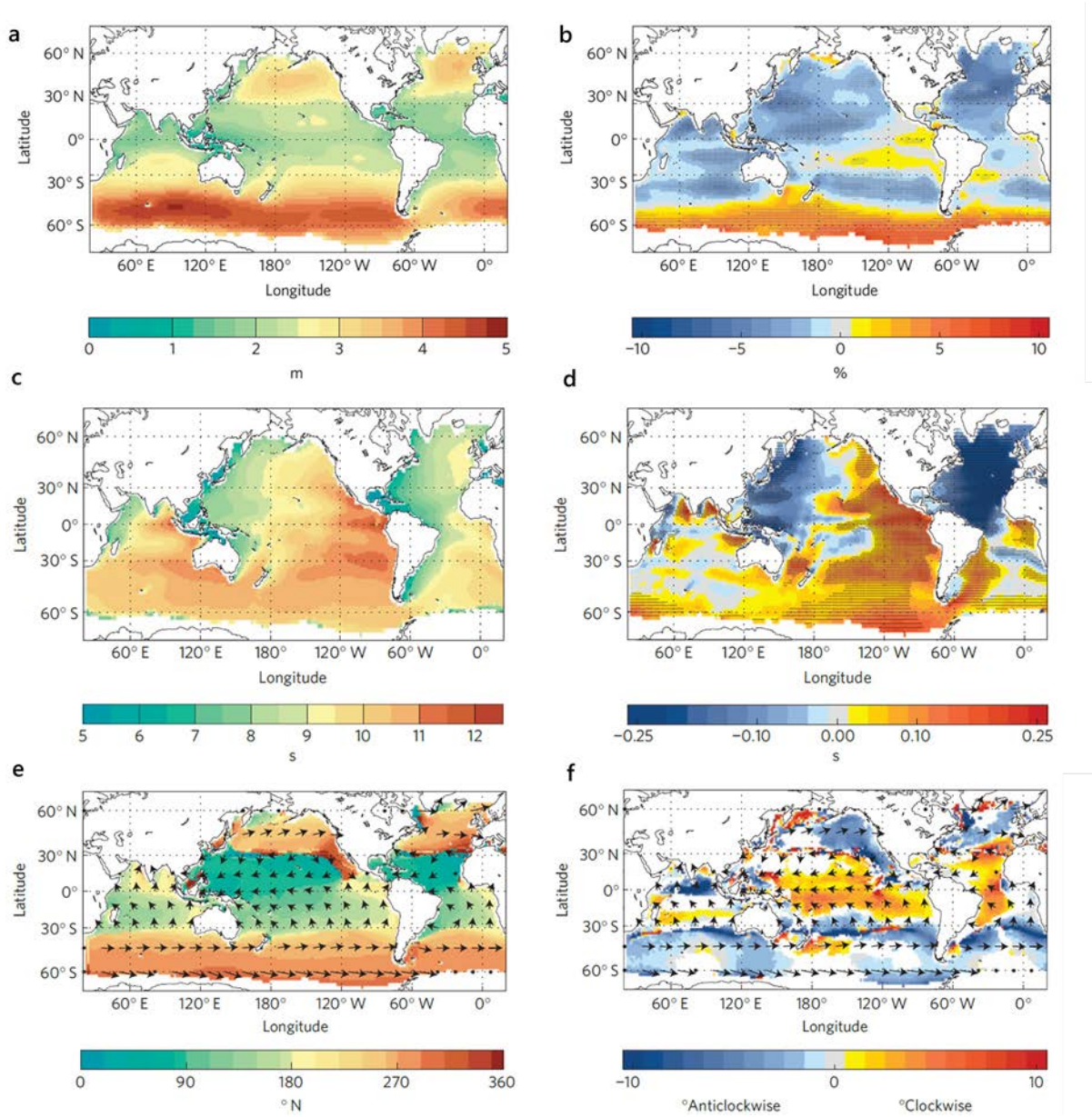

Figure 2.14. Projected future change in DD multi-model averaged wave conditions. (a) annual mean significant wave height H_s for the present climate (~1979-2009). (b) projected changes in annual mean H_s for the future climate (~2070-2100) relative to the present climate (~1979-2009) (% change). (c) annual mean wave period T_M for the present climate (~1979-2009). (d) projected changes in annual mean T_M for the future climate (~2070-2100) relative to the present climate (~1979-2009) (absolute change (s)). (e) annual mean wave direction θ_M (degrees clockwise from the North) for the present climate (~1979-2009). (f) projected changes in wave direction θ_M for the future climate (~2070-2100) relative to the present climate (~1979-2009) (absolute change, degrees clockwise) (from Hemer et al. 2013).

Dynamical projections are generated using surface wind from GCMs or Regional Climate Models (RCMs) to force spectral wind-wave models. Hemer et al. (2013) make a comparison of five independent model studies (four of them DD projections) to determine the level of agreement between the model projections of wave climate. They found that the models agree about a decrease in annual significant wave height (H_S) over the 25.8% of the global areas, which will be greater during boreal winter than austral winter.

Likewise, Hemer et al. (2013) predict an increase of the H_S over 7.1% of the ocean area, predominantly in the Southern Ocean, which could cause more swell waves propagating northward. This leads to an increase in the annual wave period in 30.2% of the area throughout the globe. Additionally, an anticlockwise rotation of mean wave direction is suggested in the westerly regions, whereas a clockwise rotation is predicted around the equatorial belt (Figure 2.14).

SD approach stands in the idea to perform a regression between hindcast atmospheric data (e.g., sea level pressure) and hindcast wave data. Here, the global wave projections are estimated from the future probability of weather types and the statistics calculated for each grid point (Camus et al. 2014). Therefore, other than DD approaches, SD approaches do not provide a time series as results.

Perez et al. 2015 presented an SD approach for regional wave climate projection in the European region for three different scenarios (RCP2.6, RCP4.5, and RCP8.5). As shown in previous studies of global wave climate projections (e.g., Hemer et al. 2013), they estimate a general decrease in wave heights and period in the European Atlantic Ocean for the late 21st Century. Later, Camus et al. (2017) extended the same study to a global scale, which we use for the projected wave climates at both sites.

2.3.4. CC driven variations in river-flow

Variations in precipitation and temperature due to CC may lead to changes in runoff and availability of water (Duong et al. 2016). IPPC AR5 global projections for all four RCPs shown that the runoff consistently decreases in southern Europe, the Middle East, and the southwestern USA (Figure 2.15), and increases in Southeast Asia, tropical East Africa, and high northern latitudes by the end of the 21st Century (Collins et al. 2013).

Hulme et al. (2001) calculated the change of the rainfall over Africa during the 20th century, showing that the precipitation decreased by approximately 10% along the catchment basin of the Mfolozi River. Moreover, they projected the changes of the rainfall for 2080's for an SRES A2 scenario, obtaining a decrease from 10-20% for the same catchment area.

Similarly, the IPPC AR5 projects a decrease in the precipitation of approximately 5-10% for an RCP2.6 scenario and of 10-20% for an RCP8.5 scenario (Niang et al. 2014). The evaporation is expected to be stronger by the end of the 21st century in the area of interest. Nohara et al. (2006) projected a decrease of the evaporation of 0.2 mm/day for an SRES1B scenario, becoming in a decrease of 10-20% on the mean river discharge by the end of the 21st Century.

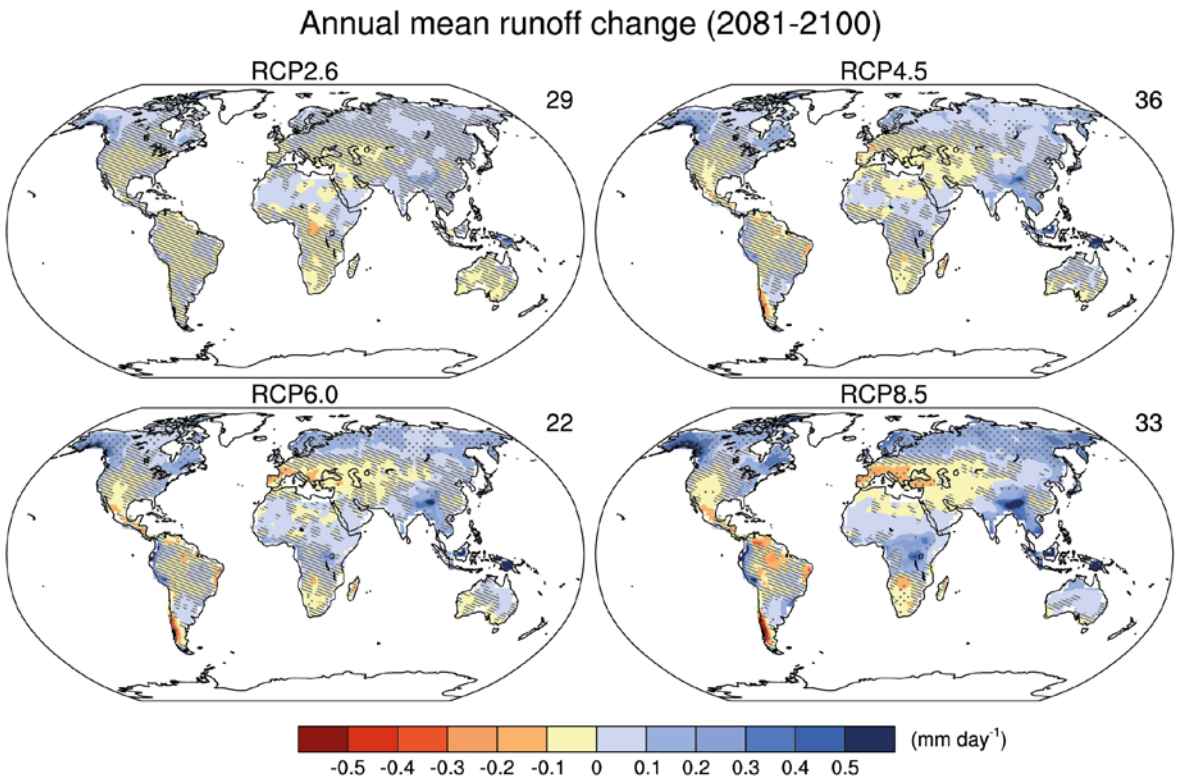

Figure 2.15. Change in annual mean runoff relative to the reference period 1986–2005 projected for 2081–2100 from the CMIP5 ensemble. Hatching indicates regions where the multi-model mean change is less than one standard deviation of internal variability. Stippling indicates regions where the multi-model mean change is greater than two standard deviations of internal variability and where at least 90% of models agree on the sign of change (see Box 12.1). The number of CMIP5 models used is indicated in the upper right corner of each panel (Collins et al. 2013).

CHAPTER 3. METHODOLOGY

CHAPTER SUMMARY

This chapter explains the methodology applied to analyze the CC impact on Katama Bay and Santa Lucia Estuary. First, we introduce the wave data analysis used to derive wave boundary conditions for the present and future state simulations. Then, we discuss the process-based modeling with Delft3D, examining the assumptions, key model parameters and the general model set up at each site. Hydrodynamics and morphodynamics validations are also discussed at both sites. Finally, we review the techniques used to analyze the results.

The current thesis is divided into three parts:

- CC data analysis for the present and future states.
- Numerical modeling of the tidal inlet systems via coupled Delft3D and SWAN models for the present and future state simulations.
- Results analysis and comparisons with previous literature.

3.1. Climate Change Data Analysis

Katama Bay is a migrating tidal inlet, formed when a sandy barrier is breached by large storms (J. A. Hopkins 2017). The inlet migrates and closes in a decadal cycle, suggesting that characterizing littoral drift changes is crucial to predict the response of the system to CC. Additionally, changes in mean sea level will alter the currents through the inlet, likely impacting migration. In contrast, Santa Lucia Estuary is forced by river, tides, and waves. The inlet is kept open by the river discharge and the tidal currents, whereas waves tend to close it. For this system, an understanding of the balance of tidal, river and waves forcings is necessary to characterize the response to CC.

Table 3.1 summarizes the different data used at each site for the present and the future state simulations (year 2100). Changes in wave climate and mean sea level are analyzed in Katama Bay, whereas changes in wave climate, mean sea level, and mean river discharge are implemented in Santa Lucia Estuary.

Table 3.1. Forcings implemented at each system for the present and the future state simulations.

	Katama Bay	**Santa Lucia Estuary**
Present State	Tide (Amplitudes & Phases) Waves (H_S, T_P, θ)	Tide (Amplitudes & Phases) Waves (H_S, T_P, θ) River-flow (Q)
Future State	RSLR & tidal range changes Waves (H_S, T_P, θ)	RSLR & tidal range changes Waves (H_S, T_P, θ) River-flow (Q)

Table 3.2. Projected changes by 2100 for an RCP4.5 scenario.

		Katama Bay	**Santa Lucia Estuary**
Wave Climate	H_S (annual change)	-1.80%	-1.00%
	T_P (annual change)		-1.50%
	Wave direction (annual change)	±10°N	±10°N
RSLR		53 cm	54 cm
River Discharge (annual change)			-15%
Tidal Climate	M2 amplitude (decadal change)	-0.22%	
	M2 phase (decadal change)	+0.15°N	
	S2 amplitude (% decadal change)	-1.48%	
	S2 phase (decadal change)	+0.29°N	

Statistical analysis (copula analysis) is necessary to quantify the wave climates (present and future). Present wave climates are obtained from WaveWatch III (WWIII) hindcast data. Projected wave climate changes are collected from SD projections (Perez et al. 2015; Camus et al. 2017) or DD projections (Hemer et al. 2013). Table 3.2 summarizes the implemented changes based on the literature review (changes in mean sea level (i.e., SLR), tidal constituents, and river discharges) and the wave climate changes after the forecast data analysis.

3.1.1. Hindcast wave data analysis

A copula is a function that combines marginal distributions to form a joint multivariate distribution. The concept was introduced by Sklar (1959) and has been a common practice in different fields, including finance and economics (Dias and Embrechts 2004; Gronwald et al. 2011; Yang and Hamori 2013; and many others), hydrology (Favre et al. 2004; Zhang et al. 2015; and many others), flood risk assessment (Chen et al. 2012; Wahl et al. 2012; Masina et al. 2015; and many others), and coastal structure design (Salvadori et al. 2014; Arns et al. 2017; and many others). Nevertheless, these methods are not a standard practice to derive the wave boundary conditions in process-based models.

Here, we use these statistical tools (copula distributions) to derive the wave boundary conditions along the SWAN outermost domains at both sites using WWIII hindcast data. Wave directions (θ) and peak periods (T_P) are fitted using a Kernel distribution (nonparametric representation of probability density function defined by a smoothing function and a bandwidth value), whereas the significant wave height (H_S) is best represented by a generalized extreme value (GEV) distribution. The joint probability between these marginal distributions is calculated using an empirical copula (multivariate probability distribution where the marginal distributions of each variable are uniform). This procedure is used as a wave reduction method for both sites when a morphological acceleration factor (MORFAC) is applied in Delft3D. However, the copula analysis can induce some physical inaccuracies (e.g., high wave steepness). For the current simulations, wave propagation (using SWAN) is inaccurate when the wave steepness at the boundaries is higher than 0.05. Therefore, a wave steepness correction (restricting it below 0.05) is applied at the copula analysis output.

Katama Bay

WWIII hindcast data (2006-2017) shows that there is spatial variation of wave conditions along the outermost grid. Therefore, U.S. East Coast WWIII data is used to generate an average yearly wave climate every 7.4 km along the open boundaries. The multivariate (H_S, T_P, and θ) copula is fitted using an empirical copula. Wave height is not introduced into the copula analysis due to the low correlation between the significant wave height and the other variables (see Appendix B). Moreover, angles between 270 and 90ºN (degrees in nautical) are not input into the copula analysis for two reasons; waves from the north would not have an impact on the inlet dynamics, and angles around 360ºN introduce numerical instabilities into the SWAN model (Booij, Ris, and Holthuijsen 1999).

A MORFAC of 12 is applied to reduce the computational time in Delft3D. Therefore, the wave climate is reduced via the copula analysis to represent a full year with only 30 days and 12 hours. Figure 3.1

illustrates the wave reduction results for winter (December – February). The other season results are detailed in Appendix B. On average, winter has higher waves, characterised by a storm climate, whereas summer (June – August) has lower waves owing to the presence of a swell climate from the Southern Atlantic. The current statistical analysis captures the wave direction distribution, showing two fluctuating directional peaks (130ºN and 200ºN) amongst the seasons.

Santa Lucia Estuary

Similarly, WWIII hindcast data (2005-2017) is used to determine the boundary conditions in the process-based model. A grid point (28.5S, 32.5E) of the Global WWIII model (half degree resolution) is used along all boundaries owing to the fact that available buoy data is 60 km south of the grid. The multivariate (H_S, T_P, and θ) copula is fitted using an empirical copula. Wave height is not introduced into the copula analysis owing to a low correlation between the significant wave height and the other variables (see Appendix B).

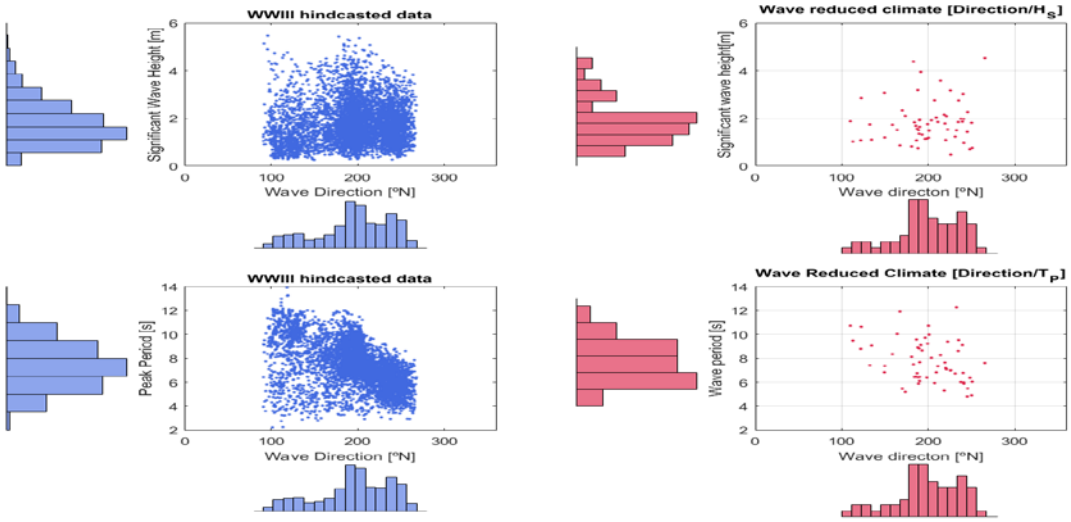

Figure 3.1. Winter reduced wave climate in Katama Bay (crimson color) using a MORFAC of 12. The reduction is made by applying a copula analysis from the WWIII hindcast data (blue color).

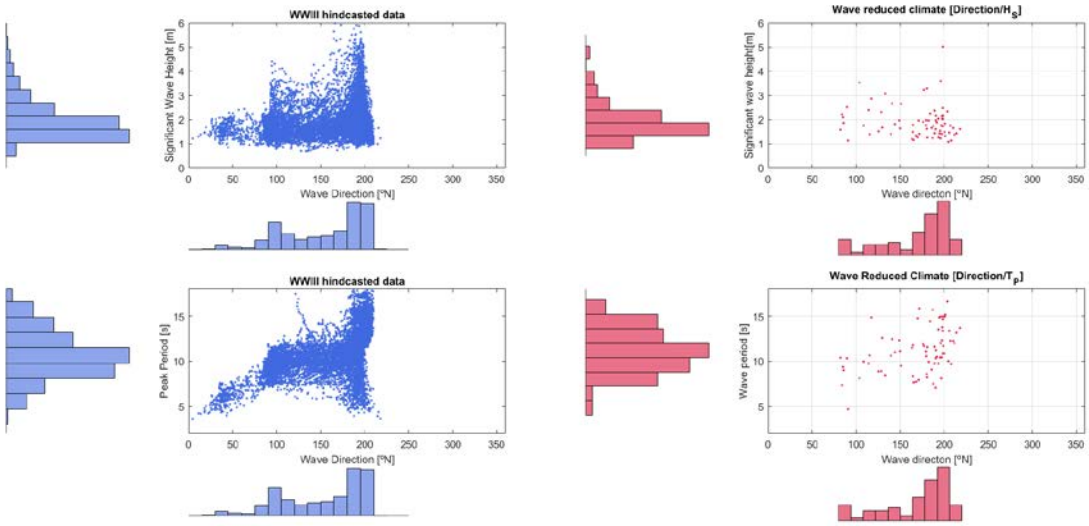

Figure 3.2. Winter reduced wave climate in Santa Lucia Estuary (crimson color) using a MORFAC of 10. The reduction is made by applying a copula analysis from the WWIII hindcast data (blue color).

A MORFAC of 10 is applied to reduce the computational time in Delft3D. Therefore, the wave climate needs to be reduced to be able to represent a full year with a timeframe of 36 days and 12 hours. Figure 3.2 shows the wave reduction results for winter (June-August), whereas other season results are illustrated in Appendix B. Winter waves are higher (H_S up to 6 meters) and with larger wave angles than during summer. During winter, cut-off lows generate south-easterly swells, whereas during summer cyclones originating in the Mozambique Channel produce north-easterly swells.

3.1.2. Forecast wave data derivation

For the future state, annual and seasonal wave climates are analyzed following the methodology presented in Figure 3.3. Wave climate projections from SD models (Perez et al. 2015; Camus et al. 2017) for an RCP4.5 scenario are used to evaluate the changes in significant wave height and peak wave period owing to CC. Wave directions are changed within an interval (-10ºN/+10ºN) (Hemer et al. 2013) due to the uncertainty in predicted change to wave direction in the selected SD models.

SD analysis by Camus et al. (2017) uses 30 GCMs, which provides a robust multi-model projection ensemble. Figure 3.4 shows time series of annual and monthly mean H_S of historical and forecast projections for each model (thin lines) and the average result (bold lines). Santa Lucia shows a smaller dispersion of its results than Katama Bay owing to higher waves at this second site. Averaging the projected changes (for an RCP4.5 scenario) of all 30 GCMs, the H_S is expected to decrease 1.73% in Katama Bay and 0.8% in Santa Lucia by the end of the 21st century. Moreover, the T_P is projected to decrease a 1.86% in Katama Bay and around a 4% in Santa Lucia, whereas the mean wave period (T_M) is likely to decrease a 1.25% in Katama Bay and a 2.54% in Santa Lucia Estuary.

Changes in wave climate are isolated in our analysis for each season (winter, spring, summer, and autumn) to include effects of seasonality. We force changes in wave height by changing the mean of the seasonal generalized extreme value distributions. The joint probability among the marginal distributions is assumed to remain constant along the time. Therefore, the same random values are used for the present and future state simulations. We change the peak period directly on the present state values, whereas we increase or decrease the wave angle by 10º depending on the simulation.

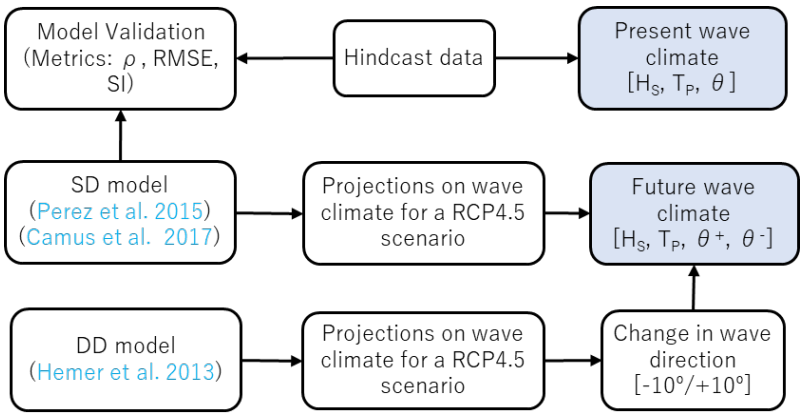

Figure 3.3. Forecast wave data derivation and validation. θ^+ represent positive changes in wave direction, whereas θ^- depicts negative changes in wave direction. The model validation metrics are the correlation coefficient (ρ), the root-mean-square error (RMSE), and the scatter index (SI)

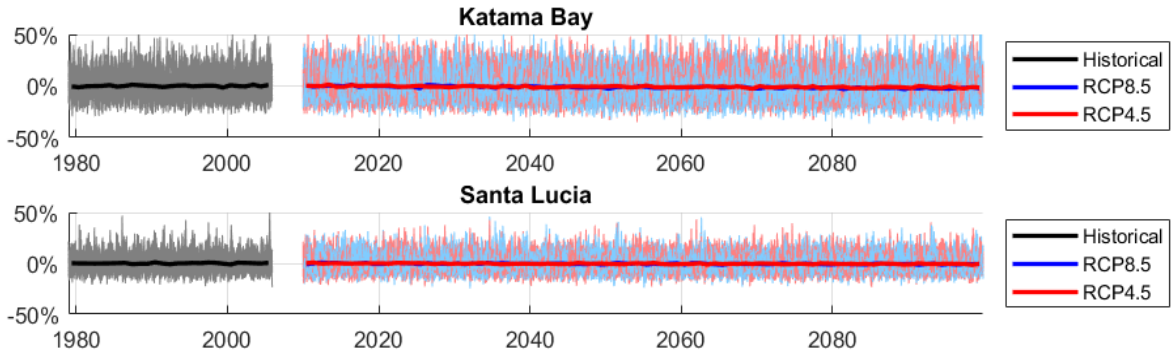

Figure 3.4. Time series of annual mean H_S change (bold lines) and monthly mean H_S for each GCM (thin lines) relative to the historical period (1979-2005). Grey lines represent the historical hindcast data, red lines illustrate the H_S projections for an RCP4.5 scenario, and blue lines show the Hs projections for an RCP8.5 scenario.

Katama Bay

The five best-fit GCMs are used to obtain forecast data at Katama Bay. Monthly and seasonal changes are presented in Figure 3.5. Winter (December–February), spring (March-May), and autumn (September–November) show decreasing significant wave heights, whereas summer (June–August) exhibits an increase of approximately 5%. This demonstrates an increase of swell (more persistent during summer) and a decrease of the mean storm climate (characteristic of winter).

A validation analysis from 2010 to 2017 comparing projections with a 50-meter water depth buoy data (NOAA 49047) is performed to verify the skill of the chosen SD method. Monthly averaged H_S, T_P, and the energetic term $H_S^2T_m$ are compared. The correlation coefficient (ρ), root-mean-square error (RMSE), and scatter index (SI) are calculated to compare predicted with observed data (see Figure 3.6).

The simulated monthly wave climate from the SD model can reproduce the hindcast wave climate. The correlation factor is 0.78 for the H_S, 0.7 for $H_S^2T_m$ term, and 0.35 for the peak period. The RMSE is about 0.22 m for H_S, 0.66 s for the T_P, and 5.15 m^2s for $H_S^2T_m$. The SD model skillfully reproduces the significant wave height seasonality and the energetic term seasonality (see Figure 3.6). It does not project the peak period seasonality, and hence these changes are not introduced into the process-based modeling.

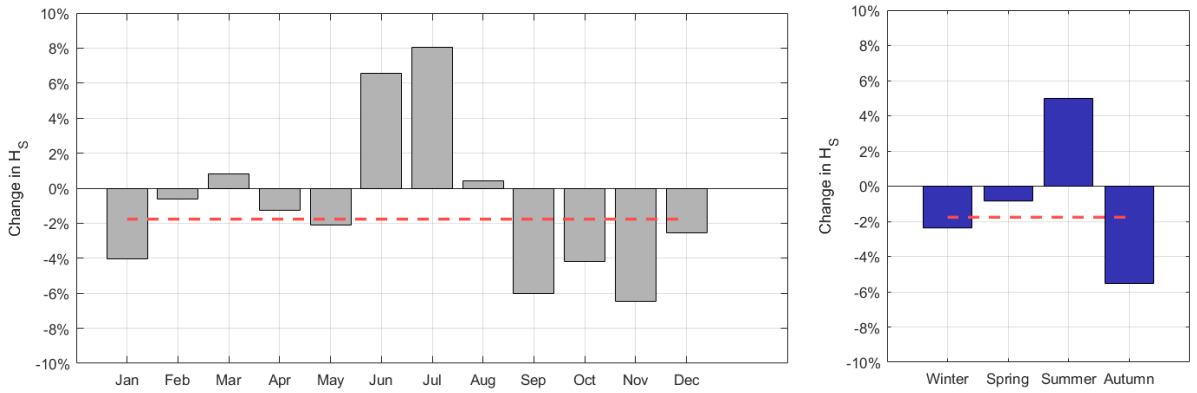

Figure 3.5. Katama Bay projected changes (in percentage) on significant wave height (H_S) by the end of the 21st Century relative to the historical period (1979-2005). The change is computed as the average of the 5 GCM ensemble. Grey and blue bars show the monthly and seasonal projected changes. Red dashed line shows the annual averaged change.

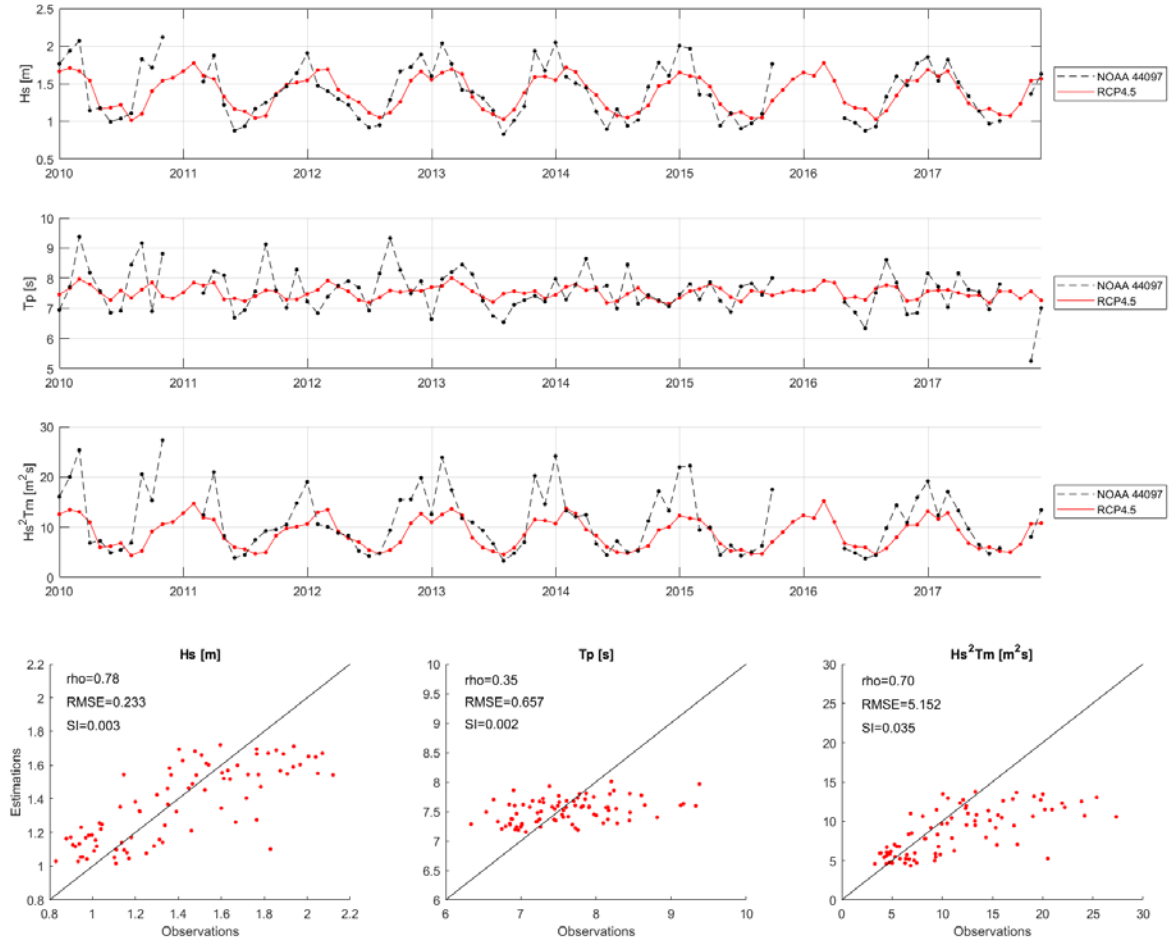

Figure 3.6. Monthly time series (2010-2017) comparison of the sea-state variables: (Hs, Tp, and $H_S^2T_m$) at Katama Bay. Scatter plots show the linear correlation between estimations and predictions for the sea state parameters. Correlation factor (ρ), RMSE, and SI are presented for each sea-state variable.

Santa Lucia

Similarly, the five best-fit GCMs are used to obtain the forecast changes in Santa Lucia Estuary. Monthly and seasonal changes in significant wave height (blue) and wave peak period (green) are illustrated in Figure 3.7. An average decrease of 1% in H_S is projected for Santa Lucia. Summer (December–February), autumn (March-May), and winter (June-August) exhibit a decrease greater than a 1%, whereas no change is expected for spring. The peak period is projected to decrease by 1.5%, with summer and spring having higher projected decreases (2.5-3%). Additionally, a decrease of 1% is expected during autumn, and no significant change is projected during winter.

Analogous to Katama Bay, a validation of the five best-fitted GCMs is performed by comparing WWIII hindcast data (from 2010 to 2017) with the SD projected climate during the same period (see Figure 3.8). The same statistics are checked (ρ, RMSE, SI) for the H_S, the T_P, and the energetic term $H_S^2T_P$. The estimated and observed data is less correlated than in Katama Bay. Nevertheless, the SD models show the seasonality of T_P within a year. The correlation factor is 0.54 for H_S, 0.60 for $H_S^2T_P$ term, and 0.61 for T_P., whereas the RMSE is 0.2 m for H_S, 0.82 s for T_P, and 8.26 m^2s for $H_S^2T_P$. Therefore, seasonally averaged changes in H_S and T_P are implemented in the process-based modeling.

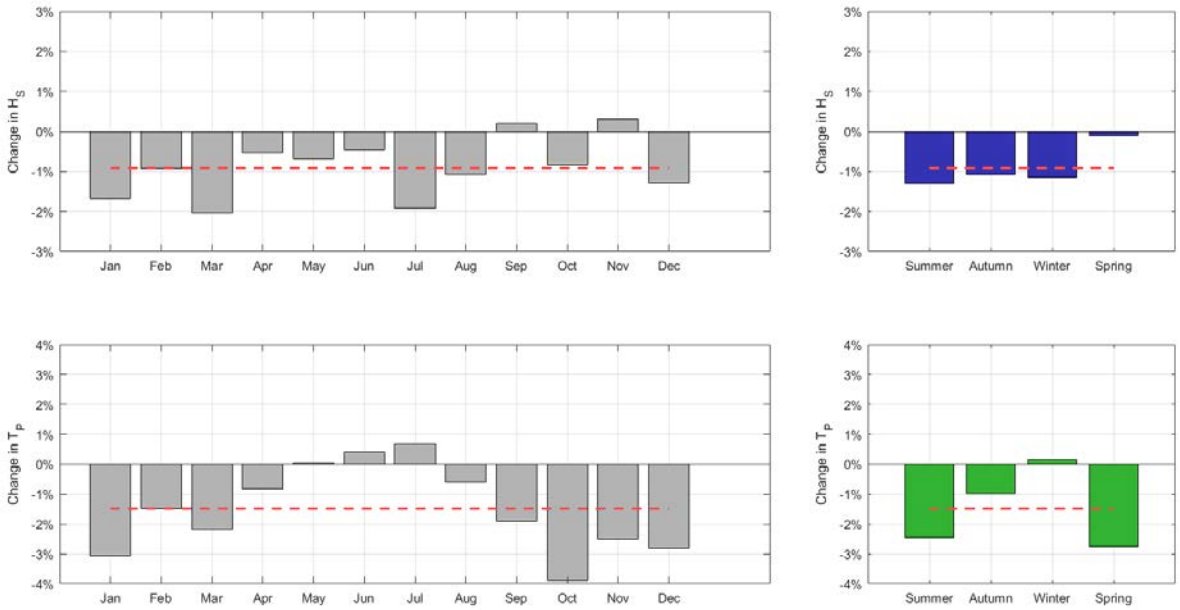

Figure 3.7 Santa Lucia Estuary projected changes (in percentage) on significant wave height (H_S) and wave peak period (T_P) by the end of the 21st Century relative to the historical period (1979-2005). The changes are computed as the average of the 5 GCM ensemble. Grey bars show the monthly projected changes and blue (for H_S) and green (for T_P) bars illustrates the projected seasonal changes. Red dashed lines indicate the annual averaged changes.

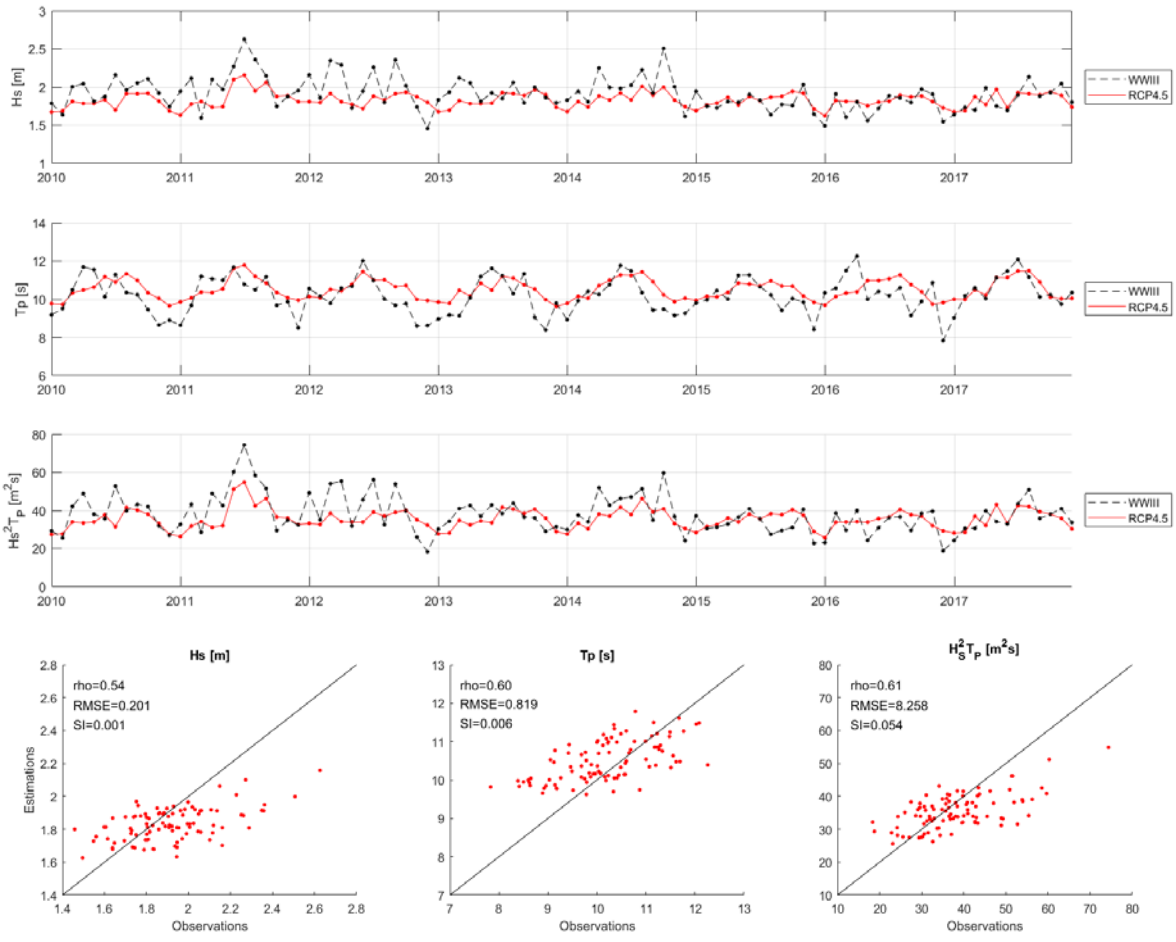

Figure 3.8. Monthly time series comparison of the sea-state variables: H_S, T_P, and $H_S^2T_m$ during the period 2010-2017 at Santa Lucia Estuary. Scatter plots show the linear correlation between estimations and predictions for the sea state parameters. Correlation factor (ρ), RMSE, and SI are presented for each sea-state variable.

3.2. Process-based modeling of decadal CC in tidal inlets

Coupled wave (SWAN) and flow (Delft3D-FLOW) models are used to investigate the inlet system hydrodynamics and morphodynamics at both sites. Waves are simulated over several nested SWAN model domains, whereas water levels, currents, and sediment transport are modeled using Delft3D-Flow. The same "snap-shot" methodology is applied at both sites (Figure 3.9). First, a present state (PS) simulation is run. Next, future state (FS) simulations are run by changing the forcings to introduce CC effects. This section defines in detail the methodology followed at each site, describing which are the principal parameters selected and the validation followed to calibrate both models.

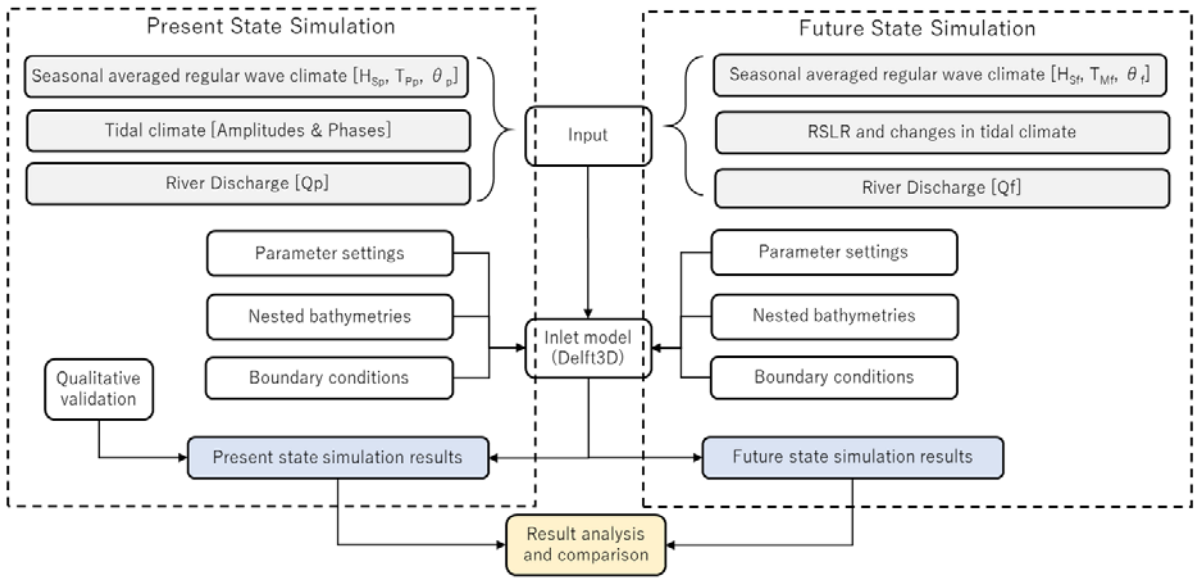

Figure 3.9. Methodology scheme used to analyze the potential CC impacts at both sites. Subscripts 'p' and 'f' refer to 'present' and 'future' situation.

3.2.1. Katama Bay

A coupled wave (SWAN) and flow (Delft3D-FLOW) model is used to investigate the inlet migration (after the inlet breaching of April 2007). The migration is evaluated for one year to capture seasonal trends. SWAN is run over three nested grids (Figure 3.10a) applying wave boundary conditions in the outermost one. Calculations on the coarser grids serve as boundary conditions to finer ones, reducing the computational time. The outermost grid (1 km of resolution) extends 180 km along the North and the South boundaries and 100 km along the West and East boundaries. Nested in it is a grid of 200-meter resolution and a grid of 29-meter resolution, which allow high-resolution results in the area of interest.

The large-scale bathymetry within the model domain was obtained during 1998 and 2008 USGS surveys (Northeast Atlantic 3 arc second map (National Geophysical Data Center 1999) and Nantucket 1/3 arc-second map (Eakins et al. 2009)) with a horizontal resolution of 10 to 90 meters. The bathymetry near the shoreline and bay was obtained during the summer of 2011 with a GPS and an acoustic altimeter mounted on a jet ski, with a horizontal resolution of around 10 meters. The 2007 inlet location, the 2007 barrier geometry, and the southeastern corner of Chappaquiddick Island are estimated from satellite images. Furthermore, the average barrier height around the inlet is set to 1 meter (Smith 2012).

Wave boundary conditions are imposed using a JONSWAP frequency-directional spectrum with 36 directional bins and 37 frequency bands logarithmically spaced between 0.03 and 1.00 Hz. Time and space-varying boundary conditions are forced every 3 hours based on the results of the copula analysis done with WWIII data (H_S, T_P, θ). SWAN is run in stationary mode with a depth-limited wave breaking formulation without rollers (Battjes and Janssen 1978), and the default breaking parameter (Appendix C).

The JONSWAP bottom friction coefficient is set lower (0.058 m^2/s^3) than the default (0.067 m^2/s^3). Hasselmann et al. (1973) suggested a mean dissipation coefficient of 0.038 m^2/s^3 to measure the decay of swell in the JOWSAP experiment. Later, Bouws and Komen (1983) proposed a bottom friction coefficient of 0.067 m^2/s^3 for a steady wind sea state owing to low dissipation using the value proposed by Hasselmann et al. (1973). The present site has a combination of swell and storm waves, and hence a value of 0.058 m^2/s^3 produces better wave height results than the default value (steady wind sea state).

The model includes depth- and current-induced refraction, and dissipation owing to white-capping (Komen and Hasselmann 1984). More persistence swell during spring and summer narrows the wave spectrum. Therefore, different directional spreading (N) is applied for each season (N=20 for autumn and winter and N=4 for spring and summer). Previous studies at the location (J. A. Hopkins 2017) shown that wind has no significant impact on the hydrodynamic results, and hence it is not included in this model.

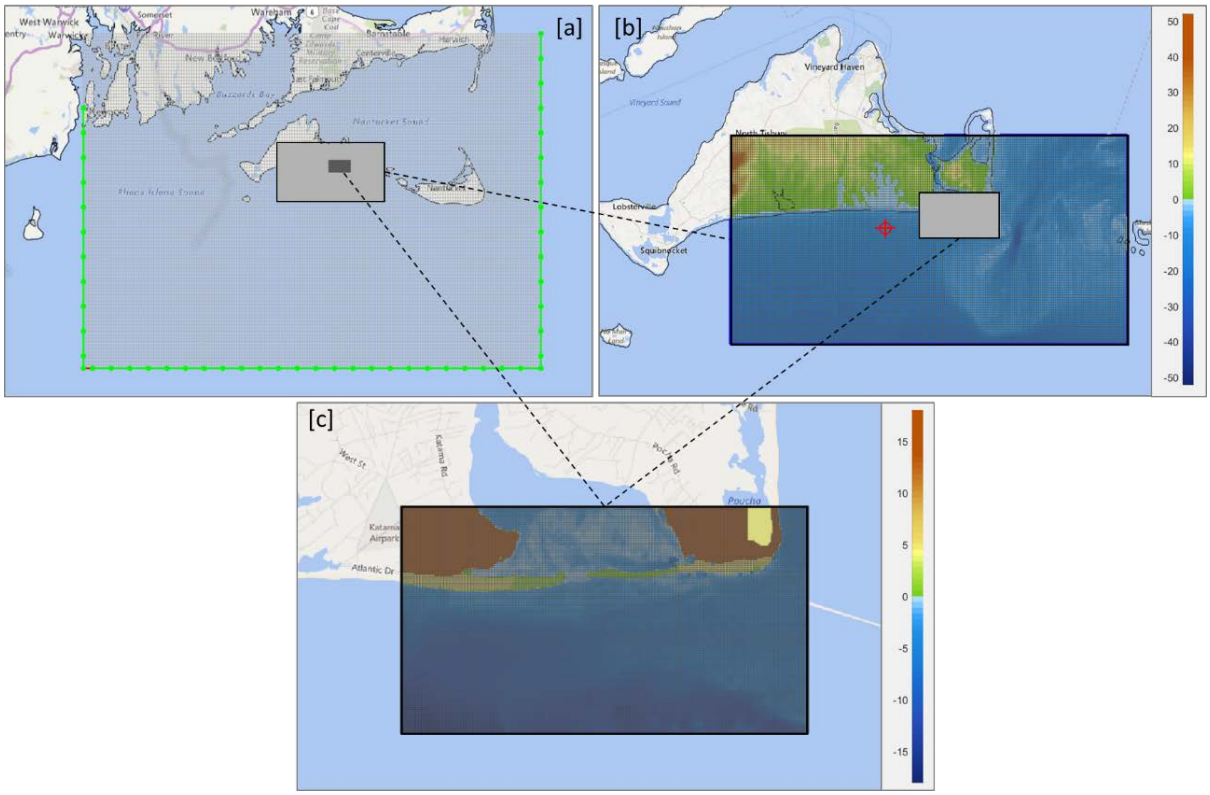

Figure 3.10. Bathymetry (color patches, scales on the right (in meters)) and nested grids for SWAN (a) and Delft3D-FLOW (b) models. Grids of Martha's Vineyard East region (b), and Katama Bay shoreline region (c) are nested in the full grid domain (a) The red circle in (b) is the Martha's Vineyard Coastal Observatory (MVCO) 12-meter buoy. Wave boundary conditions are applied at the green dotted line in (a).

Delft3D-FLOW is run over a 29-meters grid nested in a 200-meters grid (Figure 3.10b). The 13 most energetic tidal constituents are applied in the outermost grid as boundary conditions, dominated by M2 and N2 constituents. The model uses a free slip condition at closed boundaries, a spatially uniform Chezy roughness of 65 $m^{0.5}/s$ at bottom boundaries, and the default parameters for coupling both models, SWAN and Delft3D-FLOW (Deltares 2011). A time step of 12 seconds is used for both grids owing to numerical stability.

Sediment transport (van Rijn, Walstra, and van Ormondt 2004) is simulated using the modeled waves and currents. The TRANSPOR2004 model (described in Appendix D) is used instead of the default formulation (van Rijn 1993) owing to better results on the erosion and sedimentation patterns along the shoreline. The default model gives unrealistic accretion along the shoreline (up to 4 meters). The grain size is set to 500 µm based on sediment samples collected around Katama Bay in 2013 (J. A. Hopkins 2017). Most of the morphological parameters are defined as default, except for the reference height (changed to 0.5) and the calibration parameters. The current-related reference concentration factor is changed to 0.4 (from 1.0) owing to unrealistic results on the inlet migration and smoothing of all the bedforms. The bedload and suspended load transport factors are reduced to 0.25. Default values (1) give unrealistic sedimentation in the shoreline, smoothing the berm in front of the shoreline.

A present-day simulation, using averaged wave boundary conditions obtained from the copula analysis, starts in spring because most breaching events occur during winter (Dunlop 2014), and hence the initial bathymetric conditions are more likely to apply during spring. A MORFAC of 12 is used for this and all the simulations, which shows similar results to J. A. Hopkins (2017) using a MORFAC of 1 and of 10.

Six future state simulations (projected in 2100) are run changing different boundary conditions to match projected CC scenarios (Table 3.3). Two simulations (FSK1 and FSK2) have projected significant wave heights (Figure 3.5) and wave direction (increasing by 10º clockwise in simulation FSK1 and by 10º anticlockwise for simulation FSK2). Both simulations include an SLR of 53 cm and a bulk increase of the barrier height owing to the adaptability of the coastline to SLR, as well as predicted changes to tidal amplitudes and phases (Chapter 2.3.2). Two simulations (FSK3 and FSK4) emphasize the wave direction by only changing this parameter (+/-10 degrees). Finally, a simulation is run which emphasizes SLR and changes in tidal conditions (FSK5), and again only changes in tidal conditions (FSK6).

Table 3.3. Forcing conditions implemented at the future state simulations in Katama Bay. θ^{+} represents an increase (clockwise) of 10ºN on the wave direction, whereas θ^{-} indicates a decrease (anticlockwise) of 10º in the wave direction

Simulation	Wave Height	Wave direction	Wave direction	SLR	Tidal changes
FSK1					
FSK2					
FSK3					
FSK4					
FSK5					
FSK6					

Hydrodynamic validation

Overall, the model predicts the averaged seasonal wave conditions successfully and shows expected spatial inhomogeneity of wave heights (Figure 3.12a) and directions (Figure 3.12b) owing to the complex bathymetry and the wave/current interaction around Muskeget Channel. Observed data (significant wave height, mean wave period, and mean wave direction) from the Martha's Vineyard Coastal Observatory (MVCO) 12-meter depth buoy (see location in Figure 3.10b) is compared to modeled data. Figure 3.11 shows the seasonal averaged values for both the modeled and the observed data. The model predicts the averaged values for wave height and wave directions. However, modeled wave periods are slightly higher than observed. These small errors are likely due to the wave steepness correction (Chapter 3.1.1) that lower some periods, and the absence of wind within the domain which may induce the formation of locally storm waves with shorter periods.

The model predicts the flow separation around the southeast corner of Chappaquiddick Island (Figure 3.12c). Maximum depth-averaged velocities are around 2 m/s during ebb (Figure 3.12c), and flood (Figure 3.12d), showing similar results as previous models of the site (J. A. Hopkins 2017). J. Hopkins, Elgar, and Raubenheimer (2017) showed that the radius of curvature of Chappaquiddick Island determines the flow separation, and thus influences the sediment transport around the shoreline. Moreover, similarly to previous models (J. A. Hopkins 2017), velocities through the inlet are around 1 m/s, with maximum velocities up to 2 m/s, showing a flood-dominant behavior.

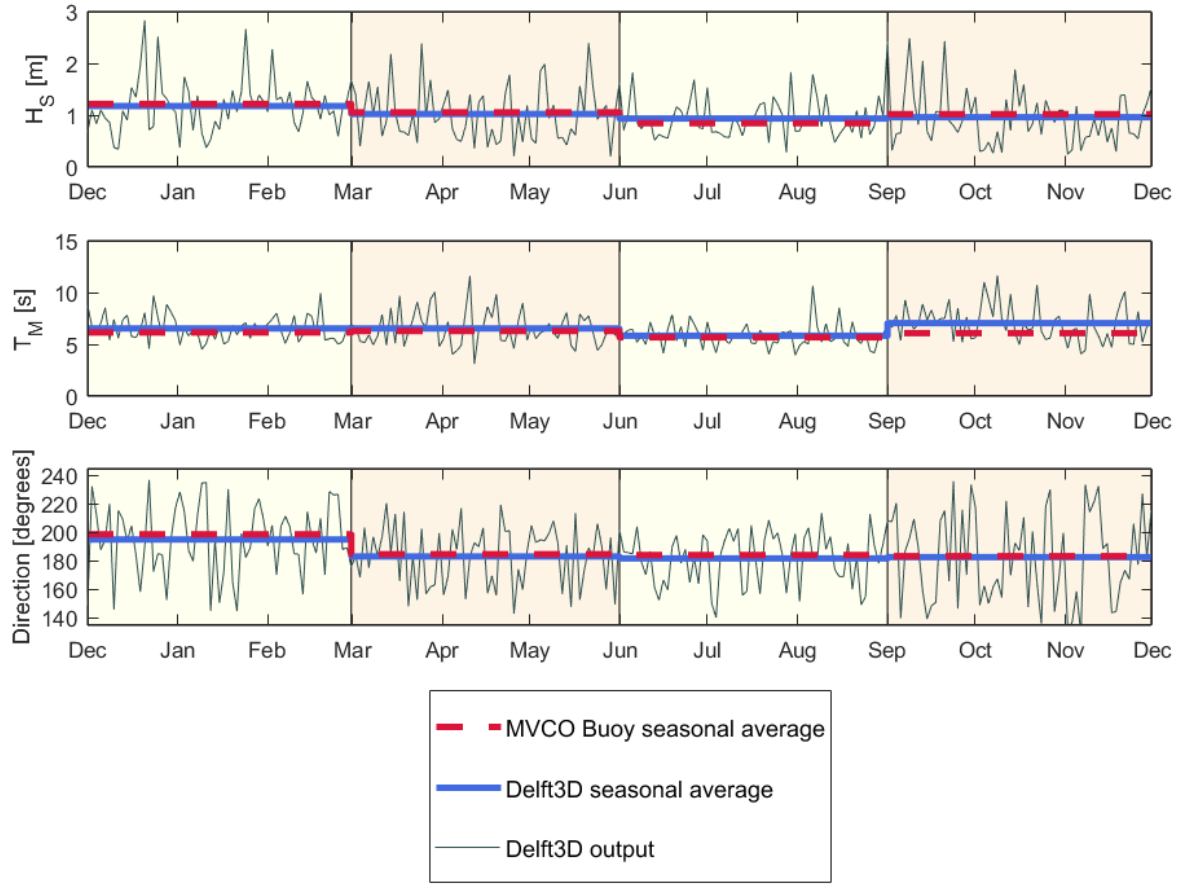

Figure 3.11. Wave validation. Comparison between the seasonal average modeled wave climate and the seasonal average observed wave climate at 12-meter water depth buoy.

Morphodynamic validation

There is no existing bathymetric measurement focused on the inlet before 2011. The nearshore bathymetry used was measured in 2011 with the barrier modified (i.e., moving the inlet from 2011 position to 2007 position). Figure 3.13 illustrates the initial shoreline position of the bathymetry compared to 2007 and 2012 satellite images.

A model with a closed barrier is run for a year (using the same model parameters) to address the bathymetric inaccuracies. No apparent changes are observed inside the basin, whereas outside the basin, currents and waves cause changes in the shoals on the east side. Closing the inlet produces accretion along the middle part of the shoreline where updrift the 2007 inlet position, the initial shoreline matches the 2007 shoreline (Figure 3.13). Changes in the shoreline position may affect the results. Therefore, a compromise is achieved to provide a near-equilibrium bathymetry but with a similar 2007 shoreline. Appendix E describes the methodology followed to obtain this new bathymetry, which is used on the validation model, the present state model, and the future state simulations.

A validation model is run from 15 of April 2007 to 30 of June 2008 using the same parameters described previously. Here, satellite images are used to qualitatively validate the inlet migration. Figure 3.14 illustrates the inlet position in July 2007 (a) and July 2008 (b), where the inlet gets wider (from 300 to 900 meters) and both barrier edges migrate towards the east. A red contour represents the modeled shoreline after the validation period in Figure 3.14c. The model predicts the correct inlet migration direction (300 meters per year towards the east) and the widening of it (from 300 to 730 meters). However, the model updrift barrier does not migrate.

Previous studies (Smith 2012; J. A. Hopkins 2017) showed that the presence of big storms enhances the morphological evolution at this site, and in particular the migration of Katama Inlet. As storms of this nature are not included in our simulations, this could be a source of error. For instance, bathymetric data

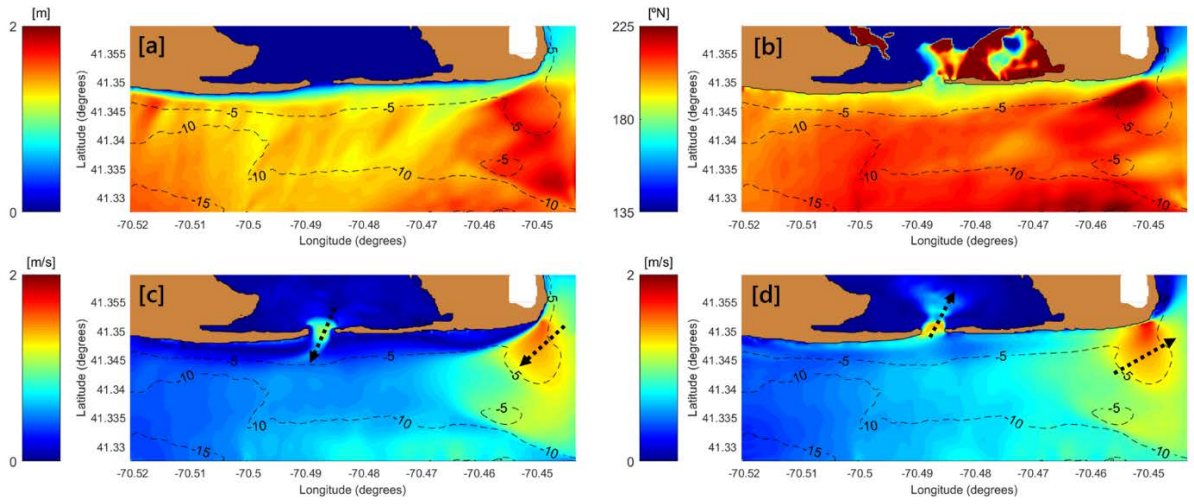

Figure 3.12. Spatial distribution of the modeled significant wave height (a) and the incoming mean wave direction (b) (jet colormap, scales on the left). Wave direction is measured clockwise from the North. Black dashed curves are depth contours every 5 meters. Depth-averaged velocity [m/s] on the inner domain (jet colormap, scales on the left) during (c) ebb and (d) flood. Black dashed curves are depth contours every 5 meters. Black dotted arrows represent the predominant flow direction.

indicates that Hurricane Irene caused the 54% of the total sand volume change in the region during 2011-2012 (Smith 2012). Also, Delft3D does not simulate overwash, which might enhance erosion in the barrier. For instance, during Hurricane Sandy, a total of 39,000 m^3 of sediment was eroded from the barrier owing to overwash (Smith 2012).

Nevertheless, the model does show good qualitative results. The wave conditions are accurately simulated (Figure 3.11), and the flow velocity through the inlet is in the same order of magnitude (maximum values from 1 m/s to 2 m/s) as previous studies (Smith 2012; Orescanin et al. 2014; J. A. Hopkins 2017). The down-drift barrier migration rate is in the order of magnitude (300 meters per year), seeing as from 2007 to 2015 the inlet migrated 2.5 km (i.e., 312 m/year).

Figure 3.13. Shoreline position of the bathymetry used in the Delft3D model (red). 2007 satellite image (left) and 2012 satellite image (right). Satellite images from (Google Earth 2018a).

Figure 3.14. Satellite images of the validation period; July 2007 (a) and July 2008 (b). Red arrows illustrate the inlet width, whereas orange arrows indicate the inlet barriers migration. Initial inlet bathymetry (green contour line) and after the validation simulation (red line). Satellite images from (Google Earth 2018a).

Furthermore, the inlet becomes wider (from 320 meters to 730 meters), and shallower from ~3 meters (by the end of 2007) to ~2 meters (July 2008), following the same behavior explained by different authors (Dunlop 2014; Orescanin et al. 2014). The model also develops ebb- and flood-tidal deltas (see Figure 3.15), and they migrate following the inlet, which shows an appropriate balance between the tidal currents and wave forcings.

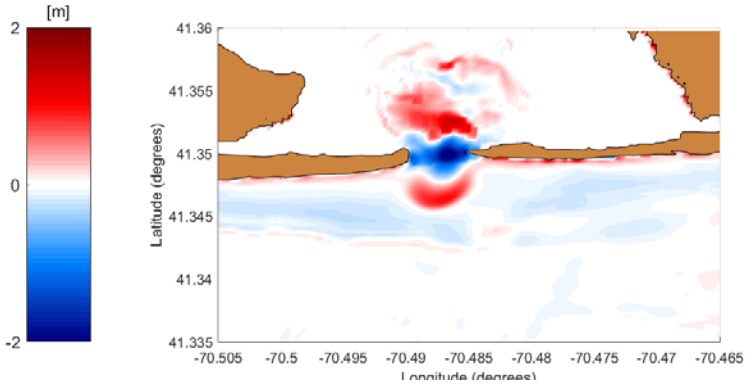

Figure 3.15. Erosion (blue) and sedimentation (red) patterns at the end of summer (August).

3.2.2. Santa Lucia Estuary

Like Katama Bay, a coupled wave (SWAN) and flow (Delft3D-FLOW) model is used to investigate the system hydrodynamics and morphodynamics. Grids, bathymetries and coupled parameters are obtained from a previous model (Hoek 2017). Changes in wave boundaries conditions, river discharges, and calibration parameters adapt the previous model to the present analysis. SWAN is run over two nested grids (Figure 3.16b), applying wave boundary conditions at the outermost one. This grid (200-meter resolution) extends for 11 km offshore and 22 km along the west and east boundaries. Nested in it is a 5 km (cross-shore) and 3 km (longshore) grid with a varying grid resolution which allows for high-resolution in the area of interest. At the boundaries, the grid resolution is 84 x 96 m and around the inlet and the surf zone, the grid resolution increases 20 m. The maximum step change on the grid resolution is 10% to preserve the computational stability on the simulation.

The outer bathymetry is obtained from General Bathymetric Chart of the Oceans (GEBCO 08), whereas the fine grid bathymetry is obtained from LIDAR and bathymetric surveys from August 2013 and September 2014 (AOC Geomatics 2013; Environmental Mapping & Surveying 2014). This bathymetry includes Santa Lucia Estuary, the Narrows, Santa Lucia barrier and adjoining offshore area

Wave boundary conditions are imposed using a JONSWAP frequency-directional spectrum with 36 directional bins and 24 frequency bands logarithmically spaced between 0.05 and 1.00 Hz. Time-varying boundary conditions are forced every 3 hours based on the results of the copula analysis. SWAN is run in stationary mode with a depth-limited wave breaking formulation without rollers (Battjes and Janssen 1978), and the default breaking parameter (see Appendix C). Furthermore, the JONSWAP bottom friction coefficient is set lower (0.038 m^2/s^3), which corresponds to the value suggested by Hasselmann et al. (1973) for swell climates. The model includes depth- and current-induced refraction, dissipation owing to white-capping (Komen and Hasselmann 1984), and a directional wave spreading of 4 degrees typical of swell.

Delft3D-FLOW is run over the high-resolution grid (Figure 3.16a) with a time step of 6 s to preserve numerical stability and model accuracy. Tidal forcing is modeled with an M2 constituent with a mean tidal range of 1.3 meters at the East boundary. Northern and southern boundaries have Neumann water level boundary conditions, which enforces an alongshore water level gradient equal to zero. The model uses a free slip condition at closed boundaries, a spatially uniform Chezy roughness of 50 $m^{0.5}/s$ at bottom boundaries, and the default parameters for coupling both models, SWAN and Delft3D-FLOW (Deltares 2011).

The Mfolozi River discharge is implemented by dividing the mean annual run-off into five equal inputs of 6 m^3/s. Grenfell and Ellery (2009) showed that a concentration of 1 kg/m^3 is expected for a MAR of 30 m^3/s. Furthermore, samples indicate an average diameter of 0.0052 mm (very fine silt) in the Mfolozi River discharge, with suspended load 5-6 times larger than the bed load (Grenfell and Ellery 2009). Nevertheless, the present study does not include cohesive sediment into the modeling. Therefore, only the river bedload transport is input (coarser sediment) with the sediment concentration decreased by a factor of 6 (set to 0.15 kg/m^3). The Narrows discharge is implemented as a single input (6.6 m^3/s) without sediment content. It is assumed that the water coming from the lakes has low contents of sediment. The low water velocities in the lakes lead sediment to settle, reducing the sediment concentration on the discharges trough the Narrows.

Sediment transport (van Rijn 1993) is simulated using the modeled waves and currents. The grain size is set to 200 µm based on sediment samples collected around the estuary in the 1980's (C. I. Wright and Mason 1990). Hoek (2017) changed the current-related calibration parameters to 20 and the wave-related transport factors to 0.31 to get reasonable longshore sediment transport measurements. Nevertheless, these calibration parameters give unrealistic erosion patterns along the barrier. Results of a copula analysis show a different wave climate than was implemented by Hoek (2017), who based their wave reduction analysis (10 wave conditions) in a buoy located 60 km south of Santa Lucia. New results should a more oblique incident angle for both: swell climates (northeasterly and southeasterly swells).

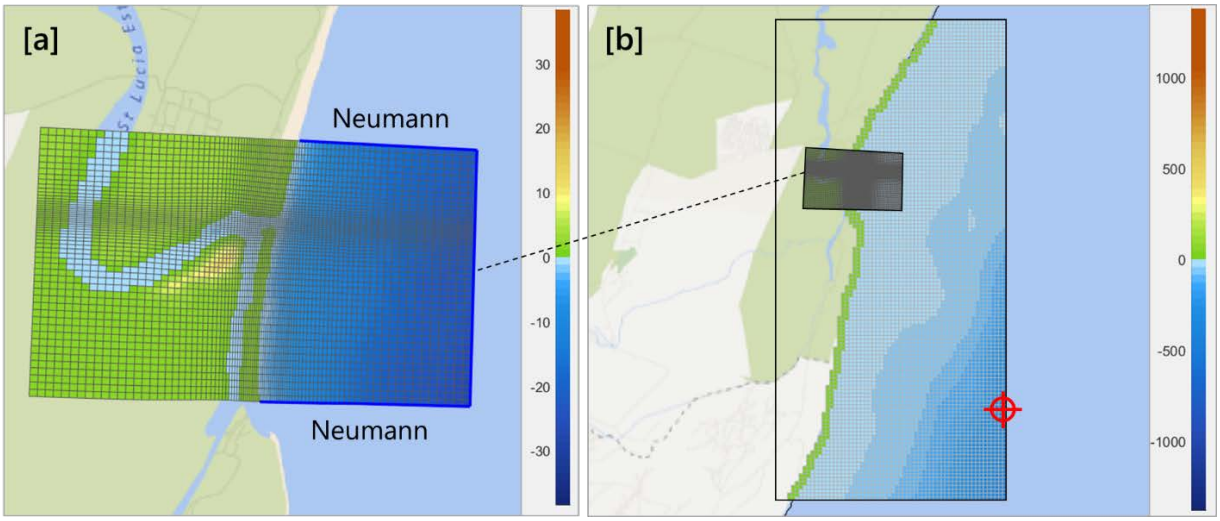

Figure 3.16 Bathymetry (color patches, scales on the right (in meters)) and nested grids for Delft3D-FLOW (a) and SWAN (b) models. Flow boundary represented by blue lines. The red circle in (b) is the WWIII wave data point applied in the open boundaries.

Furthermore, we implemented 293 wave conditions throughout the simulated year capturing higher waves (storms). Therefore, the modeled rates of sediment transport are higher, allowing allows us to reduce the current calibration parameters by half (10).

We change the bed and suspended wave related load transport factor to 0.4 from 0.31 to get reasonable sediment transport measurements and reduce the unrealistic erosion patterns along the shoreline due to strong current-related transport. Other site studies with similar grain characteristics have successfully implemented the same wave-related transport factors (Hansen et al. 2017).

A present state simulation, using averaged wave boundary conditions obtained from the copula analysis, runs for a year (spring, summer, fall, and winter). Hoek (2017) performed a MORFAC sensitivity analysis showing that a MORFAC of 10 displayed realistic values, whereas higher values (20) produced unrealistic changes. Therefore, the present state and six future state simulations to match projected CC scenarios (Table 3.4) runs with a MORFAC of 10. Two simulations (FSSL1 and FSSL2) have projected significant wave heights, peak wave periods (Figure 3.7) and wave directions (increasing 10º clockwise in simulation FSSL1 and 10º anticlockwise for simulation FSSL2). Both simulations include an SLR of 54 cm and a bulk increase of the barrier height owing to the adaptability of the coastline to SLR, as well as a projected river discharge reduction of 15% (Nohara et al. 2006). Two simulations (FSSL3 and FSSL4) emphasize the wave direction by only changing this parameter (+/-10 degrees). Finally, a simulation is run which emphasizes SLR (FSSL5), and river discharges changes (FSSL6).

Table 3.4. Forcing conditions implemented at the future state simulations in Santa Lucia Estuary.

Simulation	Wave Height	Wave Period	Wave	Wave	SLR	River discharge
FSSL1						
FSSL2						
FSSL3						
FSSL4						
FSSL5						
FSSL6						

Model Calibration

Hoek (2017) calibrated the model against field measurements of velocities through the inlet and longshore sediment transport to ensure realistic model results. This calibration was divided into two parts: a tidal prism validation and an alongshore sediment transport evaluation.

The tidal calibration was performed without river discharge and for three different tidal stages (neap, spring, and mean). He calibrated the Chezy parameter to reproduce tidal prism field measurements (Table 2.1), suggesting a value of 50 $m^{1/2}/s$ (applied in the current model). The modeled tidal prism during spring tidal range was 1,860,000 m^3 (against 1,600,000 – 2,080,000 m3 in measurements), 1,340,000 m^3 during mean tide (against 800,000 – 1,000,000 m^3 in measurements), and 550,000 m^3 during neap tide (against 350,000 – 800,000 m^3 in measurements).

Hoek (2017) calibrated the longshore sediment transport rate using a wave reduced climate of 10 wave conditions. He obtained an average longshore transport rate of 500,000 m^3 per year, which is similar to the measured values in Richards Bay (60 km southwards). Measurements in Richards Bay show a large variability in sediment transport rates (from -500,000 m^3/year to ~2,000,000 m3/year) from 1980 – 1993, with an average rate of 800,000 m^3 to the north (Schoonees 2000). Years with higher cut-off lows result in a strong longshore transport from south to north, whereas years with strong waves from the northeast shift the net longshore transport towards the south.

With the new calibration parameters implemented here, the net longshore transport rate is equal to 400,000 m^3/year in the southern side and 360,000 m^3/year in the northern side (see Figure 3.17). As most of the measured values in Richards Bay (60 km south from Santa Lucia), the net longshore sediment transport is north directed. Moreover, modeled values are in the same order of magnitude as field measurements.

The Gamede Cyclone breached the barrier on the 27th of February, 2007, and the inlet closed 175 days later. The breaching occurred during a drought season where the river discharge was minimum. Here, we run a simulation to reproduce the closure of the inlet using the model parameters defined above, with 2007 wave boundary conditions, and without river discharge. The cross-section of the inlet is measured throughout the simulated year, and the inlet closes after 220 days owing to energetic southeasterly swell.

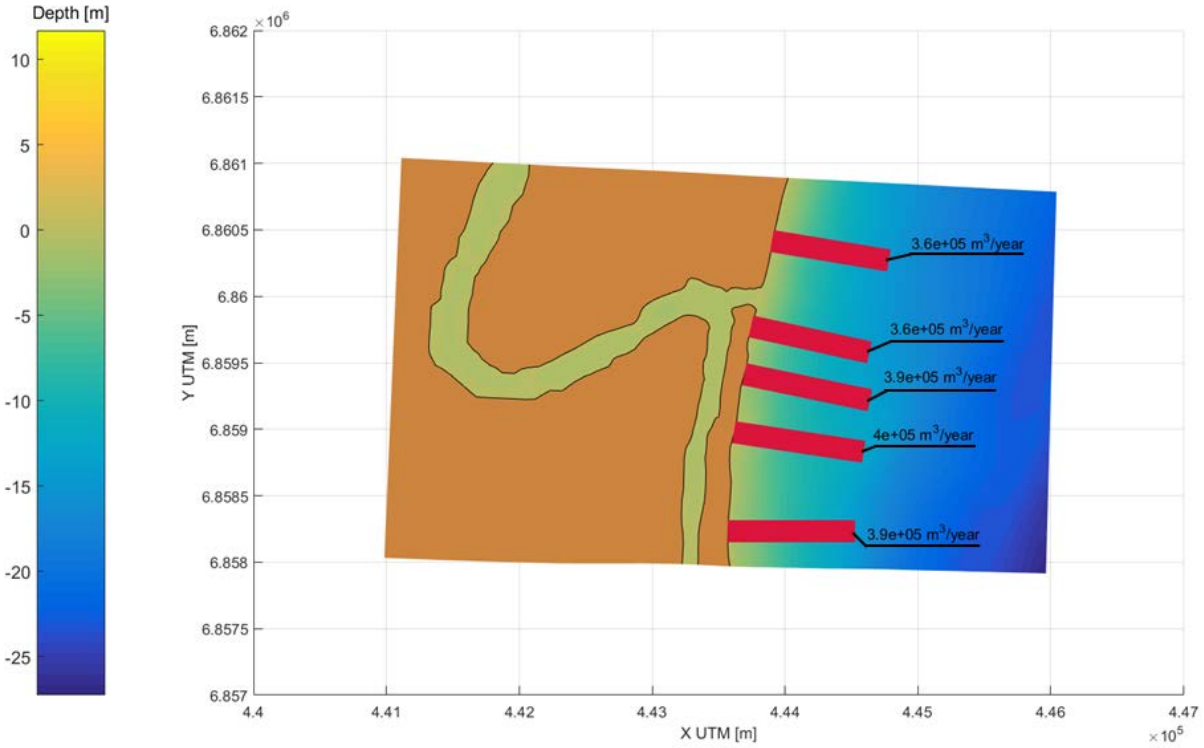

Figure 3.17. Modeled longshore sediment transport rate (m^3/year) at five different locations along the shoreline (crimson bars). Water depth is plotted as the background (scale on the left (in meters)).

3.3. Methodology for model output analysis

Outcomes are focused on comparing the stability of the inlets (e.g., inlet migration and inlet migration speed, Bruun stability criterion), changes in geometry (e.g., inlet width, and depth) and sediment pathways causing inlet migration (e.g., littoral sediment bypassing, sediment transport through the inlet, and import of sediment into the basin) for all scenarios.

The inlet migration is analyzed by determining the migration of the barriers and of the inlet centroid. The centroid migration allows an evaluation of the inlet migration in both directions (barrier-parallel and barrier-transverse). Therefore, not only the longitudinal migration is captured but also the transversal migration, leading to a better understanding of the inlet behavior (e.g., changes in flood or ebb-dominance or wave intrusion).

Sediment pathways are analyzed by building control volumes. These boxes are defined to capture the principal features of each system (e.g., ebb-tidal delta, flood-tidal delta, main inlet), and are discretized on the inlet migration direction, to capture the migration of all the other features. Each box is delimited by four profiles, where the cumulative transport calculated between them. The representation of the transport is done with arrows, changing in width depending on the transport value. Moreover, a sediment budget is done by calculating the volume change at each box. Detailed figures for each simulation are created, and then each FS simulation is compared with the PS simulation. This is a robust analysis to understand the behavior of the systems and the potential changes that can occur due to CC driving forcings.

Lastly, the results for both sites are compared for similarities and differences. The discussion is focused on the link between the result divergences and the particular conditions of each site. In a similar way, results are qualitatively compared with other previous studies in other sites (Duong et al. 2017; Duong et al. 2018).

CHAPTER 4. KATAMA BAY RESULTS

CHAPTER SUMMARY

This chapter contains the Katama Bay results analysis. First, we evaluate the present state simulation to understand the system behavior by analyzing the hydrodynamics (wave heights, wave directions, currents) and the morphodynamics (cumulative erosion/sedimentation patterns, inlet profile section development, barrier migration, inlet centroid migration, and sediment pathways). Finally, we compare the present state results with the future state simulations (Table 3.1), focusing on the inlet migration and the sediment pathways analysis.

4.1. Present State Simulation

The model operates with the specifications previously explained in Chapter 3.2.1 and the wave boundary conditions derived in Chapter 3.1. A model run takes for 30 days and 18 hours for a period of a year, starting the 1st of March (beginning of spring) and finishing the 28th of February (end of winter).

4.1.1. Hydrodynamic Results

Orbital velocities, wave breaking induced currents, tidal currents, and flows through the inlet induces the inlet to migrate (J. Hopkins, Elgar, and Raubenheimer 2017). Therefore, we need an understanding of the hydrodynamics (e.g., waves heights, wave directions, flows through the inlet and surroundings) to contextualize the morphodynamics.

Wave conditions around Katama Bay are heterogeneous (Figure 3.12). Shoals induce energy dissipation processes (e.g., breaking, bottom friction, refraction, shoaling, and wave breaking) altering wave proprieties differently throughout the domain. Figure 4.1 shows the significant wave heights (b) and mean wave directions (d) of two 5-meter depth points; updrift (red point), and downdrift (blue point) the inlet. Although both points present a similar average significant wave height (~0.86 meters), the highest waves are smaller in the downdrift point.

Extensive shoals in front of the Wasque Point (green rectangle in Figure 4.1a) dissipate wave energy via wave breaking and bottom friction. Additionally, these shoals refract the waves increasing the wave directional spreading at the downdrift point (Figure 4.1d). Waves become more oblique than updrift the inlet (e.g., differences of 20° are appreciable between the points) increasing the average mean wave direction by 4 degrees (190°N downdrift and 186°N updrift).

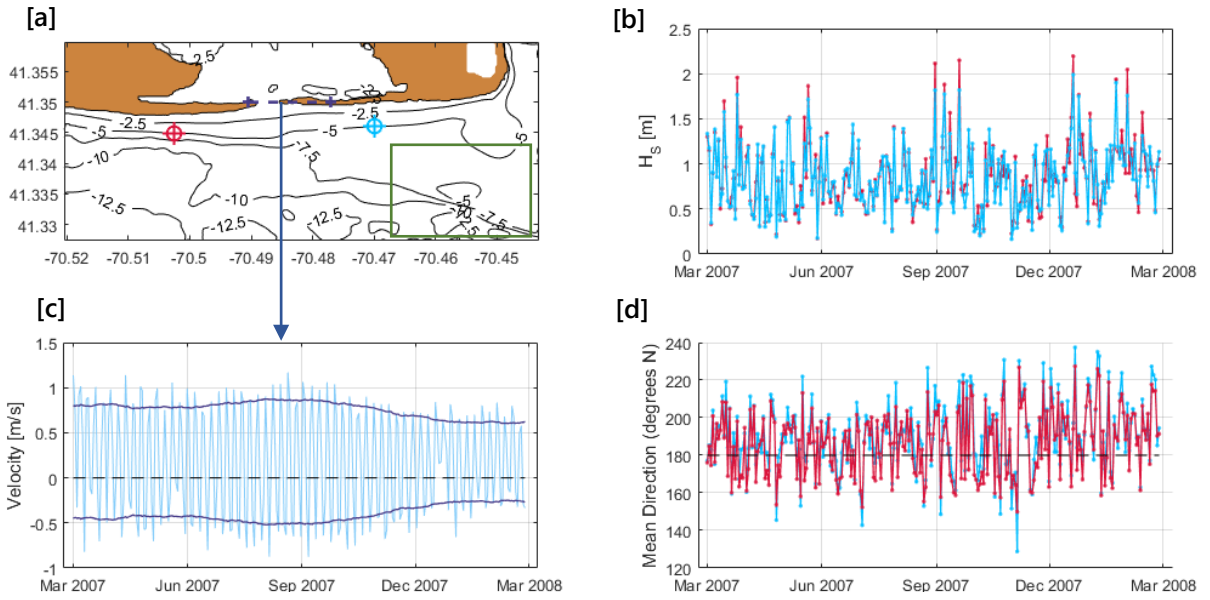

Figure 4.1. Hydrodynamic results at the area of interest (Katama Inlet surroundings). Red and blue markers [a] represent wave height sample points at 5-meter water depth. The blue dashed-line (a) shows the profile where depth-averaged velocity is checked [b]. [b] and [d] illustrate the significant wave heights and mean wave directions respectively for both points. [c] shows the mean depth-average velocity (seaward positive) through the inlet. The dark blue line is an RMS envelope obtained from the mean depth average velocity signal (light blue line).

Water level differences between Katama Bay and the open sea induce strong currents (up to 2 m/s) through the inlet. Figure 4.1c illustrates the mean depth-averaged velocity (seaward component) along the inlet for a year. The signal reveals that higher currents are present during flood (positive values) than during ebb (negative values). However, velocities in both directions are high (averaged values up to 1m/s) anticipating that the model will develop flood- and ebb- tidal deltas.

Mean depth-averaged velocities remain nearly constant during the first half of the simulation and then diminish by 25% owing to the inlet widening while it migrates. The cross-section of the channel increases at a higher rate than the discharge, hence mean and maximum velocities through the inlet decrease. The flow separation around the southeast corner of the island is simulated (Figure 3.12) with maximum velocities up to 2 m/s during ebb and flood. The flow separation creates a quiescent zone which extends towards the west for approximately 1.5 km during ebb (Figure 3.12).

4.1.2. Morphodynamic results

Figure 4.2 shows the resulting morphological development regarding bed level change and cumulative erosion/ sedimentation patterns. The first column corresponds to the isolated bed level change for each season (in the following order; spring, summer, autumn, and winter), and the right column shows the accumulated bed level changes at the end of each season. During spring (Figure 4.2a) the inlet erodes leading to the formation of both tidal deltas (ebb and flood), with the flood delta more extensive and shallower than the ebb delta.

Throughout summer (Figure 4.2b) the morphological behavior becomes more ebb-dominant. The ebb-tidal delta grows and migrates offshore. Furthermore, it rotates anticlockwise, and the terminal lobe presents a semilunar shape pointing to SSE. This tilting is due to more persistent waves coming from the SE. The flood-tidal delta continues to expand inside the basin, causing erosion to the ebb spits of the flood-tidal delta. The inlet starts to migrate, following the littoral drift direction, and hence eroding the downdrift barrier at the east side of the inlet. Consequently, the inlet becomes wider and larger.

During fall (Figure 4.2c) the inlet continues its migration, eroding the downdrift barrier. Strong currents through the east side of the inlet cause new rushes of sediments into the existing tidal deltas, creating new flats. The ebb-tidal delta grows on the east side (due to inlet migration) while big waves are coming from the SW-SSW causing erosion on the west side. This combination leads to an ebb-tidal delta oriented to the south. Additionally, the central part of the inlet exhibits sedimentation owing to a decrease inlet currents.

Finally, during winter (Figure 4.2d) the inlet continues its migration, becoming shallower in the west side. In fact, there is sedimentation around the updrift barrier owing to stronger littoral drift than in other seasons, and smaller currents through the inlet (Figure 4.1c). The flood-tidal delta continues its expansion within the bay, whereas the ebb-tidal delta travels downdrift with a persistent erosion on the west side owing to the higher waves coming from the SW (see Figure 2.2 and Figure 4.1d).

Figure 4.3 illustrates the inlet profile evolution throughout the simulation and shows the migration of the inlet centroid (bar plot on the right). The centroid is obtained by averaging the inlet centroid of each grid (29 x 29 meters) over an area that extends 100 meters offshore and 100 landwards along the inlet width. Initially, the inlet is shallow (~0.25 meters), and narrow (320 meters). During the initial 25% of the simulation (spring), the inlet becomes deeper (down to 2 meters) and slightly wider (360 meters) owing to strong tidal-driven currents.

Later (during summer), the inlet becomes deeper (2.7 meters), broader (500 meters), and the downdrift barrier migrates more than 100 meters. Autumn presents the biggest downdrift barrier migration (110 meters) making the inlet wider and displacing the centroid by 50 meters downdrift. Finally (during winter) the inlet becomes shallower, owing to a decrease in the currents, and the migration decreases. Overall, the centroid migrated 127 meters and the downdrift barrier 300 meters, making the inlet ~700 meters wide.

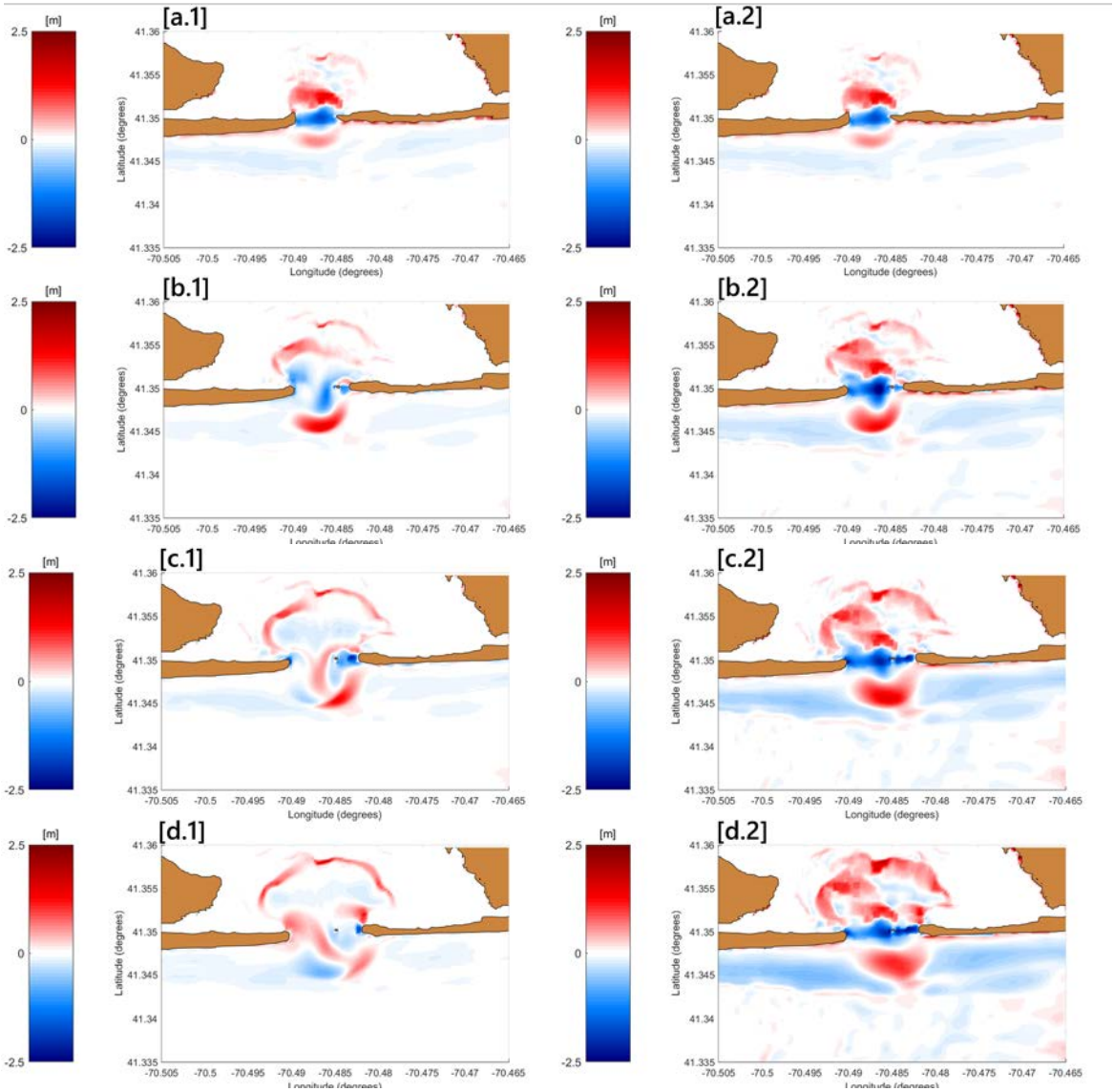

Figure 4.2. Erosion and sedimentation patterns of the present state simulation. The left column shows the changes in bed level of each isolated season (in the following order; spring, summer, autumn, and winter). Right column illustrates the accumulated changes throughout a year, with the last picture as the final result of the simulation. Red shades indicate sedimentation, whereas blue shades show erosion.

Figure 4.4 shows a qualitative sediment pathways analysis used to understand the whys and wherefores behind the changes in bed levels. The black arrows indicate the direction and volume of the annual net sediment transport rates (increasing in width if the sediment transport increases) through each profile (grey dashed lines). The values are normalized by the highest sediment transport (corresponding to profile 5-9). A sediment budget is calculated by accounting for the amount of sediment incoming and leaving each control volume. Blue cells indicate a deficit (i.e., erosion) whereas red cells designate a surplus (i.e., sedimentation). Like the sediment transport arrows, the changes in volume are normalized by the highest volume change (cell 7-8-11-12).

Here, the littoral drift is directed east, as expected with a mean wave direction of ~186°N (and a shoreline orientation of 91°N) which results in an incident wave angle of ~5 degrees. Velocities through the inlet (residual flood velocities) induce flood directed residual transport causing a decrease in the longshore transport. Differences between profile 5-9 and 7-11 indicate that the bay traps half of the annual longshore sediment rate. Furthermore, the sediment budget indicates that the shoreline erodes and the import of material into the basin causes sedimentation. The control volumes are showing sedimentation offshore of the inlet indicate that ebb delta migrates towards the east.

Modeled suspended and bedload transport rates are in the same order of magnitude throughout the domain. Bedload transport rates (blue bars in Figure 4.4) are higher (than suspended rates) in the cross-shore direction, whereas suspended sediment rates (brown bars in Figure 4.4) are higher (than bedload rates) in the longshore direction. Most of the suspended sediment transport is driven by currents (10^{-4}-10^{-5} $m^3/s/m$), which follows the same direction as the depth-averaged velocities. Therefore, the annual residual current-driven suspended sediment transport is directed east (flood dominant) and shifts north at the corner of Chappaquiddick Island. The offshore transport on the profile from point 9 to 11 shows a southward shift owing to current bypass of the ebb-tidal delta.

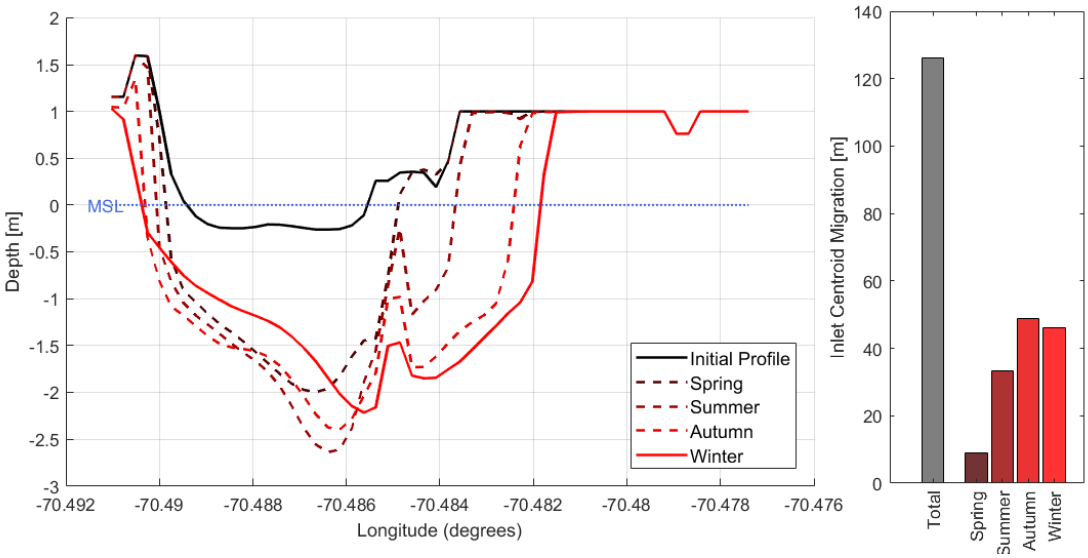

Figure 4.3. Katama inlet profile evolution throughout a year (PS simulation). The black line illustrates the initial condition and the red line denotes the inlet profile after one simulated year. Dashed-lines indicate the inlet profile for 25%, 50%, and 75% of the simulation time. The dotted blue line represents the mean sea level (MSL). On the right, the bar graph shows the inlet centroid migration (total and seasonal values).

Conversely, suspended sediment transport, primarily directed cross-shore owing to waves (which stir up the sediment in suspension), is an order of magnitude smaller (10^{-6} $m^3/s/m$) than bedload. These suspended loads shift slightly east due to wave obliqueness (5 degrees). Modeled bedload sediment transport owing to currents is on the same order of magnitude as the wave-driven fraction (10^{-5} $m^3/s/m$). Like the suspended fraction, the wave-related bedload has a cross-shore direction, whereas the current-related fraction is longshore directed (east).

Residual modeled transports through the inlet (and inside the bay) are flood-dominant. Most of the wave energy is dissipated (primarily owing to wave breaking) offshore of the inlet. Therefore, most of the transport in the inlet and the bay is due to currents. However, while the bedload and suspended fractions (owing to the currents) are even throughout the domain, the bedload fraction increases inside the bay relative to the surf zone.

Equation [4] shows the current-related friction coefficient implemented in the TRANSPOR2004 model (more detail in Appendix D). The depth is logarithmically inverse proportional to the friction. Therefore, the friction coefficient increases when the depth decreases inside the bay (~1 meter). This raises the instantaneous grain-related bed-shear stress ($\tau'_{b,cw,t}$), and hence the bed load fraction owing to currents.

$$f_c' = 0.24\left(\log\left(\frac{12h}{k_{s,grain}}\right)\right)^{-2} \qquad [4]$$

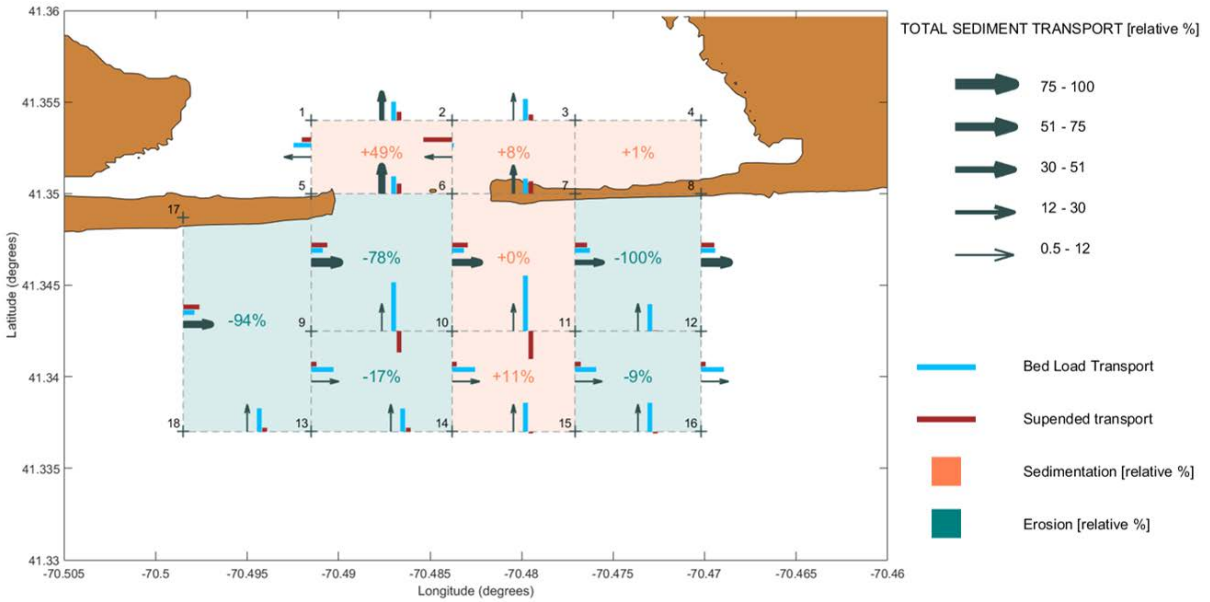

Figure 4.4. Sediment pathways analysis for the present state simulation. Black arrows represent the sediment transport through each profile (delimitated by crosses). The wider is the arrow; the bigger the sediment transport. The transport is divided into the bed load transport (blue bar) and suspended load transport (brown bar). Each cell (between four profiles) represent, a sediment budget, either erosion (teal color) or sedimentation (coral color). The shoreline position (brown surface) corresponds at the end of the simulated year.

4.2. Future State Simulations

We analyze six future state simulations by comparing them with the present state simulation. First, we discuss the changes on the hydrodynamics (wave conditions and depth-averaged velocities). Next, we analyze the impacts of the forcing changes on the morphodynamics.

4.2.1. Hydrodynamic Impacts

Figure 4.5 shows the changes in significant wave height (a and c), and mean wave direction (b and d) for the six future state simulations updrift (blue point in Figure 4.1) and downdrift (red point in Figure 4.1) of the inlet. SLR (purple markers) increases the significant wave heights from 0.5% (updrift) to 2.5% (downdrift) owing to raised water levels. There is no substantial impact on the wave heights and wave directions owing to changes in tidal constituents (yellow markers).

Clockwise changes in wave direction (+10ºN offshore and +5ºN nearshore) induce an increase in the annual averaged significant wave height of ~0.5% (blue markers), whereas anticlockwise changes (-10ºN offshore and -5% nearshore) produce a decrease of around 2% in the averaged wave heights (green markers). Simulations with all the forcing changes (FSK1 and FSK2) show a similar change in the nearshore wave direction at both points (-5ºN comparing with the PS simulation) either for clockwise and anticlockwise offshore changes in the wave direction. SLR reduces the energy dissipation along the shoals in front of Wasque Point, increasing the average wave height of the swell coming from the SE. Therefore, waves updrift the inlet have similar decreases in wave heights (~2%) than offshore, whereas wave heights downdrift of the inlet increase by 2-3% compared with the offshore changes.

Figure 4.6 illustrates the changes in depth-averaged velocities during ebb (c) and flood (d) produced by SLR. Simulations including SLR (FSK1, FSK2, and FSK5) result in higher velocities through the inlet, with currents penetrating more into the basin during flood (Figure 4.6d) and expanding offshore during ebb (Figure 4.6c). Furthermore, the implementation of SLR into the model induces changes in the flow separation. Figure 4.6c (ebb regime) shows a blue streak (representing velocity reduction) along the flow separation indicating an increase of the quiescent zone for the simulations that include SLR (simulation FSK5 in Figure 4.6). Contrarily, during flood the quiescent zone becomes smaller (red streak along flow separation in Figure 4.6d).

4.2.2. Morphodynamic Impacts

The inlet profile evolution is similar to the PS results for the simulation where SLR is not included. Figure 4.7 shows that these profiles migrate towards the east, becoming deeper in the east edge. In contrast, when SLR is included the inlet profiles are deeper (down to 2.7 meters), symmetric shaped (i.e., the centroid is in the middle of the inlet) and showing steeper inlet edges. When clockwise changes in wave direction, decrease of wave height, and SLR are combined the deepest point displaces towards the east, but the updrift edge has a milder slope, which decrease the inlet centroid migration. Therefore, the influence of the transverse bed-slope parameter in Delft3D on the slope of the inlet edges becomes important. Future work should focus on this parameter.

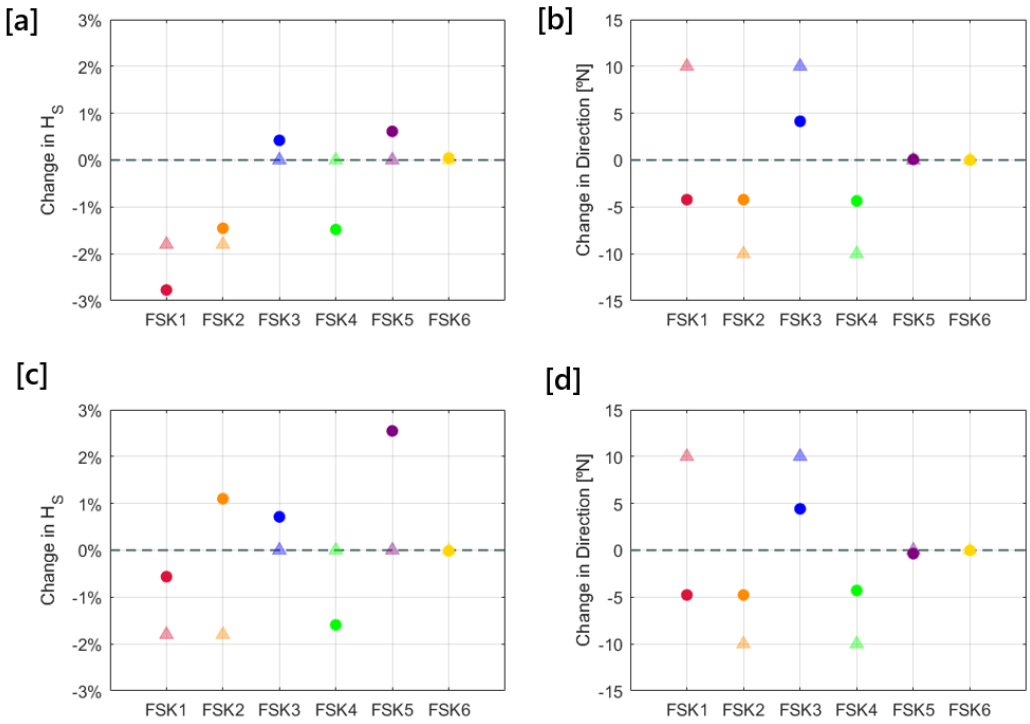

Simulation	$\Delta H_{F,}$	θ^+	θ^-	SLR	ΔTide
FSK1	x	x		x	x
FSK2	x		x	x	x
FSK3		x			
FSK4			x		
FSK5				x	x
FSK6					x

Figure 4.5. Changes in significant wave height (a and c) and mean wave direction (b and d) for future state simulations compared with present state simulation (grey-dashed line). Triangles indicate mean annual changes in the outermost boundaries, whereas dots show changes at the 5-meters water depth points analyzed in Figure 4.1 (updrift (a and c) and downdrift (b and d) of the inlet).

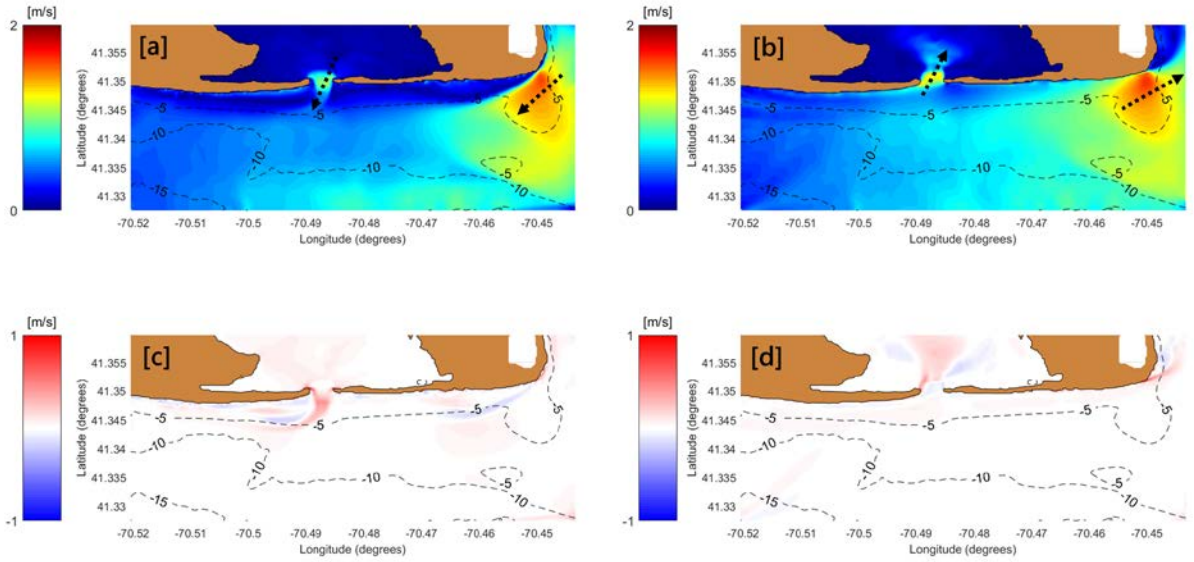

Figure 4.6. Changes in depth-averaged velocities for the FSK5 simulation (including SLR and changes in tidal constituents) during ebb (c) and flood (d) (scale bars on the left [m/s]) compared with the present state simulation during ebb (a) and flood (b).

Figure 4.8 illustrates the inlet centroid migration (a and c), and the downdrift barrier migration (b). Clockwise changes in wave direction (blue dots) induce the largest inlet migration for both; the centroid (140 meters), and the downdrift barrier (325 meters). Nonetheless, the inlet migration is less sensitive to anticlockwise changes in wave direction (green dots in Figure 4.8a and Figure 4.8b) owing primarily to the decrease in annual averaged wave heights (green dots in Figure 4.6a and Figure 4.6c). Changes in tidal constituents have a small impact on the inlet centroid migration (decreasing by 7 meters), and no impact on the downdrift barrier migration. Therefore, SLR (purple dots) is the main forcing reducing the inlet migration due to stronger currents (than present water levels) through the inlet (Figure 4.6c and Figure 4.6d) which reduce the wave-driven forcing along the inlet. When all the forcing changes are combined (simulations FSK1 and FSK2), the inlet centroid migrates at the same rate as the present state simulation. However, simulation FSK1 shows a wider profile (than present state simulation) with the deepest point located east balanced by a higher migration of the updrift barrier.

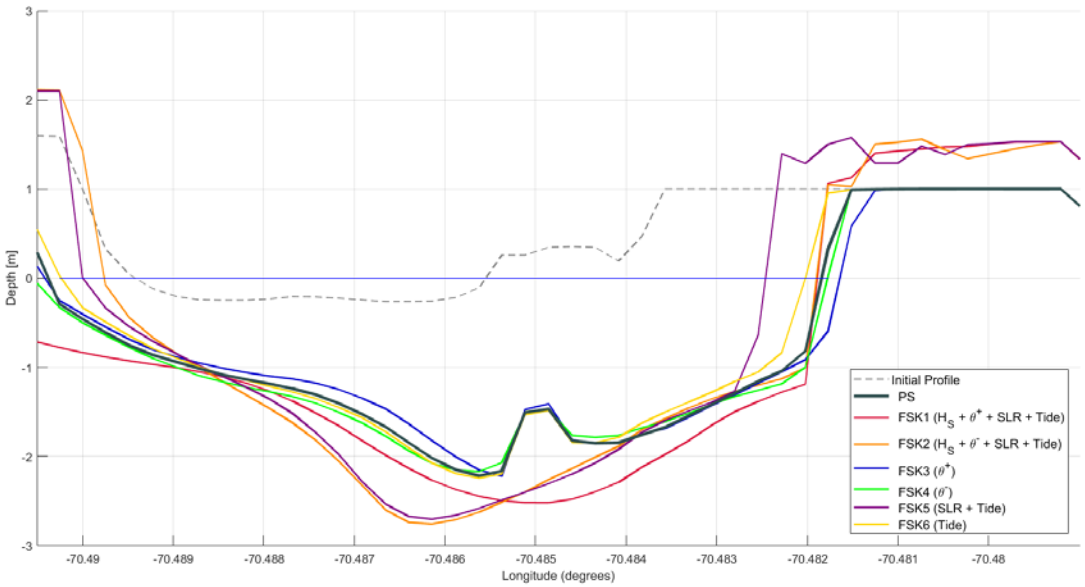

Figure 4.7. Inlet profile after the simulated year for the present state (black line) and the future state simulations (colored lines, a legend on the right). The grey-dashed line illustrates the initial profile.

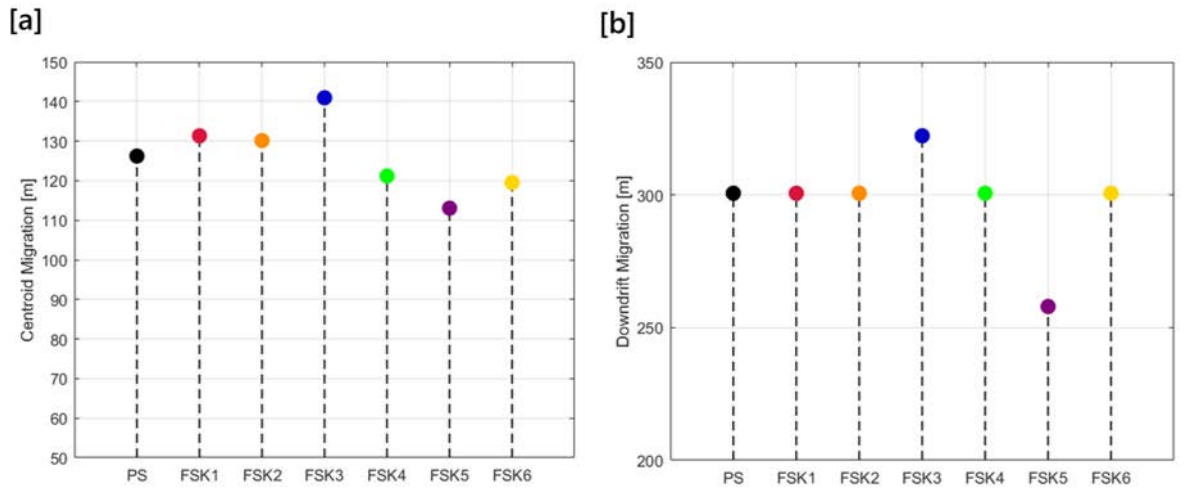

Figure 4.8. Longitudinal inlet centroid migration (a), and downdrift barrier migration (b) for the present state simulation (black markers) and future state simulations (colored lines and markers).

Here, the discussion focuses on the sediment transport changes through the inlet, inside the bay, and on the littoral drift first for the simulations with isolated forcing changes (FSK3, FSK4, FSK5, and FSK6), and then for the simulations with a combination of forcing changes (FSK1 and FSK2). Appendix F shows the sediment pathway figures for each of the future state simulations, which are then combined in Figure 4.9, Figure F.7, and Figure F.8 to illustrate the total sediment transport, the bedload sediment transport, and the suspended sediment transport respectively. A bar plot is drawn at each profile showing the annual transport rates for all the simulations. These values are normalized with respect to the highest transport value (like in Figure 4.4), being the transport larger where the grey bar is wider.

The most significant impact on the sediment pathways is by SLR, whereas changes in tidal phases and amplitudes do not have a significant impact in any of the transports throughout the domain (see Figure 4.9). SLR (purple bars) increases the total sediment transport through the inlet by 12% (compared with the PS simulation). Here, suspended sediment transport increases by 50% (see Figure F.7) owing to a increase in the depth-averaged velocities (Figure 4.6). However, the bedload transport decreases by a 10% due to a higher water-depth (i.e., reducing the current-related friction coefficient (Equation [4])). This leads to a decrease of the instantaneous grain-related bed-shear stress ($\tau'_{b,cw,t}$), and hence smaller (than in PS simulation) current-driven bedload sediment transport.

Clockwise changes in wave direction lead to higher waves propagating through the inlet (very shallow waters), increasing the wave skewness. Therefore, the forward orbital velocities are larger, affecting the term $U^4_{\delta,for} - U^4_{\delta,back}$ used in the wave-driven suspended transport equation in the TRANSPOR2004 model (detailed information in Appendix D). This increases the wave-driven suspended transport through the inlet by 10% with respect to the PS simulation. The bedload transport does not change (similar depth-averaged velocities) leading to a total transport change of ~5%. Contrary, anticlockwise changes in wave direction (green bars) lead to a 7% reduction of the suspended sediment transport (or ~3% reduction of the total transport) through the inlet owing to smaller forward-orbital velocities than the PS simulation.

Simulations FSK1 and FSK2 produce an increase of ~5% of the sediment transport through the inlet, which is smaller than the SLR-driven change. This is primarily owing to a decrease in wave heights around the inlet (Figure 4.5). Therefore, the current-related bedload transport increases, whereas the wave-driven suspended transport decreases.

The bay import is quantified as the sum of the profiles from points 5 to 1, 1 to 2, and 2 to 3. There is no apparent impact on this transport owing to changes in wave direction (either clockwise or anticlockwise). Wave energy rapidly dissipates when waves reach the bay because of the shallow bathymetry. Nevertheless, SLR increases significantly (~40%) the sediment transport (both suspended and bedload) into the bay due to an expansion of the flood velocities throughout the bay (Figure 4.6c). Simulations FSK1 and FSK2 show a similar increase in the wave import transports (~50%) than the SLR-driven one, which indicates than SLR is the primary forcing affecting the sediment import on the bay.

The modeled littoral drift increases owing to clockwise changes in wave direction (blue bars in Figure 4.9), whereas it decreases when anticlockwise changes are implemented (green bars in Figure 4.9). SLR increases the littoral drift updrift the inlet (owing to an increase of the flood velocities), but it decreases downdrift of the inlet due to the increase of sediment trapped by the bay. Here, the influence of the inlet on the littoral drift is quantified by analyzing the difference in transport between the longshore updrift (profile from point 5 to 13) and downdrift (profile from point 7 to 15) of the inlet. Overall, the bay traps more suspended sediment than bedload sediment (i.e., expecting finer material inside the bay than in the nearshore barrier). The longshore suspended sediment transport downdrift of the inlet reduces by ~70% on the simulations including SLR and by ~60% on simulations without SLR. The bedload sediment transport decreases by a 25% for simulations without SLR and 35% for simulations with SLR. This leads to a littoral drift reduction of a 45% for simulations that not include SLR and of 55% for simulations with SLR.

The profile from point 9 to 10 is used as a qualitative indicator of the ebb-tidal delta migration (which migrates east for all the simulations). If the transport is higher than in the PS simulation, it indicates less flux resistance, which means that the ebb delta is migrating faster (than the PS simulation) towards the east, whereas if the transport is smaller (i.e., biggest flux resistance) the ebb-tidal delta is migrating slower than the PS simulation. SLR and anticlockwise changes in wave direction produce a smaller (than PS simulation) ebb-tidal delta migration. Contrary, clockwise changes in wave direction cause the ebb-tidal delta to migrate faster towards the east. The decrease in wave heights combined with SLR in simulations FSK1 and FSK2 cause the most substantial decrease in the ebb-tidal migration.

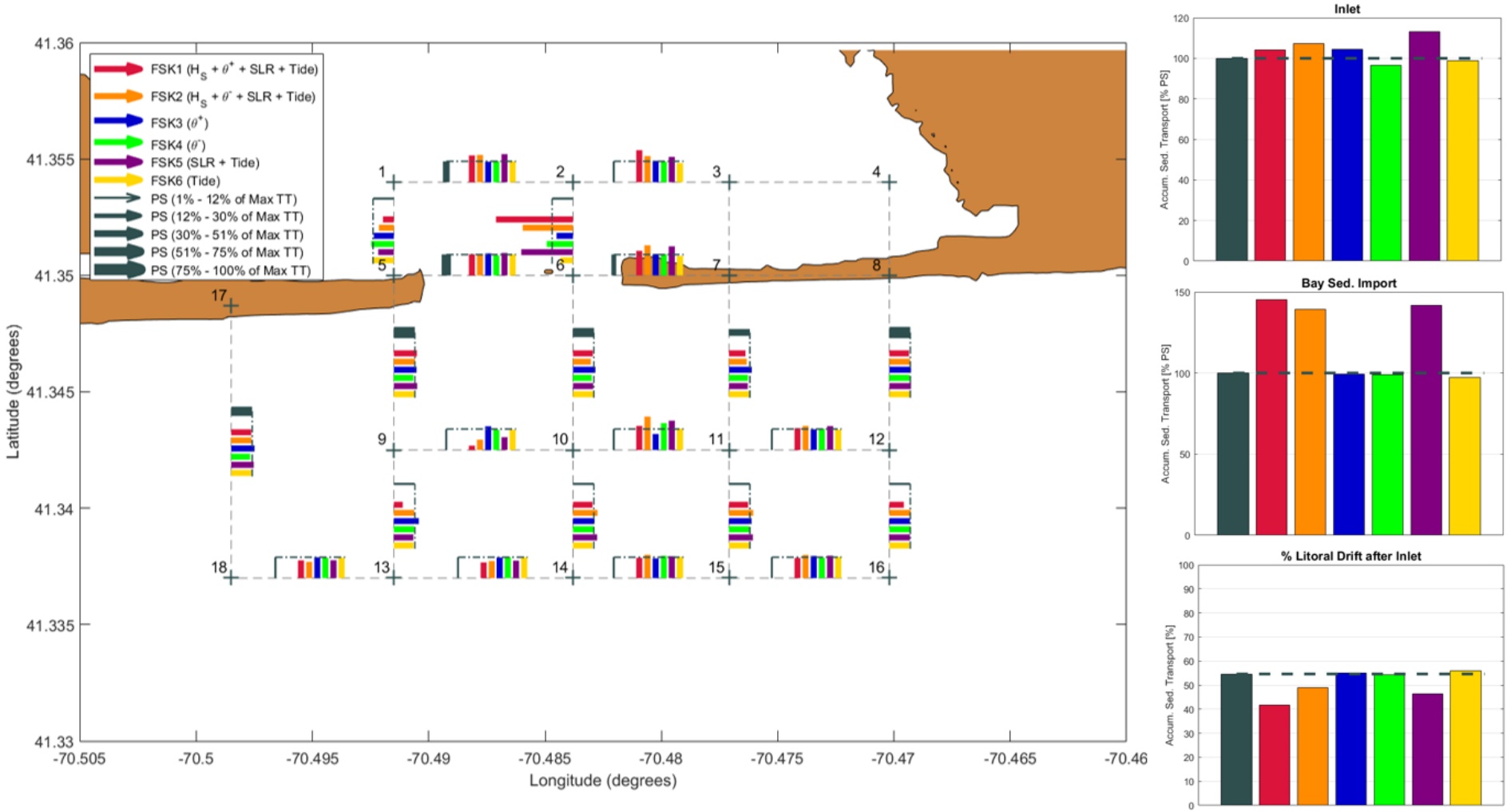

Figure 4.9. Accumulated total sediment transport map. Grey dashed lines show the output profiles from Delft3D labeled between numbers on grey crosses. At each profile, a bar plot shows the year cumulative sediment transport for all the scenarios. Grey bars (present state simulation) are wider when the sediment transport is larger (percentage of the maximum total transport (TT) in the legend). The dashed-dotted lines indicate the value for the present state to highlight the comparison with other simulation. On the right, three bar plots illustrate the inlet profile accumulated transport (top), the sum of the profiles 1-2, 2-3 and 3-5 (i.e., the sediment intrusion into the bay) (middle), and the bypassing fraction (the difference between profiles 5-13 and 7-15) (bottom).

CHAPTER 5. ST. LUCIA RESULTS

CHAPTER SUMMARY

This chapter contains the Santa Lucia Estuary results analysis. First, we evaluate the present state simulation to understand the system behavior, analyzing the hydrodynamics (wave heights, wave directions, currents) and the morphodynamics (cumulative erosion/sedimentation patterns, inlet profile section development, barrier migration, inlet centroid migration, and sediment pathways). Finally, we compare the present state results with the future state simulations (Table 3.4), focusing on the inlet migration and the sediment pathways analysis.

5.1. Present State Simulation

The model operates with the specifications previously explained in Chapter 3.2.2 and the wave boundary conditions obtained in Chapter 3.1. A model run takes 36 days and 12 hours to for a year, starting the 1st of September (beginning of spring) and finishing the 31st of August (end of winter).

5.1.1. Hydrodynamic Results

Like Katama Bay, we need an understanding of the hydrodynamics (e.g., changes in wave heights, wave directions, flows through the inlet and surroundings) to contextualize the morphodynamics. Here, Figure 5.1 shows the significant wave heights (b) and mean wave directions (d) of two points in 5-meter depth; one south of the inlet (red colored) and the other north of the inlet (blue colored). Contrary to Katama Bay, Santa Lucia has a more homogenous wave distribution throughout the domain, and hence significant wave heights are similar ($\overline{H_S}$~1.4 m) on both sides of the inlet (Figure 5.1b). Nevertheless, waves refract more in the southern region of the domain than in the northern region owing to a less shore parallel bathymetry throughout the south region. Therefore, waves are more oblique in the north ($\overline{\theta_m}$=118ºN) than in the south ($\overline{\theta_m}$=113ºN) (see Figure 5.1d).

The harmonic tidal forcing implemented in Delft3D (M2 component with an amplitude of 65 cm) induces currents up to 1.5 m/s through the inlet (Figure 5.6). Tides travel from south to north, and there is an average tidal prism of 1.32x10^{6}m^3. The river discharge plays an important role in determining the behavior of the inlet (Hoek 2017). Here, the 30 m^3/s discharge maintains the residual flow directed seawards through the inlet, but during drought seasons (small or zero river discharge) the estuary shows flood-dominant behavior (Table 2.1).

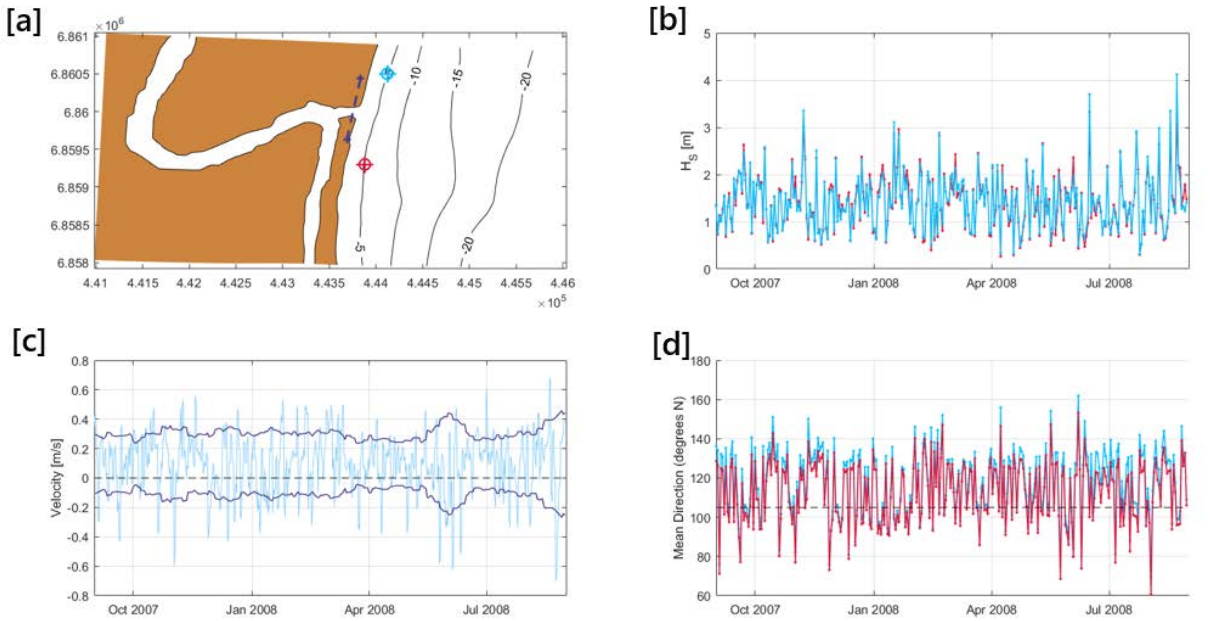

Figure 5.1. Hydrodynamic results at Santa Lucia. Red and blue markers (a) are wave climate sample points at 5-meter water depth. [b] and [d] illustrate the significant wave heights and mean wave directions, respectively, for the markers present in [a]. [c] shows the mean depth-averaged velocity (seaward positive) along the profile drawn in [a] (blue dashed line). The dark blue line in [d] is an RMS-envelope obtained from the mean depth-averaged velocity signal (light blue line). The dashed-line in [d] shows the waves parallel to the shoreline.

Figure 5.1c illustrates the mean depth-averaged velocity (seaward positive) along the inlet region for a year. Tidal and river forcings are constant throughout the simulation, and hence variations in depth-averaged velocities are due to changes in inlet dimensions (e.g., length, width, and depth). When the inlet cross-section increases, the mean depth-averaged velocity decreases, and vice versa. The residual depth-averaged velocity in Figure 4.1c is positive. Therefore, the inlet has an ebb-dominant behavior, with erosion expected in the basin and deposition predicted in the nearshore region.

5.1.2. Morphodynamic results

Figure 5.2 shows the resulting modeled morphological development in terms of bed level change and cumulative erosion/ sedimentation patterns. The first column corresponds to the isolated bed level changes for each season (in the following order; spring, summer, autumn, and winter), and the right column shows the accumulated bed level changes at the end of each season.

During spring (Figure 5.2a) the inlet erodes, leading to the formation of channels inside the estuary and sedimentation on the flats. The sediment carried by the river is mostly deposited outside the estuary (along the updrift shoreline and the surf zone north and south of the inlet). The wave climate is bimodal (Figure 3.2) with two predominant swells (northeasterly and southeasterly) whose dominance varies throughout the seasons (Figure B.11, Figure B.12, Figure B.13, and Figure B.14 in Appendix B), encouraging a seasonal behavior to the morphodynamics.

During summer, wave climate bimodality forms two ebb-tidal lobes in the nearshore inlet region (Figure 5.2b). Where the inlet discharge meets the open sea, it shifts direction towards north or south depending on the predominant wave direction. Figure 5.2b shows a larger migration of the southern ebb-delta (than the northern ebb-delta) owing to north-easterly swell. The inlet becomes deeper and larger due to a less energetic summer wave climate (compared with other seasons).

During fall, both swell directions occur at similar rates (Figure B.13), so the northern ebb-delta migrates offshore and fills the bathymetry irregularities whereas the southern ebb-delta migrates south and diffuses (Figure 5.2c). Meanwhile, the inlet becomes narrower and deeper in the northern side.

Finally, the most energetic winter wave climate with the most significant presence of southeasterly swell washes out the southern ebb-delta and displaces river sediment discharge towards the barriers (Figure 5.2d). The inlet becomes wider and shallower in the northern side reducing the velocities through the inlet and hence, making the inlet shorter.

Figure 5.3 shows the longitudinal migration (Y UTM component) of the inlet profile. The inlet migration is towards the north owing to overall dominance off southeasterly swell. Most of the migration (~80%) occurs during the first quarter of the simulation. Later, the inlet becomes deeper (down to 6 meters), and finally (during winter) wider (from 100 to 150 meters). Therefore, the migration of the southern barrier is primarily during spring whereas the northern barrier migration is distributed throughout the year.

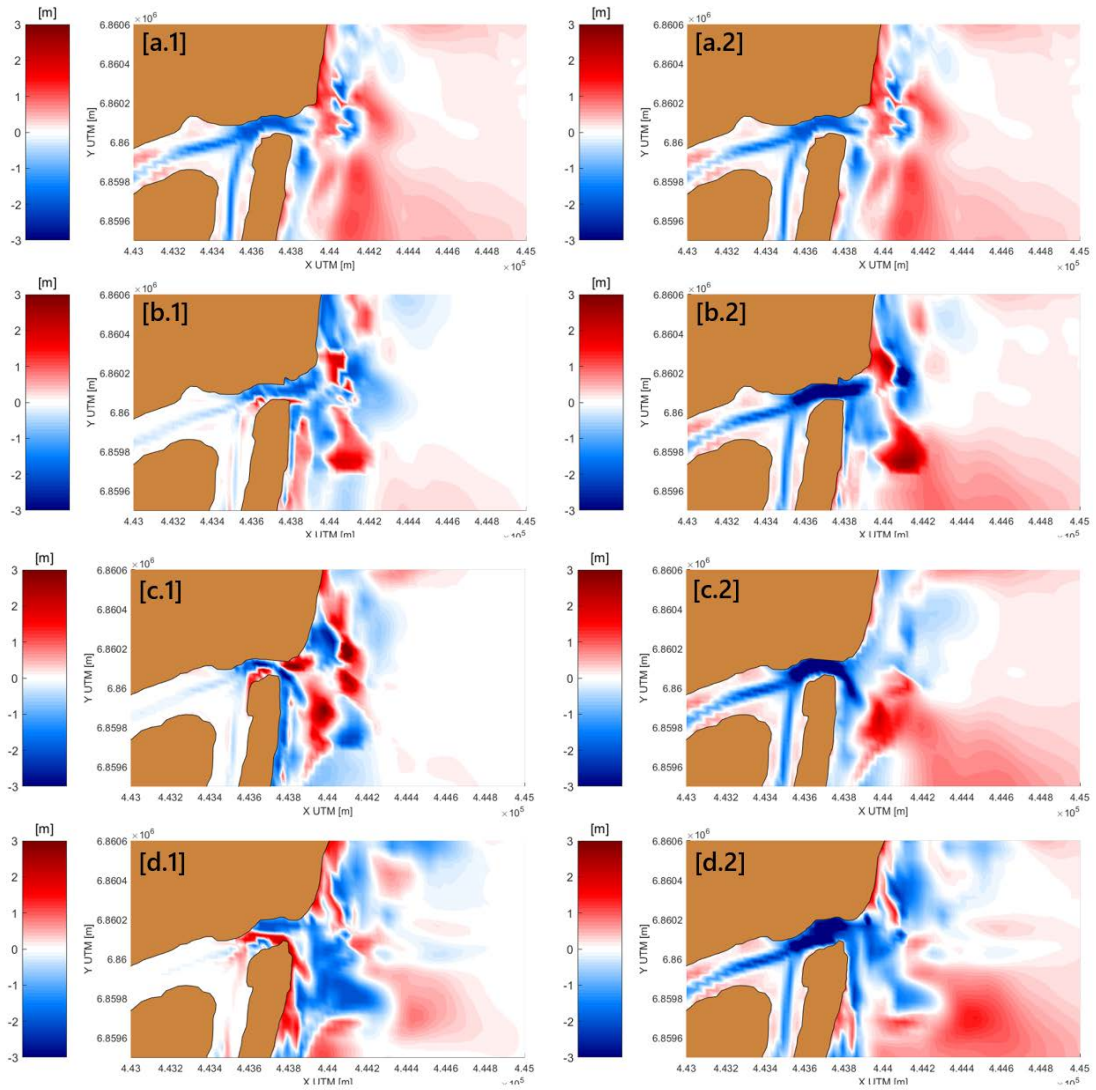

Figure 5.2. Erosion and sedimentation patterns of the present state simulation at Santa Lucia Inlet Region. The left column shows the changes in bed level of each isolated season (in the following order; spring, summer, autumn, and winter). Right column illustrates the accumulated changes during the year. Red colors indicate sedimentation, whereas blue colors are showing erosion.

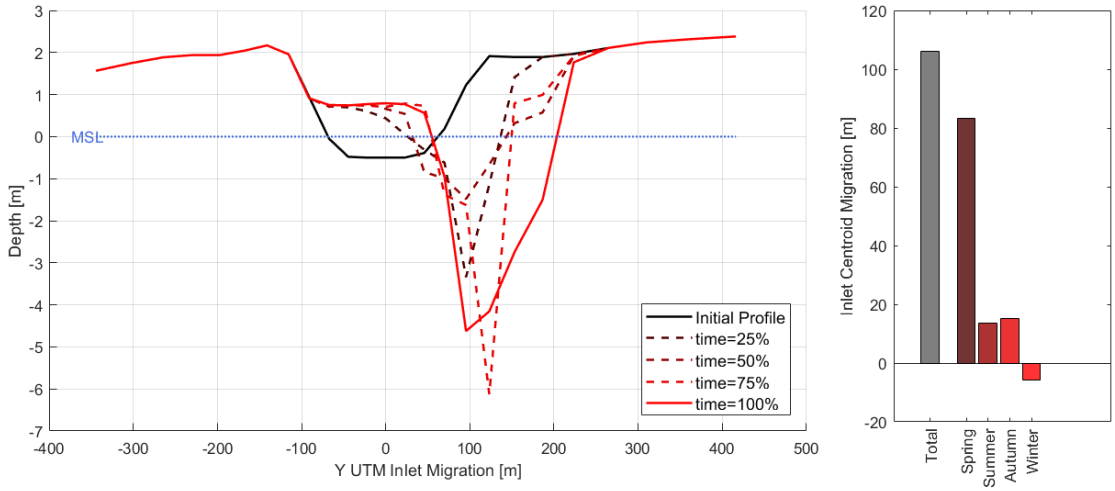

Figure 5.3. Santa Lucia Inlet profile evolution throughout a year (PS simulation). The black line illustrates the initial condition and the red line denotes the inlet profile after one simulated year. Dashed-lines indicate the inlet profile for 25%, 50%, and 75% of the simulation time. The dotted blue line represents the mean sea level (MSL). On the right, the bar graph shows the inlet centroid migration (total and seasonal values).

We use the same approach as in Katama Bay for a qualitative sediment pathways analysis (Figure 5.4), where sediment transport values (grey arrows) are normalized by the highest sediment transport (corresponding to the profile from point 13 to point 14). The volume change in the cells is also normalized by the highest control volume change (cell 1-5-21-22).

For the present state simulation, the littoral drift (~400,000 m^3/year) has a northerly direction owing to the averaged mean wave direction (~115ºN), and the tidal-driven current direction (towards the north). The estuary is ebb-dominant (i.e., the residual sediment transport through the inlet is seaward directed) leading to erosion in the estuary (25,400 m^3/year) and sedimentation nearshore. Moreover, the major fraction of the total sediment transport is suspended due to the small grain size (200µm) used in the process-based model.

The residual bedload transport in the cross-shore profiles (profiles from point 2 to 14 in Figure 5.4) is owing to waves pushing sand bars onshore (blue bars in Figure 5.4), whereas the residual suspended transport (offshore) is owing to currents bypassing the offshore discharge generated by the tidal inlet. The residual longshore transport is directed north. When waves break, they stir up material that is moved towards the north by tidal currents and wave-driven currents.

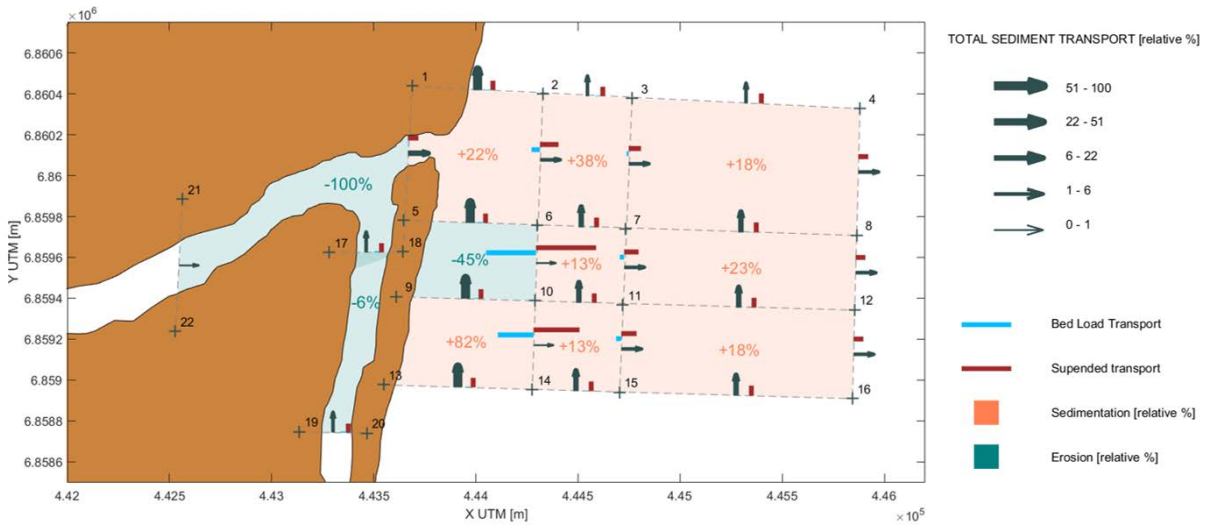

Figure 5.4 Sediment pathways analysis for the PS simulation. Grey arrows represent the sediment transport through each profile (delimitated by crosses). The wider the arrow; the larger the sediment transport relative to the biggest transport (legend on the right). The transport is divided into the bed load transport (blue bars) and suspended load transport (brown bars). Both transport loads use a scale of 0.5 relative to the total transport for better visualization. Each cell (between four profiles) represent a sediment budget, either erosion (teal color) or sedimentation (coral color). The shoreline position (brown surface) corresponds to the end of the simulated year.

5.2. Future State Simulations

We analyze six future state simulations by comparing with the present state simulation. First, we discuss the changes in the hydrodynamics (wave conditions and depth-averaged velocities). Next, we analyze the changes in impacts of the forcing on the morphodynamics.

5.2.1. Hydrodynamic Impacts

Figure 5.5 shows the changes in wave height and wave direction for the two points analyzed in Figure 5.1. Clockwise changes in wave direction at the offshore boundaries (simulation FSSL1 and FSSL3) are neutralized nearshore, where there is no effective change in the mean direction (b and d in Figure 5.5), but they lead to a decrease of >5% in the wave heights on both sides of the inlet. Southeasterly swell has a predominant direction of 190ºN (Figure 3.2), so increasing it by 10ºN enhances the refraction. Waves have to refract more dissipating more wave energy and hence decreasing the wave heights. In contrast, simulations (FSSL2 and FSSL4) with anticlockwise wave direction changes show a -5ºN wave angle swing in the nearshore and an increase >5% in nearshore significant wave height. This is due to the bimodality of the wave climate. The north-easterly swell has a predominant direction of 90ºN and if the angle increases by 10ºN the refraction decreases owing to a shore parallel bathymetry with parallel waves.

SLR (simulation FSSL5) and changes in river discharge (simulation FSSL6) do not alter the wave proprieties (wave direction and significant wave height) at the analyzed points. Nonetheless, SLR moves the wave breaking onshore and causes more wave intrusion into the inlet. Similarly, a decrease in river flow reduces the ebb-peak flows, and hence the wave-breaking owing to wave-blocking is moved onshore.

Simulations with all the forcing changes (FSSL1 and FSSL2) show similar results to those with wave direction changes only. The wave heights are smaller due to a decrease in the wave height of the offshore boundary conditions. Simulation FSSL1 (red markers in Figure 5.5) has the most significant decrease in average wave heights at the analyzed points (10% respect the PS simulation), whereas simulation FSSL2 (orange markers in Figure 5.5) shows small increases in average wave heights at both points (~3%).

SLR makes the inlet wider increasing inlet discharge through it. As such, the tidal prism increases by 18% (P_{SLR}=1.55x10^6 m^3) and the inlet exhibits flood-dominant behavior. Figure 5.6 shows the SLR-driven changes in the depth-averaged velocities throughout the inlet domain. With a broader inlet than in the PS simulation, the depth-averaged velocities during ebb (a) and flood (b) are higher in the southern edge and smaller in the northern edge.

5.2.2. Morphodynamic Impacts

Figure 5.7 shows the resulting inlet profiles for the simulations with SLR (top), and without SLR (bottom). The inlet migration is most sensitive to wave direction changes. The profile is similar to the present state simulation for clockwise changes of the wave direction (blue and red profiles), whereas the migration shifts direction for anticlockwise changes in wave direction (green and orange profiles).

The inclusion of SLR makes the inlet shallower and broader than in the PS simulation owing to enhanced intrusion of waves into the inlet that push material in it. The widening of the inlet changes the velocity patterns, moving the most prominent depth-averaged velocities towards the southern edge (Figure 5.6), and hence, shifting the migration towards the south.

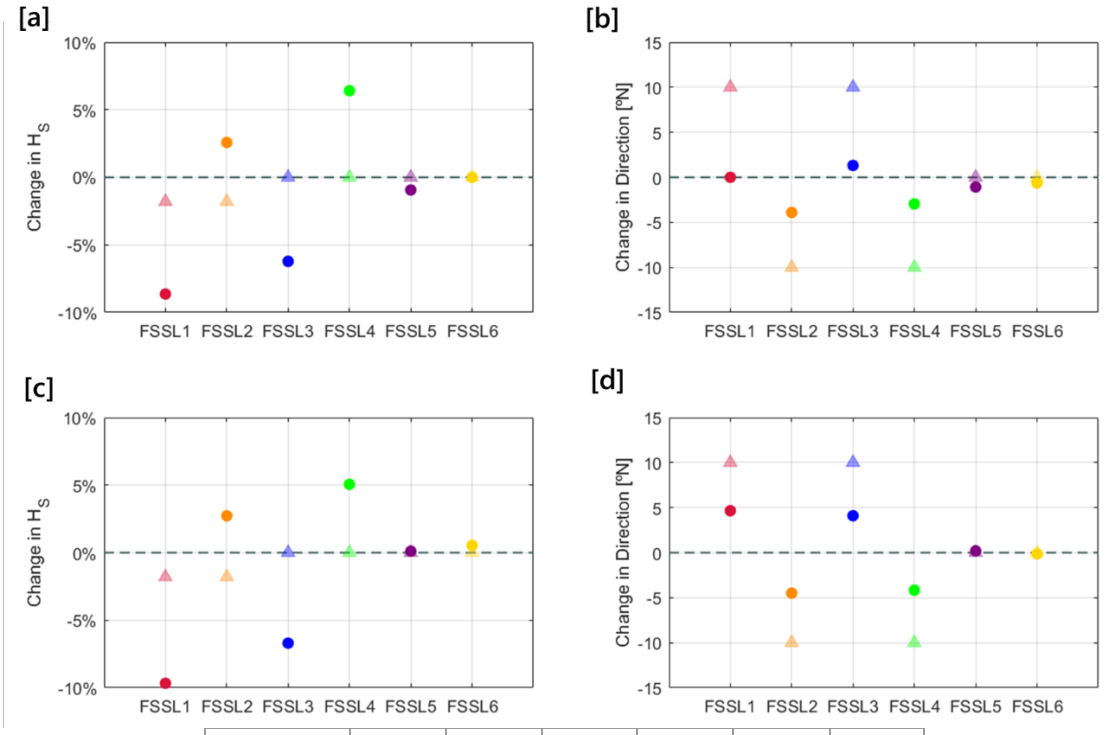

Simulation	ΔH_F,	ΔT_P	θ^+	θ^-	SLR	Q_F
FSSL1	x	x	x		x	x
FSSL2	x	x		x	x	x
FSSL3			x			
FSSL4				x		
FSSL5					x	
FSSL6						x

Figure 5.5. Changes in significant wave height (a and c) and mean wave direction (b and d) for future state simulations compared with present state simulation (grey-dashed line). Triangles indicate the mean annual changes in the outermost boundaries, whereas circles show changes at 5-meters water-depth points analyzed in the south of the inlet (a and b) and north of the inlet (c and d).

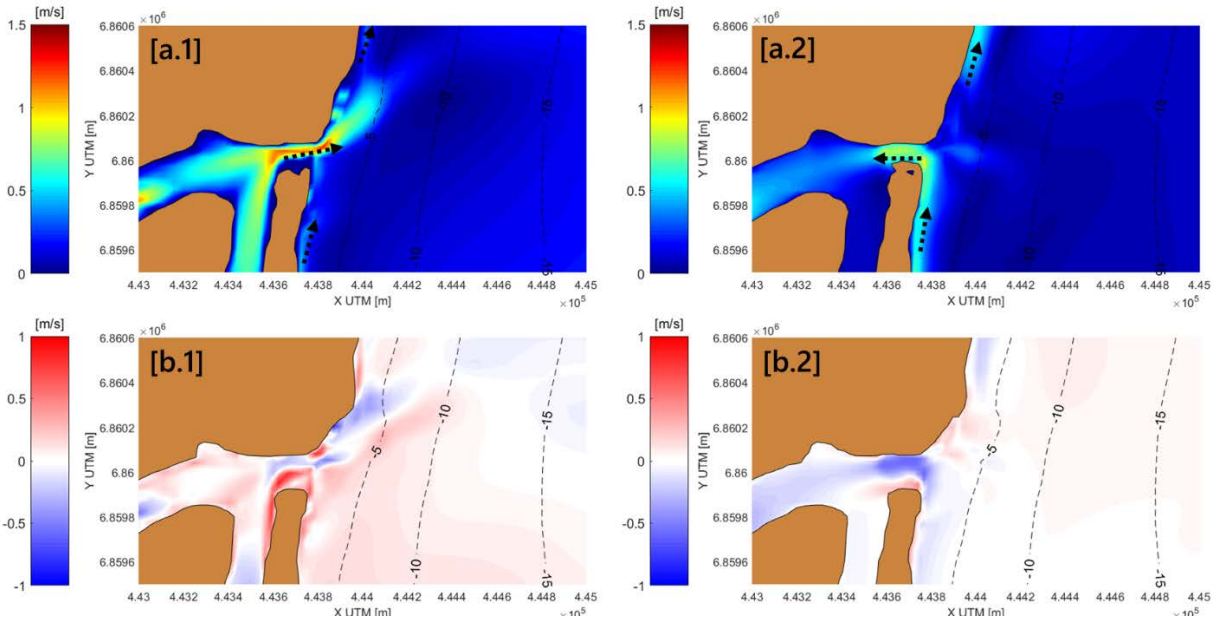

Figure 5.6. Changes in depth-averaged velocities for the FSSL5 simulation (including SLR) during ebb (b.1) and flood (b.2) (scale bars on the left [m/s]) compared with the present state simulation (a.1 and a.2).

Figure 5.8 shows the migration of the inlet centroid (a), the south barrier migration (b), and the north barrier migration (c). The modeled system is dynamic, and hence the migration rates vary on position and direction throughout the simulation. To evaluate this, Figure 5.8 shows the position of the initial (crosses), final (dots), and extreme (triangles) migrations throughout the simulation.

The centroid and barriers migrations are similar within each simulation. Anticlockwise changes in wave direction (green markers) shift the direction of the inlet migration. Here, the centroid and the barriers migrate around 100 meters. In contrast, if there is a clockwise change in the wave direction the migration is directed north with a similar rate than the present state simulation (105 meters) (i.e., increases in wave height compensate the clockwise change in wave direction).

SLR also shifts the inlet migration; the centroid and the north barrier migrate 75 and 100 meters towards the south respectively, whereas the south barrier remains in the same position. Simulations with SLR show considerable variability of the inlet migration throughout the year suggesting that the system becomes more dynamic than simulations without SLR (i.e., is further away from the equilibrium position). This is even more visible in the simulation with all the forcing changes (red and orange markers in Figure 5.8), where the range of migration of the three features is around 300 meters. Simulation FSSL1 presents the most significant migration towards the north; the centroid migrates 130 meters, the south barrier 160 meters, and the north barrier 105 meters. Simulation FSSL2 shows the most significant migration towards the south; the centroid migrates 200 meters, the south barrier 180 meters, and the north barrier 210 meters.

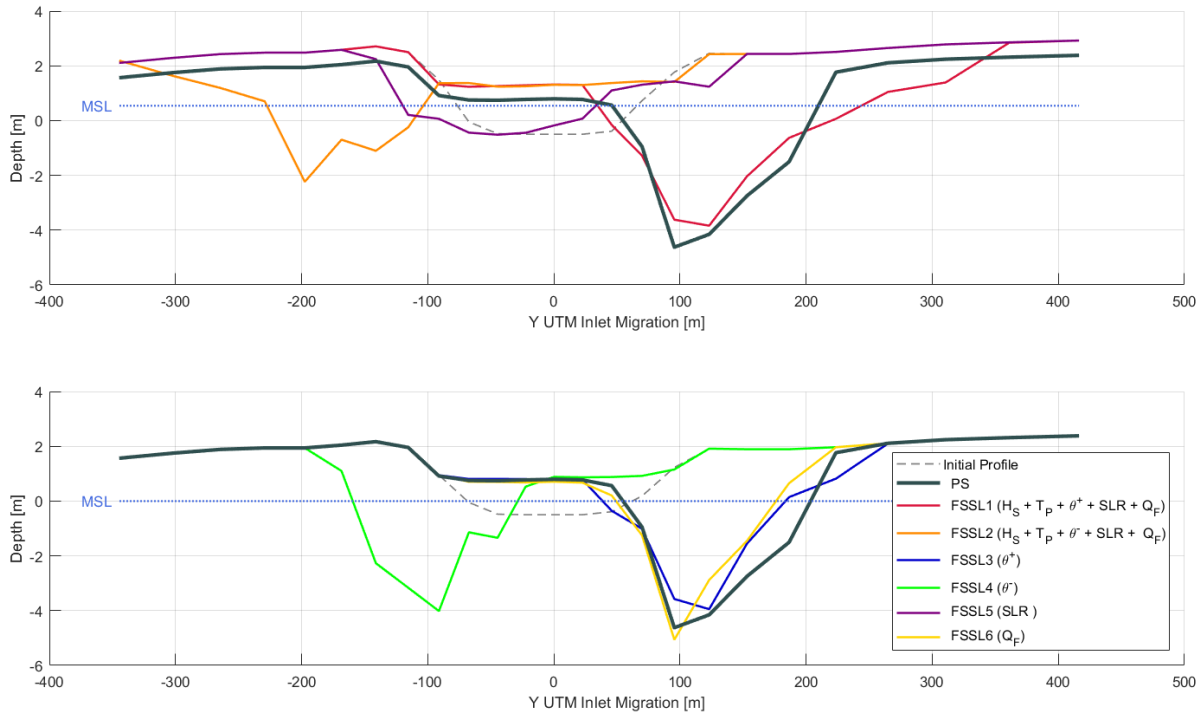

Figure 5.7. Santa Lucia Inlet profile after the simulated year for the present state (black line) and the future state simulations including SLR (top) or without SLR (bottom) (colored lines, a legend on the right). The grey-dashed lines illustrate the initial profile position.

Figure 5.9 illustrates the littoral drift (towards the north) for the PS and the future state simulations. SLR (purple bars) reduces the littoral drift in the north side of the domain by 14% owing to a decrease of the tidal-driven currents in the surf zone and an increase of sediment demand in the estuary. SLR also increases the depth-averaged velocities in the south area of the domain inducing a stronger (than in PS simulation) littoral drift northward. Clockwise changes in wave direction (blue bars) produce a decrease in the littoral drift owing to smaller (than in PS simulation) wave heights (Figure 5.5), whereas anticlockwise changes (green bars) increase the littoral drift by ~15%.

Moreover, a decrease in river discharge (yellow bars) reduces slightly (~5%) the littoral drift throughout the domain as less material is available to be transported by currents and waves. Simulations with all the forcing changes (red and orange bars) show a significant reduction (~20%) of the longshore transport updrift the inlet. Orange bars (simulation FSSL2) have a slightly smaller reduction owing to the increase in wave height due to anticlockwise changes in the direction.

Figure 5.8d shows the Bruun stability criterion (r), explained in Chapter 2, to be the ratio between the tidal prism and the annual littoral drift. Overall, the inlet can be classified as a seasonally open inlet (Type 3) as the stability criterion is smaller than 5 for all the simulations (Duong et al. 2016). For the present state simulation, the Bruun stability criterion is 3.4. SLR increases the stability of the inlet owing to the increase in the tidal prism. Conversely, anticlockwise changes in wave direction (green dots) makes the inlet more unstable (r = 2.6) owing to littoral drift increase. Simulation FSSL1 (including all forcing changes with clockwise changes in wave direction) is the more stable simulation (r=4.6), whereas simulation FSSL2 (including all forcing changes with clockwise changes in wave direction) presents similar stability to the PS simulation.

Here, the discussion focuses on the sediment transport changes through the inlet, inside the bay, and in the nearshore, first for the simulations with isolated forcing changes (FSSL3, FSSL4, FSSL5, and FSSL6), and then for the simulations with a combination of forcing changes (FSSL1 and FSSL2). Appendix G shows the sediment pathway figures for each of the future state simulations, which are then combined in Figure 5.10, Figure G.7, and Figure G.8 to illustrate the total sediment transport, the bedload sediment transport, and the suspended sediment transport respectively. The same methodology as used with Katama Bay is used here to plot these figures.

The most significant impact on the sediment pathways is owing to SLR (purple bars in Figure 5.10), which changes the inlet behavior from ebb-dominant to a zero residual sediment transport through the inlet. The tidal prism increases, and the tidal signal becomes symmetric. Tidal currents make the inlet flood-dominated, but river discharge preserves the symmetry of the discharge signal. Therefore, during drought seasons (mean annual discharge<5m^3/s) the estuary is flood-dominated.

Most of the transport through the inlet is suspended and moved by currents. The residual suspended transport (which is seaward directed) reduces by half due to SLR (purple bars in Figure G.8) owing to the discharge increase in the flood direction. Alternatively, the bedload transport (which is landward

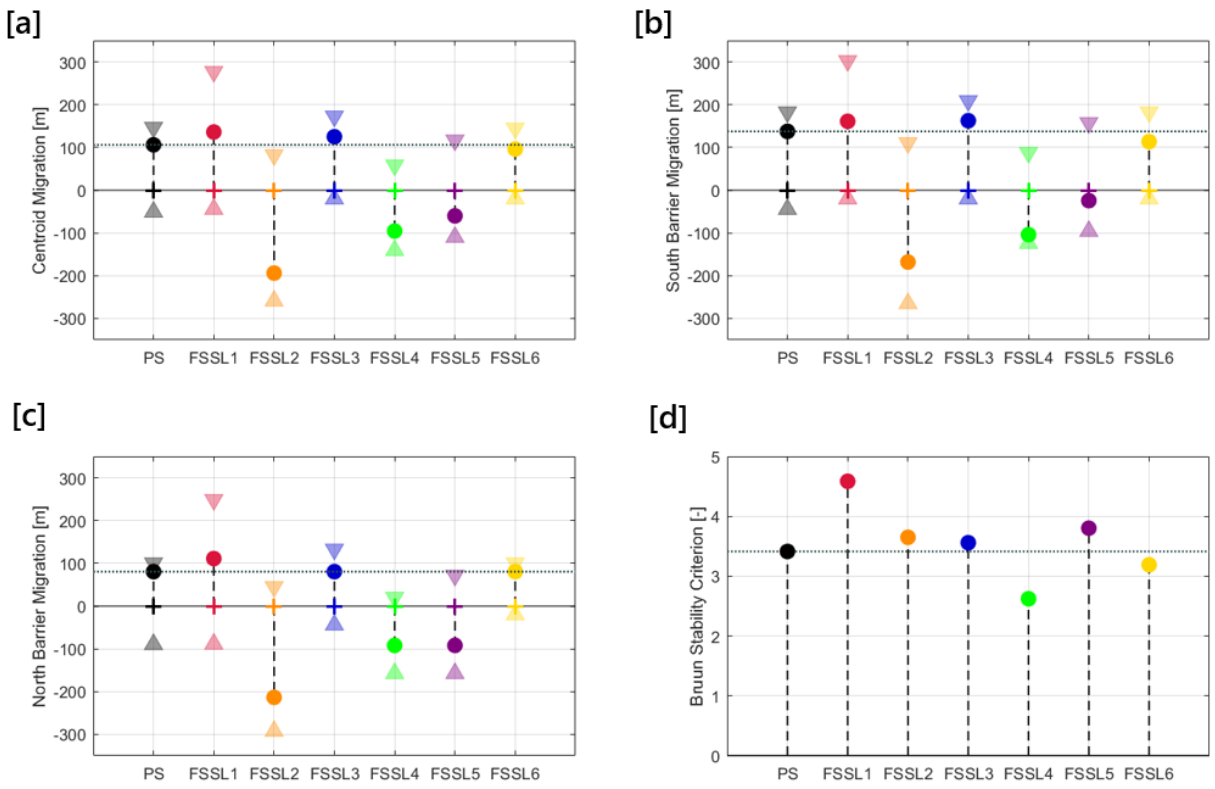

Figure 5.8. Inlet centroid migration (a), southern (downdrift) barrier migration (b), northern (updrift) barrier migration (c), and Bruun stability parameter (d) for the present state simulation (black markers) and future state simulations (colored lines and markers). Dots illustrates the final position, crosses indicate the initial position, and triangles show the maximum and minimum values for the migration of each feature.

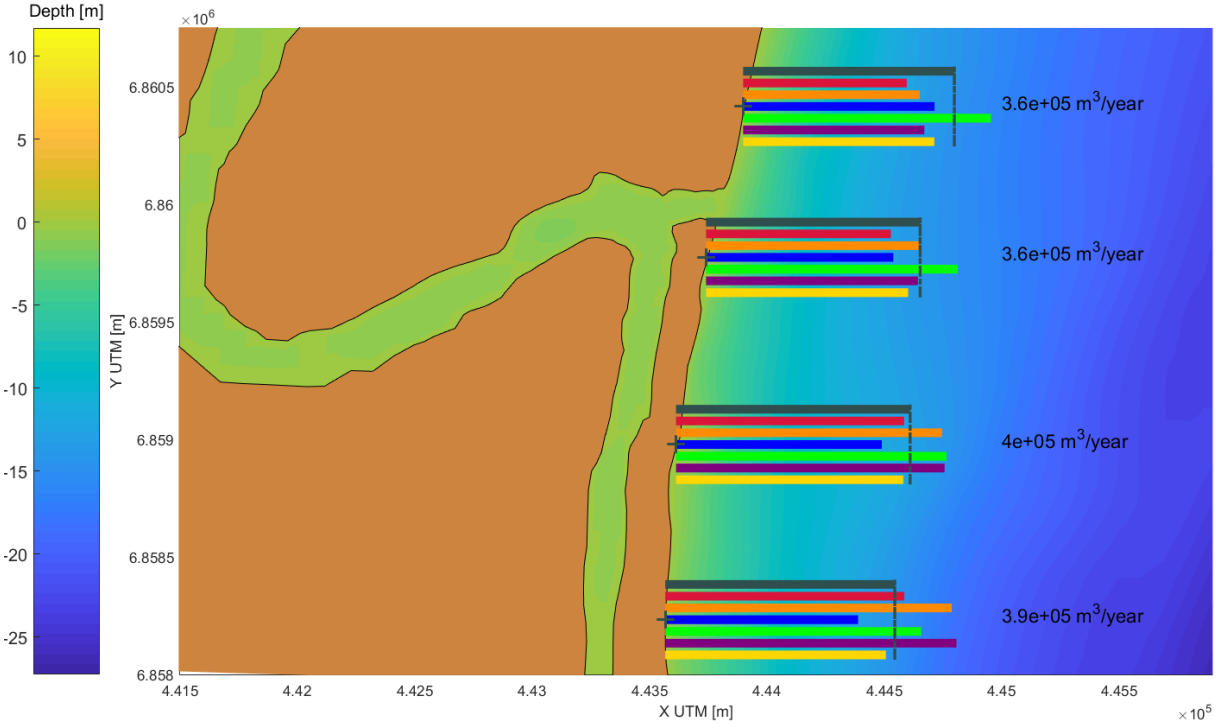

Figure 5.9. Littoral drift along the shoreline for the PS simulation (grey bars) and future state simulations. Numbers on the right are the littoral drift for the PS simulation. The shoreline position (brown shape) corresponds to the PS simulation position after a year.

directed) increases by 1300% for simulation FSSL5, and hence become relatively more significant to the total. SLR simulations have broader and shallower inlet profiles which allow a more significant discharge but smaller water depth.

Here, TR1993 (van Rijn 1993) is used to calculate the morphodynamics, which integrates the same equation (Equation [4]) as the TRANSPOR2004 model to calculate the current-related friction coefficient. Water depths through the inlet are smaller for simulations including SLR (i.e., reducing the current-related friction coefficient). This leads to a decrease of the instantaneous grain-related bed-shear stress ($\tau'_{b,cw,t}$), and hence smaller (than in PS simulation) current-driven bedload sediment transport.

Changes in wave directions (blue and green bars in Figure 5.10) have no substantial impact on the transport through the inlet owing to the small wave-driven transport fraction on the estuary. Nonetheless, when SLR is included (i.e., wave penetration into the estuary is higher), changes in wave direction affect the transport through the inlet. Clockwise changes in wave direction lead to less oblique waves which penetrate further into the estuary generating larger transport loads.

Changes (reduction) in river-discharge reduce the transport by a 20%. Therefore, simulations including all the forcing changes have flood-dominated behavior, with sedimentation increasing inside the estuary (e.g., 11,500 m^3/year in simulation FSSL1 and 17,000 m^3/year in simulation FSSL2).

The sum of the profile from point 17 to 18 and profile from point 21 to 22 shows the import of sediment into the estuary. As with the residual sediment through the inlet, SLR changes the behavior of the sediment import into the estuary (purple bars in Figure 5.10). Furthermore, anticlockwise changes in wave direction (simulations FSSL2 and FSSL4) cause a larger sediment transport (directed flood) due to more prominent currents reaching internal points in the estuary. The inlet migration is directed south (Figure 5.7), and hence the currents have less resistance to reach that points.

The cross-shore transport in the nearshore area changes primarily owing to SLR. Profiles from point 6 to point 10 in Figure 5.10 shows that simulations with SLR show a higher suspended sediment transport through the profile owing to the increase in tidal prism (~18%). Furthermore, the bedload transport (directed onshore) decreases due to the rise in water levels, which reduces the wave skewness and hence the term $U^4_{\delta,for} - U^4_{\delta,back}$ used in the wave-driven bedload transport equation in TR1993.

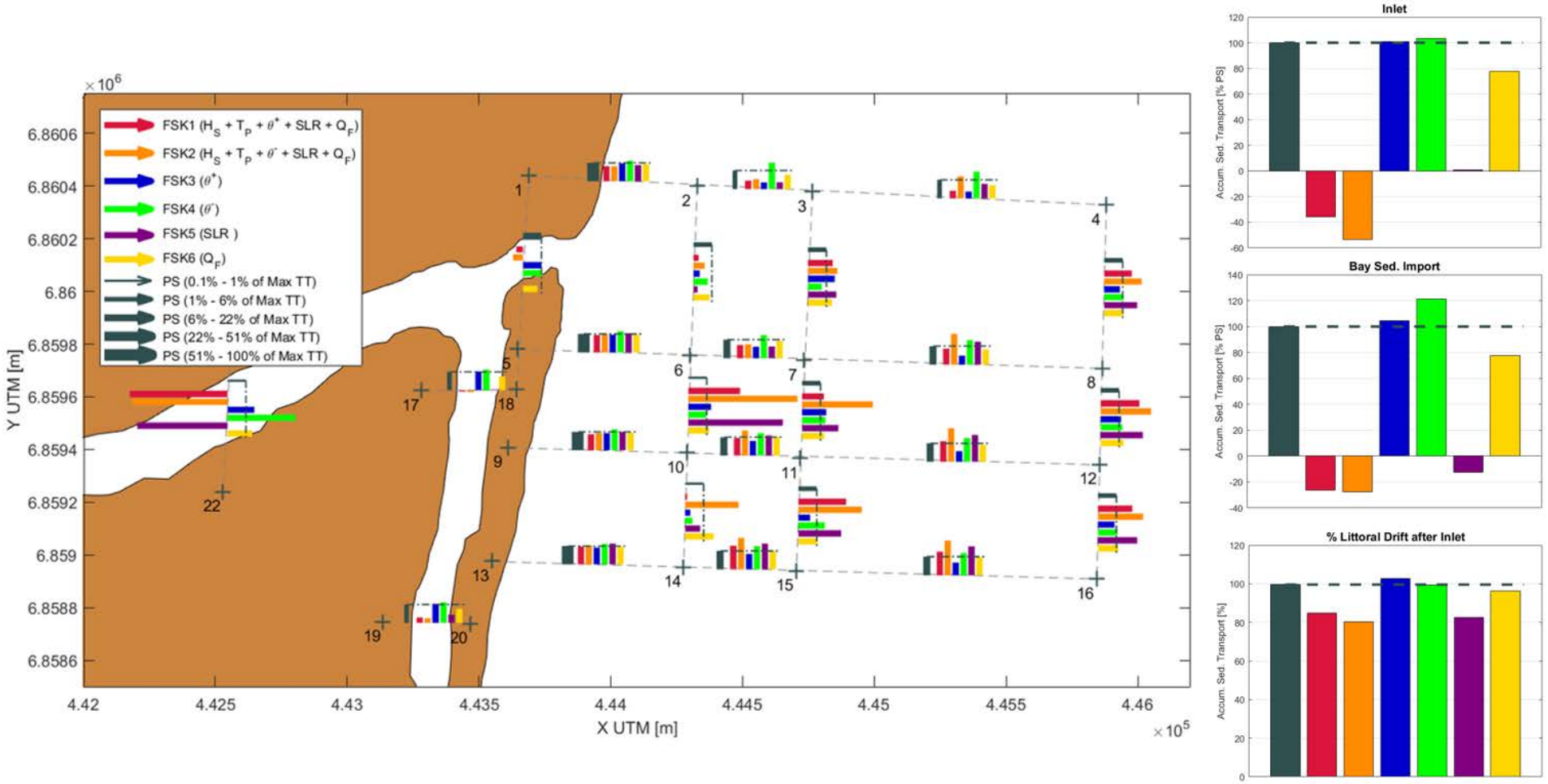

Figure 5.10. Accumulated total sediment transport map for Santa Lucia Estuary. Grey dashed lines show the output profiles from Delft3D. At each profile a bar plot shows the yearly cumulative sediment transport for all scenarios. Grey bars (present state simulation) are wider when the sediment transport is larger (percentage of the maximum total transport (TT) in legend). The dashed-dotted lines across the bars indicate the value for the present state to highlight the comparison with other simulations. On the right, three bar plots illustrate the inlet profile accumulated transport (top), the sum of the profiles 17-18 and 21-22 (i.e., the sediment intrusion into the bay) (middle), and the remaining littoral drift after the inlet (difference between profiles 5-8 and 1-4) (bottom).

CHAPTER 6. DISCUSSION

CHAPTER SUMMARY

This chapter discusses the results of the analyses presented in Chapter 4 and Chapter 5, identifies model limitations, and suggests opportunities for future research. Coupled SWAN and Delft3D models are generally capable of reproducing hydrodynamic and morphodynamic phenomena at each site. Here, SLR is the primary CC forcing impacting the overall morphodynamics at both sites; while changes in wave climate mostly affect the inlet dynamics. Comparisons with recent literature suggests that diverse impacts owing to changes in wave climate are characteristic for each site.

The proposed methodology presents some limitations, including the paucity of field measurements, the uncertainty of projected CC, the omission of extreme events, the incapability of Delft3D to reproduce some phenomena (e.g., overwash), the utilization of a MORFAC, and the way in which adaptation to CC is implemented.

Finally, we outline other paths for future research by presenting a list of proposals; foremost being the application of a morphodynamic connectivity network to assess CC on tidal inlet systems and the inclusion of extreme events into the analysis.

6.1. Model Discussion

A snap-shot simulation approach using process-based modeling has been applied to assess CC impact for an RCP4.5 scenario on the dynamics of sandy nearshore inlet systems. Here, we discuss the methodology implemented and the results obtained.

6.1.1. Copula Analysis

We based the derivation of the wave boundary conditions on a statistical analysis called a copula analysis. For this analysis, marginal distributions are fit to WWIII hindcast data (significant wave height, peak wave period, and mean wave direction) and then the joint probability between the marginal distributions is combined into an empirical copula. Standard normal distribution figures (Appendix B) show that mean wave directions and peak wave periods are correlated ($\rho \sim 0.5$) at both sites throughout the year, whereas the other pairs are uncorrelated ($\rho < 0.25$). Therefore, the empirical copula is only fitted between the peak wave periods and the mean wave directions. Resulting copulas replicate the bimodality of the wave climates at both sites (Figure 3.1 and Figure 3.2), reproducing the correlation between the peak wave periods and the mean wave directions throughout the year.

This methodology produces more accurate results than standard wave reduction methods (Walstra et al. 2013) used in Santa Lucia by Hoek (2017) owing to the utilization of more accurate hindcast data and the implementation (using the same MORFAC) of 292 characteristic waves climates instead of 10. The increase of wave conditions using the copula analysis provides a bigger range of values (extreme and calm conditions) than standard practices, and subsequent range of sediment transport rates. For instance, the present wave reduction method captures waves up to 6 meters in Santa Lucia, which have the most significant impact on the littoral drift, and hence on the inlet dynamics. Furthermore, using copula functions allow us to treat each wave conditions as a group of variables, adding statistical foundation into the methodology. In standard practices (Walstra et al. 2013), the correlation is of secondary importance, and usually the wave period is not included in the analysis.

The copula analysis gives flexibility to incorporate projected wave climate changes, which can be implemented directly to the marginal probabilistic function parameters (e.g., mean, or standard deviation). Here, we change the mean of the generalized extreme value distributions to match the projected CC on significant wave heights obtained from statistical downscaling (SD) models.

The provided GCM projections on significant wave height obtained with an SD framework (used to derive the future conditions using the copula analysis) show a good correlation with hindcast data at both sites. Nevertheless, the wave period seasonality is not well reproduced in Katama Bay, and hence not included in Delft3D. Global SD models may not well reproduce the regionality of the wave climates, and hence a validation is needed before implementing the projected future changes in wave period.

Projected changes in wave height at Katama Bay show distinct variations throughout the year. During autumn and winter, the significant wave heights decrease by 6% and 2% respectively, whereas during summer the significant wave height increases by 5% (Figure 3.5). Therefore, the storms (winter) become

on average less energetic, and the swell (summer) increases. In Santa Lucia, there is a reduction of the significant wave height and the peak and mean wave periods throughout the year (Figure 3.7), and hence both projected swells will be less energetic. This enhances the importance of the study of the seasonality in the wave climate. For instance, if the averaged decrease (~2%) in significant wave height had been implemented in Katama Bay for the whole future wave climate, swell energy would decrease, contradicting the projected trends.

6.1.2. CC impacts

In Katama Bay, SLR exhibits the most significant impact on the morphodynamics of the system. The sediment transport through the inlet (directed landwards) increases by 12% (for the simulation with only changes in SLR) owing to an increase of the depth-averaged velocities through the inlet. Similarly, the bay import is only altered by SLR (increasing by 50%) which also induces changes in the inlet profile (making it deeper) reducing the inlet migration towards the east by 10%.

Changes in wave direction primarily affect the littoral drift (and hence, the inlet migration). Clockwise changes in wave direction increase the littoral drift by 10% enhancing inlet migration towards the east (increasing by 12%), whereas anticlockwise changes in wave direction decrease the littoral drift by 10% reducing the inlet migration by 4%. Nonetheless, the inlet migration for simulations with all the forcing changes exhibit similar behavior as the present state simulation owing to a compensation for waves by inlet currents.

In Santa Lucia, SLR has the most significant impact on the sediment pathways, while anticlockwise changes in wave direction exhibit the most significant impact on the inlet migration. Changes in river discharge play a secondary role in the inlet migration and the sediment pathways. SLR makes the inlet wider, increasing the tidal prism by 18% and shifting the behavior of the inlet (from ebb-dominant to flood-dominant). The sediment transport through the inlet and the sediment import becomes flood directed for simulations with SLR, and the inlet migrates 70 meters towards the south (shifting direction). The increase in discharge through the inlet supposes an increase on the Bruun stability criterion.

Anticlockwise changes in wave direction increase the longshore transport in both directions and the residual littoral drift (towards north) owing to bigger waves throughout the domain. The inlet migrates 95 meters towards the south while the migration is 105 meters towards the north for the present state simulation. A larger littoral drift enhances instability of the inlet, decreasing the Bruun stability criterion. In contrast, clockwise changes in wave direction decrease the littoral drift and play a secondary role in the dynamics of the system, not altering significantly the inlet migration. When all the forcing changes are combined, the impacts intensify; the inlet migration is 120 meters towards the north for simulation FSSL1 and 200 meters towards the south for simulation FSSL2.

To sum up, SLR and changes in wave direction play a primary role in the inlet dynamics at both sites, whereas changes in wave height or river discharge (Santa Lucia) play a secondary role. Figure 6.1 shows the relative impact on three variables (centroid migration, littoral drift, and residual sediment transport

through the inlet) for all the future state simulations. We have chosen these three variables to represent an overall behavior of the system; the centroid migration relates to the inlet migration, the sediment transport through the inlet correlates to the basin behavior, and the littoral drift links to changes in the nearshore area. The impacts are normalized by the maximum difference between the future and present state simulations at each site. Then, the impacts are normalized again by the sum of the three impacts so as to be represented in a ternary plot. The first column of ternary plots follows the same color pattern described in Figure 4.5 (Katama Inlet) and Figure 5.5 (Santa Lucia Inlet). Highlighted markers (salmon color) show the simulations with SLR in the second column and the simulations with clockwise changes in wave direction in the third column.

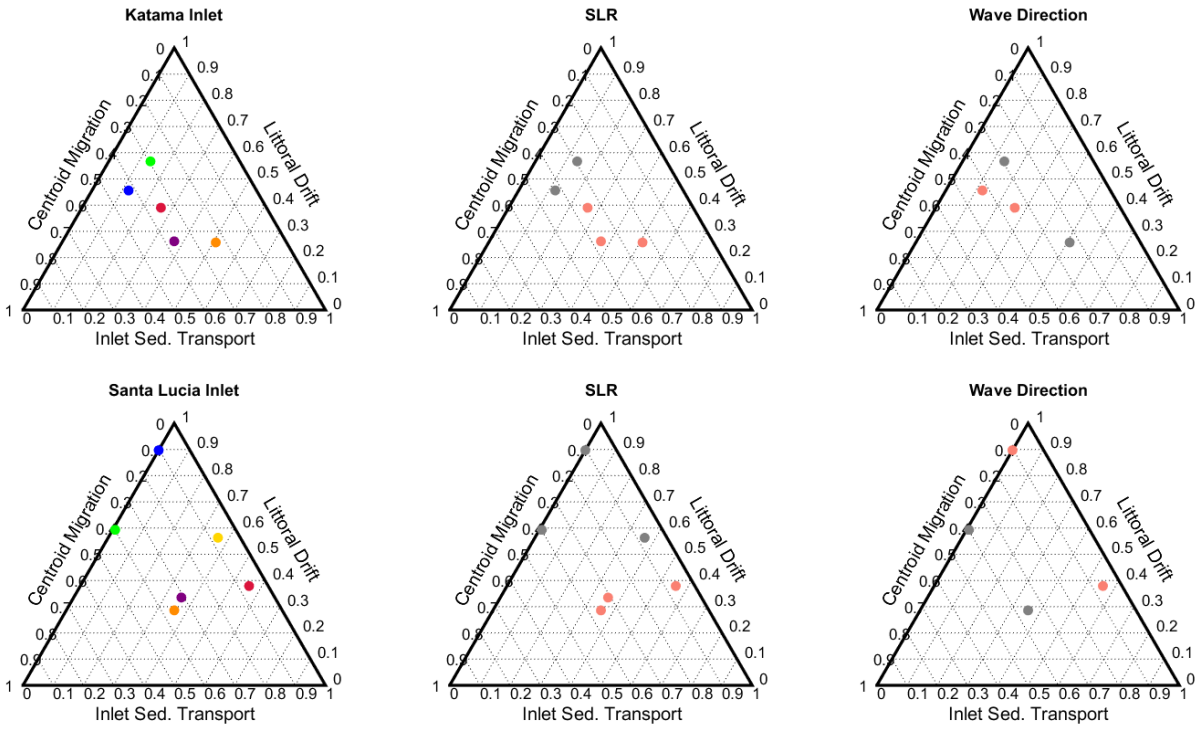

Katama Bay	Simulation	2nd Column	3rd Column	ΔH_F	θ^+	θ^-	SLR
	FSK1			x	x		x
	FSK2			x		x	x
	FSK3				x		
	FSK4					x	
	FSK5						x

Santa Lucia Estuary	Simulation	2nd Column	3rd Column	ΔH_F	ΔT_P	θ^+	θ^-	SLR	Q_F
	FSSL1			x	x	x		x	x
	FSSL2			x	x		x	x	x
	FSSL3					x			
	FSSL4						x		
	FSSL5							x	
	FSSL6								x

Figure 6.1. Relative impact on the centroid migration, the residual sediment through the inlet, and the littoral drift for the future state simulations in Katama Inlet (top) and Santa Lucia Inlet (bottom). The impact on the different factors is normalized to achieve a sum of one for each simulation. The ternary plot on the left shows all the simulations for each site (same color pattern used in Chapter 4 and Chapter 5). In the middle, the ternary plots with highlighted dots (salmon) show simulations with SLR, whereas grey dots indicate simulations without SLR. To the right, the highlighted dots (salmon) represent simulations with clockwise changes in wave direction, whereas grey dots show simulation with anticlockwise changes in wave direction. Katama Bay simulation FSK6 is not included owing to an insignificant impact on the inlet compared with the present state simulation.

Overall, markers are closer in Katama Bay than in Santa Lucia Estuary indicating that Santa Lucia Estuary is more sensitive (than Katama Bay) to CC driven variations in physical processes. Colored dots in the second column in Figure 6.1 show that SLR has a relatively larger impact on the sediment transport through the inlet (i.e., the basin behavior), whereas it has a relatively smaller impact on the littoral drift. When SLR is included, both sites show an average increase of 25%-30% on the sediment through the inlet and no significant impact on the inlet migration.

The relative importance of changes in wave direction varies along the centroid migration axes (last column of Figure 6.1). One variation in wave direction (clockwise or anticlockwise) enhances inlet migration, whereas the other one (anticlockwise or clockwise) shows similar inlet migration as the present state simulation. In Katama Bay, clockwise changes in wave direction have a larger relative impact on the centroid migration than the anticlockwise changes. Conversely, Santa Lucia results show that anticlockwise changes in wave direction have a relatively larger impact on the centroid migration than clockwise changes. Therefore, the impacts on the variation in the wave direction (clockwise or anticlockwise) are specific for each site, especially in bimodal wave climates.

This can be explained by the distinct wave climates (storm or swell) in Katama Bay and Santa Lucia. Storms tend to move sand rapidly offshore causing erosion in the surf zone, while under low-energy conditions (mostly swell), sand moves onshore accreting the beach (Komar 1998). Therefore, sites with storm climates are characterized to have reflective beaches or "winter profiles" with coarser grain size and steeper slopes, whereas sites with swell climates normally have dissipative beaches or "summer profiles" with finer grain size and milder slopes (L. D. Wright and Short 1984).

Here, this is well reproduced. Katama Bay exhibits a steeper profile with coarser grain size (500 µm) than Santa Lucia (200 µm). Therefore, milder profiles in Santa Lucia move wave breaking, and hence the wave energy, onshore with SLR. This pushes sediment into the inlet, making the inlet shallower, but broader (owing to an increase of discharge). In Katama Bay the wave breaking is moved less onshore with SLR, and the inlet becomes deeper owing to stronger currents. Therefore, it is expected that SLR decreases the inlet depth in swell climates and increase the inlet depth in storm climates.

The projected changes in tidal constituents do not alter the dynamics in Katama Bay. However, large (time-scale) tidal nodal cycles may have an impact on the morphodynamics of this system. The 18.61-year nodal cycle modulates tidal amplitudes and currents around the world, enhancing changes in the morphodynamics. Oost et al. (1993) studied the influence of this nodal cycle on the Dutch Wadden Sea showing the potential impacts along the Dutch barrier islands and sedimentary filling of abandoned channels. Here, the tidal signal of the closest tidal station (Woods Hole) does not display any significant cyclical trend for the next 20 years (Figure 6.2), and hence it is not expected to have an impact on the morphodynamics. This corroborates results found by Haigh et al. (2011), which showed that the nodal modulation is largest in diurnal (rather than semidiurnal) regions with tidal ranges >4 m.

For management purposes, SLR is projected to bring more sediment material into Katama Bay, affecting navigation. However, the lower migration rate of the inlet owing to SLR suggests a more extended inlet

presence, enhancing good navigation to the Atlantic and water quality for the Bay shellfish farms (Arpin 1970). Clockwise changes in wave direction, on the other hand, suggest faster inlet migration and a subsequently shorter time with the inlet present. Compared with the present-day, this leads to a shorter period when currents through the Bay can strain mooring lines at Edgartown Marina, but decreases the period of higher flushing and hence better water quality.

The change in basin behavior (from ebb to flood) in Santa Lucia Inlet due to SLR suggests that the current management measures (dredging spoils) to reduce the salinity on the lakes during drought seasons maybe not as efficient in the future. Furthermore, the increase in inlet stability seen in simulations with SLR suggest that the inlet will be opened longer during drought seasons.

Overall, SLR changes the sediment behavior in the inlets, and hence the sediment erosion/sedimentation patterns inside the basins. For management purposes, SLR will have an impact on navigation owing to potentially larger sediment import into the bays. Management measures should be focusing on enhanced dredging for navigational purposes. Changes in wave direction have the most significant impact on the inlet stability. In intermediately open inlet systems these changes may play a role altering the presence (in time) of the inlet in this type of systems. Therefore, the evaluation of the variations in inlet closure time is a fundamental step in management measures.

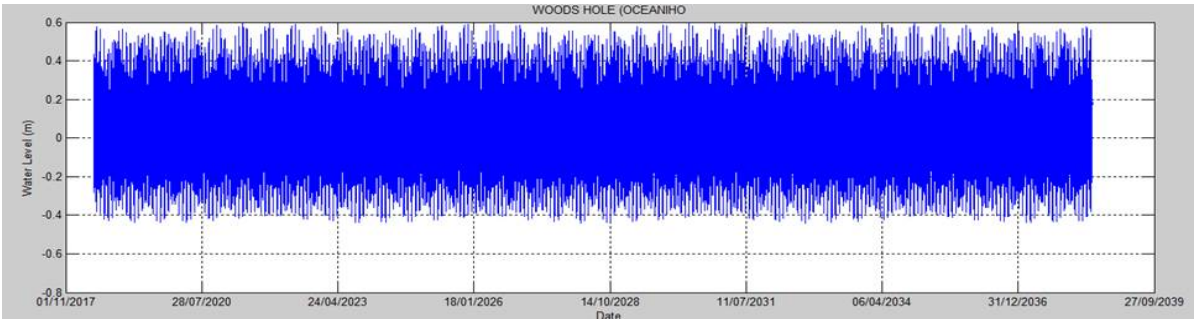

Figure 6.2. The tidal signal at Woods Hole for the next 20 years (2018-2038). It is appreciable interannual variation of tidal levels with a semidiurnal component. However, the signal does not display any significant cyclical trend for the next 20 years (18.61-years nodal cycle).

6.1.3. Comparison with previous studies

The current results are compared with previous studies to contextualize this thesis with the existing body of CC assessment in inlet systems. Duong et al. (2017) analyzed the stability of three tidal inlets in Sri Lanka (Negombo Inlet, Kalutara Inlet, and Maha Oya Inlet) for CC driven variations (RCP8.5 scenario). The first inlet is permanently open, locationally stable (Type 1), the second one is permanently open, alongshore migrating (Type 2), and the third one is seasonally-interpedently open, locationally stable (Type 3).

Maha Oya Inlet and Santa Lucia Inlet results are compared owing to similar Bruun stability criterion (r), indicating that both inlets are Type 3 (Table 2.3). Santa Lucia Inlet exhibits a Bruun stability criterion in the range from 2.5 to 5 for all the simulations (Figure 6.3a), which supports the previous conclusion that a Type 3 inlet will not change Type ($r<10$) under CC forcing (Duong et al. 2017).

The stability of Maha Oya Inlet is more sensitive to changes in wave direction than in Santa Lucia Inlet (Figure 6.3b). Sri Lanka has a monsoonal bimodal wave climate, with two monsoon seasons; the Northeast (NE) monsoon from November-February and the Southwest (SW) monsoon from May-September. In the Maha Oya Inlet, the SW monsoon is the primary contributor to longshore sediment transport, and anticlockwise changes in wave direction increase the littoral drift considerably owing to an incident wave angle close to 45°. The impact of changes in wave direction on the morphodynamics are different in the literature review sites and in the studied sites. Therefore, future work must avoid using the results from one site as a general behavior on the assessment of CC impacts in tidal inlet systems.

Duong et al. (2017) suggest that SLR enhances inlet closure, which the present study finds to be very site-specific instead of a general rule. In Santa Lucia, SLR increases the Bruun stability criterion owing to a larger discharge through the inlet (Figure 6.3a). In Katama Bay, SLR increases also the discharge through the inlet, decreasing the migration. Therefore, each site is unique and can behave differently with similar changes in the forcings.

Besides the forcings, the way in which CC adaptation is implemented into the model may have an impact on the results. Duong et al. (2017) rose the estuary bed level by approximately half the SLR amount (which is 1 meter) following the premise that a small basin strives to maintain an equilibrium volume, but with a time lag of 50% (Ranasinghe et al. 2013). In the current study, only the upward movement of the barrier is included. Different adopted methodologies may impact the results, where models without adaptation of the level of the basin may have a larger discharge through the inlet (increasing the stability) than models with an adaptation of the level of the basin. This suggests the need to study the sensitivity of the basin adaptation to CC on the inlet dynamics.

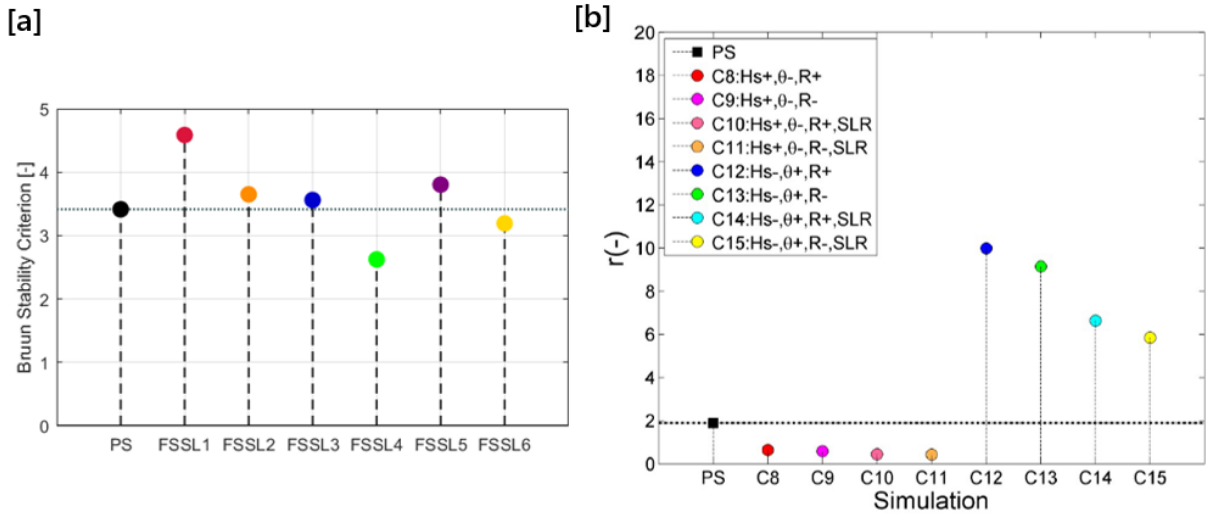

Figure 6.3. [a] exhibits the results in the Bruun stability criterion for CC driven variation in Santa Lucia. [b] shows the Bruun stability criterion for CC driven variations in physical processes at the Type 3 inlet (Maha Oya River, Sri Lanka) calculated by Duong et al. (2017). Black square shows the present state (PS) simulation results. The future state simulations (colored dots) have an increase (H_S+) or decrease (H_S-) of an 8% in the significant wave heights, an increase (θ+) or decrease (θ-) of 10°N on the wave directions, an increase (R+) or decrease (R-) of a 40% in the river flow and 1 m SLR.

6.2. Limitations

This study is limited by four main factors: the way in which present and future boundary conditions are implemented, the paucity of field observations against which to calibrate and validate the models, the model set-up, and the capability of the selected process-based models to reproduce the physical processes to evaluate the impacts of CC on the dynamics of inlet systems.

6.2.1. Copula analysis

The copula analysis is presented as a reliable tool that shows good performance compared with standard practices (Walstra et al. 2013). Nevertheless, this novel methodology has some limitations.

We use a whole wave climate to calculate the empirical copulas, instead of dividing the wave climate in frequency or direction within each season. We conclude that only the peak wave period and the mean wave direction are correlated. However, the inclusion of all the data in the same copula may interfere with the correlation between other pairs (H_S/T_P, H_S/θ_m). By dividing the data (e.g., in frequency or wave direction), other trends may be found allowing the implementation of theoretical copulas (e.g., Gaussian, t-copula, Gumbel, Clayton) with more of a statistical foundation.

Peak wave period and mean wave direction data is fitted using Kernel distributions. These distributions are nonparametric, hindering the implementation of projected future changes. Fitting parametric distributions would allow a similar methodology to project the future distributions as used for the significant wave heights, adding again more statistical foundation.

The derivation of the boundary conditions along the SWAN outermost boundaries does not distinguish between regular and extreme climates. In Katama Bay, it is shown (Smith 2012; Orescanin et al. 2016; J. A. Hopkins 2017) that extreme wave climates have a large contribution to the bed level changes throughout the domain. Therefore, the importance of the timing and frequency of episodic events for the present state, and the extrapolated changes in the future climate, will alter the morphodynamics. The inclusion of such events may improve the morphodynamic results (e.g., enhancing the migration of the updrift barrier in Katama Bay owing to larger littoral drift).

We set up the wave conditions randomly throughout the seasons. Nevertheless, groups of storms usually enhance larger morphological changes than that of an individual storm (Lee, Nicholls, and Birkemeier 1998). Therefore, the randomness on which storms are implemented may alter the results obtained. Adding wave condition sequencing to the copula analysis should be studied in future applications.

6.2.2. Future state forcings derivation

The projections used in the current study to adapt the present study to the future (the year 2100) are based on projected climate scenarios (in this case RCP4.5) that rely on several assumptions. Therefore, the projected changes are themselves uncertain. The output from Delft3D can also be associated with at least an equal level of uncertainty than the input.

Changes in wave direction are based on a projected global range (Hemer et al. 2013) owing to the scarcity of regional SD or DD projections. The implementation of the same range of values at both sites does not reflect reality. Wave directions may vary differently at both sites, and probably with smaller values. Hence, we may be overpredicting the impact of the wave direction changes.

The assumption that the joint probability between the wave variables will not change throughout time may not be accurate. Changes in the joint probability may impact the resulting future state wave climates. Other models outside of SD models (e.g., DD frameworks), provide time-series results which will facilitate the derivation of future joint probabilities.

We based the future changes in river discharge at Santa Lucia on changes in precipitation and run-off seen on the scale of the African Continent. The uniqueness of each river basin needs to be considered for future run-off changes. Moreover, the changes in sediment concentration in the river, which are not addressed here, will change the input of sediment to be mobilized throughout the domain, and hence the morphology.

6.2.3. The paucity of field measurements

The research has been limited by the lack of input data, and the available data is of questionable accuracy. The most important limitation is the absence of bathymetric data at the desired point in time. In Katama Bay, we had to apply the methodology presented in Appendix E to improve the initial bathymetry. At both sites, the initial dimensions and position of the inlet were manually introduced. Above all, the model is sensitive to the bathymetry, and hence the inaccuracy of this initial condition adds uncertainty to the results. Implementing an accurate (in time and resolution) initial bathymetry is one of the main premises to improve the results.

The scarcity of field observations against which to calibrate and validate the models is another primary limitation. In Katama Bay, no measurements of velocities through the inlet are available during 2007. Moreover, the lack of repeated bathymetric surveys through all stages of the inlet migration made a quantitative morphodynamic validation impossible. We based our validation in satellite images, and hence the profile evolution cannot be validated. In Santa Lucia, only averaged values of tidal prism and peak flows are available. Longshore sediment transport was validated against field measurements 60 km south of the studied domain, which may differ to the longshore transport in Santa Lucia.

6.2.4. Delft3D

The implementation of a MORFAC assumes a linear relationship between the morphological response and the hydrodynamic response. However, real-life situations are likely to incorporate highly non-uniform morphology and non-linear time forcing (tides, waves, wind). Furthermore, a MORFAC can induce errors in the bed form celerity and amplitude, and numerical errors due to advection/diffusion scheme (Ranasinghe et al. 2011).

The set-up of the tidal boundary conditions is another constraint on the results. In Katama Bay, the close proximity of the outer flow grid to the Vineyard's Sound may influence the tidal signal, and thus the

behavior of the inlet. Nesting the outer grid in another grid which extends towards the north may improve the results. In Santa Lucia, we simplify the tidal signal to a single uniform M2 signal to reduce the complexity of the modeling. This simplification impacts the hydrodynamics, and hence the morphology. Furthermore, in the open sea, the proximity of the model grid boundary to the inlet can induce to some boundary effects disturbing to the flow patterns throughout the domain.

The Santa Lucia model does not include the whole Isimangaliso system, which plays an important role on the hydrodynamics (thus morphodynamics) of the system. Enlarging the model to include the Santa Lucia lakes and a larger part of the Mfolozi River will contribute to a more realistic model. This will enable the option to incorporate a complete hydrological cycle (evaporation, precipitation, groundwater flows and discharge of each river) and the water levels of the St Lucia Lakes.

The calibration parameters play a crucial role in the model set-up. In Santa Lucia, Hoek (2017) implemented current-related calibration parameters (Sus and Bed) of 20 in Delft3D to match longshore transport measurements. Here, we decreased them to 10, and the model shows a realistic morphodynamic behavior, making it apt for the current study. Nevertheless, the high calibration parameters indicate that this model does not well represent some physical processes. For instance, the longshore sediment transport is underestimated when the calibration parameters are the default values (1). The grid size along the coast (away from the inlet), which has a resolution of 100 meters, may be too coarse, influencing these sediment transport rates. Similarly, the implemented value of the horizontal eddy diffusivity (1 m^2/s) is a parameter to check for future modeling in this site.

The slope of the inlet edges and the depth incision of the inlet may affect the inlet migration. In Katama Bay, different edge slopes alter the inlet centroid migration rates. Wang et al. (2016) suggested that the transverse bed slope parameter (α_{bn}) plays an essential role in the inlet incision, and hence the inlet edge slopes. The calibration of α_{bn} to bathymetric surveys would be a good practice to obtain more accurate results (inlet migration).

In Katama Bay, overwash owing to big storms (e.g., Hurricane Irene) plays a significant role on the morphodynamics of the back barrier (Smith 2012). In Santa Lucia, sediment transport owing to long waves may alter the morphodynamics of the barrier and the inlet. Nevertheless, Delft3D does not reproduce both processes, likely underestimating the sediment transport throughout the domains.

Finally, a cohesive sediment transport analysis is out of the scope of the current study. However, fine sediment may alter the morphodynamics, especially in Santa Lucia where a significant amount of the sediment carried by the river is cohesive (Grenfell and Ellery 2009).

6.2.5. Adaptation to CC

Comparison with existing literature (Duong et al. 2017; Duong et al. 2018) show that the methodology used to implement adaptation to CC into the model may impact the results. Other than changing the mean sea level, three main physical processes contribute to coastline change adjacent to basins owing to SLR: basin infilling due to SLR-induced increase in basin accommodation space, SLR upward

movement of the cross-shore profile, and landward movement of the coastline (Ranasinghe et al. 2013). Furthermore, variations in river flow into the basin may impact the basin volume. In theory, an inlet-basin system will strive to maintain cross-sectional equilibrium velocities (van der Wegen, Dastgheib, and Roelvink 2010).

In Katama Bay, the morphology of the flats is only altered when the inlet is present. In Santa Lucia, we believe that the adaptation of the basin levels is driven mainly by changes in river discharge. Owing to the uncertainty of these assumptions, we decided not to change the basin levels. Nevertheless, the bed level of the basin plays a primary role in defining the behavior of the basin, and hence any assumption adopted adds uncertainty to the results. On the other hand, we modified the barrier height to adapt to SLR. However, modifying the future state bathymetry manually is a rough approximation to reality, and it is unknown how sensitives are the models towards these practices.

6.3. Next Steps

Many additional analyses and ideas lay beyond the scope of this thesis. This chapter serves as a proposal section for future investigation of CC-driven impacts on tidal inlet systems. We suggest a list of possible proposals which will contribute to building on the existing body of CC impacts on tidal inlet systems. These are:

- Climate change impacts on the sediment transport pathways using a morphodynamic connectivity network. A multifaction grain size analysis.
- Assessment of CC-driven extreme wave climate impacts on the dynamics of tidal inlet systems.
- Sensitivity analysis of RCP scenarios on the dynamics of tidal inlets.
- Assessment of climate changes impacts on cohesive sediment transport in Santa Lucia Estuary.
- Predicting changes in breaching of sand barriers using a Bayesian Network. A case study: Katama Barrier.

Proposal 1 – Climate change impacts on the sediment transport pathways using a morphodynamic connectivity network. A multifaction grain size analysis.

A novel methodology (Pearson et al. 2017) focuses on analyzing the connectivity between different regions of the Ameland Inlet (Wadden Sea) using the sediment pathways of multiple grain size fractions. This approach can be used to advance the understanding of extensively complex tidal systems. Here, we suggest using this methodology to predict the impacts of CC on tidal inlet systems, developing a framework to be used as a tool for management purposes.

Research Question:

How does climate change impact the sediment pathways and the morphodynamics connectivity of nearshore inlet systems?

This study will first focus on defining the main morphological units in Delft3D from which connectivity will be assessed. Then, the hydrodynamic and morphodynamic connectivity will be established using particle tracking from each morphological unit. Finally, the results (present and future) will be introduced in a graphical network to determine the sediment pathways from different grain sizes.

The framework proposed by Nienhuis & Ashton (2016) can be used to quantify the inlet migration. The bypassing fraction, the flood delta fraction, and the barrier fraction can be determined and, most important, the origin of the sediment (e.g., downdrift barrier, updrift barrier, tidal deltas).

The comparison of the present state and the future state simulations by using the methodology proposed by Pearson et al. (2017) will provide a robust tool to quantify the impacts of CC. Nevertheless, this methodology is sophisticated and requires extensive field measurements (or an appropriate existing Delft3D model) to be implemented. Therefore, only a single site will be analyzed (e.g., Ameland Inlet), providing an example study replicable in other sites.

Key References:

Pearson, S.G., van Prooijen, B.C., Wang, Z.B., Bak, J.P. (2017) Sediment Connectivity and Transport Pathways in Tidal Inlets: A Conceptual Framework with Application to Ameland Inlet. American Geophysical Union Fall Meeting 2017, December 11, 2017, New Orleans, Louisiana

Pearson, S.G., van Prooijen, B.C., Wang, Z.B., Bak, J.P. (2018) Sediment Connectivity and Exchange in Ameland Inlet. NCK Symposium on Sediment Sorting, January 11, 2018, Delft, the Netherlands.

Nienhuis, Jaap H., and Andrew D. Ashton. 2016. "Mechanics and Rates of Tidal Inlet Migration: Modeling and Application to Natural Examples." Journal of Geophysical Research: Earth Surface 121 (11): 2118–39. doi:10.1002/2016JF004035.

Proposal 2 – Assessment of CC-driven extreme wave climate impacts on the dynamics of tidal inlet systems.

After the accomplishment of the present study, the lack of analysis on extreme events is seen to be one of the main limitations. We suggest that a future study introduce the impact of extreme events on the analysis of the present and the future state of the morphodynamics of nearshore tidal systems.

Research Question:

How does projected climate changed extreme events impact the dynamics of nearshore inlet systems?

This study will first focus on analyzing the significance of CC-driven changes on extreme events in the present-day dynamics of inlet systems with different kind of wave climates. For instance:

- Inlet system with a storm climate: Katama Bay, Massachusetts.
- Inlet with a swell climate: Santa Lucia Estuary, South Africa.
- Inlet with a monsoonal climate: Tu Hien Inlet, Vietnam (van der Biezen 2014).

The study will focus initially on determining the importance of extreme climates on present-day inlet dynamics. Then, regular and extreme climates will be analyzed separately to derive the conditions for future simulations. Shope et al. (2016) defined the extreme wave values as the mean of the top 5% of H_S and associated T_P and θ_M. Their approach to analyzing CC impacts on extreme climates can be adopted for this study.

Process-based models (e.g., coupled SWAN and Delft3D) will then be used to analyze the CC-driven impacts on the dynamics of the selected sites. The results should discuss the relative importance of changes in extreme wave climate on the dynamics of tidal inlet systems focusing on differencing the distinct wave climates.

Key References:

Chapters 3, 4 and 5 of this report.

van der Biezen, T.F. 2014. "Climate Change and the Morphological Stability of the Tu Hien Inlet, Vietnam." Master's Thesis. Delft University of Technology. https://repository.tudelft.nl/islandora/object/uuid%3Ad80b095b-9e54-42e8-a06e-d144ae8d14ee.

Shope, James B., Curt D. Storlazzi, Li H. Erikson, and Christie A. Hegermiller. 2016. "Changes to Extreme Wave Climates of Islands within the Western Tropical Pacific throughout the 21st Century under RCP 4.5 and RCP 8.5, with Implications for Island Vulnerability and Sustainability." Global and Planetary Change 141. Elsevier B.V.: 25–38. doi:10.1016/j.gloplacha.2016.03.009.

Proposal 3 – Sensitivity analysis of RCP scenarios on the dynamics of tidal inlet systems.

The present thesis focuses on the impacts on the tidal inlet for projected changes using an intermediate climate change scenario (RCP4.5). Nevertheless, the Fifth Assessment Report (AR5) of Intergovernmental Panel on Climate Change (IPCC 2014b) uses four different Representative Concentration Pathways (RCP) scenarios (RCP2.6, RCP4.5, RCP6.0, and RCP8.5) proposed by van Vuuren et al. (2011). Here, we suggest evaluating the impacts of CC on the dynamics of sandy nearshore inlet systems for the rest of the scenarios to evaluate the sensitivity of each change across scenarios.

Research Question:

How does climate change impact the dynamic of sandy nearshore inlet systems across the different RCP scenarios?

This study will first focus on analyzing the significance of CC-driven changes on forcings (e.g., wave climate, river discharge, SLR) in the same systems as the current thesis:

- Inlet system with a storm climate: Katama Bay, Massachusetts.
- Inlet with a swell climate: Santa Lucia Estuary, South Africa.

The idea is to examine which forcings are most impactful across scenarios. Therefore, it will require the use of the copula analysis, developed in this thesis to determine all the wave climates applying the projected changes (Camus et al. 2017) in the marginal distributions. Projected changes in other variables can be obtained from the AR5 report (IPCC 2014b).

We suggest applying the same methodology as the current thesis for the Delft3D outcomes. The sensitivity of each forcing change can be obtained by comparing the input range of values (hydrodynamic forcings) with the output range of values (e.g., centroid migration, centroid geometry, or sediment pathways). This will provide a range of results, which adds robustness to the methodology.

Key References:

Chapters 3, 4 and 5 of this report.

IPCC. 2014b. Climate Change 2014: Synthesis Report. Contribution of Working Groups I, II and III to the Fifth Assessment Report of the Intergovernmental Panel on Climate Change. Edited by R.K. Pachauri and L.A. Meyer Core Writing Team. Geneva, Switzeland: IPCC. doi:10.1017/CBO9781107415324.004.

Camus, Paula, Iñigo J. Losada, Cristina Izaguirre, Antonio Espejo, Melisa Menéndez, and Jorge Pérez. 2017. "Statistical Wave Climate Projections for Coastal Impact Assessments." Earth's Future 5: 918–33. doi:10.1002/2017EF000609.

Proposal 4 – Assessment of climate changes impacts on cohesive sediment transport in Santa Lucia Estuary.

The present study focuses on the physics of non-cohesive sediment transport. Nevertheless, fine sediment does not behave as non-cohesive sediment (Mehta et al. 1990), and its presence may have an impact on the morphodynamics of many small tidal basins (van Ledden et al. 2004). Grenfell and Ellery (2009) showed that the Mfolozi River (in the Santa Lucia Estuary) has a significant fraction of silt which suggests that cohesive sediment transport may impact the morphodynamics of this system. We propose to analyze the CC impacts on the cohesive sediment transport in Santa Lucia Estuary.

Research Question:

How does climate change impact the cohesive sediment transport in Santa Lucia Estuary?

The thesis will first investigate the seasonality of the sediment concentration in the Mfolozi River for the present and the future states. Particular attention must be paid to the potential changes in the sediment concentration owing to CC-driven changes in river discharge.

Cohesive and non-cohesive fractions will be then defined and implemented in Delft3D. The analysis of the cohesive fraction may require enlarging the model to include the Santa Lucia lakes and a larger part of the Mfolozi River. This will lead to a more realistic model and will include the influence on the silt content in the lakes. For future simulations, the basin infilling owing to changes in river discharge should be investigated.

The results from this proposal should be compared with the outcomes of the current thesis to evaluate the impacts of the cohesive fraction. We recommend focusing on the sediment pathways analysis and the differentiation between the cohesive and the non-cohesive fraction.

Key References:

Grenfell, S. E., and W. N. Ellery. 2009. "Hydrology, Sediment Transport Dynamics and Geomorphology of a Variable Flow River: The Mfolozi River, South Africa." Water SA 35 (3): 271–82. doi:10.4314/wsa.v35i3.

van Ledden, Mathijs, Zheng Bing Wang, Han Winterwerp, and Huib De Vriend. 2004. "Sand-Mud Morphodynamics in a Short Tidal Basin." Ocean Dynamics 54 (3–4): 385–91. doi:10.1007/s10236-003-0050-y.

Mehta, By Ashish J, Earl J Hayter, W Reginald Parker, Ray B Krone, and Allen M Teeter. 1990. "Cohesive Sediment Transport. I: Process Description." Hydraulic Engineering 115 (8): 1076–93.

Proposal 5 – Predicting changes in breaching of sand barriers using a Bayesian Network. A case study: Katama Barrier.

In the present thesis, we focus our study on the implications of CC when the inlet is present. Nevertheless, CC may impact the probability of barrier breaching. Several studies suggested the use of Bayesian Networks to study storm impacts (den Heijer et al. 2012; Poelhekke 2015; and many others). Here, we suggest developing a synthetic dataset using XBeach to cast these results in a Bayesian Network.

Research Question:

How does climate change impact the probability of breaching of the Katama Bay Barrier?

The study will first focus on determining the correlation between the hydrodynamic forcings in Katama Bay using copulas. These forcings will then be implemented in XBeach, which is capable of reproducing the physical phenomena necessary to analyze erosion and breaching in sandy barriers (Roelvink et al. 2009). We recommend using an idealized bathymetry to save computational time. Finally, the output from XBeach will be used to train a Bayesian Network (BN) to take over its function. The BN will be trained and validated for the present state, and then it will be used for the future state simulations.

Here, we propose the BN presented in Figure 6.4. This network implements the most significant hydrodynamic forcings at Katama Bay as input, and the maximum overwash depth, the barrier volume change, and the overwash transport as hazard outputs. We suggest dividing the barrier into different sections to predict the location of the weakest point (breaching) and the changes of the location for future state simulations. Furthermore, using BNs allow to check the sensitivity of the model against changes in sediment propeties (e.g., grain size or sediment compaction), which will require an extension of the proposed BN.

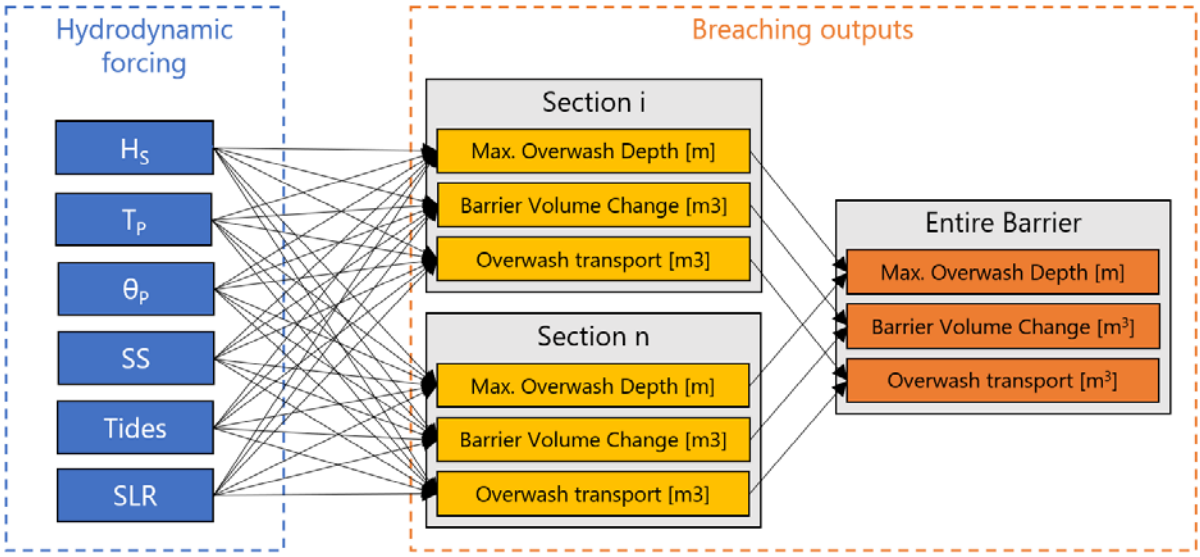

Figure 6.4. Proposed Bayesian Network to determine the breaching of the site barrier. Six hydrodynamic forcings are suggested; significant wave height (H_S), peak wave period (T_P), peak wave direction (θ_P), storm surge (SS), tides, and SLR. The breaching outputs are divided into sections (from i=1:n) to predict the weakest point along the barrier.

Key References:

den Heijer, C., Dirk T.J.A. Knipping, Nathaniel G. Plant, Jaap S.M. van Thiel de Vries, Fedor Baart, and Pieter van Geer. 2012. "Impact Assessment of Extreme Storm Events Using a Bayesian Network." Coastal Engineering Proceedings, 15. doi:10.9753/icce.v33.management.4.

Poelhekke, L., 2015. Predicting Coastal Hazards with a Bayesian Network. Master's Thesis. Delft University of Technology. Available at: http://resolver.tudelft.nl/uuid:8875d3be-5686-4272-b8e5-394f760157cf.

Roelvink, Dano, Ad Reniers, Ap van Dongeren, Jaap van Thiel de Vries, Robert McCall, and Jamie Lescinski. 2009. "Modelling Storm Impacts on Beaches, Dunes and Barrier Islands." Coastal Engineering 56 (11–12). Elsevier B.V.: 1133–52. doi:10.1016/j.coastaleng.2009.08.006.

CHAPTER 7. CONCLUSIONS

CHAPTER SUMMARY

Key Findings:

- Sea Level Rise is the primary contributor affecting the overall morphodynamics at both sites.
- Clockwise changes in wave direction enhance the largest inlet migration in Katama Inlet, whereas anticlockwise changes suppose the most significant migration in Santa Lucia Estuary.
- Changes in wave height and changes in river discharge (Santa Lucia) play a secondary role in the morphodynamics of both sites.
- Changes in tidal constituents at Katama Bay do not alter the dynamics of the site.
- Coupled Delft3D and SWAN models are a suitable tool to analyze the dynamics of tidal inlet systems under CC-driven forcings.
- The proposed methodology is flexible, easily replicable, and can be used as a systematic analytical method to analyze the impact of CC on different sandy nearshore inlet systems.

Recommendations:

- Collect more field data for validation.
- Implement accurate initial bathymetry.
- Use a copula analysis to derive the wave boundary conditions.
- Introduction of seasonality on the wave climate for present and future simulations in Delft3D.
- Consider implementing basin adaptation owing to SLR and river discharge.
- Physical processes not included in Delft3D.

This study analyzed the future impacts of CC forcings (for an RCP4.5 scenario) on the hydrodynamics and morphodynamics of sandy nearshore inlet systems. Process-based models (coupled SWAN and Delf3D) were used to examine the impact of changes in wave conditions, depth-averaged velocity, inlet geometry, inlet migration, inlet stability, sediment transport, and sediment pathways for six future state simulations at Katama Bay and Santa Lucia Estuary. Model results were compared to existing CC case studies from the literature.

7.1. Key Findings

At the beginning of this study, we posed several main research questions. Here are the key findings based on the outcome of our study:

1. **To what degree does SLR affect sandy nearshore inlet systems?**

   SLR is the primary contributor affecting the overall morphodynamics at both sites with the most significant impact on sediment transports and fluxes between the open sea and the tidal systems. A comparison of all the future simulations shows that SLR increases the relative impact of the sediment transport through the inlet (i.e., the import of sediment into the tidal system) by 25-30% compared with simulations without SLR. However, it does not significantly alter the inlet migration or the littoral drift.

   Results show that SLR impacts systems with distinct wave climates differently. SLR moves the wave energy onshore, enhancing onshore transport and pushing sediment on the inlet, in swell climates. Conversely, in storm climates, the increase of energy onshore (which is smaller owing to steeper profiles) enhances wave-driven offshore transport. Therefore, it is expected that SLR decreases the inlet depth in swell climates whereas it increases the inlet depth in storm climates.

   A comparison to recent studies (Duong et al. 2017; Duong et al. 2018) indicates that the way in which SLR adaptation is implemented into the model may have a substantial impact on the results. The uncertainty behind the assumptions adopted in the literature review suggest that is necessary a sensitivity analysis to determine the range of results adopting, for example, different infillings at the basin.

2. **Other than SLR, which are the most critical CC processes that impact sandy nearshore inlet systems?**

   Changes in wave direction have the most significant impact on the migration of tidal inlets, whereas changes in wave height and changes in river discharge play a secondary role on the hydrodynamics and morphodynamics of the analyzed sites. Projected changes in tidal constituents at Katama Bay do not alter either the hydrodynamics or the morphodynamics.

3. **How do changes in wave direction affect sandy nearshore inlet systems?**

   Clockwise changes in wave direction enhance the largest inlet migration in Katama Inlet, whereas anticlockwise changes suppose the most significant migration in Santa Lucia Estuary. The inlet

migration direction is constant for all the simulations in Katama Inlet, while it shifts in direction (towards the south) in Santa Lucia Inlet for the simulations with anticlockwise changes in wave direction.

Results indicate that the sensitivity to inlet stability owing to changes in wave direction is smaller in Santa Lucia than in the studied sites in recent assessments (Duong et al. 2017; Duong et al. 2018) on CC impacts on tidal inlets. Here, we show that the impact on the hydrodynamics and morphodynamics owing to changes in wave direction depends on the peculiarity of each wave climate. The degree to which changes in wave direction enhance refraction is different at both studied sites, and hence affecting morphodynamics differently. Therefore, the impacts on changes in wave direction must be addressed specifically for each tidal inlet. Consequently, the results from one site cannot be used to determine a general behavior for the assessment of CC impacts in tidal inlet systems.

4. **Are process-based numerical models suitable for this analysis?**

Coupled Delft3D and SWAN models are a suitable tool to analyze the dynamics of tidal inlet systems owing to CC-driven forcings. The models reproduce the inlet migration and the morphodynamic behavior at both sites. Nevertheless, some critical processes cannot be reproduced by these models (e.g., overwash, aeolian transport, or transport due to long waves). Other process-based numerical models (like XBeach) should be used to analyze the implementation of such processes and their impacts on the dynamics owing to CC-driven forcings.

5. **Can these tools be applied to develop a systematic analytical method to analyze the impact of CC on different sandy nearshore inlet systems?**

The proposed methodology is flexible, easily replicable, and can be used as a systematic analytical method to analyze the impact of CC on different sandy nearshore inlet systems. The implementation of the copula analysis to derive the wave boundary conditions is adaptative to different approaches to implement projected changes in wave climate. The result analysis methodology is easily replicable and gives an overall understanding of the system rather than focusing on the inlet.

7.2. Advances

The present research signifies an advance in the analysis of CC-driven forcings on the morphodynamics of inlet systems in that is not just focused on the stability and migration of the inlets, but also on the sediment pathways. It intends to be a bridge for future studies to use a similar result analysis to look at the impacts of CC-driven forcings on the sediment pathways using a morphodynamic connectivity network. These new practices can be used as a tool for management purposes to adapt to CC.

To the author's knowledge, this is the first study to apply a copula analysis to assess climate change impacts on the dynamics of tidal inlets with process-based models. This thesis serves as a proof-of-concept demonstrating the potential for copula analysis as a wave reduction methodology for the

derivation of the present and future state scenarios implemented in Delft3D. The proposed methodology is flexible regarding applying different future state scenarios or MORFAC coefficients, and it can be applied at different sites by merely changing the hindcast data.

7.3. Recommendations

Based on the findings of this report, we make several recommendations for future research and practical applications:

1. **Collect more field data for validation.**

   A scarcity of field data with which to validate the process-based models is one of the key limitations of this thesis. Hence, additional data collection is essential for future work. Specifically, water level and velocity measurements (in the inlet) are needed to validate the models. The use of acoustic Doppler current profilers and similar instruments has been a common practice to collect this type of data in tidal inlets (Staneva et al. 2009; Defendi et al. 2010; Dodet et al. 2013; J. Hopkins, Elgar, and Raubenheimer 2017; and many others). Furthermore, repeated bathymetric surveys through all stages of an inlet migration should be undertaken to provide a field data for a quantitative morphodynamic validation.

2. **Implement an accurate initial bathymetry**

   The model is most sensitive to the initial bathymetry. We had to adjust the bathymetry in Katama Bay to reach a near-equilibrium conditions, and artificially adjust the initial bathymetry at both sites to reproduce the breaching of the inlet. We recommend acquiring the bathymetry of the years a study requires in its analysis and finding accurate measurements of the inlet, especially after the breaching event has taken place.

3. **Copula analysis to derive the wave boundary conditions.**

   This thesis develops a novel framework to derive present and future wave boundary conditions. The utilization of copula distributions to examine the joint probability between the different wave variables provides a robust and flexible framework that adds statistical reasoning to wave reduction methodology. The resulting probability distributions allows changes in the main wave parameters and the joint probability between these parameters to artificially adapt the climate (regular or extreme) to future changes.

4. **Seasonality differentiation**

   This thesis illustrates the different behavior of the systems throughout the seasons. Systems with the following characteristics require a seasonality study: variable wave climate (especially if it is multimodal), irregular river discharge, or unstable tidal inlets with rapid closure (<1 year). We suggest the study of quarterly seasons in boreal or austral locations and two seasons (dry and humid) at sites with equatorial latitudes.

5. Differentiation of projected CC in multimodal wave climates

Changes in wave climate are not projected to be the same around the world. As illustrated in Katama Bay, projections in wave heights suggested that storm waves will be on average less energetic, whereas swell waves will increase in height by 2100. We recommend investigating the changes in wave climate for the different climate types focused on sensitivity to either in direction or frequency. This is specially the case for those sites that present different energetic wave climates (i.e., swell and storm).

6. Implementation – Sea Level Rise

We recommend investigating the sensitivity of the model towards the way the sea level rise is implemented. Other than changing the mean sea level, three main physical processes contribute to coastline change adjacent to basins owing to SLR: basin infilling due to the SLR-induced increase in basin accommodation space, SLR-induced upward movement of the cross-shore profile, and landward movement of the coastline (Ranasinghe et al. 2013). To study each of these in turn, we recommend a bulk increase of the barrier height equal to the SLR. As a first estimator of the shoreline erosion due to SLR, we suggest using the data from the global Dynamic Interactive Vulnerability Assessment (DIVA) (Hinkel et al. 2013). Ranasinghe et al. (2013) proposed that the basin will infill with a lag time of 0.5; therefore in some recent analyses (van der Biezen 2014; Duong et al. 2017; Duong et al. 2018), the basin bed level was increased by approximately half of the SLR amount. The proposed 0.5 lag time value is based on the results from a linearized single-element version of the Aggregated Scale Morphological Interaction between Tidal basin and Adjacent coast (ASMITA) model. Therefore, we recommend performing a sensitivity analysis of the lag time of the basin infilling (e.g., obtain results for a lag time of 0, 0.25, 0.5, and 0.75).

7. Implementation – River Discharge

We suggest investigating the effect of CC-driven variation in the annual river flow into the basin on the basin volume change. In theory, an inlet-basin system will strive to maintain cross-sectional equilibrium velocities (van der Wegen, Dastgheib, and Roelvink 2010). Ranasinghe et al. (2013) suggested an empirical model that can be applied to small tidal basins. Nevertheless, the uniqueness of each site leads us to advise taking these empirical models as what they are; an uncertain simplification of reality.

8. Physical processes not included in Delft3D

We suggest investigating the importance of processes that are not well reproduced by Delft3D (e.g., overwash, transport owing to long waves or aeolian transport). The impact that these processes have on the dynamics of a site may require the implementation of other process-based models (e.g., XBeach).

REFERENCES

AOC Geomatics. 2013. "LIDAR Aerial Survey, St. Lucia, Kwa-Zulu Natal, South Africa." Isimangaliso Wetland Park Authority.

Arkema, Katie K., Greg Guannel, Gregory Verutes, Spencer A. Wood, Anne Guerry, Mary Ruckelshaus, Peter Kareiva, Martin Lacayo, and Jessica M. Silver. 2013. "Coastal Habitats Shield People and Property from Sea-Level Rise and Storms." *Nature Climate Change* 3 (10): 913–18. doi:10.1038/nclimate1944.

Arns, Arne, Sönke Dangendorf, Jürgen Jensen, Stefan Talke, Jens Bender, and Charitha Pattiaratchi. 2017. "Sea-Level Rise Induced Amplification of Coastal Protection Design Heights." *Scientific Reports* 7. Nature Publishing Group: 1–9. doi:10.1038/srep40171.

Arpin, Oscar E. 1970. "Tidal Inlet Problems along the New England Coast." *Coastal Engineering*. Waltham, Massachusetts, 1171–85.

Bate, G C, Alan K Whitfield, and Anthony T Forbes. 2011. "A Review of Studies on the Mfolozi Estuary and Associated Flood Plain, with Emphasis on Information Required by Management for Future Reconnection of the River to the St. Lucia System." *WRC Report*. Gezina, South Africa.

Battjes, J.A., and J. P. M. Janssen. 1978. "Energy Loss and Set-Up Due to Breaking of Random Waves." *Coastal Engineering 1978*. doi:10.1061/9780872621909.034.

Bender, Morris A, Thomas R Knutson, Robert E Tuleya, Joseph J Sirutis, Gabriel A Vecchi, Stephen T Garner, and Isaac M Held. 2009. "Modeled Impact of Anthropogenic Atlantic Hurricanes." *Science* 327 (28): 454–58.

Beukema, J J. 2002. "Expected Changes in the Benthic Fauna of Waden Sea Tidal Flats as a Result of Sea Level Rise or Bottom Subsidence." *Journal of Sea Research* 47: 25–39. doi:10.1016/S1385-1101(01)00095-8.

Booij, N., R. C. Ris, and Leo H. Holthuijsen. 1999. "A Third-Generation Wave Model for Coastal Regions: 1. Model Description and Validation." *Journal of Geophysical Research* 104 (C4): 7649–66. doi:10.1029/98JC02622.

Boothroyd, Jon C. 1985. "Tidal Inlets and Tidal Deltas." In *Coastal Sedimentary Environments*, edited by Richard A Davis, 187–224. New York, NY: Springer New York. doi:10.1007/978-1-4612-5078-4_7.

Bouws, E., and G. J. Komen. 1983. "On the Balance Between Growth and Dissipation in a Extreme Depth-Limited Wind-Sea in the Southern North Sea." *Jornal of Physical Oceanography* 13: 1653–58. doi:10.1175/1520-0485(1983)013<1653:OTBBGA>2.0.CO;2.

Boyd, R., R. Dalrymple, and B. A. Zaitlin. 1992. "Classification of Clastic Coastal Depositional Environments." *Sedimentary Geology* 80 (3–4): 139–50. doi:10.1016/0037-0738(92)90037-R.

Brandon, Tess. 2006. "Hydrodynamics of Tidal Flow Across A Submarine Sand Ridge. Lessons from Middle Ground." Cambridge, MA: Massachusetts Institute of Technology, M.I.T. https://seagrant.mit.edu/publications/MITSG_07-21.pdf.

Bruun, Per, A.J. Mehta, and I. G. Johnsoon. 1978. *Stability of Tidal Inlets, Theory and Engineering*. *Developments in Geotechnical Engineering*. Vol. 23. Amsterdam: Elsevier Scientific Publishing Company. doi:10.1016/B978-0-444-41728-2.50002-3.

Camus, Paula, Iñigo J. Losada, Cristina Izaguirre, Antonio Espejo, Melisa Menéndez, and Jorge Pérez. 2017. "Statistical Wave Climate Projections for Coastal Impact Assessments." *Earth's Future* 5: 918–33. doi:10.1002/2017EF000609.

Camus, Paula, Melisa Menéndez, Fernando J. Méndez, Cristina Izaguirre, Antonio Espejo, Verónica Cánovas, Jorge Pérez, Ana Rueda, Iñigo J. Losada, and Raúl Medina. 2014. "A Weather-Type Statistical Downscaling Framework for Ocean Wave Climate." *Journal of Geophysical Research: Oceans* 119: 7389–7405. doi:10.1002/2014JC010141.

Carbognin, Laura, Pietro Teatini, Alberto Tomasin, and Luigi Tosi. 2010. "Global Change and Relative Sea Level Rise at Venice: What Impact in Term of Flooding." *Climate Dynamics* 35 (6): 1055–63. doi:10.1007/s00382-009-0617-5.

Chen, Lu, Vijay P. Singh, Guo Shenglian, Zenchao Hao, and Tianyuan Li. 2012. "Flood Coincidence Risk Analysis Using Multivariate Copula Functions." *Journal of Hydrologic Engineering* 17 (6): 742–55. doi:10.1061/(ASCE)HE.1943-5584.0000504.

Chrystal, C., and Derek D. Stretch. 2014. "Tidal Flows and Inlet Dynamics of the St Lucia/Mfolozi Estuarine System, South Africa." *Estuarine Coastal and Shelf Science*.

Church, J.a., P.U. Clark, A. Cazenave, J.M. Gregory, S. Jevrejeva, A. Levermann, M.a. Merrifield, et al. 2013. "Sea Level Change." In *Climate Change 2013: The Physical Science Basis. Contribution of Working Group I to the Fifth Assessment Report of the Intergovernmental Panel on Climate Change*, edited by V. Bex and P.M. Midgley Stocker, T.F., D. Qin, G.-K. Plattner, M. Tignor, S.K. Allen, J. Boschung, A. Nauels, Y. Xia, 1137–1216. Cambridge: Cambridge University Press, United Kingdom and New York, NY, USA. doi:10.1017/CB09781107415315.026.

Collins, Matthew, Reto Knutti, Julie Arblaster, Jean-Louis Dufresne, Thierry Fichefet, Pierre Friedlingstein, Xuejie Gao, et al. 2013. *Long-Term Climate Change: Projections, Commitments and Irreversibility*. Edited by V. Bex and P.M. Midgley Stocker, T.F., D. Qin, G.-K. Plattner, M. Tignor, S.K. Allen, J. Boschung, A. Nauels, Y. Xia. *Climate Change 2013: The Physical Science Basis.*

Contribution of Working Group I to the Fifth Assessment Report of the Intergovernmental Panel on Climate Change. Cambridge: University Press, Cambridge, United Kingdom and New York, NY, USA. doi:10.1017/CBO9781107415324.024.

Corbella, S., and D.D. Stretch. 2014. "Directional Wave Spectra on the East Coast of South Africa." *Journal of the South African Institution of Civil Engineering* 56 (3): 53–64. http://www.scielo.org.za/pdf/jsaice/v56n3/07.pdf.

Corbella, S, and D.D. Stretch. 2012. "The Wave Climate on the KwaZulu-Natal Coast of South Africa." *Journal of the South African Institution of Civil Engineering* 54 (2): 45–54. http://www.scielo.org.za/scielo.php?script=sci_arttext&pid=S1021-20192012000200005.

Davies, A.G., and C. Villaret. 1999. "Eulerian Drift Induced by Progressive Waves above Rippled and Very Rough Beds." *Journal of Geophysical Research* 104 (C1): 1465. doi:10.1029/1998JC900016.

Davis, R.A., and D.M. FitzGerald. 2009. *Beaches and Coasts*. John Wiley & Sons.

Davis, Richard A., and Miles O. Hayes. 1984. "What Is a Wave-Dominated Coast?" *Developments in Sedimentology* 39 (C): 313–29. doi:10.1016/S0070-4571(08)70152-3.

Defendi, V., V. Kovačević, F. Arena, and L. Zaggia. 2010. "Estimating Sediment Transport from Acoustic Measurements in the Venice Lagoon Inlets." *Continental Shelf Research* 30 (8): 883–93. doi:10.1016/j.csr.2009.12.004.

Deltares. 2011. "Delft3D-FLOW. Simulation of Multi-Dimensional Hydrodynamic Ows and Transport Phenomena, Including Sediments. User Manual." Rotterdamseweg 185, The Netherlands. www.deltaressystems.nl.

den Heijer, C., Dirk T.J.A. Knipping, Nathaniel G. Plant, Jaap S.M. van Thiel de Vries, Fedor Baart, and Pieter van Geer. 2012. "Impact Assessment of Extreme Storm Events Using a Bayesian Network." *Coastal Engineering Proceedings*, 15. doi:10.9753/icce.v33.management.4.

Dias, Alexandra, and Paul Embrechts. 2004. "Dynamic Copula Models for Multivariate High-Frequency Data in Finance." *Manuscript, ETH Zurich*, no. November: 1–42. http://www2.warwick.ac.uk/fac/soc/wbs/subjects/finance/research/wpaperseries/wf06-250.pdf.

Dissanayake, D. M.P.K., R. Ranasinghe, and J. A. Roelvink. 2012. "The Morphological Response of Large Tidal Inlet/Basin Systems to Relative Sea Level Rise." *Climatic Change* 113 (2): 253–76. doi:10.1007/s10584-012-0402-z.

Dodet, Guillaume, Xavier Bertin, Nicolas Bruneau, André B. Fortunato, Alphonse Nahon, and Aron Roland. 2013. "Wave-Current Interactions in a Wave-Dominated Tidal Inlet." *Journal of Geophysical Research: Oceans* 118 (3): 1587–1605. doi:10.1002/jgrc.20146.

Dunlop, Tom. 2014. "Revised: A History of the Openings (and Closings) Through Norton Point."

Duong, Trang Minh, Roshanka Ranasinghe, A. Luijendijk, D. Walstra, and D. Roelvink. 2017. "Assessing Climate Change Impacts on the Stability of Small Tidal Inlets: Part 1 - Data Poor Environments." *Marine Geology*. doi:10.1016/j.margeo.2017.05.008.

Duong, Trang Minh, Roshanka Ranasinghe, Marcus Thatcher, Sarith Mahanama, Zheng Bing Wang, Pushpa Kumara Dissanayake, Mark Hemer, et al. 2018. "Assessing Climate Change Impacts on the Stability of Small Tidal Inlets: Part 2 - Data Rich Environments." *Marine Geology* 395 (September 2017). Elsevier: 65–81. doi:10.1016/j.margeo.2017.09.007.

Duong, Trang Minh, Roshanka Ranasinghe, Dirkjan Walstra, and Dano Roelvink. 2016. "Assessing Climate Change Impacts on the Stability of Small Tidal Inlet Systems: Why and How?" *Earth-Science Reviews* 154. Elsevier B.V.: 369–80. doi:10.1016/j.earscirev.2015.12.001.

Eakins, B W, L A Taylor, K S Carignan, R R Warnken, E Lim, P R Medley, and Geophysics Division. 2009. *Digital Elevation Model of Nantucket, Massachusetts: Procesures, Data Sources and Analysis. NOAA Technical Memorandum NESDIS NGDC-26 DIGITAL*. Boulder, CO.

Elias, E. P.L., A. J.F. Van Der Spek, Z. B. Wang, and J. De Ronde. 2012. "Morphodynamic Development and Sediment Budget of the Dutch Wadden Sea over the Last Century." *Geologie En Mijnbouw/Netherlands Journal of Geosciences* 91 (3): 293–310. doi:10.1017/S0016774600000457.

Elias, Edwin P L. 2006. "Morphodynamics of Texel Inlet." Delft University of Technology. https://repository.tudelft.nl/islandora/object/uuid:92ad4ac0-9d54-4f5f-8536-80b7782a6aa6?collection=research.

Environmental Mapping & Surveying. 2014. "Lidar & Bathymetric Survey of St Lucia Beach Barrier & Adjoining Offshore Area September 2014. Isimangaliso Wetland Park Authority."

Escoffier, F.F. 1940. "The Stability of Tidal Inlets." *Shore Beach* 8: 111–14.

Eysink, W.D. 1993. "Impact of Sea-Level Rise on the Morphology of the Wadden Sea within the Scope of Its Ecological Function." Delft.

Favre, Anne Catherine, Salaheddine El Adlouni, Luc Perreault, Nathalie Thiémonge, and Bernard Bobée. 2004. "Multivariate Hydrological Frequency Analysis Using Copulas." *Water Resources Research* 40 (1): 1–12. doi:10.1029/2003WR002456.

Flemming, Burghard W., and Alexander Bartholomä. 1997. "Response of the Wadden Sea to a Rising Sea Level: A Predictive Empirical Model." *Deutsche Hydrografische Zeitschrift* 49 (2): 343–53. doi:10.1007/BF02764043.

Galloway, W.E. 1975. "Process Framework for Describing the Morphological and Stratigraphic Evolution of Deltaic Depositional Systems." *Deltas: Models for Exploration*, 87–98.

Glaeser, J Douglas. 1978. "Global Distribution of Barrier Islands in Terms of Tectonic Setting." *The Journal of Geology* 86 (3). The University of Chicago Press: 283–97. doi:10.1086/649691.

Google Earth. 2018a. "Katama Bay, Edgartown, Massachusetts, EE. UU, 41°21'24.13"N 70°29'4.27"W, February 2018." http://www.google.com/earth/.

Google Earth. 2018b. "Santa Lucía Estuary, South Africa, 28°23'13.16"S, 32°25'16.81"E, Febraury 28, 2018." http://google.com/earth/.

Grenfell, S. E., and W. N. Ellery. 2009. "Hydrology, Sediment Transport Dynamics and Geomorphology of a Variable Flow River: The Mfolozi River, South Africa." *Water SA* 35 (3): 271–82. doi:10.4314/wsa.v35i3.

Gronwald, Marc, Janina Ketterer, and Stefan Tr??ck. 2011. "The Relationship between Carbon, Commodity and Financial Markets: A Copula Analysis." *Economic Record* 87 (SUPPL. 1): 105–24. doi:10.1111/j.1475-4932.2011.00748.x.

Haigh, Ivan D., Matt Eliot, and Charitha Pattiaratchi. 2011. "Global Influences of the 18.61 Year Nodal Cycle and 8.85 Year Cycle of Lunar Perigee on High Tidal Levels." *Journal of Geophysical Research: Oceans* 116 (6): 1–16. doi:10.1029/2010JC006645.

Hansen, Jeff E., Britt Raubenheimer, Steve Elgar, Jefrrey H. List, and Thomas C. Lippmann. 2017. "Physical Linkages between an Offshore Canyon and Surf Zone Morphologic Change." *Journal of Geophysical Research: Oceans* 122: 3451–60. doi:10.1002/2016JC012319.

Hasselmann, K., T.P. Barnett, E. Bouws, H. Carlson, D. E. Cartwright, K. Enke, J. A. Ewing, et al. 1973. "Measurements of Wind-Wave Growth and Swell Decay during the Joint North Sea Wave Project (JONSWAP)." *Deutsche Hydrografische Zeitschrift* 12 (A8): 95.

Hayes, M.O. 1979. "Barrier Island Morphology as a Function of Tidal and Wave Regime." *Academic Press*, no. July: 1–27.

Hayes, Miles O. 1975. *Morphology of Sand Accumulation in Estuaries: An Introduction to the Symposium*. Edited by L Eugene B T - Geology and Engineering Cronin. Academic Press. doi:10.1016/B978-0-12-197502-9.50006-X.

Hemer, Mark A., Yalin Fan, Nobuhito Mori, Alvaro Semedo, and Xiaolan L. Wang. 2013. "Projected Changes in Wave Climate from a Multi-Model Ensemble." *Nature Climate Change* 3 (5). Nature Publishing Group: 471–76. doi:10.1038/nclimate1791.

Hinkel, Jochen, Robert J. Nicholls, Richard S.J. Tol, Zheng B. Wang, Jacqueline M. Hamilton, Gerben Boot, Athanasios T. Vafeidis, Loraine McFadden, Andrey Ganopolski, and Richard J.T. Klein. 2013. "A Global Analysis of Erosion of Sandy Beaches and Sea-Level Rise: An Application of DIVA." *Global and Planetary Change* 111. Elsevier B.V.: 150–58. doi:10.1016/j.gloplacha.2013.09.002.

Hirabayashi, Yukiko, Roobavannan Mahendran, Sujan Koirala, Lisako Konoshima, Dai Yamazaki, Satoshi Watanabe, Hyungjun Kim, and Shinjiro Kanae. 2013. "Global Flood Risk under Climate Change." *Nature Climate Change* 3 (9). Nature Publishing Group: 816–21. doi:10.1038/nclimate1911.

Hoek, J. 2017. "Process-Based Modelling of the St Lucia Estuary." Delft University of Technology. https://repository.tudelft.nl/islandora/object/uuid%3A9838976f-a838-4f74-9ce1-8892e718906b?collection=education.

Hopkins, J.A. 2017. "Field Observations and Numerical Model Simulations of a Migrating Inlet System." Massachusetts Institute of Technology (M.I.T.). https://dspace.mit.edu/handle/1721.1/113475.

Hopkins, Julia, Steve Elgar, and Britt Raubenheimer. 2017. "Flow Separation Effects on Shoreline Sediment Transport." *Coastal Engineering* 125 (October 2016). Elsevier: 23–27. doi:10.1016/j.coastaleng.2017.04.007.

Hulme, Mike, Ruth Doherty, Todd Ngara, Mark New, and David Lister. 2001. "African Climate Change: 1900-2100." *Climate Research* 17: 145–68. doi:10.3354/cr017145.

IPCC. 2000. "Summary for Policymakers: Emissions Scenarios. A Special Report of Working Group III of the Intergovernmental Panel on Climate Change." *Group*, 20. doi:92-9169-113-5.

IPCC. 2014a. *Climate Change 2014: Mitigation of Climate Change. Summary for Policymakers and Technical Summary*. *Climate Change 2014: Mitigation of Climate Change. Part of the Working Group III Contribution to the Fifth Assessment Report of the Intergovernmental Panel on Climate Change.* doi:10.1017/CBO9781107415416.005.

IPCC. 2014b. *Climate Change 2014: Synthesis Report. Contribution of Working Groups I, II and III to the Fifth Assessment Report of the Intergovernmental Panel on Climate Change*. Edited by R.K. Pachauri and L.A. Meyer Core Writing Team. Geneva, Switzeland: IPCC. doi:10.1017/CBO9781107415324.004.

Isobe, Masahiko, and Kiyoshi Horikawa. 1982. "Study on Water Particle Velocities of Shoaling and Breaking Waves." *Coastal Engineering in Japan* 25 (1). Taylor & Francis: 109–23. doi:10.1080/05785634.1982.11924340.

Johnson, Jennifer M., Laura J. Moore, Kenneth Ells, A. Brad Murray, Peter N. Adams, Richard A. Mackenzie, and John M. Jaeger. 2015. "Recent Shifts in Coastline Change and Shoreline Stabilization Linked to Storm Climate Change." *Earth Surface Processes and Landforms* 40 (5): 569–85. doi:10.1002/esp.3650.

Jonsson, Ivar G, and Niels A Carlsen. 1976. "Experimental and Theoretical Investigations in an Oscillatory Turbulent Boundary Layer." *Journal of Hydraulic Research* 14 (1). Taylor & Francis: 45–60. doi:10.1080/00221687609499687.

Kamphuis, J.W. 1991. "Alongshore Sediment Transport Rate." *Journal of Waterway, Port, Coastal, and Ocean Engineering* 117 (6): 624. doi:10.1061/(ASCE)0733-950X(1991)117:6(624).

Kirwan, Matthew L., and J. Patrick Megonigal. 2013. "Tidal Wetland Stability in the Face of Human Impacts and Sea-Level Rise." *Nature* 504 (7478): 53–60. doi:10.1038/nature12856.

Komar, P.D. 1998. *Beach Processes and Sedimentation*. Edited by Pretice Hall. 2nd ed. New Jersey: Pretice-Hall, Inc.

Komen, G. J., and K. Hasselmann. 1984. "On the Existence of a Fully Developed Wind-Sea Spectrum." *Journal of Physical Oceanography*. doi:10.1175/1520-0485(1984)014<1271:OTEOAF>2.0.CO;2.

Kriel, J. 1966. "Report of the Commission of Inquiry into the Alleged Threat to Plant and Animal Life in St Lucia Lake." Pretoria: Government Printer.

Lawrie, Robynne A., and Derek D. Stretch. 2011. "Anthropogenic Impacts on the Water and Salt Budgets of St Lucia Estuarine Lake in South Africa." *Estuarine, Coastal and Shelf Science* 93 (1). Elsevier Ltd: 58–67. doi:10.1016/j.ecss.2011.04.005.

Lee, Guan hong, Robert J. Nicholls, and William A. Birkemeier. 1998. "Storm-Driven Variability of the Beach-Nearshore Profile at Duck, North Carolina, USA, 1981-1991." *Marine Geology* 148 (3–4): 163–77. doi:10.1016/S0025-3227(98)00010-3.

Leendertse, J J. 1987. "A Three-Dimensional Alternating Direction Implicit Model with Iterative Fourth Order Dissipative Non-Linear Advection Terms." *Report WD-3333-NETH*. Rijkswaterstaat.

Lopes, Carina L., Paulo A. Silva, João M. Dias, Alfredo Rocha, Ana Picado, Sandra Plecha, and André B. Fortunato. 2011. "Local Sea Level Change Scenarios for the End of the 21st Century and Potential Physical Impacts in the Lower Ria de Aveiro (Portugal)." *Continental Shelf Research* 31 (14): 1515–26. doi:10.1016/j.csr.2011.06.015.

Masina, Marinella, Alberto Lamberti, and Renata Archetti. 2015. "Coastal Flooding: A Copula Based Approach for Estimating the Joint Probability of Water Levels and Waves." *Coastal Engineering* 97. Elsevier B.V.: 37–52. doi:10.1016/j.coastaleng.2014.12.010.

McGranahan, Gordon, Deborah Balk, and Bridget Anderson. 2007. "The Rising Tide: Assessing the Risks of Climate Change and Human Settlements in Low Elevation Coastal Zones." *Environment and Urbanization* 19 (1): 17–37. doi:10.1177/0956247807076960.

Mehta, By Ashish J, Earl J Hayter, W Reginald Parker, Ray B Krone, and Allen M Teeter. 1990. "Cohesive Sediment Transport. I: Process Description." *Hydraulic Engineering* 115 (8): 1076–93.

Mori, Nobuhito, Tomoya Shimura, Tomohiro Yasuda, and Hajime Mase. 2013. "Multi-Model Climate Projections of Ocean Surface Variables under Different Climate Scenarios-Future Change of Waves, Sea Level and Wind." *Ocean Engineering* 71. Elsevier: 122–29. doi:10.1016/j.oceaneng.2013.02.016.

Müller, M., B. K. Arbic, and J. X. Mitrovica. 2011. "Secular Trends in Ocean Tides: Observations and Model Results." *Journal of Geophysical Research: Oceans* 116 (5): 1–19. doi:10.1029/2010JC006387.

National Geophysical Data Center. 1999. "Coastal Relief Model." U.S. Department of Commerce. doi:10.7289/V5MS3QNZ.

Niang, I., O.C. Ruppel, M.A. Abdrabo, A. Essel, C. Lennard, J. Padgham, and P. Urquhart. 2014. *Africa*. Edited by and L.L. White Barros, V.R., C.B. Field, D.J. Dokken, M.D. Mastrandrea, K.J. Mach, T.E. Bilir, M. Chatterjee, K.L. Ebi, Y.O. Estrada, R.C. Genova, B. Girma, E.S. Kissel, A.N. Levy, S. MacCracken, P.R. Mastrandrea. *Climate Change 2014: Impacts, Adaptation and Vulnerability - Contributions of the Working Group II to the Fifth Assessment Report of the Intergovernmental Panel on Climate Change*. Cambridge, United Kingdom and New York, NY, USA: Cambridge University Press. doi:10.1017/CBO9781107415386.002.

Nicholls, R.J., P P Wong, V. Burkett, J Codignotto, and J. Hay. 2007. "Coastal Systems and Low-Lying Areas." *Climate Change 2014 Impacts, Adaptation, and Vulnerability*, 361–410. doi:10.1017/CBO9781107415379.010.

Nicholls, Robert J., Susan E. Hanson, Jason A. Lowe, Richard A. Warrick, Xianfu Lu, and Antony J. Long. 2014. "Sea-Level Scenarios for Evaluating Coastal Impacts." *Wiley Interdisciplinary Reviews: Climate Change* 5 (1): 129–50. doi:10.1002/wcc.253.

Nienhuis, Jaap H., and Andrew D. Ashton. 2016. "Mechanics and Rates of Tidal Inlet Migration: Modeling and Application to Natural Examples." *Journal of Geophysical Research: Earth Surface* 121 (11): 2118–39. doi:10.1002/2016JF004035.

Nohara, Daisuke, Akio Kitoh, Masahiro Hosaka, and Taikan Oki. 2006. "Impact of Climate Change on River Discharge Projected by Multimodel Ensemble." *Journal of Hydrometeorology* 7 (5): 1076–89. doi:10.1175/JHM531.1.

O'Brien, M.P., and R.G. Dean. 1972. "Hydraulics and Sedimentary Stability of Coastal Inlets." *Coastal Engineering*. Proceedings. Vancouver, British Columbia, Canada: American Society of Civil Engineers. doi:doi:10.1061/9780872620490.044.

Oost, A. P., H. de Haas, F. Ijnsen, J. M. van den Boogert, and P. L. de Boer. 1993. "The 18.6 Yr Nodal Cycle and Its Impact on Tidal Sedimentation." *Sedimentary Geology* 87 (1–2): 1–11. doi:10.1016/0037-0738(93)90032-Z.

Orescanin, Mara M., Steve Elgar, and Britt Raubenheimer. 2016. "Changes in Bay Circulation in an Evolving Multiple Inlet System." *Continental Shelf Research* 124. Elsevier: 13–22. doi:10.1016/j.csr.2016.05.005.

Orescanin, Mara, Britt Raubenheimer, and Steve Elgar. 2014. "Obervations of Wave Effects on Inlet Circulation." *Continental Shelf Research* 82: 37–42. doi:10.1016/j.csr.2014.04.010.

Pearson, S.G., B.C. van Prooijen, Z.B. Wang, and J.P. Bak. 2017. "Sediment Connectivity and Transport Pathways in Tidal Inlets: A Conceptual Framework with Application to Ameland Inlet." In *American Geophysical Union Fall Meeting*. New Orleands, Louisiana.

Perez, Jorge, Melisa Menendez, Paula Camus, Fernando J. Mendez, and Inigo J. Losada. 2015. "Statistical Multi-Model Climate Projections of Surface Ocean Waves in Europe." *Ocean Modelling* 96. Elsevier Ltd.: 161–70. doi:10.1016/j.ocemod.2015.06.001.

Perissinotto, Renzo, Derek D. Stretch, and R. H. Taylor. 2013. *Ecology and Conservation of Estuarine Ecosystems. Lake St Lucia as a Global Model*. First. Barcelona: Cambridge University Press.

Pickering, M. D., K. J. Horsburgh, J. R. Blundell, J. J.M. Hirschi, R. J. Nicholls, M. Verlaan, and N. C. Wells. 2017. "The Impact of Future Sea-Level Rise on the Global Tides." *Continental Shelf Research* 142 (February). Elsevier Ltd: 50–68. doi:10.1016/j.csr.2017.02.004.

Poelhekke, Laurens. 2015. "Predicting Coastal Hazards with a Bayesian Network." Delft University of Technology. http://resolver.tudelft.nl/uuid:8875d3be-5686-4272-b8e5-394f760157cf.

Ranasinghe, Roshanka. 2016. "Assessing Climate Change Impacts on Open Sandy Coasts: A Review." *Earth-Science Reviews* 160. Elsevier B.V.: 320–32. doi:10.1016/j.earscirev.2016.07.011.

Ranasinghe, Roshanka, Trang Minh Duong, Stefan Uhlenbrook, Dano Roelvink, and Marcel Stive. 2013. "Climate-Change Impact Assessment for Inlet-Interrupted Coastlines." *Nature Climate Change* 3 (1). Nature Publishing Group: 83–87. doi:10.1038/nclimate1664.

Ranasinghe, Roshanka, Cilia Swinkels, Arjen Luijendijk, Dano Roelvink, Judith Bosboom, Marcel Stive, and DirkJan Walstra. 2011. "Morphodynamic Upscaling with the MORFAC Approach: Dependencies and Sensitivities." *Coastal Engineering* 58 (8). Elsevier B.V.: 806–11. doi:10.1016/j.coastaleng.2011.03.010.

Ray, Richard D. 2009. "Secular Changes in the Solar Semidiurnal Tide of the Western North Atlantic Ocean." *Geophysical Research Letters* 36 (19): 1–5. doi:10.1029/2009GL040217.

Reed, Denise J. 1995. "The Response of Coastal Marshes to Sea‐level Rise: Survival or Submergence?" *Earth Surface Processes and Landforms* 20 (1): 39–48. doi:10.1002/esp.3290200105.

Rego, João L., and Chunyan Li. 2010. "Storm Surge Propagation in Galveston Bay during Hurricane Ike." *Journal of Marine Systems* 82 (4). Elsevier B.V.: 265–79. doi:10.1016/j.jmarsys.2010.06.001.

Roelvink, Dano, Ad Reniers, Ap van Dongeren, Jaap van Thiel de Vries, Robert McCall, and Jamie Lescinski. 2009. "Modelling Storm Impacts on Beaches, Dunes and Barrier Islands." *Coastal Engineering* 56 (11–12). Elsevier B.V.: 1133–52. doi:10.1016/j.coastaleng.2009.08.006.

Salvadori, G., G. R. Tomasicchio, and F. D'Alessandro. 2014. "Practical Guidelines for Multivariate Analysis and Design in Coastal and Off-Shore Engineering." *Coastal Engineering* 88. Elsevier B.V.: 1–14. doi:10.1016/j.coastaleng.2014.01.011.

SANHO. 2018. "Ocean Rhythm - Wind, Swell, Tidal, Solar and Lunar Rhythms around South Africa." http://www.satides.co.za/.

Schoonees, J. S. 2000. "Annual Variation in the Net Longshore Sediment Transport Rate." *Coastal Engineering* 40 (2): 141–60. doi:10.1016/S0378-3839(00)00009-0.

Schumann, E. 2013. "Sea Level Variability in South African Estuaries." *South African Journal of Science* 109 (3–4): 1–7. http://www.scielo.org.za/scielo.php?pid=S0038-23532013000200010&script=sci_arttext&tlng=pt.

Shope, James B., Curt D. Storlazzi, Li H. Erikson, and Christie A. Hegermiller. 2016. "Changes to Extreme Wave Climates of Islands within the Western Tropical Pacific throughout the 21st Century under RCP 4.5 and RCP 8.5, with Implications for Island Vulnerability and Sustainability." *Global and Planetary Change* 141. Elsevier B.V.: 25–38. doi:10.1016/j.gloplacha.2016.03.009.

Singleton, A. T., and C. J. C. Reason. 2007. "A Numerical Model Study of an Intense Cutoff Low Pressure System over South Africa." *Monthly Weather Review* 135 (3): 1128–50. doi:10.1175/MWR3311.1.

Sklar, A. 1959. *Fonctions de Répartition à n Dimensions et Leurs Marges. Publ. Inst. Statist. Univ. Paris*. 8th ed. Vol. 8. Publications de l'Institut de Statistique de L'Université de Paris. doi:10.1007/978-3-642-33590-7.

Smith, Maddie. 2012. "Sediment Transport in Katama Bay and Inlet, Martha's Vineyard, Massachusetts" 1921 (1974): 1–15.

Staneva, Joanna, Emil V. Stanev, Jörg Olaf Wolff, Thomas H. Badewien, Rainer Reuter, Burghard Flemming, Alexander Bartholomä, and Karsten Bolding. 2009. "Hydroynamics and Sediment Dynamics in the German Bight. A Focus on Observations and Numerical Modelling in the East Frisian Wadden Sea." *Continental Shelf Research* 29 (1): 302–19. doi:10.1016/j.csr.2008.01.006.

Stelling, Guus S, and Jan J Leendertse. 1992. "Approximation of Convective Processes by Cyclic AOI Methods." In *Estuarine and Coastal Modeling*, 771–82. ASCE.

Sterl, Andreas, Alexander M R Bakker, Henk W Van Den Brink, Rein Haarsma, Andrew Stepek, Ine L. Wijnant, and Renske C De Winter. 2015. "Large-Scale Winds in the Southern North Sea Region: The Wind Part of the KNMI'14 Climate Change Scenarios." *Environmental Research Letters* 10 (3). IOP Publishing: 0–8. doi:10.1088/1748-9326/10/3/035004.

Storlazzi, Curt D., James B. Shope, Li H. Erikson, Christine A. Hegermiller, and Patrick L. Barnard. 2015. "Future Wave and Wind Projections for United States and United States-Affiliated Pacific Islands." *U.S. Geological Survey Open-File Report 2015–1001*, 426 p. doi:http://dx.doi.org/10.3133/ofr20151001.

Taylor, R. H. 1993. "Proceedings of the Workshop on Water Requirements for Lake St. Lucia, Organised by the St. Lucia Ecological and Technical Committee (SCADCO) and Held at Fanies Island, St. Lucia on 12 and 13 May 1992." In , 83. South Africa, Department of Environmental Affairs.

Turpie, J. K., J. B. Adams, A. Joubert, T. D. Harrison, B. M. Colloty, R. C. Maree, A. K. Whitfield, et al. 2002. "Assessment of the Conservation Priority Status of South African Estuaries for Use in Management and Water Allocation." *Water SA* 28 (2): 191–206. doi:10.4314/wsa.v28i2.4885.

United Nations. 2014. *World Urbanization Prospects*. New York, NY: United Nations. doi:10.18356/527e5125-en.

Valentim, J. M., N. Vaz, H. Silva, B. Duarte, I. Caçador, and J. M. Dias. 2013. "Tagus Estuary and Ria de Aveiro Salt Marsh Dynamics and the Impact of Sea Level Rise." *Estuarine, Coastal and Shelf Science* 130. Elsevier Ltd: 138–51. doi:10.1016/j.ecss.2013.04.005.

van de Kreeke, J. 1992. "Stability of Tidal Inlets. Escoffier's Analysis." *Shore and Beach* 60 (1): 9–12.

van der Biezen, T.F. 2014. "Climate Change and the Morphological Stability of the Tu Hien Inlet, Vietnam." Delft University of Technology. https://repository.tudelft.nl/islandora/object/uuid%3Ad80b095b-9e54-42e8-a06e-d144ae8d14ee.

van der Wegen, M., A. Dastgheib, and J. A. Roelvink. 2010. "Morphodynamic Modeling of Tidal Channel Evolution in Comparison to Empirical PA Relationship." *Coastal Engineering* 57 (9). Elsevier B.V.: 827–37. doi:10.1016/j.coastaleng.2010.04.003.

van Goor, M. A., T. J. Zitman, Z. B. Wang, and M. J.F. Stive. 2003. "Impact of Sea-Level Rise on the Morphological Equilibrium State of Tidal Inlets." *Marine Geology* 202 (3–4): 211–27. doi:10.1016/S0025-3227(03)00262-7.

van Ledden, Mathijs, Zheng Bing Wang, Han Winterwerp, and Huib De Vriend. 2004. "Sand-Mud Morphodynamics in a Short Tidal Basin." *Ocean Dynamics* 54 (3–4): 385–91. doi:10.1007/s10236-003-0050-y.

van Rijn, Leo C. 1993. *Principles of Sediment Transport in Rivers, Estuaries and Coastal Seas*. Blokzijl, Netherlands: Aqua Publishing.

van Rijn, Leo C., D.J.R. Walstra, and M. van Ormondt. 2004. "Description of TRANSPOR2004 and Implementation in Delft3D, WL | Delft Hydraulics Report Z3748.00," no. May.

van Rijn, Leo C., and Dirkjan Walstra. 2003. "Modelling of Sand Transport in DELFT3D." *WL Delft Hydraulics*. Delft.

van Vuuren, Detlef P., Jae Edmonds, Mikiko Kainuma, Keywan Riahi, Allison Thomson, Kathy Hibbard, George C. Hurtt, et al. 2011. "The Representative Concentration Pathways: An Overview." *Climatic Change* 109 (1): 5–31. doi:10.1007/s10584-011-0148-z.

Wahl, T., C. Mudersbach, and J. Jensen. 2012. "Assessing the Hydrodynamic Boundary Conditions for Risk Analyses in Coastal Areas: A Multivariate Statistical Approach Based on Copula Functions." *Natural Hazards and Earth System Science* 12 (2): 495–510. doi:10.5194/nhess-12-495-2012.

Walstra, Dirkjan, R. Hoekstra, P. K. Tonnon, and B. G. Ruessink. 2013. "Input Reduction for Long-Term Morphodynamic Simulations in Wave-Dominated Coastal Settings." *Coastal Engineering* 77. Elsevier B.V.: 57–70. doi:10.1016/j.coastaleng.2013.02.001.

Wang, Yunwei, Qian Yu, Jian Jiao, Pieter Koen Tonnon, Zheng Bing Wang, and Shu Gao. 2016. "Coupling Bedform Roughness and Sediment Grain-Size Sorting in Modelling of Tidal Inlet Incision." *Marine Geology* 381 (September): 128–41. doi:10.1016/j.margeo.2016.09.004.

Wang, Z. B., P. Hoekstra, H. Burchard, H. Ridderinkhof, H. E. De Swart, and M. J.F. Stive. 2012. "Morphodynamics of the Wadden Sea and Its Barrier Island System." *Ocean and Coastal Management* 68. Elsevier Ltd: 39–57. doi:10.1016/j.ocecoaman.2011.12.022.

Wang, Z. B., T. Louters, and H. J. de Vriend. 1995. "Morphodynamic Modelling for a Tidal Inlet in the Wadden Sea." *Marine Geology* 126 (1–4): 289–300. doi:10.1016/0025-3227(95)00083-B.

Warner, Natalya N., and Philippe E. Tissot. 2012. "Storm Flooding Sensitivity to Sea Level Rise for Galveston Bay, Texas." *Ocean Engineering* 44. Elsevier: 23–32. doi:10.1016/j.oceaneng.2012.01.011.

Whitfield, A. K., and R.H. Taylor. 2009. "A Review of the Importance of Freshwater Inflow to the Future Conservation of Lake St Lucia." *Aquatic Conservation: Marien and Freswater Ecosystems* 19 (September): 838–48. doi:10.1002/aqc.1061.

Wright, C. I., and T. R. Mason. 1990. "Sedimentary Environment and Facies of St Lucia Estuary Mouth, Zululand, South Africa." *Journal of African Earth Sciences* 11 (3–4): 411–20. doi:10.1016/0899-5362(90)90020-F.

Wright, L. D., and A. D. Short. 1984. "Morphodynamic Variability of Surf Zones and Beaches: A Synthesis." *Marine Geology* 56 (1–4): 93–118. doi:10.1016/0025-3227(84)90008-2.

Yang, Lu, and Shigeyuki Hamori. 2013. "Dependence Structure among International Stock Markets: A GARCH–copula Analysis." *Applied Financial Economics* 23 (23). Routledge: 1805–17. doi:10.1080/09603107.2013.854296.

Young, I. R., S. Zieger, and A. V. Babanin. 2011. "Global Trends in Wind Speed and Wave Height." *Science* 159: 451–55. doi:10.1126/science.1197219.

Zhang, Qiang, Mingzhong Xiao, and Vijay P. Singh. 2015. "Uncertainty Evaluation of Copula Analysis of Hydrological Droughts in the East River Basin, China." *Global and Planetary Change* 129. Elsevier B.V.: 1–9. doi:10.1016/j.gloplacha.2015.03.001.

Appendix A. TIDAL INLET FEATURES

Strong velocities through the inlet cause exchange of sediment between the basins and the open sea, leading to the formation of a flood delta inside the basin and an ebb delta in the nearshore area. Velocities through the inlet decrease when the water diverges either inside the basin or in the open sea, facilitating the settlement of sediment. This sediment is then transported either by the residual tidal currents or by the wave-induced currents.

The ebb-tidal delta (see Figure A.1) typically includes the following morphological components (Miles O Hayes 1975):

- A deep main ebb channel scoured by high current velocities.
- Marginal flood channels (to either side of the inlet), shallow channels shaped by flood currents.
- Channel margin linear bars. These are bars that flank the main ebb channel and are built by the interaction of ebb and flood-tidal currents with wave generated currents.
- Swash bars. These have an arc-shape and migrate onshore within the ebb-tidal delta owing to wave action.
- Terminal lobe, formed by sediment deposited out of the main channel where the ebb velocities are smaller than the threshold velocity of motion.

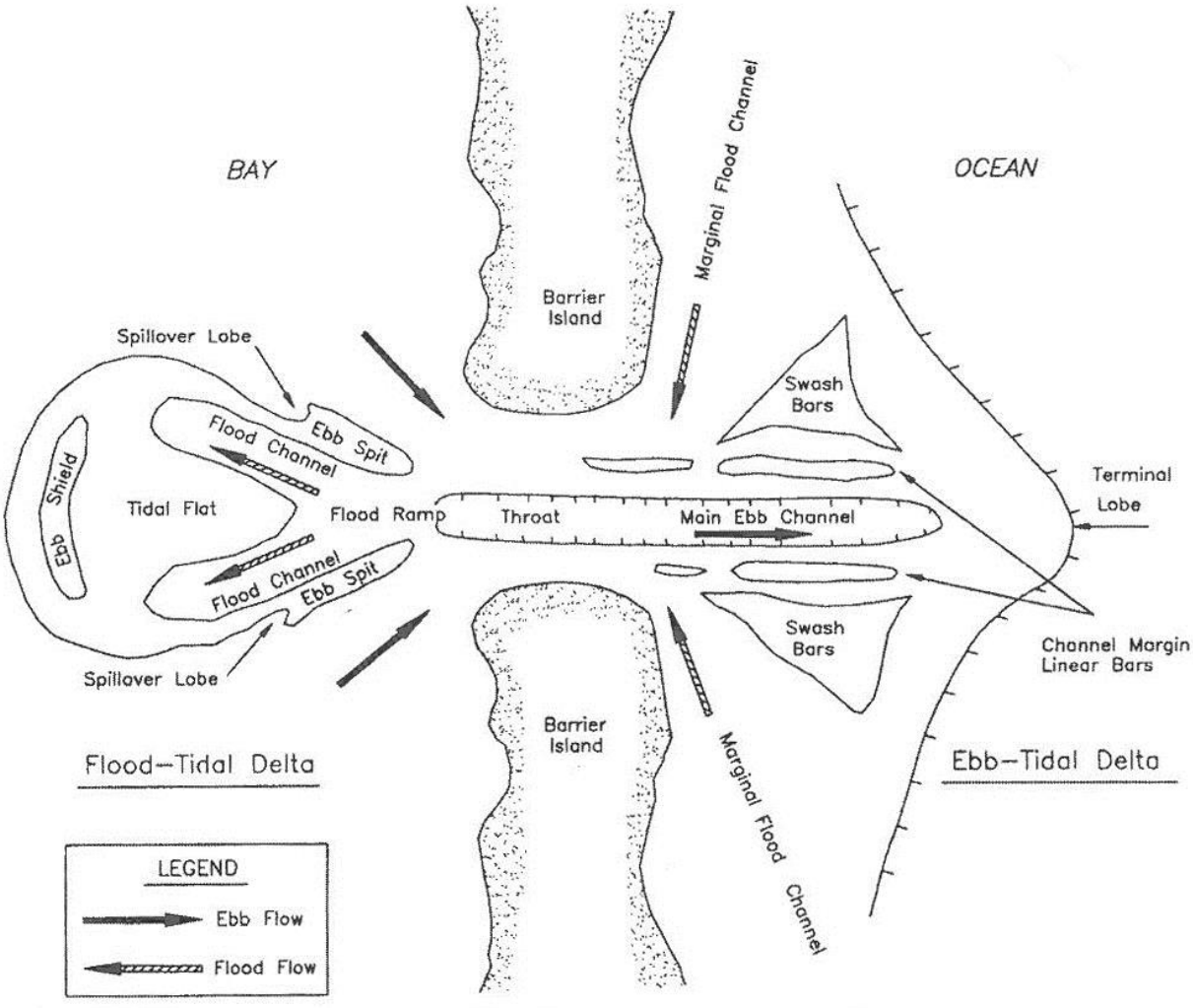

Figure A.1. Morphological elements of a tidal inlet (Boothroyd 1985).

The flood-tidal delta (see Figure A.1) typically contains the next morphological elements (M.O. Hayes 1979):

- Ebb shield. The diverge of currents along the edge of the flood delta creates the ebb shield. It is the equivalent of the terminal lobe of the ebb tidal deltas.
- Flood Ramp. A sediment body that slopes upwards and ends at the ebb shield.
- Flood Channels. The flood ramp branches into two shallow channels dominated by flood-tidal currents. These channels are the sand path to the flood delta.
- Ebb spits. They form when sand is eroded from the ebb shield and transported back through the inlet by ebb-tidal currents.
- Spillover lobes. Interaction of flood and ebb currents breach the ebb spits creating the spillover lobes.

Appendix B. COPULA RESULTS

B.1 Katama Bay

A correlation analysis between the significant wave height, the peak wave period, and the wave direction is performed to determine the need to include these variables into the copula distribution. Table B.1 summarizes the correlation illustrated in Figure B.1, Figure B.2, and Figure B.3. Wave peak period and wave direction have the highest correlation (around 0.4), which is higher in summer owing to a more persistent swell. Significant wave height has a low correlation with the other two variables (most values between 0.1 and 0.2). Therefore, we do not include the significant wave height in the empirical copula.

Table B.1. Correlation factor between wave direction (θ_p), significant wave height (H_s), and peak wave period (T_p) in Katama Bay.

Correlation Factor ρ				
	Winter	Spring	Summer	Fall
Dp/Hs	0.097	0.081	0.257	0.084
Dp/Tp	-0.441	-0.425	-0.477	-0.309
Hs/Tp	0.212	0.191	-0.102	0.136

We use generalized extreme value distributions (GEV) to fit the significant wave heights, and kernel distributions to fit the peak wave periods and the wave directions. We use empirical copulas with a resolution of 200 points to represent the joint probability between the peak wave period and the wave direction. We use this methodology as a wave reduction method owing to the implementation of a MORFAC of 12 in Delft3D. Figure B.4, Figure B.5, Figure B.6, and Figure B.7 show the winter, spring, summer, and autumn copula results respectively.

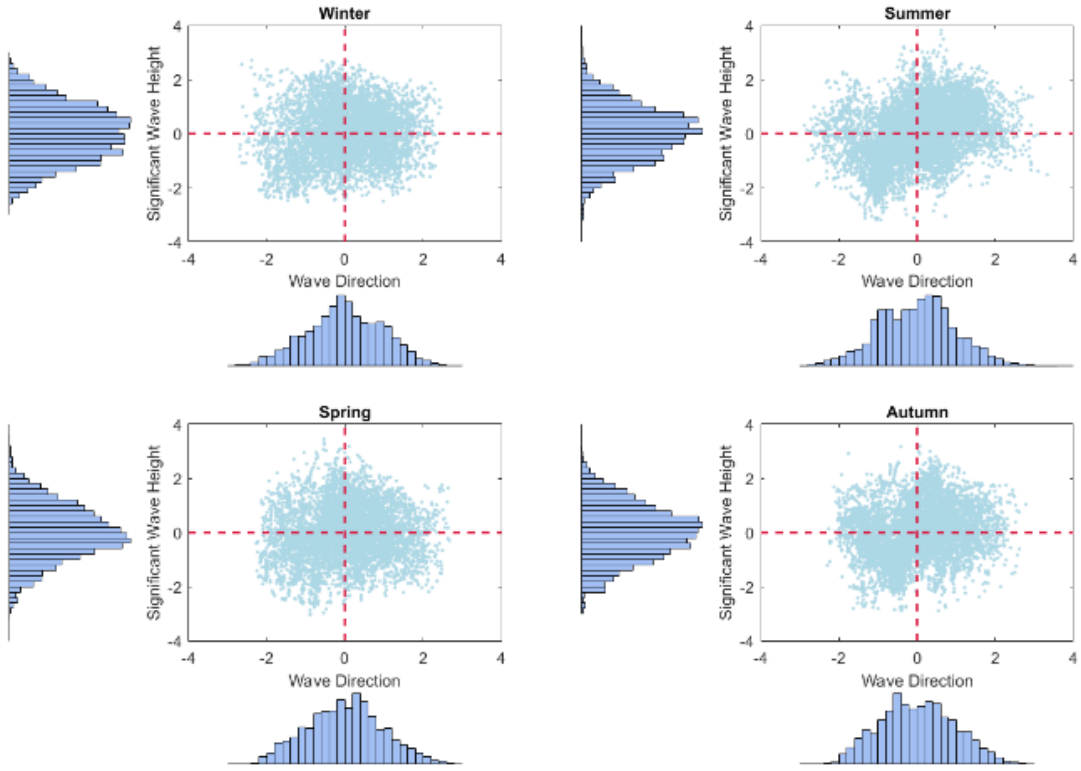

Figure B.1. Correlation between significant wave height (H_s) and wave direction (θ_p) at Katama Bay. The marginal distributions are standard normal (μ=0 and σ=1).

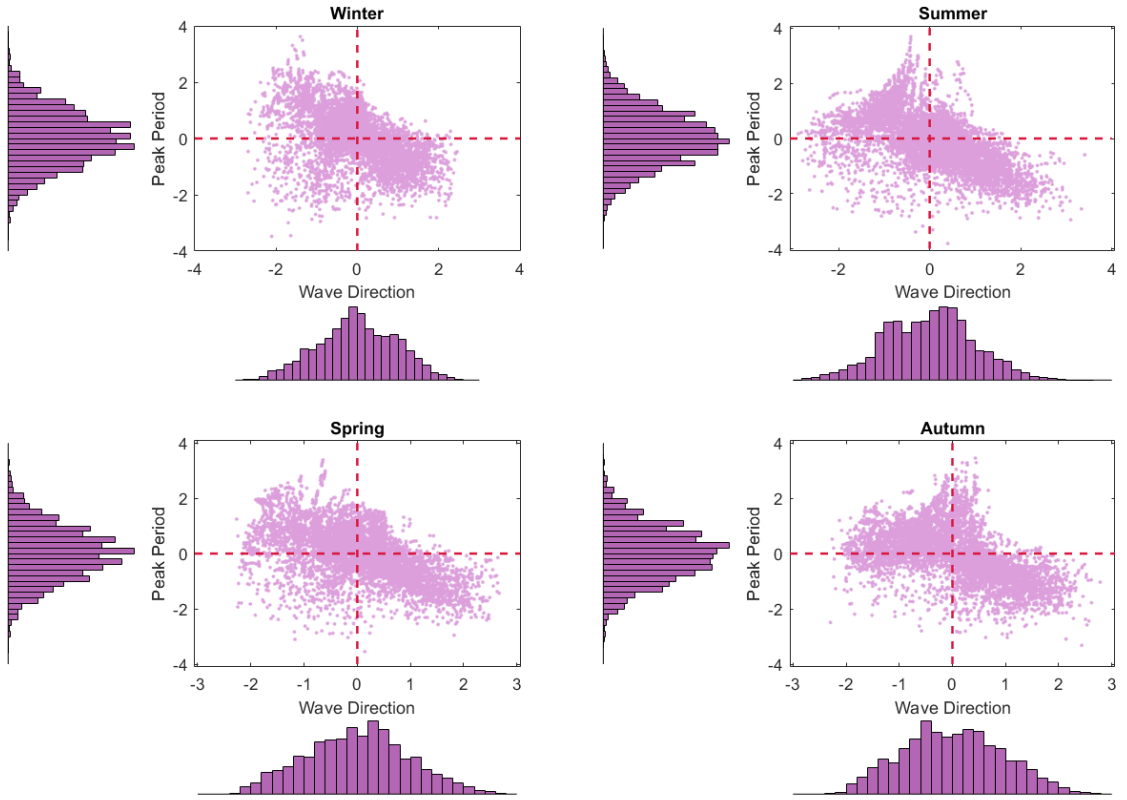

Figure B.2. Correlation between peak wave period (T_p) and wave direction (θ_p) at Katama Bay. The marginal distributions are standard normal (μ=0 and σ=1).

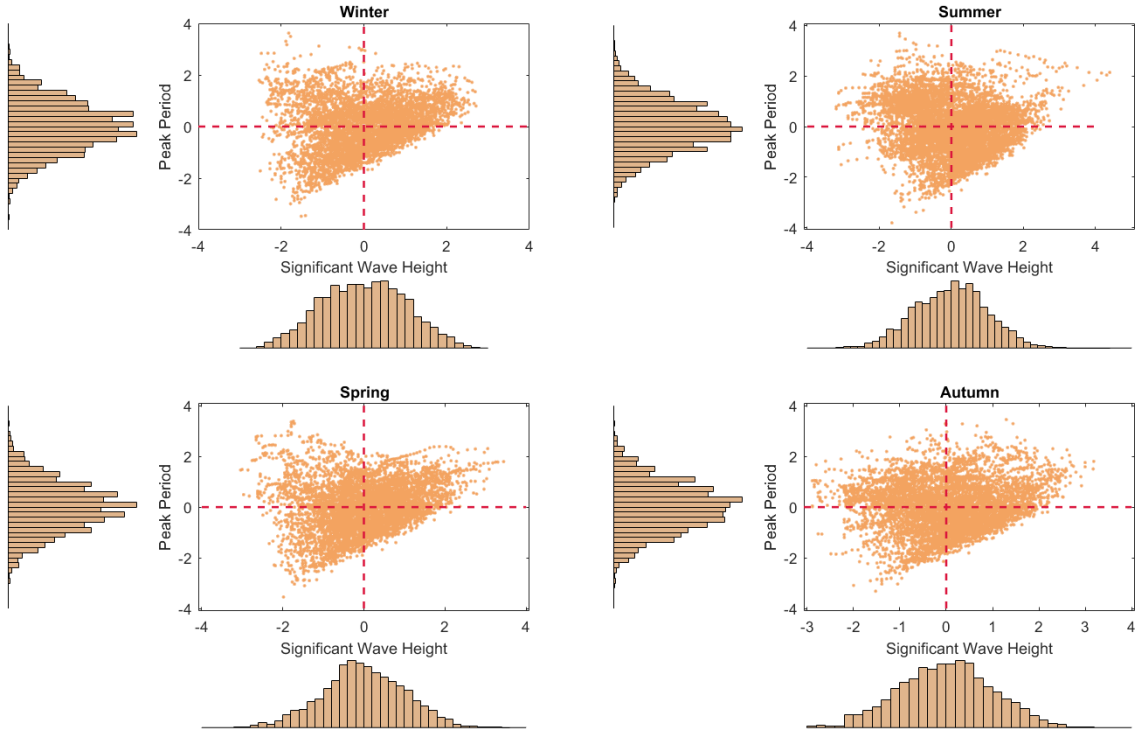

Figure B.3. Correlation between significant wave height (H_S) and peak wave period (T_p) at Katama Bay. The marginal distributions are standard normal (μ=0 and σ=1).

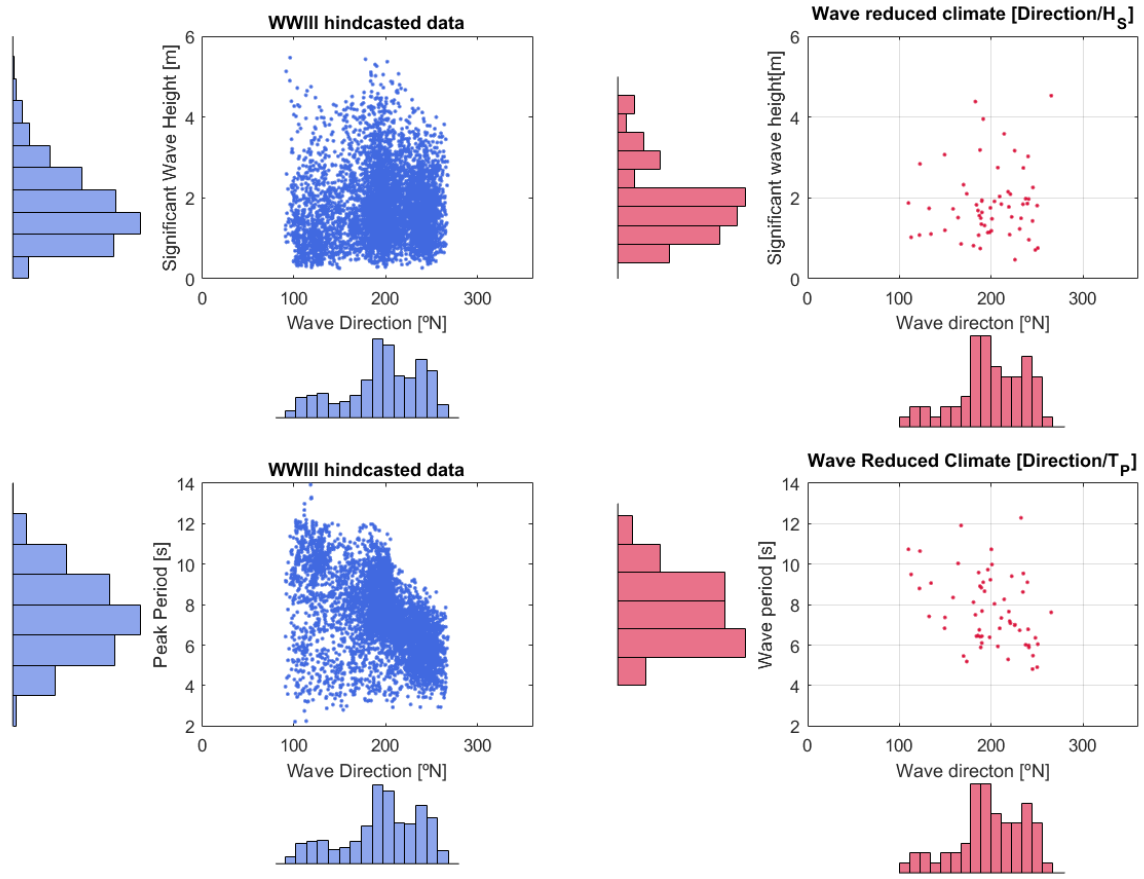

Figure B.4. Winter reduced wave climate in Katama Bay (crimson color) using a MORFAC of 12. The reduction is made by applying a copula analysis from the WWIII hindcast data (blue color).

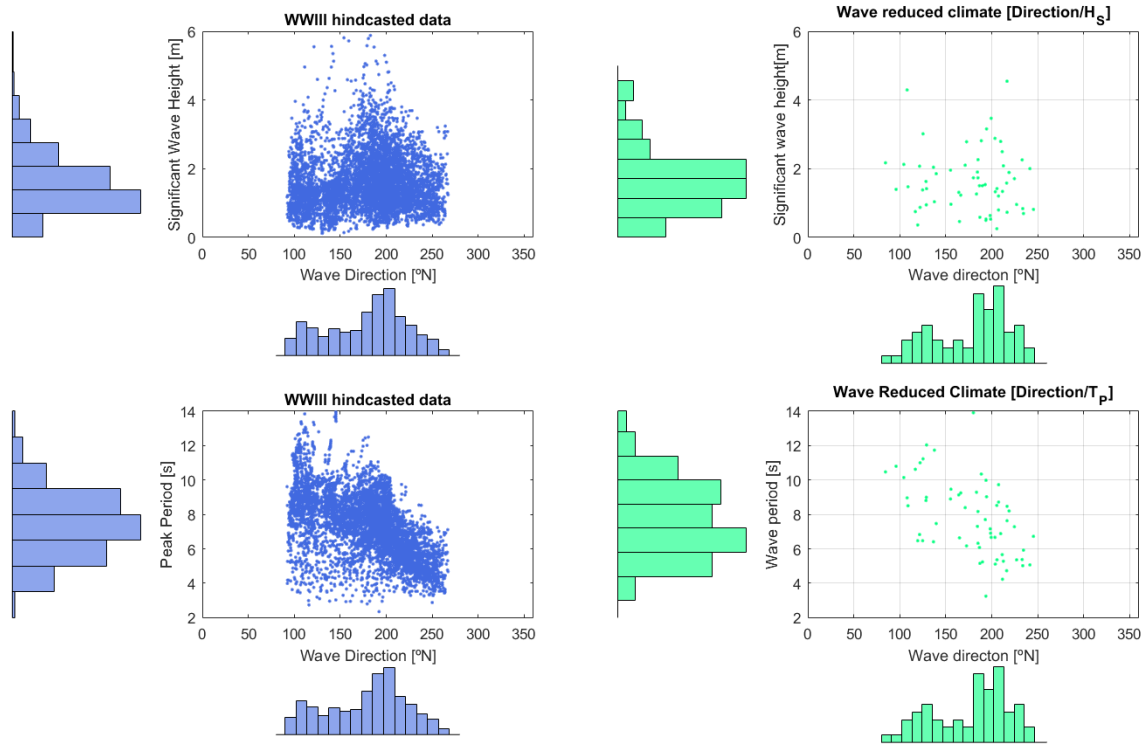

Figure B.5. Spring reduced wave climate in Katama Bay (green color) using a MORFAC of 12. The reduction is made by applying a copula analysis from the WWIII hindcast data (blue color).

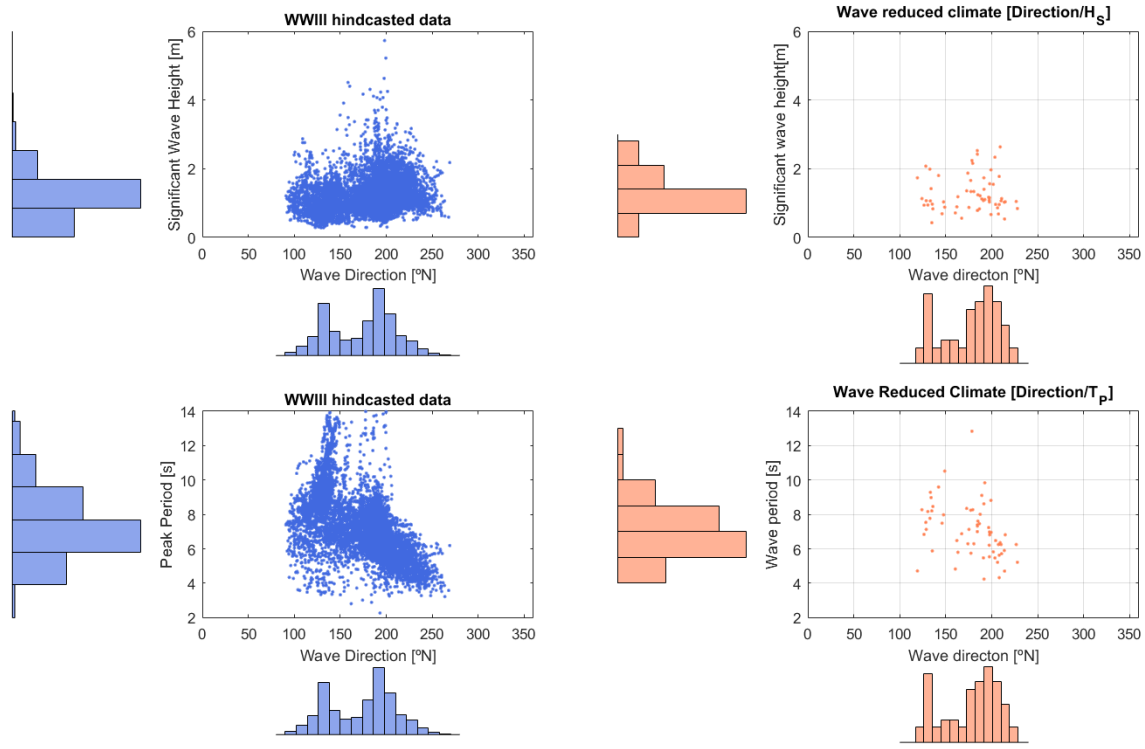

Figure B.6. Summer reduced wave climate in Katama Bay (orange color) using a MORFAC of 12. The reduction is made by applying a copula analysis from the WWIII hindcast data (blue color).

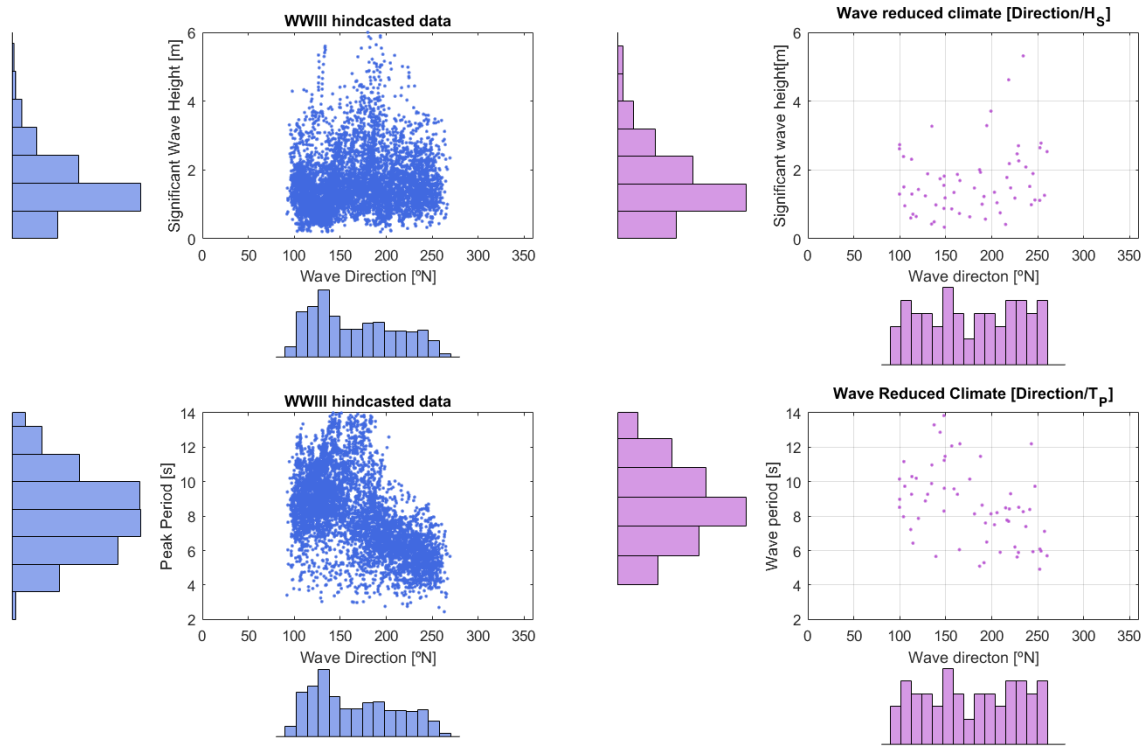

Figure B.7. Autumn reduced wave climate in Katama Bay (purple color) using a MORFAC of 12. The reduction is made by applying a copula analysis from the WWIII hindcast data (blue color).

B.2 Santa Lucia Estuary

A correlation analysis between the significant wave height, the peak wave period, and the wave direction is performed to determine the need to include these variables into the copula distribution. Table B.2 summarizes the correlation illustrated in Figure B.8, Figure B.9, and Figure B.10. Wave peak period and wave direction have the highest correlation (around 0.5). Again, significant wave height has a low correlation with the other two variables (most values between 0.1 and 0.2). Therefore, we do not include the significant wave height in the empirical copula.

Table B.2. Correlation factor between wave direction (θ_p), significant wave height (H_S), and peak wave period (T_P) in Santa Lucia.

	Correlation Factor ρ			
	Winter	Spring	Summer	Autumn
Dp/Hs	0.182	0.223	0.153	0.066
Dp/Tp	0.593	0.512	0.358	0.522
Hs/Tp	0.054	0.112	0.112	-0.015

We use generalized extreme value distributions (GEV) to fit the significant wave heights, and kernel distributions to fit the peak wave periods and the wave directions. We use empirical copulas with a resolution of 200 points to represent the joint probability between the peak wave period and the wave direction. We use this methodology as a wave reduction method owing to the implementation of a MORFAC of 12 in Delft3D. Figure B.11, Figure B.12, Figure B.13, and Figure B.14 show the winter, spring, summer, and autumn copula results respectively.

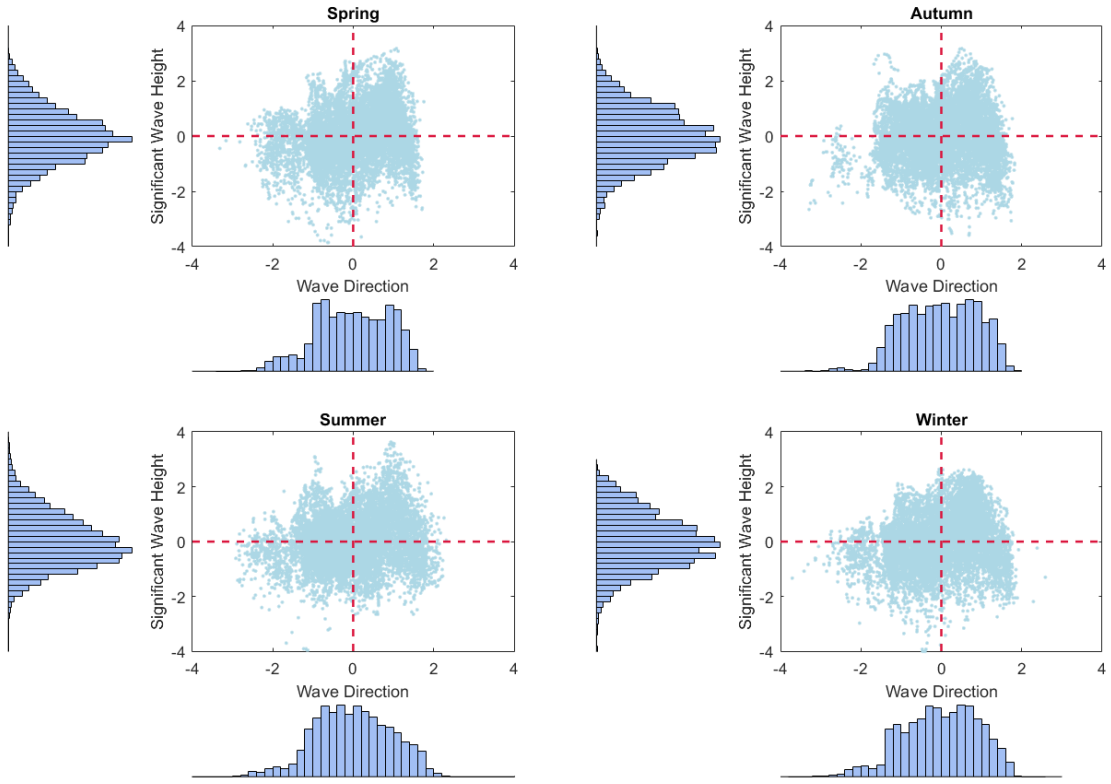

Figure B.8. Correlation between significant wave height (H_S) and wave direction (θ_p) at Santa Lucia Estuary. The marginal distributions are standard normal (μ=0 and σ=1).

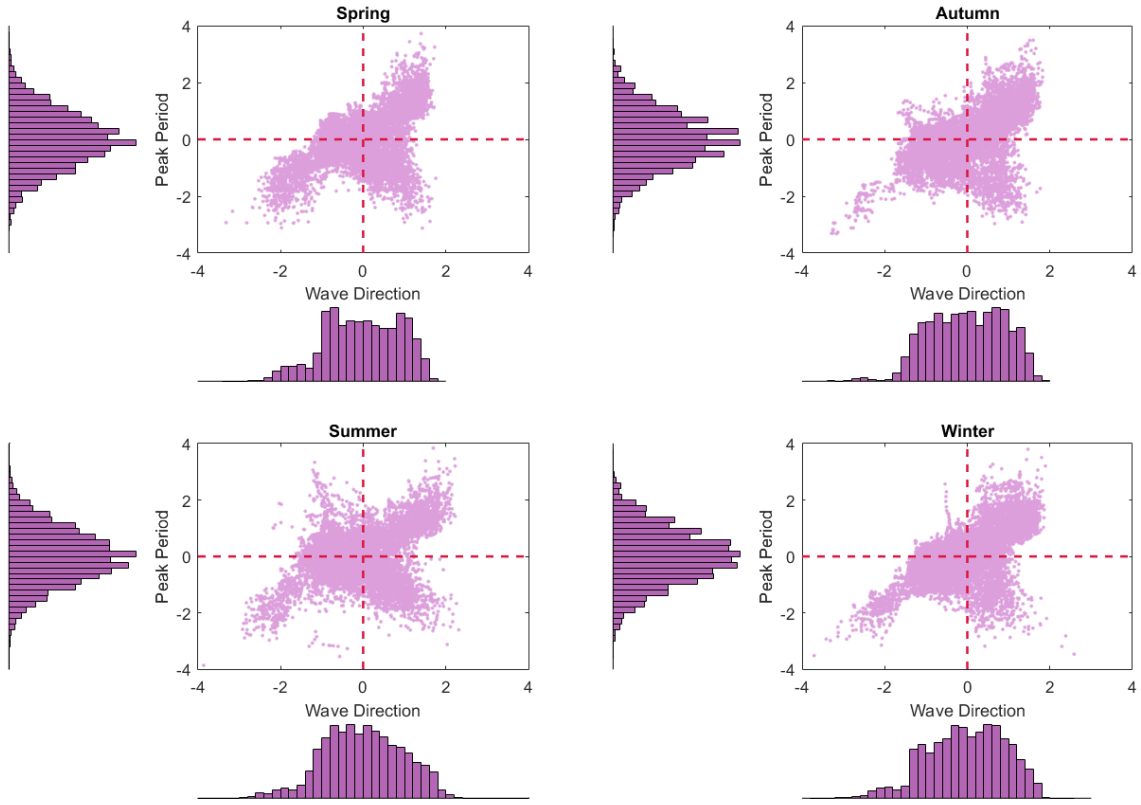

Figure B.9. Correlation between peak wave period (T_p) and wave direction (θ_p) at Santa Lucia Estuary. The marginal distributions are standard normal (μ=0 and σ=1).

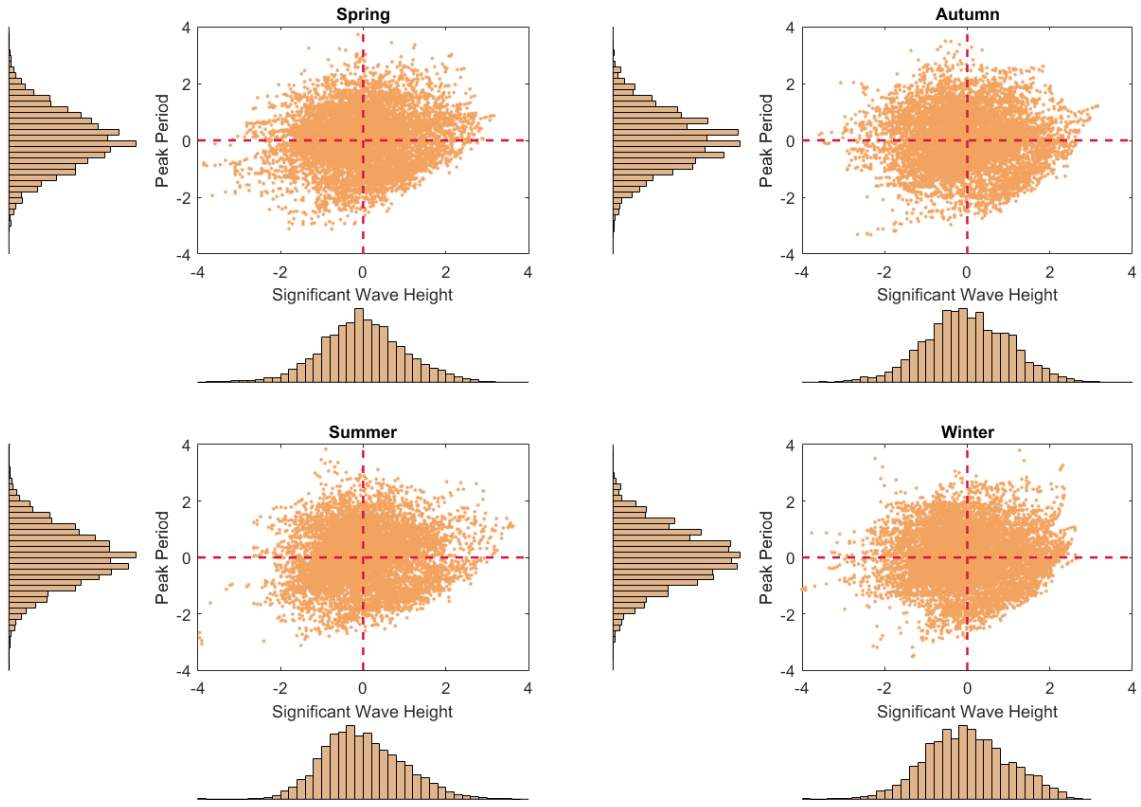

Figure B.10. Correlation between significant wave height (H_S) and peak wave period (T_p) at Santa Lucia Estuary. The marginal distributions are standard normal (μ=0 and σ=1).

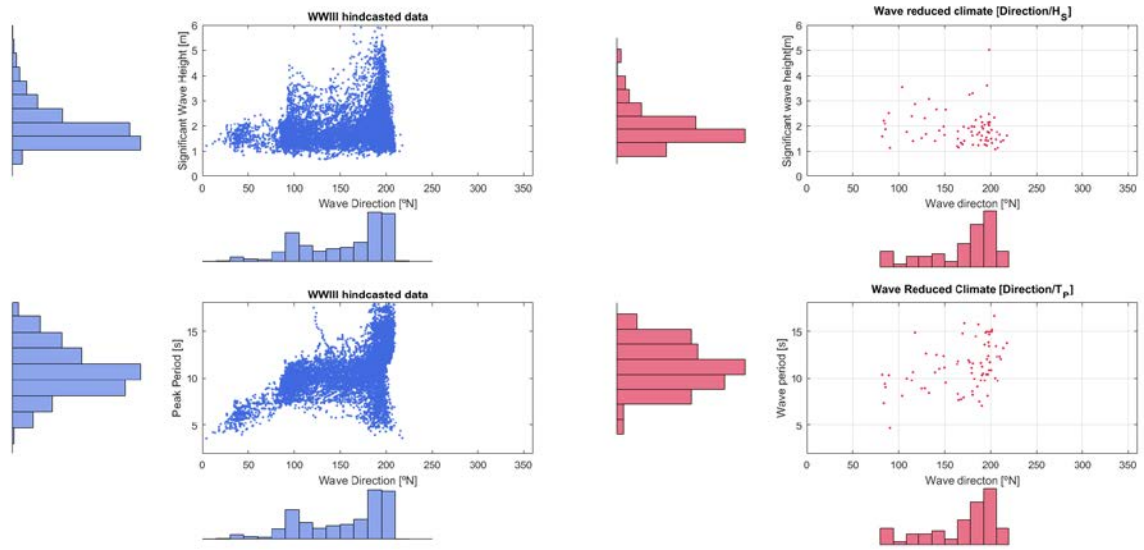

Figure B.11. Winter reduced wave climate in Santa Lucia Estuary (crimson color) using a MORFAC of 10. The reduction is made by applying a copula analysis from the WWIII hindcast data (blue color).

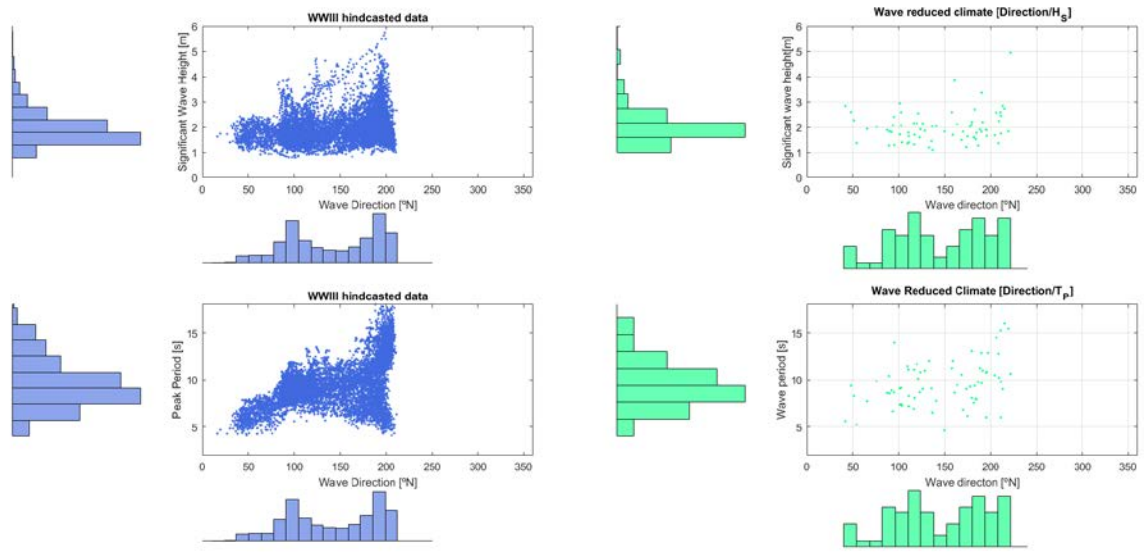

Figure B.12. Spring reduced wave climate in Santa Lucia Estuary (green color) using a MORFAC of 10. The reduction is made by applying a copula analysis from the WWIII hindcast data (blue color).

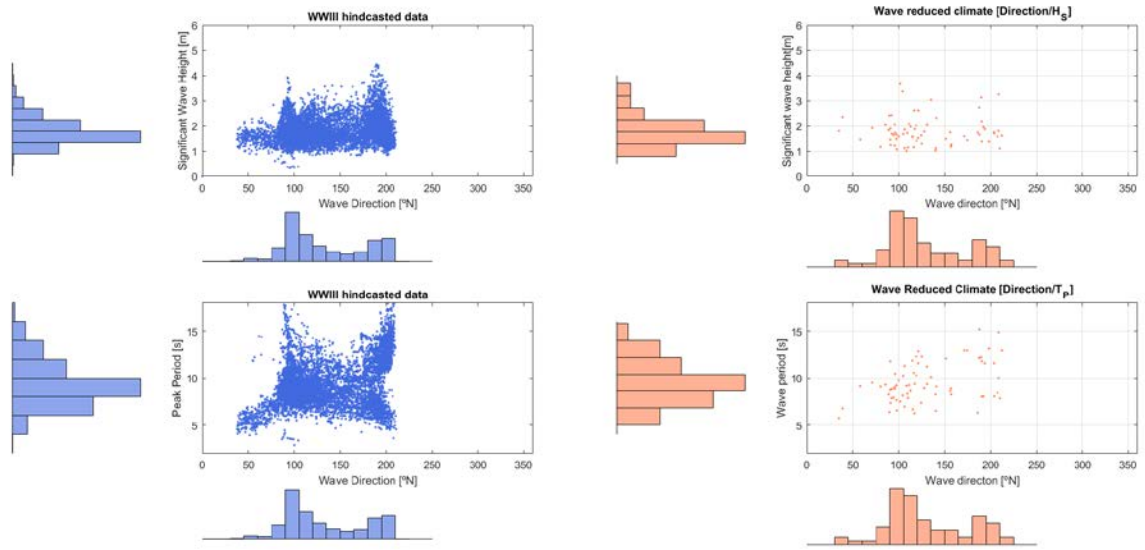

Figure B.13. Summer reduced wave climate in Santa Lucia Estuary (orange color) using a MORFAC of 10. The reduction is made by applying a copula analysis from the WWIII hindcast data (blue color).

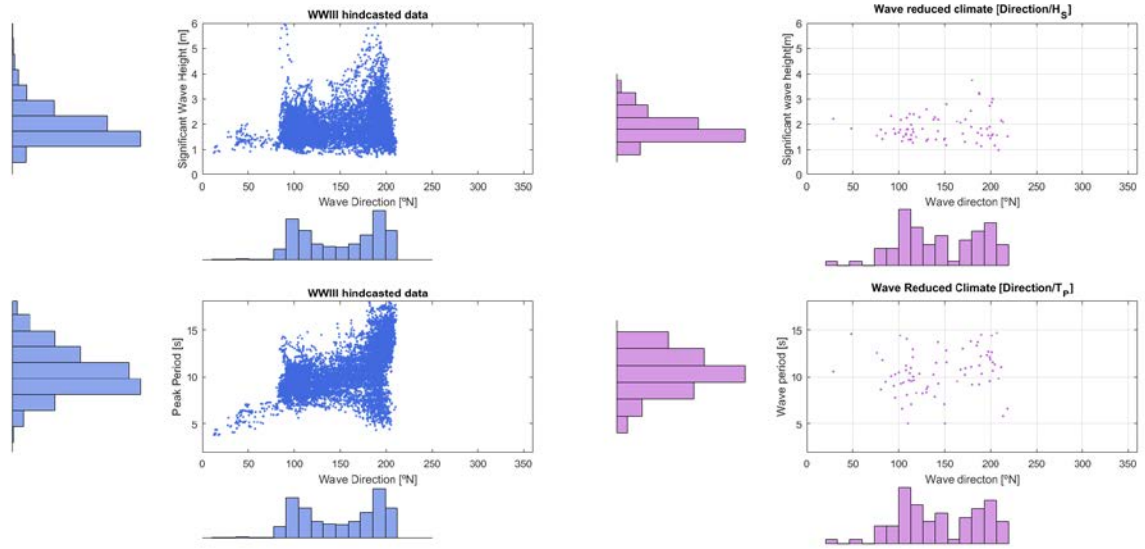

Figure B.14. Autumn reduced wave climate in Santa Lucia Estuary (purple color) using a MORFAC of 10. The reduction is made by applying a copula analysis from the WWIII hindcast data (blue color).

Appendix C. DELFT3D MODEL PARAMETERS LIST

Table C.1. Delft3D – FLOW module parameters for Katama Bay

Parameter	Description	Value
Flow - General		
Grid points in M-direction		303
Grid points in N-direction		128
Co-ordinate system	Spherical	
Number of layers		1
Bathymetry	Values specified at grid cell corners	
Bathymetry	Cell center values computed using:	Max
Time step	[s]	12
Water density	[kg/m^3]	1025
C	Chezy coefficient [m$^{1/2}$/s]	0.65
Stress formulation due to wave	Fredsoe	
Slip condition	Free	
K	Horizontal eddy viscosity [m^2/s]	1
N	Horizontal eddy diffusivity [m^2/s]	10
Flow - Sediment		
Cref	Reference density for hindered settling [kg/m^3]	1600
SedType	Sand	
RhoSol	Specific density [kg/m^3]	2650
CDryB	Dry bed density [kg/m^3]	1600
SedDia	Median sediment transport (D50) [µm]	500
IniSedThick	Initial sediment layer thickness at bed [m]	10
Flow - Morphology		
MorFac	Morphological scale factor	12
MorStt	Spin-up interval before morphological changes [min]	720
SedThr	Minimum depth for sediment calculation [m]	0.1
Transport model	TRANSPOR2004	
ThetSD	Factor for erosion of adjacent dry cells	1
Sus	Current-related reference concertation factor	0.3
Bed	Current-related transport vector magnitude factor	1
SusW	Wave-related suspended transport factor	0.25
BedW	Wave-related bedload transport factor	0.25
AlfaBn	Transverse bed gradient factor for bedload transport	1

Table C.2. SWAN parameters for Katama Bay

Parameter	Description	Value
Wave - Hydrodynamics		
Water Level	Use of FLOW results	Use and extend
Current	Use of FLOW results	Use and extend
Bathymetry	Use of FLOW results	Use but don't extend
Wind	Use of FLOW results	Don't use
Wave - Domain		
DirSpace	Directional space	circle
Ndir	Number of directions	36
FreqMin	Lowest frequency space [Hz]	0.03
FreqMax	Maximum frequency space [Hz]	1
Nfreq	Number of frequency bins	37
Wave - Physical parameters		
Forces	Computation of wave forces	Radiation Stress
Breaking	Wave breaking	TRUE
BreakAlpha	Alpha depth-induced breaking parameter	1
BreakGamma	Gamma depth-induced breaking parameter	0.73
Triads	Non-linear triad interactions	FALSE
BedFriction	Bottom friction type	JONSWAP
BedFricCoef	Bottom friction coefficient	0.58
Diffraction	Diffraction is activated for wave propagation	FALSE
Whitecapping	Formulation for white capping	Komen et al.
Refraction	Refraction is activated for wave propagation	TRUE
Frequency shift	Frequency shift is activated for wave propagation	TRUE
Wave - Output		
Coupling interval	(min)	180

Table C.3. Delft3D – FLOW module parameters for Santa Lucia Estuary

Parameter	Description	Value
Flow - General		
Grid points in M-direction		91
Grid points in N-direction		57
Co-ordinate system	Cartesian	
Number of layers		1
Bathymetry	Values specified at grid cell corners	
Bathymetry	Cell center values computed using:	Max
Time step	[s]	6
Water density	[kg/m^3]	1025
C	Chezy coefficient [m$^{1/2}$/s]	0.5
Stress formulation due to wave	Fredsoe	
Slip condition	Free	
K	Horizontal eddy viscosity [m^2/s]	1
N	Horizontal eddy diffusivity [m^2/s]	1
Flow - Sediment		
Cref	Reference density for hindered settling [kg/m^3]	1600
SedType	Sand	
RhoSol	Specific density [kg/m^3]	2650
CDryB	Dry bed density [kg/m^3]	1600
SedDia	Median sediment transport (D50) [µm]	200
IniSedThick	Initial sediment layer thickness at bed [m]	10
Flow - Morphology		
MorFac	Morphological scale factor	10
MorStt	Spin-up interval before morphological changes [min]	7200
SedThr	Minimum depth for sediment calculation [m]	0.1
Transport model	TR1993	
ThetSD	Factor for erosion of adjacent dry cells	0.1
Sus	Current-related reference concertation factor	10
Bed	Current-related transport vector magnitude factor	10
SusW	Wave-related suspended transport factor	0.4
BedW	Wave-related bedload transport factor	0.4
AlfaBn	Transverse bed gradient factor for bedload transport	1

Table C.4. SWAN parameters for Santa Lucia Estuary

Parameter	Description	Value
Wave - Hydrodynamics		
Water Level	Use of FLOW results	Use but don't extend
Current	Use of FLOW results	Use but don't extend
Bathymetry	Use of FLOW results	Use but don't extend
Wind	Use of FLOW results	Don't use
Wave - Domain		
DirSpace	Directional space	circle
Ndir	Number of directions	36
FreqMin	Lowest frequency space [Hz]	0.05
FreqMax	Maximum frequency space [Hz]	1
Nfreq	Number of frequency bins	24
Wave - Physical parameters		
Forces	Computation of wave forces	Radiation Stress
Breaking	Wave breaking	TRUE
BreakAlpha	Alpha depth-induced breaking parameter	1
BreakGamma	Gamma depth-induced breaking parameter	0.73
Triads	Non-linear triad interactions	FALSE
BedFriction	Bottom friction type	JONSWAP
BedFricCoef	Bottom friction coefficient	0.38
Diffraction	Diffraction is activated for wave propagation	FALSE
Whitecapping	Formulation for white capping	Komen et al.
Refraction	Refraction is activated for wave propagation	TRUE
Frequency shift	Frequency shift is activated for wave propagation	TRUE
Wave - Output		
Coupling interval	(min)	180

Appendix D. SAND TRANSPORT MODEL TRANSPOR2004

The DELFT3D-FLOW module solves the unsteady shallow-water equations, which consist of the horizontal momentum equations, the continuity equation, the transport equation, and a turbulence closure model (van Rijn and Walstra 2003). The model uses an alternating direction implicit (ADI) method to solve the continuity and horizontal momentum equations (Leendertse 1987). The transport equation is formulated in a conservative form (finite-volume approximation) and solved via the so-called "cyclic method" (Stelling and Leendertse 1992) where suspended sediment transport is calculated by solving the three-dimensional advection-diffusion (mass-balance) equation.

The sediment transport calculation used to simulate morphodynamics at Katama Bay is based on formulas developed by van Rijn and Walstra (2003) and then implemented in Delft3D (van Rijn, Walstra, and van Ormondt 2004). The model used here (TR2004), similarly to the default Delft3D formulation (TR1993 (van Rijn 1993)), divides the sediment motion into suspended sediment load (sand moved through the water column) and bed load (sand moved in the bed boundary layer). Therefore, sediment transport below the bed boundary level is considered bedload transport, whereas sediment transport above this boundary is considered suspended sediment. This appendix describes the equations used for non-cohesive sediment leading to the results presented in Chapter 4. Bed and suspended transport, bed roughness predictors, boundary layer thicknesses, bed shear stress, the critical Shields parameter, and the reference concentration are described, emphasizing the differences between the TR2004 and the default option (van Rijn, Walstra, and van Ormondt 2004).

D.1 Bedload Transport

The net bedload transport rate over a wave period T is obtained using a quasi-steady approach of the instantaneous transport rate:

$$q_b = \left(\frac{1}{T}\right)\int q_{b,t}dt \qquad [5]$$

Where $q_{b,t}$ is the instantaneous transport rate, is calculated as follows:

$$q_{b,t} = 0.5\rho_s d_{50} D_*^{-0.3}\left(\frac{\tau'_{b,cw,t}}{\rho}\right)^{0.5}\left(\frac{\max\left(0,\tau'_{b,cw,t}-\tau_{b,cr}\right)}{\tau_{b,cw,t}}\right) \qquad [6]$$

In which:

- $\tau'_{b,cw,t}$ is the instantaneous grain-related bed-shear stress (owing to both current and wave motion), which is defined as:

  $$\tau'_{b,cw,t} = 0.5\rho f'_{cw}\left(U_{\delta,cw,t}\right)^2 \qquad [7]$$

  Being $U_{\delta,cw,t}$ the instantaneous velocity at a reference height (Equation [27]), f'_{cw} the current- and wave-related friction coefficient, and ρ the fluid density.
- $\tau_{b,cr}$ is the critical bed-shear stress according to Shields (Equation [25]).
- ρ_s and ρ are the sediment and fluid density respectively.
- d_{50} is the particle diameter.
- D_* is the dimensionless particle diameter.

The most influential parameter of the Equation [7] is f'_{cw}. Therefore, new equations (compared with previous models) have been implemented in TR2004 based on the findings of van Rijn and Walstra (2003):

$$f'_{cw} = \alpha^{0.5}\beta_f f'_c + (1-\alpha^{0.5})f'w \quad [8]$$

where:

- β_f is a coefficient related to the vertical structure of the velocity profile.
- α is a coefficient related to the relative strength of current and wave motion.
- f'_c is the current-related friction coefficient, defined as:

$$f'_c = 0.24\left(\log\left(\frac{12h}{k_{s,grain}}\right)\right)^{-2} \quad [9]$$

  Where h is the water depth and $k_{s,grain}$ is the grain roughness equal to d_{90}.
- $f'w$ is the wave-related friction coefficient, defined as:

$$f'w = \exp\left(-6 + 5.2\left(\frac{A_\delta}{k_{s,grain}}\right)^{-0.19}\right) \quad [10]$$

  Where h is the water depth and $k_{s,grain}$ is the grain roughness equal to d_{90}.

D.2 Wave-related suspended transport

The wave-related suspended transport fraction is implemented as:

$$q_{s,w} = \gamma\left(\frac{U^4_{\delta,for} - U^4_{\delta,back}}{U^3_{\delta,for} + U^3_{\delta,back}} + u_\delta\right)\int cdz \quad [11]$$

where:

- $U_{\delta,for}$ is the onshore (wave direction) peak orbital velocity (near the bed).
- $U_{\delta,back}$ is the offshore peak orbital velocity (near the bed).
- u_δ is the wave-induced streaming.
- c is the time-averaged concentration.
- γ is a phase lag function, which is 0.1 in TR2004, instead of 0.2 in TR2000.

The model TR2004 predicts the suspended sediment size depending on the mobility parameter, as follows:

$$d_s = max\left[d_{10}\left(1 + 0.0006\left(\frac{d_{50}}{d_{10}} - 1\right)(\Psi - 550)\right)d_{50}\right] \quad for\ \Psi < 550$$

$$d_s = d_{50} \quad for\ \Psi \geq 550 \quad [12]$$

where Ψ is the mobility parameter:

$$\Psi = \frac{{U_{wc}}^2}{(s-1)gd_{50}} \quad [13]$$

$${U_{wc}}^2 = {U_{\delta,r}}^2 + {v_R}^2 \quad [14]$$

Here, $U_{\delta,r}$ is the representative peak orbital velocity near bed based on the method of Isobe-Horikawa (Isobe and Horikawa 1982), and v_R is the depth-averaged current velocity.

D.3 Bed Roughness

The TRANSPOR2004 (TR2004) model includes roughness predictors to simulate the effective roughness of various types of bedforms (e.g., mega-ripples or dunes). This model includes a bed-roughness predictor for the current-related and wave-related bed roughness parameters, whereas in other models (e.g., TR1993 or TR2000) this predictor must be defined by the user.

D.3.1 Physical current-related bed roughness

The primary assumption behind the small-scale ripples is that the physical bed roughness in natural conditions is equal to the ripple height. In all these models (e.g., TR1993, TR2000, and TR2004) the following expressions are implemented:

$$\begin{aligned} k_{s,c,r} &= 150 d_{50} && and\ 0 \le \Psi \le 50 \quad (lower\ wave - current\ regime) \\ k_{s,c,r} &= (182.5 - 0.65\Psi) d_{50} && and\ 50 \le \Psi \le 25 \quad (upper\ wave - current\ regime) \\ k_{s,c,r} &= 20 d_{50} && and\ \Psi \ge 250 \quad (linear\ approach\ in\ transitional\ regime) \end{aligned} \qquad [15]$$

The Equation [15] is valid for relatively fine sand with d_{50} between 0.1 and 0.5 mm. Therefore, the upper limit is for a diameter of 0.5 mm, with a bed roughness height of 0.075 mm.

The physical form roughness for mega-ripples $k_{s,c,mr}$ (van Rijn and Walstra 2003) should be considered when mega-ripples are present on the seabed (if water depth > 1 m and v_r=depth-averaged velocity >0.3 m/s):

$$\begin{aligned} k_{s,c,mr} &= 0.0002\Psi h && and\ 0 \le \Psi \le 50 && and\ h > 1 \\ k_{s,c,mr} &= (0.011 - 0.0002\Psi) h && and\ 50 \le \Psi \le 550 && and\ h > 1 \\ k_{s,c,mr} &= 0 && and\ \Psi \ge 550 && and\ h > 1 \end{aligned} \qquad [16]$$

$$0.02 \le k_{s,c,mr} \le 0.2$$

The current related bed roughness is the quadratic sum of the small-scale ripples bed roughness, the mega-ripples bed roughness, and the current-related friction roughness ($k_{s,c,d}$), as follows:

$$k_{s,c,mr} = \left(k_{s,c,r}^2 + k_{s,c,mr}^2 + k_{s,c,d}^2\right)^{0.5} \qquad [17]$$

D.3.2 Physical wave-related bed roughness

Only the bed forms with a length the size of the orbital diameter velocity near the bottom are relevant for the physical wave-related bed roughness. Therefore, mega-ripples are not considered to calculate this parameter, and the physical wave-related roughness of small-scale ripples is given as:

$$\begin{aligned} k_{s,w,r} &= 150 d_{50} && and\ 0 \le \Psi \le 50 \quad (lower\ wave - current\ regime) \\ k_{s,w,r} &= (182.5 - 0.65\Psi) d_{50} && and\ 50 \le \Psi \le 25 \quad (upper\ wave - current\ regime) \\ k_{s,w,r} &= 20 d_{50} && and\ \Psi \ge 250 \quad (linear\ approach\ in\ transitional\ regime) \end{aligned} \qquad [18]$$

Here, the mobility parameter is computed as explained in Equation [13].

D.3.3 Apparent bed roughness for flow over a movable bed

It is proposed by van Rijn, Walstra, and van Ormondt (2004) to use the next expression to calculate the apparent bed roughness (k_a) for a flow over a movable bed:

$$\frac{k_a}{k'_{s,c}} = \exp\left(\frac{\gamma U_{\delta,r}}{v_R}\right) \qquad and \quad \left(\frac{k_a}{k'_{s,c}}\right)_{MAX} = 10 \qquad [19]$$

Where $U_{\delta,r}$ is the peak orbital velocity (Equation [24]), v_R is the depth-averaged current velocity, $\gamma=0.8+\varphi-0.3\varphi^2$ (being φ the angle between wave and current direction), and $k_{s,c}$ is the current-related bed roughness excluding dunes.

D.4 The thickness of the wave-boundary layer, fluid mixing, and sediment mixing layer

The model TR2004 uses a wave boundary layer thickness according to Davies and Villaret (1999), replacing the wave boundary thickness based on Jonsson and Carlsen (1976) used in TR1993 and TR2000. The new formulation is defined as:

$$\delta_w = 0.36 A_\delta \left(\frac{A_\delta}{k_{s,w,r}}\right)^{-0.25} \qquad [20]$$

The thickness of the effective fluid mixing layer (δ_m) is calculated as twice the wave boundary thickness, with an upper limit of 0.2 meters, and a lower limit of 0.05 meters. Finally, the effective sediment mixing layer in TR2004 is computed as:

$$\delta_s = min(0.5, max(0.05, 2\delta_w \gamma_{br})) \qquad [21]$$

where:

$$\gamma_{br} = 1 + \left(\frac{H_S}{h} - 0.4\right)^{0.5} \qquad and\ \gamma_{br} = 1\ for\ \frac{H_S}{h} \leq 0.4 \qquad [22]$$

D.5 Wave-induced bed-shear stress

The time-averaged bed-shear stress is calculated equally in the three models (TR1993, TR2000, and TR2004):

$$\tau'_{b,cw,t} = \frac{1}{4}\rho f'_w \left(U_{\delta,r}\right)^2 \qquad [23]$$

Nevertheless, whereas the peak orbital velocity ($U_{\delta,r}$) is only based on linear wave theory for TR1993 and TR2000, in TR2004 it is refined into:

$$U_{\delta,r} = \left(0.5\left(U_{\delta,for}\right)^3 + 0.5\left(U_{\delta,back}\right)^3\right)^{\frac{1}{3}} \qquad [24]$$

where:

- $U_{\delta,r}$ = representative peak orbital velocity near the bed.
- $U_{\delta,for}$ = peak orbital velocity in the forward direction (Isobe and Horikawa 1982).
- $U_{\delta,back}$ = peak orbital velocity in the backward direction (Isobe and Horikawa 1982).

D.6 Critical Shields parameter

TR2004 implements a new representation of the critical Shields parameter based on experimental data (van Rijn 1993):

$$\theta_{cr} = \frac{\tau_{b,cr,o}}{(s-1)gd_{50}} = 0.115D_*^{-0.5} \; fot \; D_* \leq 4 \qquad [25]$$

$$D_* = d_{50}\left[\frac{(s-1)g}{v^2}\right]^{\frac{1}{3}} \qquad [26]$$

Where θ_{cr} is the critical Shields parameter, s is the relative density, ν is the kinematic viscosity coefficient, and $\tau_{b,cr,o}$ is the bead-shear stress for pure sand (no mud).

D.7 Reference concentration and the reference level

The reference level in TR2004 is implemented as follows:

$$a = \min\left(0.2h, max\left(0.5k_{s,c,r}, 0.5k_{s,w,r}, 0.01\right)\right) \qquad [27]$$

Where h is the local depth, $k_{s,c,r}$ is the current-related roughness height owing to small-scale ripples (Equation [15]), and $k_{s,w,r}$ is the wave-related roughness height due to small-scale ripples (Equation [18]). On the other hand, the reference concentration in TR2004 is described by:

$$c_a = 0.015\rho_s \frac{d_{50}T_a^{1.5}}{a(D_*)^{0.3}} \qquad with \; c_{a,\mathrm{MAX}} = 0.05\rho_s \qquad [28]$$

Appendix E. EQUILIBRIUM BATHYMETRY, KATAMA BAY

The bathymetry provided is created joining bathymetries from 2011 and barrier geometry based on 2007 satellite images. Therefore, it is not in equilibrium with the calculated forcings. To get rid of potential instabilities (i.e., obtain an equilibrium bathymetry), the model is run with a closed inlet for a full year. The model shows the rapid formation of shoals in front of the Wasque Point (Box 2 in Figure E.1) partly owing to the position of the inlet in 2011 which had washed out some of the shoals. Also, the model smooths the features (most of them from the inlet migration from 2007 to 2011) along the nearshore area in front of the barrier (Box 1 in Figure E.1). However, the shoreline accretes in the middle of the barrier due to the elimination of the inlet.

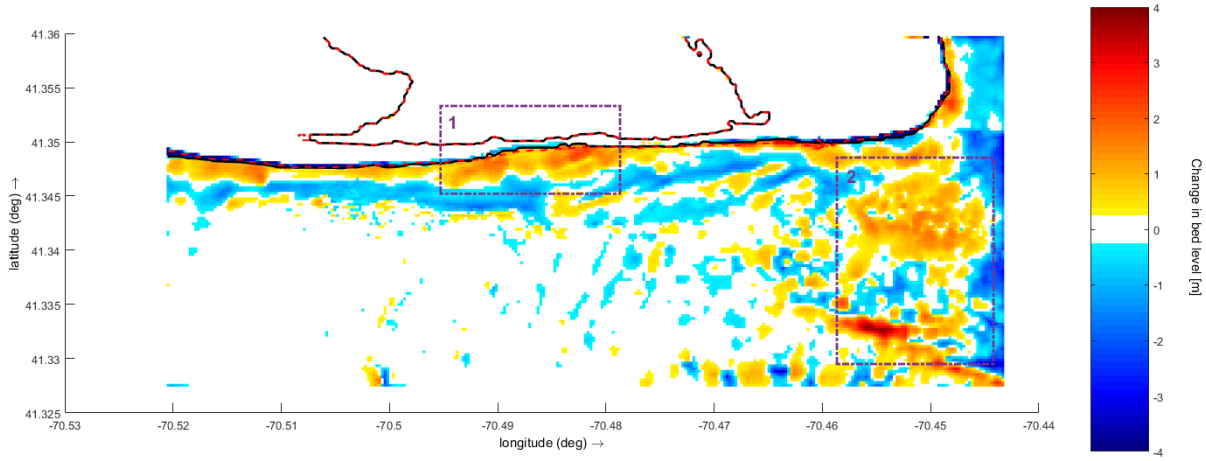

Figure E.1. Sedimentation (red) and erosion (blue) patterns (legend on the right [m]) after a year simulation with a closed inlet.

A compromise is achieved to provide an equilibrium bathymetry but with a similar 2007 shoreline. An analysis of the ratio of the bed level change is performed throughout the domain, focusing on 4 main points. Figure E.2 illustrates the ratio of sedimentation for the time step 152 of 247 (comparing with the last time step). Most of the points have reached the 70% of sedimentation by this time. Four representative points on the main features are individually analyzed (Figure E.3), showing that for the time step 152 most of the bathymetric changes (>80%) have already happened. Therefore, we select the bathymetry at timestep 152 as the near-equilibrium to be used from now on. We manually breach the barrier to represent the inlet position in 2007 (Figure E.4).

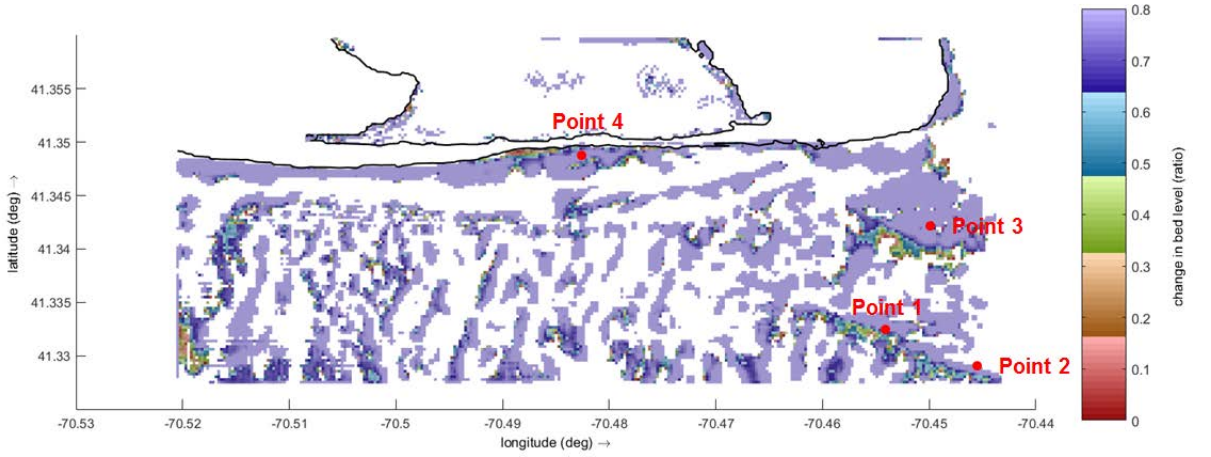

Figure E.2. Ratio of sedimentation change at timestep 152 of 247 compared with the last time step (247).

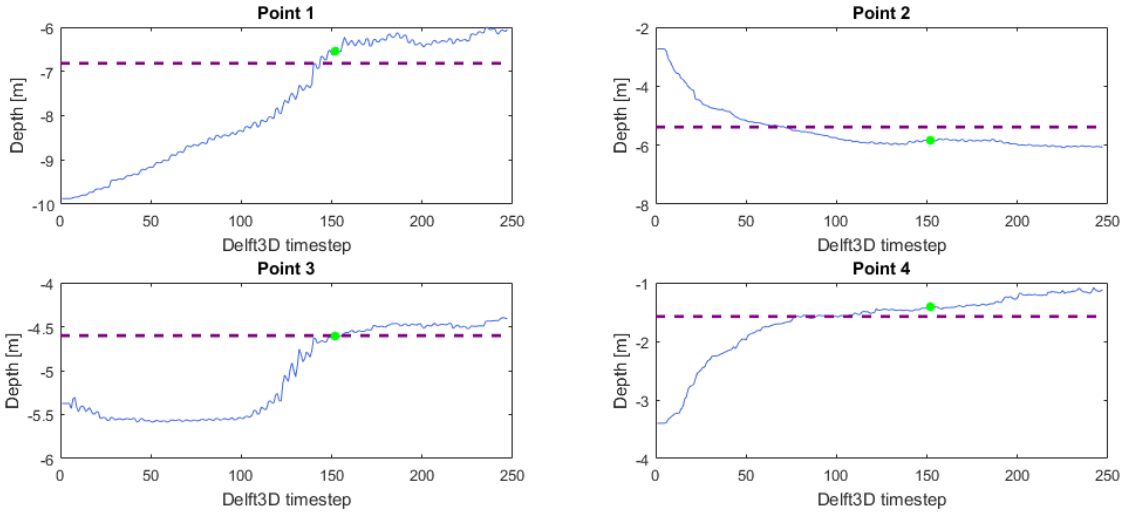

Figure E.3. Change in water depth for four points at main features (Figure E.2). Dashed-purple line indicates the 80% of bed level change, and the green dots the bed level change at time step 152.

Figure E.4. Initial near-equilibrium bathymetry used in all the simulations in Katama Bay.

Appendix F. KATAMA BAY EXTENDED RESULTS

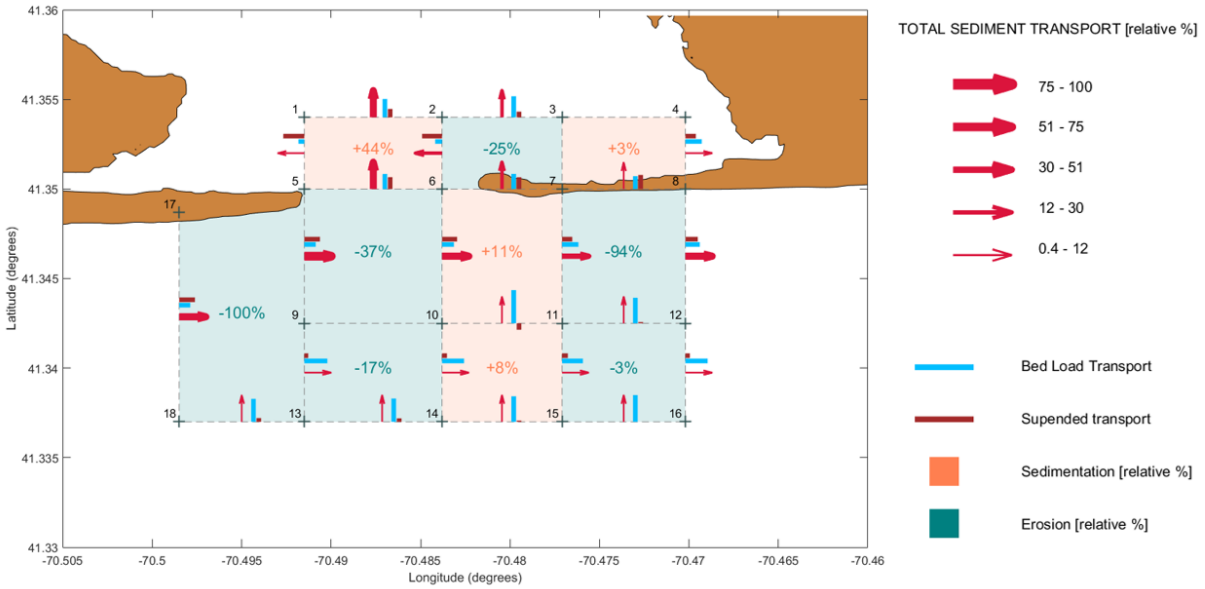

Figure F.1. Sediment pathway analysis for the FSK1 simulation (including SLR, changes in tidal constituents, changes in significant wave height, and an increase of 10ºN in the mean wave direction). Crimson arrows represent the sediment transport through each profile (delimitated by crosses). The wider the arrow, the larger the sediment transport relative to the biggest transport (legend on the right). The transport is divided into the bed load transport (blue bars) and suspended load transport (brown bars). Each cell (between four profiles) represent a sediment budget, either erosion (teal color) or sedimentation (coral color). The shoreline position (brown surface) corresponds to the end of the simulated year.

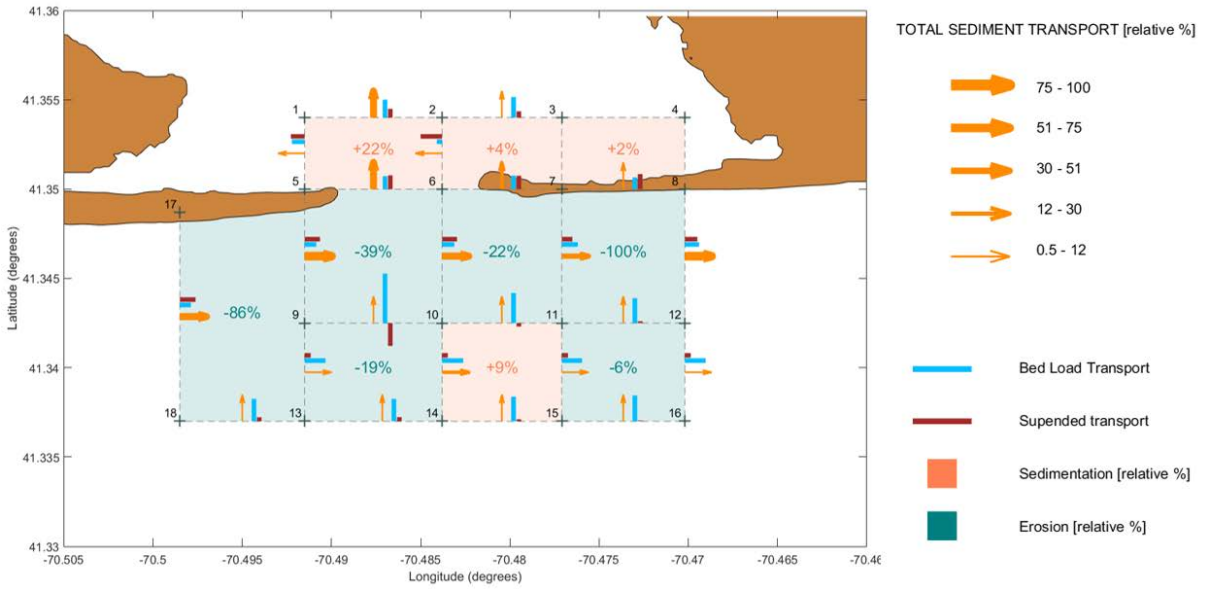

Figure F.2. Sediment pathway analysis for the FSK2 simulation (including SLR, changes in tidal constituents, changes in significant wave height, and a decrease of 10ºN in the mean wave direction). Orange arrows represent the sediment transport through each profile (delimitated by crosses). The wider the arrow, the larger the sediment transport relative to the biggest transport (legend on the right). The transport is divided into the bed load transport (blue bars) and suspended load transport (brown bars). Each cell (between four profiles) represent a sediment budget, either erosion (teal color) or sedimentation (coral color). The shoreline position (brown surface) corresponds to the end of the simulated year.

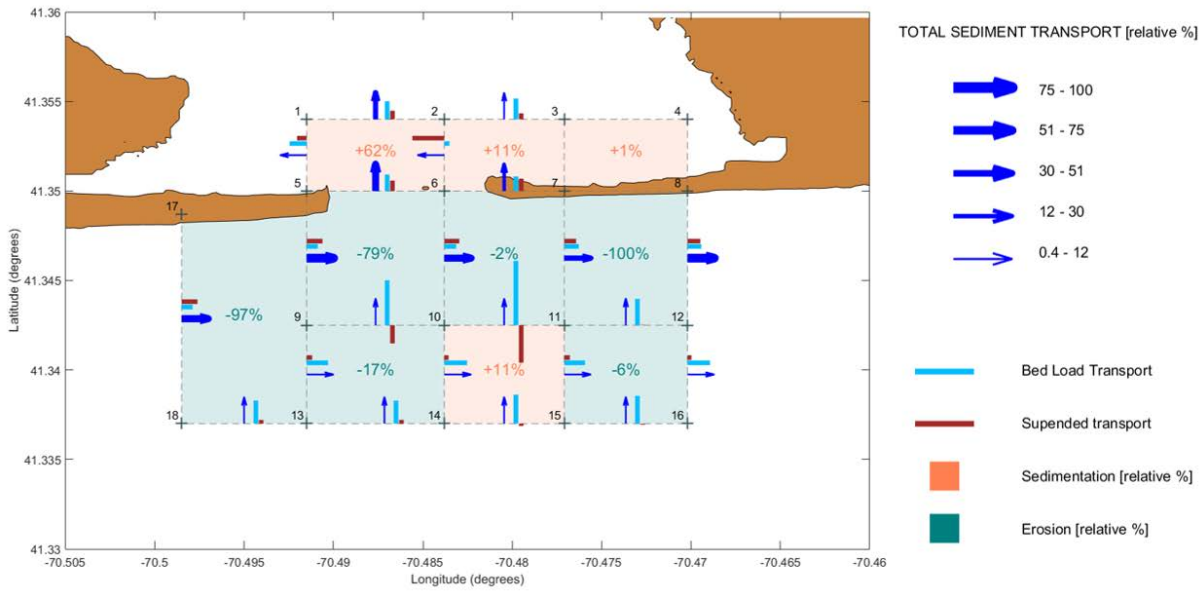

Figure F.3. Sediment pathway analysis for the FSK3 simulation (including an increase of 10ºN in the mean wave direction). Blue arrows represent the sediment transport through each profile (delimitated by crosses). The wider the arrow, the larger the sediment transport relative to the biggest transport (legend on the right). The transport is divided into the bed load transport (blue bars) and suspended load transport (brown bars). Each cell (between four profiles) represent a sediment budget, either erosion (teal color) or sedimentation (coral color). The shoreline position (brown surface) corresponds to the end of the simulated year.

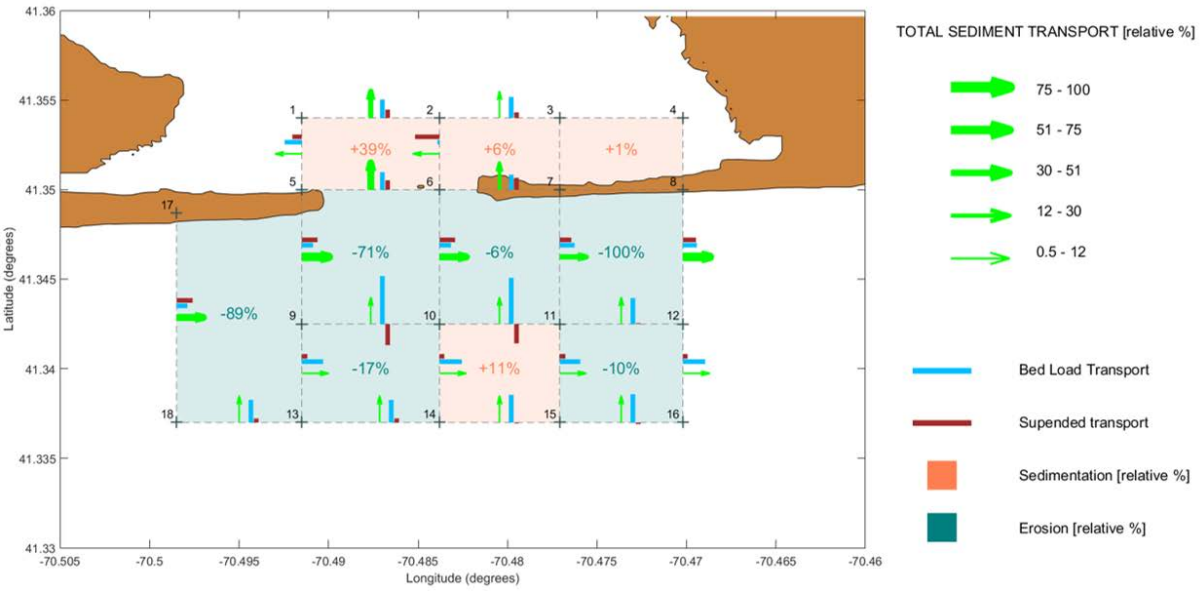

Figure F.4. Sediment pathway analysis for the FSK4 simulation (including a decrease of 10ºN in the mean wave direction). Green arrows represent the sediment transport through each profile (delimitated by crosses). The wider the arrow, the larger the sediment transport relative to the biggest transport (legend on the right). The transport is divided into the bed load transport (blue bars) and suspended load transport (brown bars). Each cell (between four profiles) represent a sediment budget, either erosion (teal color) or sedimentation (coral color). The shoreline position (brown surface) corresponds to the end of the simulated year.

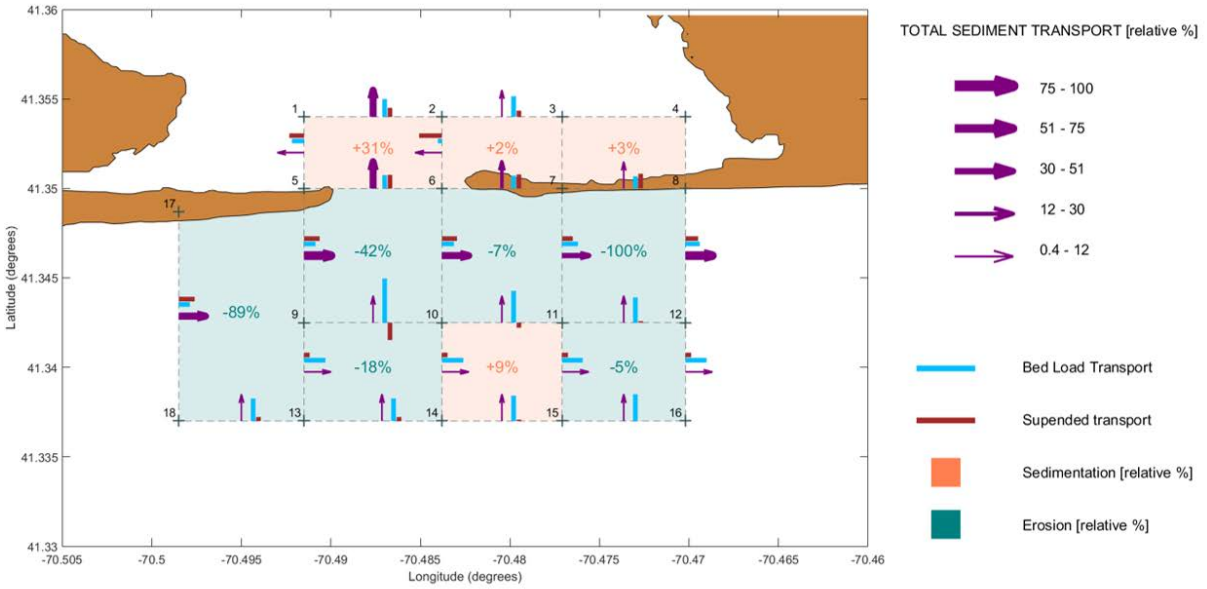

Figure F.5. Sediment pathway analysis for the FSK5 simulation (including SLR, and changes in tidal constituents). Purple arrows represent the sediment transport through each profile (delimitated by crosses). The wider the arrow, the larger the sediment transport relative to the biggest transport (legend on the right). The transport is divided into the bed load transport (blue bars) and suspended load transport (brown bars). Each cell (between four profiles) represent a sediment budget, either erosion (teal color) or sedimentation (coral color). The shoreline position (brown surface) corresponds to the end of the simulated year.

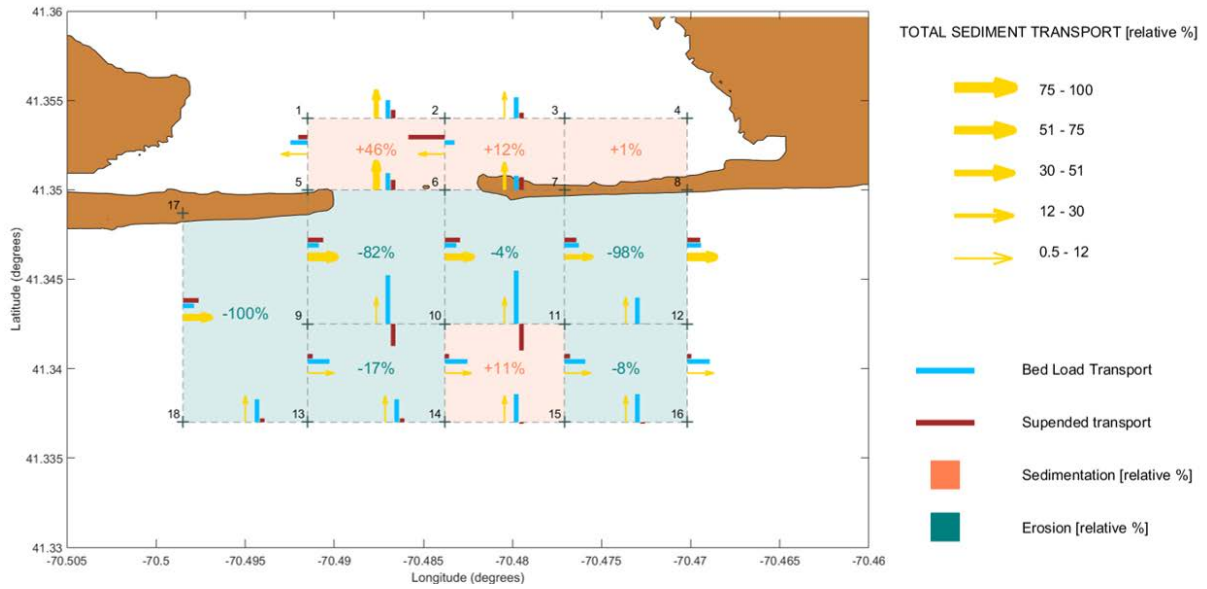

Figure F.6. Sediment pathway analysis for the FSK6 simulation (including changes in tidal constituents). Yellow arrows represent the sediment transport through each profile (delimitated by crosses). The wider the arrow, the larger the sediment transport relative to the biggest transport (legend on the right). The transport is divided into the bed load transport (blue bars) and suspended load transport (brown bars). Each cell (between four profiles) represent a sediment budget, either erosion (teal color) or sedimentation (coral color). The shoreline position (brown surface) corresponds to the end of the simulated year.

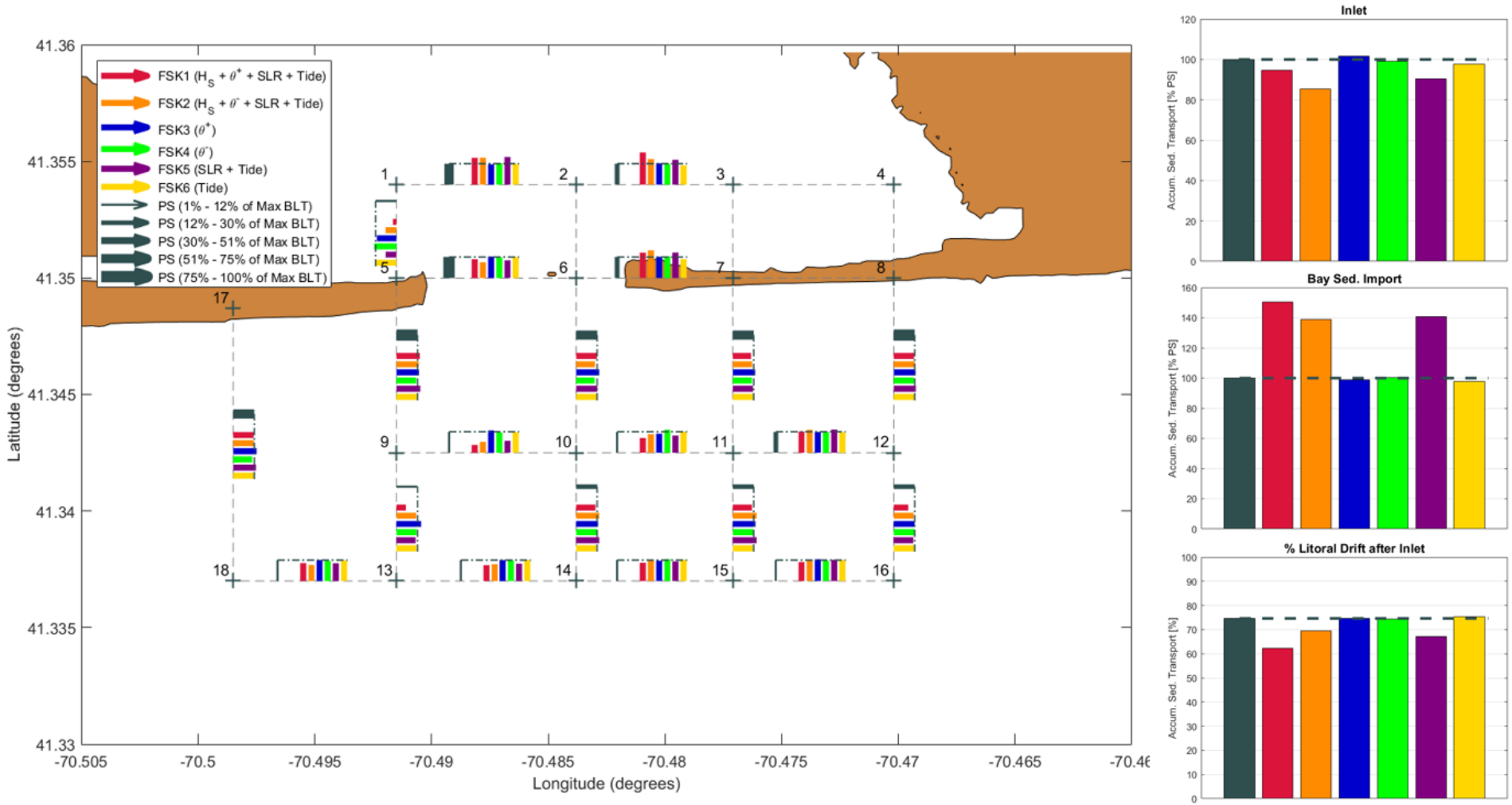

Figure F.7. Accumulated bedload sediment transport map. Grey dashed lines show the output profiles from Delft3D labeled between numbers on grey crosses. At each profile, a bar plot shows the year cumulative sediment transport for all the scenarios. Grey bars (present state simulation) are wider when the sediment transport is larger (percentage of the maximum bedload transport (BLT) in the legend). The dashed-dotted lines indicate the value for the present state to highlight the comparison with other simulation. On the right, three bar plots illustrate the inlet profile accumulated transport (top), the sum of the profiles 1-2, 2-3 and 3-5 (i.e., the sediment intrusion into the bay) (middle), and the bypassing fraction (the difference between profiles 5-13 and 7-15) (bottom).

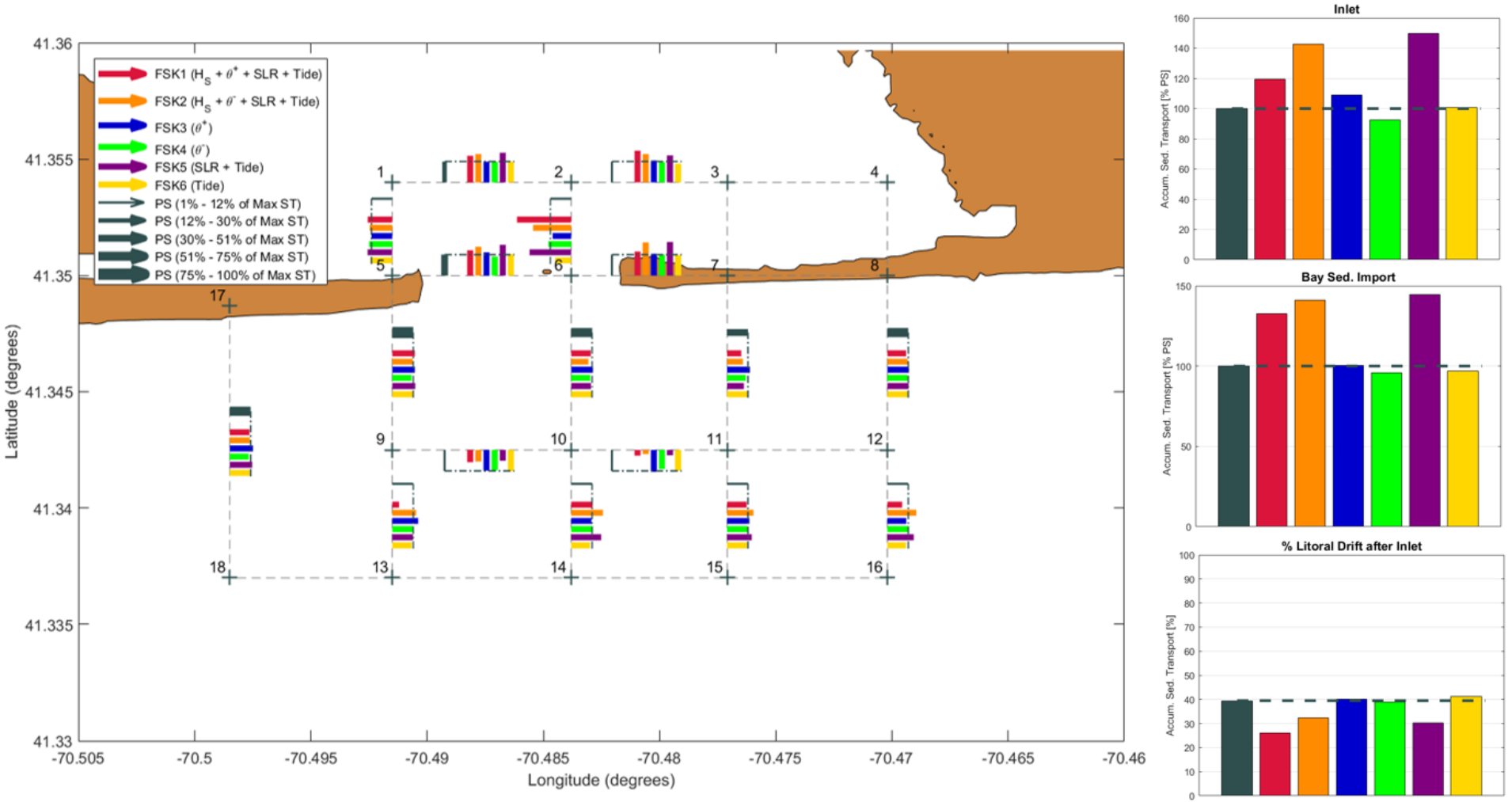

Figure F.8. Accumulated suspended sediment transport map. Grey dashed lines show the output profiles from Delft3D labeled between numbers on grey crosses. At each profile, a bar plot shows the year cumulative sediment transport for all the scenarios. Grey bars (present state simulation) are wider when the sediment transport is larger (percentage of the maximum suspended transport (ST) in the legend). The dashed-dotted lines indicate the value for the present state to highlight the comparison with other simulation. On the right, three bar plots illustrate the inlet profile accumulated transport (top), the sum of the profiles 1-2, 2-3 and 3-5 (i.e., the sediment intrusion into the bay) (middle), and the bypassing fraction (the difference between profiles 5-13 and 7-15) (bottom).

Appendix G. St. Lucia

EXTENDED RESULTS

.

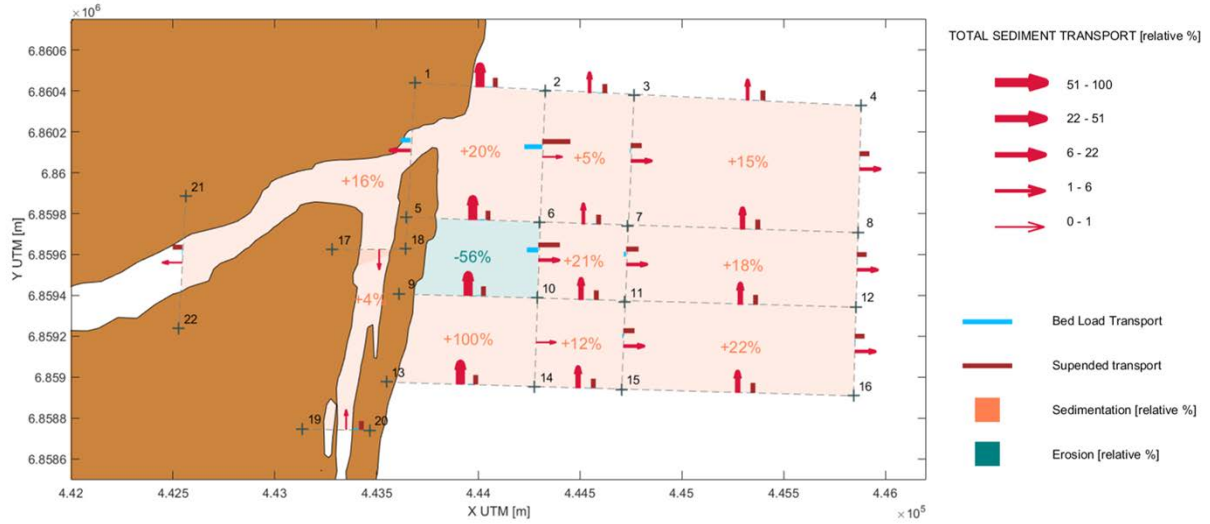

Figure G.1 Sediment pathway analysis for the FSSL1 simulation (including changes in H_S, changes in T_P, an increase of 10ºN of the wave direction, SLR, and the projected river discharge). Crimson arrows represent the sediment transport through each profile (delimitated by crosses). The wider the arrow, the larger the sediment transport relative to the biggest transport (legend on the right). The transport is divided into the bed load transport (blue bars) and suspended load transport (brown bars). Both transport loads use a scale of 0.5 relative to the total transport for better visualization. Each cell (between four profiles) represent a sediment budget, either erosion (teal color) or sedimentation (coral color). The shoreline position (brown surface) corresponds to the end of the simulated year.

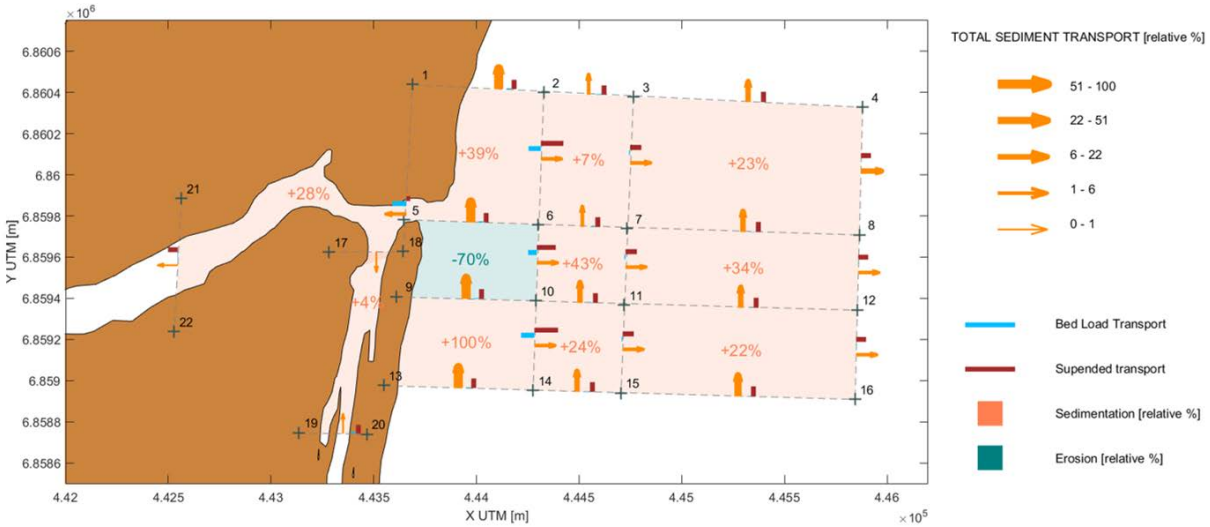

Figure G.2 Sediment pathway analysis for the FSSL2 simulation (including changes in H_S, changes in T_P, a decrease of 10ºN of the wave direction, SLR, and the projected river discharge). Orange arrows represent the sediment transport through each profile (delimitated by crosses). The wider the arrow, the larger the sediment transport relative to the biggest transport (legend on the right). The transport is divided into the bed load transport (blue bars) and suspended load transport (brown bars). Both transport loads use a scale of 0.5 relative to the total transport for better visualization. Each cell (between four profiles) represent a sediment budget, either erosion (teal color) or sedimentation (coral color). The shoreline position (brown surface) corresponds to the end of the simulated year.

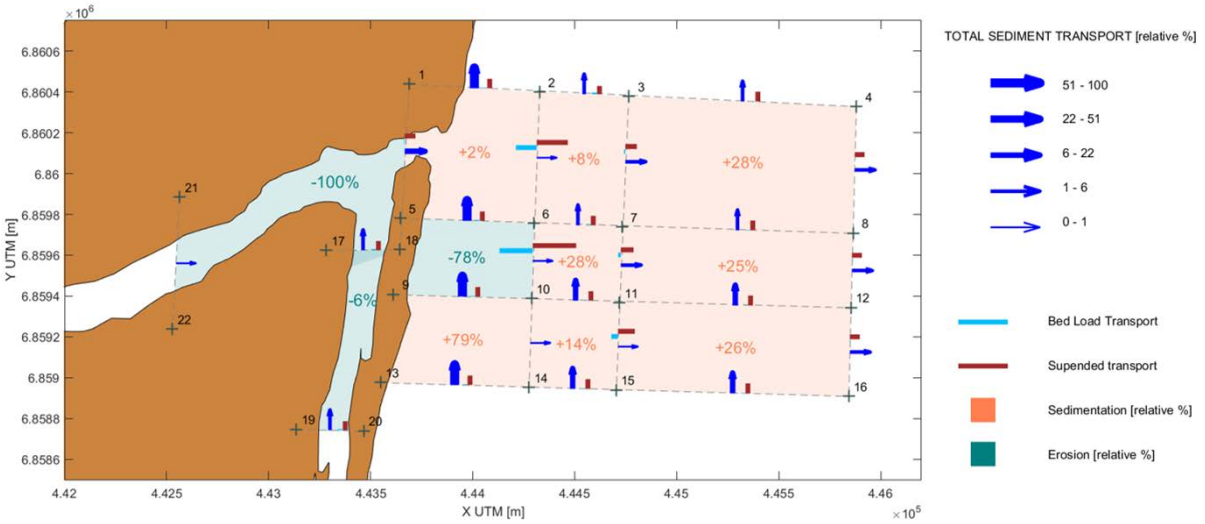

Figure G.3 Sediment pathway analysis for the FSSL3 simulation (includes a10ºN wave direction increase). Blue arrows represent the sediment transport through each profile (delimitated by crosses). The wider the arrow, the larger the sediment transport relative to the biggest transport (legend on the right). The transport is divided into the bed load transport (blue bars) and suspended load transport (brown bars). Both transport loads use a scale of 0.5 relative to the total transport for better visualization. Each cell (between four profiles) represent a sediment budget, either erosion (teal color) or sedimentation (coral color). The shoreline position (brown surface) corresponds to the end of the simulated year.

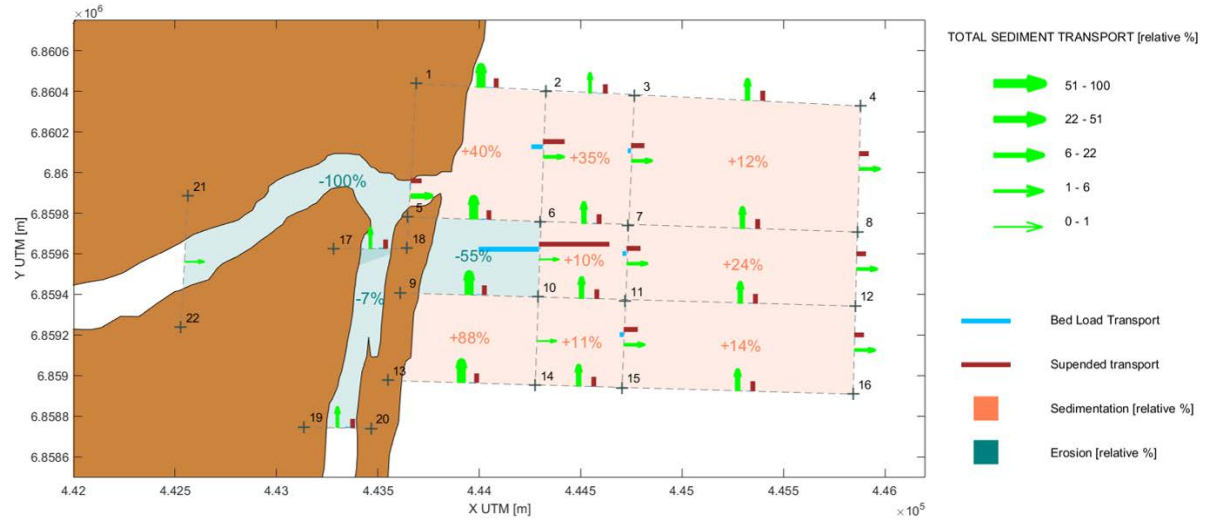

Figure G.4 Sediment pathway analysis for the FSSL4 simulation (includes a10ºN wave direction decrease). Green arrows represent the sediment transport through each profile (delimitated by crosses). The wider the arrow, the larger the sediment transport relative to the biggest transport (legend on the right). The transport is divided into the bed load transport (blue bars) and suspended load transport (brown bars). Both transport loads use a scale of 0.5 relative to the total transport for better visualization. Each cell (between four profiles) represent a sediment budget, either erosion (teal color) or sedimentation (coral color). The shoreline position (brown surface) corresponds to the end of the simulated year.

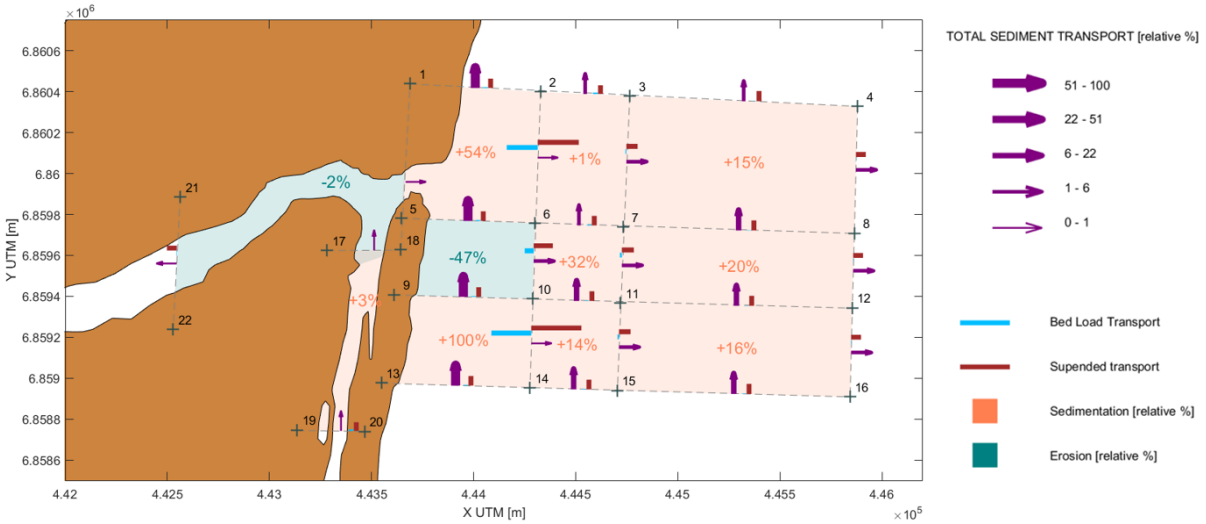

Figure G.5 Sediment pathway analysis for the FSSL5 simulation (includes SLR). Purple arrows represent the sediment transport through each profile (delimitated by crosses). The wider the arrow, the larger the sediment transport relative to the biggest transport (legend on the right). The transport is divided into the bed load transport (blue bars) and suspended load transport (brown bars). Both transport loads use a scale of 0.5 relative to the total transport for better visualization. Each cell (between four profiles) represent a sediment budget, either erosion (teal color) or sedimentation (coral color). The shoreline position (brown surface) corresponds to the end of the simulated year.

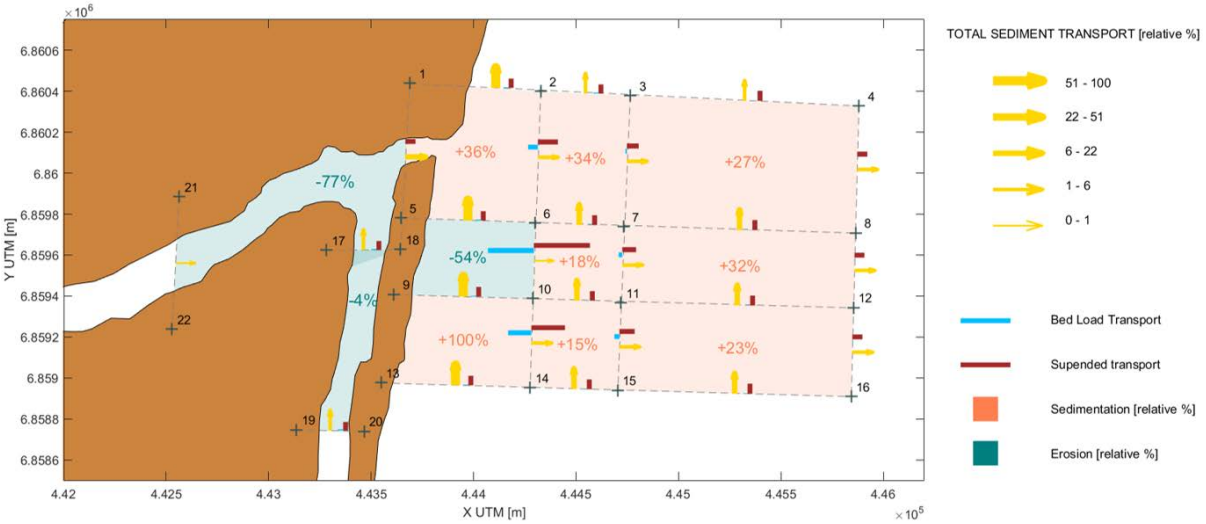

Figure G.6 Sediment pathway analysis for the FSSL6 simulation (includes the 2100 projected river discharge). Yellow arrows represent the sediment transport through each profile (delimitated by crosses). The wider the arrow, the larger the sediment transport relative to the biggest transport (legend on the right). The transport is divided into the bed load transport (blue bars) and suspended load transport (brown bars). Both transport loads use a scale of 0.5 relative to the total transport for better visualization. Each cell (between four profiles) represent a sediment budget, either erosion (teal color) or sedimentation (coral color). The shoreline position (brown surface) corresponds to the end of the simulated year.

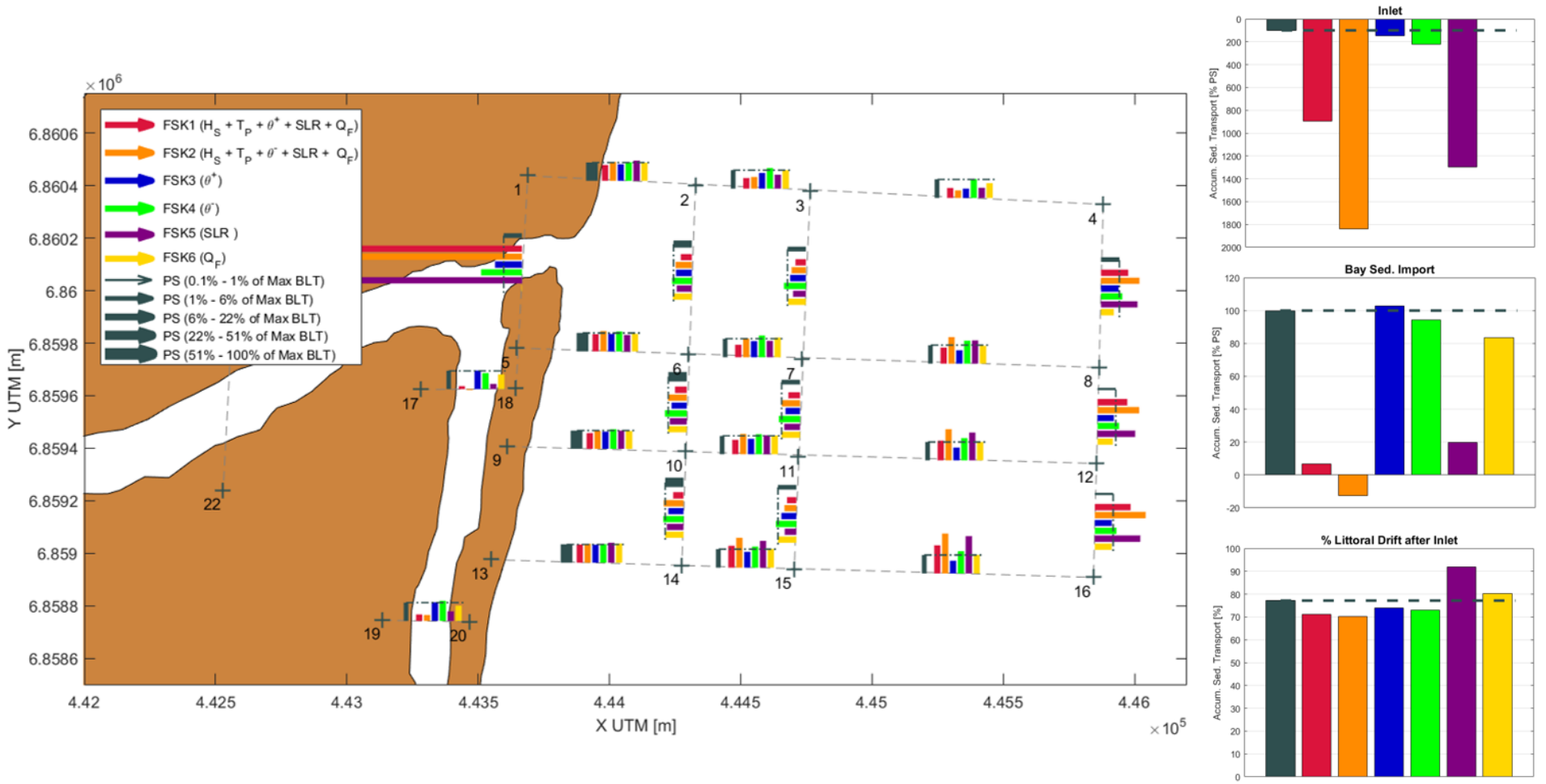

Figure G.7. Accumulated bedload sediment transport map for Santa Lucia Estuary. Grey dashed lines show the output profiles from Delft3D. At each profile a bar plot shows the yearly cumulative sediment transport for all scenarios. Grey bars (present state simulation) are wider when the sediment transport is larger (percentage of the maximum bedload transport (BLT) in legend). The dashed-dotted lines across the bars indicate the value for the present state to highlight the comparison with other simulations. On the right, three bar plots illustrate the inlet profile accumulated transport (top), the sum of the profiles 17-18 and 21-22 (i.e., the sediment intrusion into the bay) (middle), and the remaining littoral drift after the inlet (difference between profiles 5-8 and 1-4) (bottom).

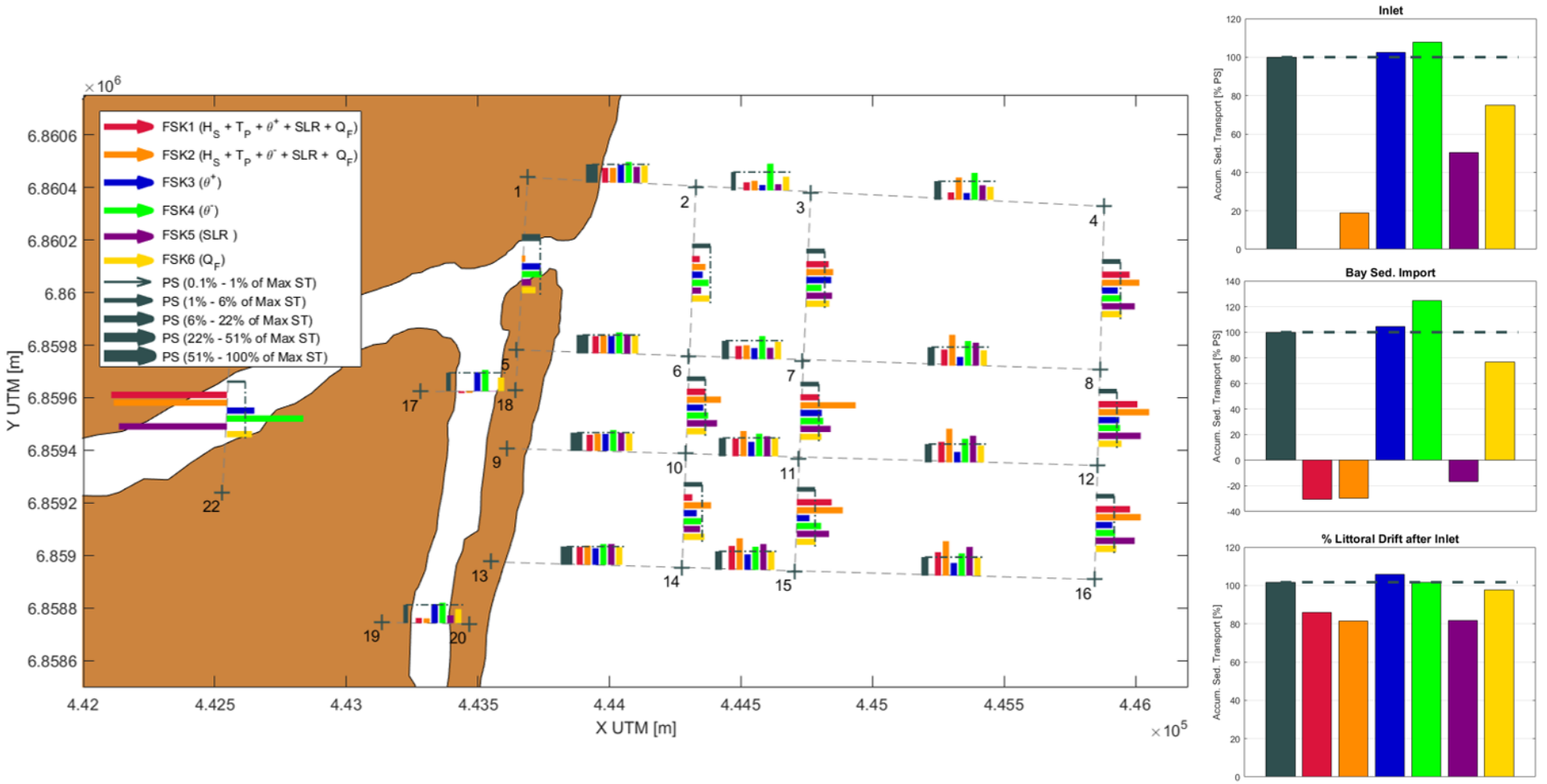

Figure G.8. Accumulated suspended sediment transport map for Santa Lucia Estuary. Grey dashed lines show the output profiles from Delft3D. At each profile a bar plot shows the yearly cumulative sediment transport for all scenarios. Grey bars (present state simulation) are wider when the sediment transport is larger (percentage of the maximum suspended transport (ST) in legend). The dashed-dotted lines across the bars indicate the value for the present state to highlight the comparison with other simulations. On the right, three bar plots illustrate the inlet profile accumulated transport (top), the sum of the profiles 17-18 and 21-22 (i.e., the sediment intrusion into the bay) (middle), and the remaining littoral drift after the inlet (difference between profiles 5-8 and 1-4) (bottom).

To walk aside your favor
I am an Astuary King*
I'll keep in a cave, your comfort and all
Unburdened and becoming

8 (circle) – Bon Iver

* Astuary is likely a combination of the Greek term for star, "aster", and estuary, a meeting point between freshwater and saltwater bodies.